

2013

RNA Dynamics in T Cell Activation

Emily Conn Gantman

Follow this and additional works at: http://digitalcommons.rockefeller.edu/student_theses_and_dissertations

 Part of the [Life Sciences Commons](#)

Recommended Citation

Gantman, Emily Conn, "RNA Dynamics in T Cell Activation" (2013). *Student Theses and Dissertations*. Paper 225.

This Thesis is brought to you for free and open access by Digital Commons @ RU. It has been accepted for inclusion in Student Theses and Dissertations by an authorized administrator of Digital Commons @ RU. For more information, please contact mcsweej@mail.rockefeller.edu.



RNA DYNAMICS IN T CELL ACTIVATION

A Thesis Presented to the Faculty of
The Rockefeller University
in Partial Fulfillment of the Requirements for
the degree of Doctor of Philosophy

by
Emily Conn Gantman

June 2013

RNA DYNAMICS IN T CELL ACTIVATION

Emily Conn Gantman, Ph.D.

The Rockefeller University 2013

Eukaryotic cells employ multiple posttranscriptional mechanisms to fine tune gene expression programs in response to external signals. Regulation of messenger RNA and microRNA by RNA-binding proteins is critical to the control of this process. Hence, disruptions of RNA regulatory processes result in neurologic diseases, cancer, and immunologic disorders among other complications. Posttranscriptional control of RNA is particularly important for precise cytokine expression in T cells during adaptive immune responses.

We have studied human lymphocyte activation as a model for correlating changes in RNA regulation with dynamic cellular state changes and stress responses. We hypothesize that RNA-binding proteins such as Argonaute (Ago) and HuR play critical roles in shaping the dynamic immune response in T cells. We have previously demonstrated the ability to map Ago-microRNA binding sites using high-throughput sequencing of RNA isolated by cross-linking immunoprecipitation (HITS-CLIP) {Chi:2009ht}. Here we used HITS-CLIP to define genome-wide maps of both Ago and HuR RNA binding sites in freshly isolated primary human T cells in the resting state and after one hour of stimulation with anti-CD3 and anti-CD28 antibodies. We also applied RNA sequencing and ribosomal profiling to these lymphocytes to establish their transcriptional and translational status.

We observed different patterns of both Ago and HuR binding from HITS-CLIP in resting and activated T cells. Comparing the Ago and HuR HITS-CLIP genome-wide maps suggests agonistic and antagonistic actions of these two proteins to confer microRNA-mediated regulation of mRNA translation. Furthermore, we overlaid these dynamic RNA binding-protein maps with ribosomal profiles of the target transcripts to investigate translational output as it relates to Ago and HuR regulation. By comparing the changes in both RNA-binding maps with ribosomal profiling results from lymphocytes before and after one hour of T cell activation, we developed a combinatorial dynamic map for these two RNA-binding proteins. Additionally, examining the function of Ago in T cells deficient in HuR helped us understand the relationship between these regulatory proteins in determining the resting and activated lymphocyte states. Our results suggest that differences in protein-RNA interactions for Ago and HuR occur quickly after T cell activation and provide important insight into the specificity of how microRNA translational regulation mediates the immune response.

For Jon.

My rock. My inspiration. My love.

ACKNOWLEDGMENTS

I would like to begin by thanking my advisor, Dr. Robert B. Darnell, for his wisdom, enthusiasm, humor, and support. Bob has been a constant source of motivation to me throughout my time in the lab. I have learned so much from him over the years and he has always found a way to pick me up whenever things have gotten the toughest. I am truly grateful for his mentorship on both professional and personal levels. I cannot express how much I appreciate everything Bob has done for me. Thank you, Bob.

Additionally, I would like to thank the past and present members of the Darnell Lab for providing a friendly and stimulating work environment. They have made my years at Rockefeller not only ones of great learning but also a lot of fun. There could not be enough pages to list all of the important impacts they have had on my scientific and personal life.

I want to extend a special acknowledgement to Dr. Nathalie Blachère for welcoming me into to the lab and teaching me practically everything I know about immunology and mouse work. She has provided constant support, encouragement, and advice. I have loved working on experiments with Nathalie and her friendship is so important to me. I would also like to thank Dr. Jennifer Darnell for her scientific training and advice. I am grateful for her support and collaboration in my experiments and for assuring me that it would possible to defend my thesis near the end of my third trimester of pregnancy.

I owe many thanks to the members of my committee, Dr. Nina Papavasiliou and Dr. Alexander Tarakhovsky, for all of their time and scientific advice. A special thank you to

Nina for chairing my committee and being a great mentor and collaborator. I have really appreciated our chats and her personal support. I am also appreciative of Dr. Alexander Rudensky for participating as my outside committee member.

Additionally, I am grateful to Dr. Sid Strickland and the Rockefeller Dean's Office staff. Thanks for always making time for me and for all of the support during my years here. I would especially like to thank Dr. Emily Harms for being such a wonderful mentor and friend, and for allowing me to be involved in teaching here through the SURF program. I would like to acknowledge the Rockefeller Women & Science Program and the Cancer Research Institute for all of their help and supporting my research.

Thank you to Dr. Bianca Santomaso and Dr. Ilana DeLuca for welcoming me into their projects when I first joined the lab. And to the rest of the ninth floor gang for their support, extra hands, friendships, and wonderful times at "lunch lunch." Especially, thank you to Dr. Julia Kaufman for her amazing friendship, mentorship, and support. Thank you to my bay mate Joe Luna, for keeping me constantly entertained and for all of our long and apparently loud chats about data and life. A huge thank you to Jeff Smith and Dr. Brian Houck-Loomis for their support throughout these years. Their friendship and guidance has meant so much to me.

Thank you to Aldo Mele and Dr. Gulayse Ince-Dunne for teaching me CLIP! I am grateful to Jak Fak and Aldo for graciously lending me an extra pair of hands in many experiments and for helping me with radioactive material during my pregnancy. To Jessica Doerner and Margo Herre, thanks for making the mouse room not so scary after all and for all of their assistance with the little guys. I would also like to thank Dr. Scott

Dewell and the Rockefeller University Genomics Resource Center for their assistance with many parts of this thesis. I am also grateful to Dr. Chaolin Zhang for his guidance and support with my bioinformatic analyses. Graeme Couture, thank you for the help with my cdr2 project. Thank you to Gabe Loeb for all of his advice and reagents. Thank you also to Dr. Nathalie Blachère, Dr. Kate Jeffrey, Dr. Julia Kaufman, Joseph Luna, and Dr. Michael Moore for taking the time to help me with this thesis.

I have been blessed with a wonderful group of friends who have supported me my whole life and most notably throughout my time at Rockefeller. I hope they all know how much I appreciate and love them.

Thank you to Mom and Dad, for always believing in me and supporting me every step of the way to explore whatever path I wanted. Their friendship and love has always overwhelmed me. To my newer Mom and Dad, thank you for all of your love, being my cheerleaders and welcoming me into you family. To my three siblings, our friendship has grown as we have, thank you for always making me smile and being my best friends. And to our newest family member, thanks for always keeping me company and giving me a swift kick to wake me up when I have grown tired. She has literally been with me for this entire writing process and I love being her incubator. We cannot wait to meet her!

I could not be any luckier than to have my husband Jon by my side. He makes me incredibly happy and amazes me with his constant enthusiasm and support of literally everything in our lives. I could not have done any of this without him. He is my best friend, my soul mate, and I love him with every part of my being.

TABLE OF CONTENTS

| | |
|---|-----------|
| ACKNOWLEDGEMENTS | iv |
| TABLE OF CONTENTS | vii |
| LIST OF FIGURES | xiii |
| LIST OF TABLES | xvii |
| CHAPTER 1. Introduction | |
| The Inflammatory and Adaptive Immune Response | 1 |
| <i>Lymphocytes as a Model System for Studying Basic Cellular Function, Immune Responses, and Disease</i> | 7 |
| <i>Paraneoplastic Neurologic Degeneration</i> | 8 |
| RNA Regulation in the Immune Response | 10 |
| <i>T cell Activation and Rapid Cellular Stress Responses</i> | 10 |
| <i>RNA-Binding Proteins in Immune Cells</i> | 12 |
| <i>HuR Regulation of RNA</i> | 14 |
| <i>HuR Regulation in T cells</i> | 15 |
| <i>Ago Regulation and microRNAs</i> | 17 |
| <i>Ago Regulation in T cells</i> | 19 |
| <i>T cell Differentiation and Responses Impacted by the Overexpression or Deletion of microRNAs in Mice</i> | 20 |
| <i>The Combinatorial Control of Ago and HuR</i> | 23 |
| <i>Previous Studies Using CLIP to Explore Co-Regulation of Ago & HuR Targets</i> | 27 |
| Perspectives | 29 |
| CHAPTER 2. Experimental Procedures | |
| <i>Peripheral Blood Isolation</i> | 31 |
| <i>Cell Culture</i> | 31 |
| <i>Negative Selection of CD8 T cells</i> | 31 |
| <i>Positive Selection of CD8 T cells</i> | 32 |
| <i>CD3/CD28 Stimulation</i> | 32 |

| | |
|---|----|
| <i>Flow Cytometry Surface Staining</i> | 33 |
| <i>Reverse Transcription and Quantitative PCR Analysis</i> | 33 |
| <i>Primers</i> | 34 |
| <i>Western Blot</i> | 34 |
| <i>Ago and HuR HITS-CLIP</i> | 35 |
| <i>Ribosomal Profiling and mRNA Sequencing</i> | 43 |
| <i>Mice</i> | 52 |
| <i>Ocular Blood Draw</i> | 52 |
| <i>Flow Cytometry Intracellular Staining</i> | 52 |
| <i>Single Linker Ligation CLIP</i> | 53 |
| <i>Adenovirus production</i> | 54 |
| <i>Adenovirus Immunizations</i> | 55 |
| <i>Mouse T cell in vitro Stimulation</i> | 55 |
| <i>T cell Receptor Codon Optimization, Synthesis, and Cloning</i> | 55 |
| <i>In vitro Transcription of RNA for Electroporation</i> | 55 |
| <i>Electroporation of in vitro transcribed RNA</i> | 56 |
| <i>Tetramer Staining</i> | 57 |
| <i>Primary Ascites Cultures</i> | 57 |
| <i>Preparation of Primary Murine Kidney Epithelial Cells (KECs)</i> | 58 |
| <i>Cell Lines</i> | 58 |
| <i>Peptides</i> | 58 |
| <i>Tumor Killing Assay</i> | 59 |
| <i>Murine and Human IFNG ELISPOT Assays</i> | 59 |
| <i>CD107a assay</i> | 60 |
| <i>HuD peptide 321 specific CD8 T cell Cloning</i> | 60 |
| <i>In Vitro CTL Chromium Release Assay</i> | 61 |
| <i>Titermax Immunization</i> | 61 |

| | |
|---|-----|
| <i>Bone Marrow Chimeras</i> | 62 |
| CHAPTER 3. The Efficiency and Activation of Purified Lymphocytes Using Different Isolation Techniques | |
| Introduction | 63 |
| Results | 67 |
| <i>Purification of CD8 T cells by Negative Selection</i> | 67 |
| <i>Purification of CD8 T cells by CD56 Depletion followed by CD8 Positive Selection</i> | 69 |
| <i>Assessment of CD8 T cell Activation</i> | 72 |
| <i>Ago protein levels with T cell activation</i> | 75 |
| Discussion | 75 |
| CHAPTER 4. Determination of HuR <i>in vivo</i> Binding Sites in Resting and Activated T cells | |
| Introduction | 81 |
| Results | 83 |
| <i>Immunoprecipitation of HuR from T cell Lysate</i> | 83 |
| <i>Pilot HuR HITS-CLIP Experiment on Human T cells expanded in Culture</i> | 87 |
| <i>Radioactive RNA Signal on the Autoradiogram is Specific to the HuR Abs</i> | 89 |
| <i>Radioactive signal on the Autoradiogram is Sensitive to RNase A Digestion</i> | 90 |
| <i>Radioactive RNA Signal on the Autoradiogram is Dependent on Crosslinking</i> | 91 |
| <i>HuR CLIP in Mouse CD8 T cells</i> | 92 |
| <i>Numbers of T Cells Necessary for HuR CLIP</i> | 94 |
| <i>HuR HITS-CLIP from Five Normal Donor Resting and Activated CD8 T cells</i> | 96 |
| <i>Overview of RNA Tag Statistics</i> | 98 |
| <i>Reproducibility of Binding between Biologic Replicate Samples</i> | 101 |
| <i>Genomic Distribution of HuR Binding Sites</i> | 104 |
| <i>Top Hexameric Sequences Represented in HuR Binding Dataset</i> | 106 |
| <i>HuR Binding Changes with Activation</i> | 110 |

| | |
|---|-----|
| Discussion | 116 |
| CHAPTER 5. Determination of Ago <i>in vivo</i> Binding Sites in Resting and Activated T cells | |
| Introduction | 120 |
| Results | 123 |
| <i>Ago HITS-CLIP from Five Normal Donor Resting and Activated CD8 T cells</i> | 123 |
| <i>Overview of RNA Tag Statistics</i> | 126 |
| <i>Reproducibility of Binding between Biologic Replicate Samples</i> | 127 |
| <i>Genomic Distribution of Ago Binding Sites</i> | 131 |
| <i>Ago bound MicroRNA Analysis</i> | 134 |
| <i>Ago mRNA Binding Changes with Activation</i> | 137 |
| Discussion | 145 |
| CHAPTER 6. Exploring the Combinatorial Control of Ago and HuR RNA Regulation During T cell Activation | |
| Introduction | 149 |
| Results | 152 |
| <i>Ago and HuR HITS-CLIP Summary</i> | 152 |
| <i>Ago and HuR Bind EGR3 and IFNG</i> | 152 |
| <i>Overlapping Binding of Ago and HuR</i> | 156 |
| <i>Examining Dynamic Changes in Ago and HuR Binding within Overlapping Transcript Regions</i> | 160 |
| <i>Examining Ago and HuR Binding in the Context of Transcriptional Levels of Target RNA</i> | 165 |
| <i>Ago and HuR and microRNAs</i> | 169 |
| Discussion | 175 |
| CHAPTER 7. Characterization of Ribosomal Profiling of Resting and Activated T cells | |
| Introduction | 181 |
| Results | 184 |
| <i>Nuclease Titration of CD8 T cells for Sucrose Gradients</i> | 184 |

| | |
|---|-----|
| <i>Poly-A mRNA selection and Alkaline Hydrolysis Titration</i> | 188 |
| <i>Preparation of CD8 T cells for Ribosomal Profiling and RNA Sequencing</i> | 188 |
| <i>Sucrose Gradient Profile of Resting and Activated Lymphocytes</i> | 190 |
| <i>Ribosomal Protected Fragments and Poly-A RNA Isolation, Size Selection, and Amplification</i> | 192 |
| <i>Ribosomal Profiling Read Statistics and Genomic Distribution of Binding</i> | 196 |
| <i>Ribosomal Profiling Changes with T cell Activation</i> | 200 |
| <i>Combining CLIP, Ribosomal Profiling and RNA Sequencing</i> | 202 |
| Discussion | 209 |
| CHAPTER 8. Studying T cell Regulation in HuR Deficient CD8 Lymphocytes | |
| Introduction | 211 |
| Results | 212 |
| <i>Lck-Cre⁺ HuR^{fl/fl} CD8 Lymphocyte Characterization</i> | 212 |
| <i>CD4-Cre⁺ HuR^{fl/fl} Mouse Characterization</i> | 216 |
| <i>Preparation of Mouse CD8 T cells for Ago CLIP</i> | 216 |
| <i>Tag Statistics</i> | 220 |
| <i>Genomic Distribution of Ago Binding Sites</i> | 222 |
| <i>Ago Binds Egr3 and Ifng in Mouse T cells with or without HuR</i> | 224 |
| <i>Revisiting Dynamic Binding Changes from the Human Dataset: IRF9 and SATB1</i> | 226 |
| <i>Exploring Ago Binding Changes between HuR Wild type and KO T cells</i> | 231 |
| Discussion | 237 |
| CHAPTER 9. Exploring Tumor Immunity and Neurologic Autoimmunity in Paraneoplastic Neurologic Degeneration | |
| Introduction | 241 |
| Results | 249 |
| <i>Cdr2 T cell Receptor Optimization</i> | 249 |
| <i>Characterization of Ovarian Cancer Patient Ascites Samples</i> | 251 |

| | |
|---|-----|
| <i>Flow Cytometry Based Killing Assay Development</i> | 254 |
| <i>Cdr2-specific CD8 T cell Responses to Primary Human Cancer Cells</i> | 258 |
| <i>HuD Specific CD8 T cell Clone Characterization</i> | 263 |
| <i>Attempts at HuD Specific CD4 T cell Epitope Discovery</i> | 265 |
| <i>Exploring Tolerance to HuD Using Wild Type and HuD KO Mouse Bone Marrow Chimeras</i> | 265 |
| <i>Development of Tools to Study Tolerance to HuD</i> | 269 |
| Discussion | 273 |
| CHAPTER 10. General Discussion | |
| <i>Summary</i> | 277 |
| <i>Overlapping RNA-Binding of Ago and HuR</i> | 278 |
| <i>Rapid Changes in RNA-Binding with CD8 T cell Activation</i> | 279 |
| <i>Analysis of CLIP Data in the Context of Translational Status</i> | 281 |
| <i>Genomic Distribution of Ago and HuR Regulation in CD8 Lymphocytes</i> | 285 |
| <i>Ago and HuR and microRNA Regulation</i> | 287 |
| <i>Conclusion</i> | 291 |
| REFERENCES | 292 |

LIST OF FIGURES

CHAPTER 3

| | |
|---|----|
| Figure 3.1 Purity of CD8 T Cells Purified by Negative Selection. | 68 |
| Figure 3.2 Purity of CD8 T Cells Purified by CD56 Depletion and CD8 Positive Selection. | 70 |
| Figure 3.3 CD8 T Cell Activation qPCR Analysis. | 73 |
| Figure 3.4 Ago Protein Levels with CD8 T Cell Activation in vitro. | 76 |

CHAPTER 4

| | |
|--|-----|
| Figure 4.1 HuR HITS-CLIP Methods Schematic. | 84 |
| Figure 4.2 HuR Immunoprecipitation. | 86 |
| Figure 4.3 HuR CLIP: mAb Specific to HuR. | 88 |
| Figure 4.4 HuR-RNA Complexes are Crosslinking Dependent. | 93 |
| Figure 4.5 HuR Mouse CD8+ T Cell CLIP. | 95 |
| Figure 4.6 HuR CLIP CD8+ T Cell Titration. | 97 |
| Figure 4.7 Pairwise Correlation of HuR CLIP Clusters. | 102 |
| Figure 4.8 HuR Clusters Activation State Distributions. | 105 |
| Figure 4.9 HuR Clusters Genomic Distribution. | 107 |
| Figure 4.10 Nucleotide Frequency in HuR Clusters. | 109 |
| Figure 4.11 Cluster Scoring System. | 111 |
| Figure 4.12 HuR Binding on Human EGR3. | 114 |
| Figure 4.13 HuR Binding on Human IFNG. | 115 |

CHAPTER 5

| | |
|---|-----|
| Figure 5.1 Ago HITS-CLIP. | 125 |
| Figure 5.2 Pairwise Correlation of Ago CLIP Clusters. | 130 |
| Figure 5.3 Ago Clusters Activation State Distributions. | 132 |
| Figure 5.4 Ago Clusters Genomic Distribution. | 133 |

| | |
|---|-----|
| Figure 5.5 Ago Binding on Human EGR3. | 142 |
| Figure 5.6 Ago Binding on Human IFNG. | 143 |
| Figure 5.7 Ago Binding in Human FYB Intron. | 144 |
| CHAPTER 6 | |
| Figure 6.1 Ago and HuR bind Human EGR3. | 154 |
| Figure 6.2 Ago and HuR bind Human IFNG. | 155 |
| Figure 6.3 Ago and HuR Cluster Overlap Parameters. | 157 |
| Figure 6.4 Histogram of Ago and HuR Cluster Overlap. | 159 |
| Figure 6.5 Ago and HuR Cluster Overlap in Resting and Activated States. | 161 |
| Figure 6.6 Dynamic Ago and HuR Changes in Overlapping Clusters. | 162 |
| Figure 6.7 Reciprocal Changes in Ago and HuR Binding in the Human IRF9 3'UTR. | 164 |
| Figure 6.8 Reciprocal Changes in Ago and HuR Binding in the Human SATB1 3'UTR. | 166 |
| Figure 6.9 Reciprocal Changes in Ago and HuR Binding in the Human FYB Gene. | 170 |
| Figure 6.10 Ago Clusters with Matches in each Seed Family. | 171 |
| Figure 6.11 Ago and HuR bind the Human microRNA-17-92 Locus. | 174 |
| Figure 6.12 HuR binding sites mapped onto miR-17-92 Locus. | 176 |
| CHAPTER 7 | |
| Figure 7.1 Ribosomal Profiling and RNA Sequencing Schematic. | 185 |
| Figure 7.2 Sucrose Gradients After Nuclease Titration. | 187 |
| Figure 7.3 Urea gel of Alkaline Hydrolysis Duration Titration. | 189 |
| Figure 7.4 CD8+ T Cell Characteristics of Donor 1 for Ribosomal Profiling Experiment. | 191 |
| Figure 7.5 Sucrose Gradient Profile of Resting and CD3/CD28 Stimulated CD8+ T Cells. | 193 |
| Figure 7.6 Urea Acrylamide Gel of RPFs and PolyA RNA. | 194 |
| Figure 7.7 RPFs and mRNA PCR Products for High-Throughput Sequencing. | 195 |
| Figure 7.8 Mapped RPFs Read Genomic Distribution. | 199 |

| | |
|--|-----|
| Figure 7.9 RPFs and mRNA Changes with T Cell Activation. | 201 |
| Figure 7.10 T Cell RPFs and mRNA in the Resting and Activated State. | 203 |
| Figure 7.11 Combining Ribosomal Profiling, mRNA Sequencing, and CLIP Data. | 204 |
| Figure 7.12 3'UTR CLIP Targets: Combining Ribosomal Profiling, mRNA Sequencing, and CLIP Data. | 208 |

CHAPTER 8

| | |
|--|-----|
| Fig 8.1 Lck-Cre HuRfl/fl Characterization. | 213 |
| Figure 8.2 HuR Intracellular Stain and Western Blot. | 215 |
| Figure 8.3 CD4-Cre HuRfl/fl Intracellular FACS from Blood. | 217 |
| Figure 8.4 Mouse CD8 T Cells: Characterization for Ago CLIP. | 219 |
| Figure 8.5 Mouse Ago Clusters Genomic Distribution. | 223 |
| Figure 8.6 Ago Binding on Mouse Egr3. | 225 |
| Figure 8.7 Ago Binding on Mouse Ifng. | 227 |
| Figure 8.8 Ago and HuR Binding in Human and Mouse: IRF9 3'UTR. | 229 |
| Figure 8.9 Ago and HuR Binding in Human and Mouse: SATB1 3'UTR. | 230 |
| Figure 8.10 Ago and HuR Combinatorial Control. | 232 |
| Figure 8.11 Ago and HuR Binding in Human and Mouse: FYB 3'UTR. | 233 |
| Figure 8.12 Ago and HuR Binding in Human and Mouse: Ppp1r15b Exon. | 235 |
| Figure 8.13 Ago and HuR Binding in Human and Mouse: Pdcd4 Exon. | 236 |

CHAPTER 9

| | |
|---|-----|
| Figure 9.1 Model of Paraneoplastic Neurologic Degeneration. | 242 |
| Figure 9.2 Hu Patient Schematic. | 244 |
| Figure 9.3 Mouse Adenovirus-HuD Immunizations. | 248 |
| Figure 9.4 cdr2 TCR Optimization Schematic. | 250 |
| Figure 9.5 cdr2 TCR Tetramer Stain of Electroporated Lymphocytes. | 252 |
| Figure 9.6 HLA-A2 Stain of Ovarian Cancer Patient PBMC. | 253 |
| Figure 9.7 Tumor Killing Assay Schematic. | 255 |

| | |
|--|-----|
| Figure 9.8 cdr2-Specific CD8 T Cell Tumor Killing Assay. | 257 |
| Figure 9.9 cdr2-Specific CD8 T Cell IFNG ELISPOT. | 260 |
| Figure 9.10 cdr2-specific CD8 T Cell CD107a and TNF Assay. | 262 |
| Figure 9.11 HuD peptide 321 CD8 T Cell Clone Characterization. | 264 |
| Figure 9.12 IFNG CD4 T Cell HuD Peptide Titermax Experiment. | 266 |
| Figure 9.13 HuD Tolerance Bone Marrow Chimera Experiment Summary. | 268 |
| Figure 9.14 Tools to Study Tolerance to HuD: Double Adenovirus Immunization. | 271 |
| Figure 9.15 Tools to Study Tolerance to HuD: Double Peptide-Titermax Immunization. | 272 |

CHAPTER 10

| | |
|---|-----|
| Figure 10.1 Ago and HuR Binding in Human and Mouse: microRNA-17-92 Locus. | 290 |
|---|-----|

LIST OF TABLES

CHAPTER 3

| | |
|--|----|
| Table 3.1 Purification of CD8 T cells from Normal Human Donor Leukapheresis. | 71 |
|--|----|

CHAPTER 4

| | |
|--|-----|
| Table 4.1 HuR CLIP Tag Statistics. | 100 |
| Table 4.2 Top Hexameric Sequences in HuR Clusters. | 108 |
| Table 4.3 Combining HuR CLIP with RNAseq. | 113 |

CHAPTER 5

| | |
|--|-----|
| Table 5.1 Ago CLIP mRNA Tag Statistics. | 128 |
| Table 5.2 Ago CLIP microRNA Tag Statistics. | 135 |
| Table 5.3 Ago CLIP: Top 35 microRNAs. | 136 |
| Table 5.4 MicroRNAs Shifting More than 1.5 Fold with Activation. | 138 |
| Table 5.5 Combining Ago CLIP with RNAseq. | 140 |

CHAPTER 6

| | |
|---|-----|
| Table 6.1 HITS-CLIP Sequencing Summary. | 153 |
| Table 6.2 Combining Overlapping Ago and HuR CLIP with RNAseq. | 168 |

CHAPTER 7

| | |
|---|-----|
| Table 7.1 RPFs and mRNA Sequencing Read Statistics. | 197 |
|---|-----|

CHAPTER 8

| | |
|--|-----|
| Table 8.1 Ago CLIP Tag Statistics from HuR cKO and WT Lymphocytes. | 221 |
|--|-----|

CHAPTER 10

| | |
|---|-----|
| Table 10.1 Dynamic Changes in Ago and HuR binding and Translational Efficiency. | 283 |
|---|-----|

CHAPTER 1. Introduction

The adaptation to environmental signals is an essential component of cellular life. In multicellular organisms, these pathways have evolved to include responses to both external stimuli and internal signals. For example, in the immune system, lymphocytes need to modify their states quickly to respond to the presence of potentially harmful antigen, such as during the recognition of virally infected or malignant cells, and then back to quiescence so as not to damage normal tissue.

The Inflammatory and Adaptive Immune Response

The spread of a pathogen is first combatted by the inflammatory response of the innate immune system. Macrophages and dendritic cells survey the host for antigen, such as in sites of infection and inflammation, and are triggered to ingest bacteria and infected cells due to their recognition of molecules shared by pathogens and distinguishable from the host. These molecules also trigger the cells to become activated and secrete cytokines, including tumor necrosis factor (TNF), and chemokines to initiate inflammation (Janeway and Medzhitov 2002). Clinically, inflammation is characterized by heat, redness, and swelling, which are caused by the cytokine induced increase in blood flow and leakage of fluid from the bloodstream into the site, and pain, due to the infiltration of white blood cells. The inflammatory neutrophil and macrophage populations help to increase the flow of lymph to bring together antigen-presenting cells (APCs) with lymphocytes to activate the adaptive immune response (Barton 2008; Nathan 2002).

Among other inflammatory signals, local cells such as fibroblasts are stimulated by TNF to produce a wide array of cytokines and chemokines that help to propagate the inflammatory response and recruit white blood cells into the injured tissue. While only short exposure to TNF is necessary for the initiation of the NF- κ B transcriptional program, which can account for much of the early response, a sustained stimulus can lead to the induction of three temporal classes of responses: transcripts that initiate expression within a half-hour and are quickly diminished, transcripts that accumulate over the first two hours and then are sustained, and transcripts that increase more gradually. These responses are highly regulated temporally to ensure the proper initiation of the inflammatory cascade. While the induction of these signals is transcriptionally controlled, the fate and regulation of the transcripts is defined largely post-transcriptionally (Bradley 2008; Hao and Baltimore 2009; Hoffmann 2002; Tian 2005).

When a dendritic cell ingests a pathogen, it becomes activated to mature into an APC that is able to stimulate pathogen-specific lymphocytes in the lymph node. These activated APCs secrete cytokines that help to shape both the innate and adaptive immune responses. Lymphocytes circulate in the host's bloodstream in a fairly quiescent state until they encounter antigen and co-stimulatory molecules in the context of an APC. Such an encounter triggers proliferation and differentiation of lymphocytes into primed effector cells that can reject the infectious agent. These initiating interactions of the adaptive immune response occur in the peripheral lymphoid organs such as the lymph nodes, spleen and mucosal lymphoid tissues (Banchereau and Steinman 1998).

While antibodies can recognize pathogens circulating in the blood and in extracellular spaces, the cytotoxic T lymphocytes of the adaptive immune system are needed to identify intracellular bacterial pathogens, parasites, viruses, and tumor antigens. Foreign proteins and tumor antigens are processed and presented as peptide fragments on major histocompatibility complex (MHC) molecules to T cells, which can kill the offensive cells. MHC I molecules generally capture and present peptides from the cytosol of the cell. MHC II molecules present exogenous peptide to cluster of differentiation four (CD4) T cells that can function as “helper” cells to orchestrate T cell responses, antibody responses, or to down regulate adaptive immune responses as suppressor cells. During lymphocyte maturation each T cell develops a unique antigen receptor, or T cell Receptor (TCR), which recognizes a specific antigenic peptide held by an MHC molecule. Thus the genotype of the MHC restricts the antigen specificity of the T cell. Lymphocytes are selected during differentiation for deletion or tolerance of lymphocytes expressing TCRs specific for self-antigen (Rock and Goldberg 1999).

Cytotoxic T cells typically express the cluster of differentiation eight (CD8) co-receptor on their surfaces which binds MHC class I. The TCR and CD8 molecules can bind to the same MHC complex simultaneously, which greatly enhances the resulting activation signal (J.-H. Wang and Reinherz 2002). Other co-stimulatory interactions may also be necessary to stimulate a productive immune response such as with the B7 proteins, which stimulate T cells via the cluster of differentiation twenty-eight (CD28) molecule (Jenkins et al. 1991). Upon engagement of cognate peptide-MHC complexes, the Src family kinases LCK and FYN are recruited to the TCR and phosphorylate tyrosine substrates in the cytoplasmic tails of the receptor’s subunits in immunoreceptor tyrosine-based

activation motifs (ITAMs). These phosphorylated receptor molecules recruit and then activate a second tyrosine kinase, ZAP-70. The FYN adaptor protein also associates with FYB, also called SLAP or ADAP, which aids in the proliferative response and cytokine production by helping to stabilize the interaction of the TCR with APCs through integrin clustering and adhesion (Griffiths et al. 2001; Peterson et al. 2001).

Activation of ZAP-70 in turn leads to the phosphorylation of adaptor proteins LAT and SLP-76 that recruit other proteins that stimulate the Ras pathway, the mobilization of calcium, and the reorganization of the cytoskeleton of the T cell. One protein that is recruited to the membrane is phospholipase C γ 1 (PLCG1) which hydrolyzes phosphatidylinositol 4,5-bisphosphate (PIP2) into inositol 1,4,5-trisphosphate (IP3) and diacylglycerol (DAG). IP3 interrogates receptors on the endoplasmic reticulum to release Ca²⁺ into the cytoplasm, triggering a cascade of calcium dependent signaling leading to the activation of NFAT and its regulated transcriptional control of interleukin-2 (IL-2) and other cytokines (Weiss and Littman 1994). DAG in turn activates numerous protein targets including protein kinase C (PKC) family members and Ras guanyl-nucleotide-releasing protein (RasGRP). These help to activate Ras signaling which eventually leads to the activation of mitogen-activated protein (MAP) kinases. This results in the phosphorylation and activation the transcription factor AP-1, which induces both FOS and JUN transcription among others changes. PKCs also are involved in activating the NF κ B transcription factor which contributes to the induction of pro-inflammatory cytokines (Cantrell 2002; Jordan, Singer, and Koretzky 2003; Weiss and Littman 1994).

The addition of co-stimulatory CD28 signaling to CD3 stimulation leads to higher expression and stabilization key inflammatory molecules such as IL-2, interferon gamma (IFNG), TNF, and granulocyte-macrophage colony stimulating factor (GM-CSF) (Lindstein et al. 1989; Thompson et al. 1989). Although it has also been reported that the primary differential effect of CD28 engagement may be related to an increase in NFAT signaling in the lymphocyte (Diehn et al. 2002). CD28 binding, in addition to TCR binding, stimulates transcription of the EGR family, Nuclear Receptor Subfamily, and CD69 (Kaye 2000; Shao et al. 1997). The interaction between a T cell and peptide-MHC complex can be mimicked in culture by interrogation of the TCR complex via anti-CD3 antibodies and co-stimulation with anti-CD28 antibodies. By using beads coated with both of these antibodies (CD3/CD28 beads), the signals are distributed on a surface comparable to the size of an APC and the lymphocyte can encounter both signals simultaneously.

Interferon gamma (IFNG) production after T cell stimulation can directly inhibit viral replication and also help kill intracellular pathogens by initiating starvation programs in their host cells. Additionally, IFNG signals for the increased production and expression of major histocompatibility complex I (MHC I) and other components of antigen processing machinery to increase the presentation of viral components to the immune system for potential recognition and attack. IFNG synergizes with TNF to activate and recruit macrophages to the site of infection or injury to aid in the clearance and killing of infected material, and in antigen presentation (Boehm et al. 1997; Rock and Goldberg 1999). IFNG mediates its antiviral and immune modulatory effects through Janus Tyrosine Kinase (JAK) signaling. Homodimers of IFNG bind to two interferon gamma

receptor (IFNGR) 1 molecules that have intracellular domains associated with JAK1. Binding of IFNG leads to the joining of each IFNGR1 subunit with one of IFNGR2 that is associated with JAK2. This brings together the active IFNG receptor complex made up of two of each receptor and two of each JAK. The JAK1 and JAK2 molecules are auto- and trans-phosphorylated creating a docking site for signal transducers and activators of transcription (STAT) 1. A homodimer of STAT1 forms after phosphotyrosine activation by the JAKs. This STAT1 homodimer translocates to the nucleus and binds to gamma-activated sequence (GAS) elements to induce transcription (Horvath 2000; Levy and Darnell 2002; Shuai and Liu 2003; Stark and Darnell 2012; Stark et al. 1998).

With the initiation of an inflammatory and adaptive immune response, it is clear that a variety of signaling pathways lead to a vast induction of transcription. While these transcriptional changes help to characterize the inflammatory response, they do not complete the regulatory picture. When lymphocytes encounter antigen, they are required to respond very quickly. Thus, it is logical that T cells not rely solely on transcriptional changes to alter protein expression. RNA-binding proteins can help to regulate translation by affecting mRNA stability, localization, inclusion in stress granules, and access to ribosomes, among other processes. RNA-binding proteins in T cells regulate rapid changes in the production of cytokines, among other proteins. The induction of cytokine production needs immediate control to ensure the production of an effective immune response to antigen, but also a transient response to protect surrounding healthy cells from destruction. RNA-binding proteins can ensure this by helping to induce translation, or targeting transcripts for degradation or translational repression (Anderson

2008). To better understand lymphocyte responses, and as a surrogate system for examining the dynamic control of mRNA, we have undertaken to study the post-transcriptional regulation of T cell activation.

Lymphocytes as a Model System for Studying Basic Cellular Function, Immune Responses, and Disease

The elaborate transcriptional and translational regulation of T cell activation, and the connection of these processes with the general mechanisms of the integrated stress response make T cells a perfect system for the study of the dynamic control of RNA regulation. Working with T cells, we can study a purified cell population rather than a tissue made up of many cellular components without significant manipulation, as compared to the dissociation of a tissue. Furthermore, we can work with normal human cells without the requirement for invasive procedures or post-mortem collection of tissue. Although CD8 T cells can have varied responses such as cytotoxic responses, immune tolerance, and anergy, they are more uniform than CD4 lymphocytes phenotypes that have various transcriptional profiles and cytokine secretion depending on their committed lineage.

In this work, we studied the regulation of CD8 lymphocytes directly *ex vivo* from normal human donors. Therefore, they represent true biologic samples and do not have the biases of cells that have been transformed or otherwise propagated in culture systems. Also, each donor sample represents a true replicate. While the donors were all normal adults, they represent different genetic background and ages which gives much more biologic complexity than multiple plates of cell lines or even genetically identical mice.

Thus, processes and events that we find consistent between donor samples are more likely to represent general mechanisms of control. Also, by pairing these studies with the mouse system we can take advantage of genetic models and utilize the power of conservation to rapidly dissect findings from the human system.

The *in vitro* activation and manipulation of lymphocytes can mimic *in vivo* biologic interactions of T cells with APCs. Here we focused on broad T cell activation by CD3/CD28 stimulation to maximize our response and best recapitulate a general stress response, but this could also be done in an antigen-specific manner to study even more specific cell populations and responses. Because lymphocyte activation is important for the control of many disease states including inflammation, infection, tumor biology, and autoimmunity, we think that studying lymphocyte stimulation is generally applicable and biologically meaningful. Much of the signaling and regulatory mechanisms studied in lymphocytes should be pertinent to other cellular systems, especially regarding general regulation of the stress response. Nevertheless, because of the connection between the translational regulation of cytokine production and the balance between stimulatory and anergic responses, we hypothesize that understanding the basic regulatory control of T cell activation could be especially informative in the understanding of tumor immunity and autoimmunity.

Paraneoplastic Neurologic Degeneration

Paraneoplastic disorders refer to symptoms resulting from the presence of a tumor at a site remote from the neoplasm and can be caused by hormone and cytokine secretion by the tumor cells or by an immune response to the tumor. In some cases, tumor cells

express proteins that are normally restricted to the brain, termed onconeural antigens. Because the antigens are normally restricted to the nervous system, the ectopic expression in the tumor makes them vulnerable to immune system surveillance, much like foreign antigens, and can help to elicit a strong tumor immune response that correlate with positive outcomes in subsequent cancer treatment. Unfortunately, the anti-tumor immune reaction can lead to severe autoimmune disease mediated by these onconeural proteins, leading to neurologic degeneration. Paraneoplastic neurologic degeneration (PND) disorders represent some of the best-known clinical cases of spontaneous tumor immunity, especially with identified antigenic targets of the immune system. Interestingly, the onconeural antigens in multiple PNDs are RNA-binding proteins (R. B. Darnell 1996; R. B. Darnell and Posner 2003a; 2003b; 2006).

While patients are often diagnosed with a PND based on the presence of onconeural-specific antibodies, their role in disease progression is unclear as disease models utilizing onconeural autoantibodies have failed to initiate disease (Sakai et al. 1995). Antibodies often mediate responses to extracellular antigens, while PND antigens are often expressed intracellularly (Okano and Darnell 1997). CD8 T cells are often key effectors of tumor immunity due to their ability to recognize the unusual protein repertoires often expressed in malignant cells. PND patients often have activated T cells in their cerebral spinal fluid and previous lab members have identified onconeural antigen-specific CD8 lymphocytes in PND patients, including the discovery of CD8 T cells that display unusual cytokine expression phenotypes (Albert et al. 1998; Albert, Austin, and Darnell 2000; Roberts et al. 2009). Studies in mice have suggested that in normal animals there is immune tolerance to onconeural antigens (DeLuca et al. 2009) and Blachère et al., unpublished. The

mechanisms mediating tolerance to these neuronal proteins are unknown and the critical method by which this tolerance is broken in PND patients leading to both tumor immunity and neuronal autoimmunity is not yet understood. By studying the basic regulatory processes mediating T cell activation, we hope to uncover insight into the control of the powerful tumor immunity and devastating autoimmunity displayed by these patients.

RNA Regulation in the Immune Response

T cell Activation and Rapid Cellular Stress Responses

When cells encounter various biologic stresses such as heat shock, amino acid starvation, oxidative stress, or viral infection, a common integrated stress response (ISR) pathway is induced to protect the cell from damage and adapt to the environmental changes. One main functional outcome of this pathway is the control of the translational status of mRNA in the cells to modulate the priority of which transcripts are made into protein during the period of new cellular demands. While different cellular cascades help to initiate these different responses, many converge upon the phosphorylation of serine 51 of the alpha subunit of the eukaryotic initiation factor two (EIF2A). Serine 51 phosphorylation blocks EIF2A from helping establish active initiation complexes at the ribosome, which decreases translation. Changes in translational control with the induction of the ISR are also accompanied by alterations in gene expression to help the cells adapt, including the induction of regulators of EIF2A phosphorylation such as GADD34 (PPP1R15A) (Harding et al. 2002; 2003; Murphy 2006). Unlike GADD34, constitutive repressor of EIF2A phosphorylation (CReP or PPP1R15B) is constitutively expressed,

but both can help dephosphorylate EIF2A blocking it from activating the ISR (Jousse et al. 2003). In addition to changes in transcription and translation, an activated ISR can also affect the localization of mRNA. mRNA present in the cell can be sequestered in stress granules and p-bodies, although the presence of the latter is not depended on EIF2A phosphorylation, to harbor latent transcripts or target them for degradation (Anderson 2008; Brengues, Teixeira, and Parker 2005; Harding et al. 2002; Kedersha and Anderson 2002; Murphy 2006; Scheu et al. 2006; Sheth and Parker 2006). RNA-binding proteins, such as Argonaute (Ago) and HuR to be discussed later, can rapidly shuttle in and out of stress granules, presumably in conjunction with bound mRNAs, to mediate translational silencing and potentially degradation (Bhattacharyya, Habermacher, Martine, Closs, and Filipowicz 2006a; 2006b; Leung and Sharp 2007; 2010).

The dissociation between the transcription of cytokine mRNA and synthesis of the protein during CD4 T cell differentiation has been linked to a pathway resembling ISR (Scheu et al. 2006). Also, in a mouse model of immune tolerance, the production of cytokine mRNA was disconnected from the generation of effector proteins in T cells specific for self but not foreign antigens (Villarino et al. 2011). T cell activation in hypoxic conditions has also been shown to increase the secretion of IFNG without increased levels of the IFNG transcript (Roman et al. 2010). Although these may not be direct representations of the classical ISR pathway, the translational control of cytokine expression and their localization to stress granules makes T cell activation an intriguing system to study the regulation of these pathways and applicable to many general cellular dynamic responses.

RNA-Binding Proteins in Immune Cells

These observations raise the general issue of how gene regulation is manifest in the dynamics of the immune response. Hao and Baltimore analyzed the inflammatory response by determining the transcriptional profiles of macrophages at various time points after the stimulation with TNF. They described that the response could be grouped into three sets of genes: ones that peaked in expression at half an hour after activation, after two hours of activation, or increased steadily with stimulation and peaked at 12 hours after activation. They concluded that transcription and mRNA turnover are important to the control of inflammation (Hao and Baltimore 2009). Another level of regulation, not excluded by these observations, is translational regulation. One predominant advantage of this point of regulatory control is in the potential for even more rapid responses of immune cells in response to stimuli.

As immune cells survey the host for antigen, they are required to adapt quickly to changes within their host. For example, when a lymphocyte encounters antigen, it needs to quickly initiate an inflammatory response including the production of cytokines. This response needs to be carefully controlled and transient so that it does not damage the surrounding tissue. Thus, it is logical that much of lymphocyte protein expression be regulated at the translational level. For instance, by harboring latent cytokine transcripts in cytoplasmic granules, RNA-binding proteins can compete for interactions with their targets. These proteins work in combination to modulate a cytokine mRNA's stability and access to ribosomes, which can be quickly accomplished without the need for new transcription to initiate a response (Anderson 2008; 2010).

AU-rich elements (ARE) are usually found in the 3'UTR of transcripts and are found in many mRNAs encoding immediate-early and early response genes, including cytokines, proliferative factors, and other functional groups that drive inflammation (Gruber et al. 2011). These *cis*-regulatory elements were first identified as binding sites for RNA-binding proteins nearly twenty-five years ago (Malter 1989). Since then it has been elucidated that many RNA-binding proteins act at these sites to both positively and negatively regulate mRNA turnover, changes in subcellular localization, and access to translational machinery in response to cellular stresses. ARE-binding proteins such as HuR (ELAVL1), TIA1/TIAR, and tristetraprolin (TTP), have been shown to have critical inflammatory functions, such as in the regulation of cytokine mRNA (Meisner and Filipowicz 2010).

For example, all of these factors have been shown to interact with ARE in the TNF 3'UTR in mediating the immune response. HuR deficient T cells in mice displayed increased levels of *Tnf* mRNA and analyses of myeloid-restricted HuR over-expression showed translational suppression of inflammatory mRNAs, including *Tnf* (Katsanou et al. 2005; Papadaki et al. 2009). TIA-1 and TIAR recruit target mRNAs to stress granules in response to different stimuli to block their translation (Kedersha et al. 1999). Macrophages from mice lacking either *Tia-1* or *Tiar* and stimulated with LPS produced increased levels of TNF protein without altering its transcript abundance or half-life (Kedersha et al. 1999; Piecyk et al. 2000). Mice deficient in *Ttp* spontaneously develop severe autoimmune disorders due to the over expression of TNF protein and other inflammatory factors which are normally targets of deadenylation and mRNA decay due to TTP destabilization (Blackshear 2002; Lai et al. 1999; Taylor et al. 1996).

HuR Regulation of RNA

HuR, also known as HuA or ELAV11, is a ubiquitously expressed RNA-binding protein that is closely related to the neuronal proteins HuB, HuC, and HuD (Ma et al. 1996; Okano and Darnell 1997). The neuronal isoforms are targets of the immune system in both lung cancer cells and the nervous system in a PND known as the Hu Syndrome. This is an interesting connection between RNA regulation and the pathology of PND and we speculate that HuR could be critical to controlling the immune response of T cell phenotypes that are altered in the targeting of its neuronal homologues. Hu proteins contain three RNA recognition motifs. These proteins were identified as binding to U-rich sequences and many U-rich and ARE binding motifs have been identified (Ma et al. 1996; Myer, Fan, and Steitz 1997).

HuR was shown to actively shuttle between the nucleus and cytoplasm in response to different stress conditions including the activation of immune cells (Meisner and Filipowicz 2010). This export of HuR into the cytoplasm is critical for its regulatory control of certain target transcripts (X. C. Fan and Steitz 1998b; Peng et al. 1998). The shuttling is mediated by two different pathways, one which utilizes the HuR nuclear localization signal and is dependent on CRM1, and the second uses transportin molecules (X. C. Fan and Steitz 1998a; Gallouzi, Brennan, and Steitz 2001; Rebane, Aab, and Steitz 2004). HuR also associates with stress granules in response to cellular stress (Gallouzi et al. 2000). In response to cellular stimuli, signaling cascades can lead to posttranslational modifications of HuR which may mediate its subcellular localization or influence its RNA binding (Abdelmohsen et al. 2007; Doller, Pfeilschifter, and Eberhardt 2008). The

levels of HuR protein have also been shown to be regulated in response to T cell stimulation and other stress responses by multiple pathways including auto-regulation and control by microRNAs (Abdelmohsen et al. 2008; Akool et al. 2003; Atasoy et al. 1998; X. Guo, Wu, and Hartley 2009; Jeyaraj et al. 2010; Papadaki et al. 2009; Sakai et al. 2003).

HuR has been demonstrated to regulate targeted transcripts by cooperative and competitive interactions with other RNA-binding proteins often by interfering with ARE-mediated decay of mRNA by other RNA-binding proteins (Anderson 2008; Brennan and Steitz 2001; Casolaro et al. 2008; X. C. Fan and Steitz 1998b; Myer, Fan, and Steitz 1997). Although much work studying HuR has focused on transcript stability, HuR has also been linked to dynamic control of translation (Katsanou, Dimitriou, and Kontoyiannis 2006; Kawai et al. 2006; Lal et al. 2004; Mazan-Mamczarz et al. 2003; Sureban et al. 2007). Still, much of the research investigating the targets and effects of HuR binding has been studied *in vitro* with reporter constructs or by over expressing HuR, in potentially biased screens for regulation and non-physiologic conditions.

HuR Regulation in T cells

As introduced in the previous section, HuR has been shown to help regulate many cellular processes including the stress response and immune pathways. The effects of HuR binding vary by mRNA target, most often involving regulation of stability and translation. HuR has been implicated in both inducing and suppressing inflammatory responses.

In T cells, HuR has been shown to regulate CD3 ζ , CD40L, Fas, IFNG, IL-4, IL-13, and TNF (Brennan and Steitz 2001; Izquierdo 2008; Katsanou et al. 2005; Moulton et al. 2008; Myer, Fan, and Steitz 1997; J. G. Wang et al. 2006; Yarovinsky et al. 2006). During lymphocyte activation, HuR promotes the stabilization of cytokine transcripts by binding to AU-rich elements (ARE) in the 3' untranslated region (3'UTR). By interacting both cooperatively and competitively with other RNA-binding proteins, these associations can promote or inhibit translation of cytokines to determine the fate of the transcript (Anderson 2008; Casolaro et al. 2008; X. C. Fan and Steitz 1998b; Myer, Fan, and Steitz 1997). HuR levels have also shown to be up-regulated following T cell activation (Atasoy et al. 1998; Papadaki et al. 2009; Sakai et al. 2003).

Mice deficient in HuR are not viable, while post-natal conditional ablation of HuR causes gastrointestinal inflammation, along with depletion of hematopoietic lineages and death within the first two weeks of life (Ghosh et al. 2009; Katsanou et al. 2009). Animals lacking HuR only in their T cells proceed throughout development. Still, these mice have altered lymphocyte phenotypes. HuR deficient T cells show altered maturation and do not exit the thymus at normal rates due to diminished chemotactic responses to cytokines that have been shown to alter HuR subcellular localization. Upon CD3/CD28 stimulation, T cells lacking HuR showed a reduced proliferative response and a decreased apoptotic response. HuR deficient cells displayed increased levels of Tnf mRNA (Papadaki et al. 2009).

While the role of HuR in regulating cytokines has been pervasive, the majority of the work has been done in cell culture systems that do not necessarily represent physiologic

conditions. Furthermore, much of work studying the association of HuR with targets, including during T cell activation, has been studied without crosslinking, which may lead to the identification of false targets of regulation due to the potential association of RNA-binding proteins with transcripts after cell lysis for immunoprecipitation (Mili and Steitz 2004; Mukherjee et al. 2009). Genome-wide HuR binding sites have been mapped using photoactivatable ribonucleoside crosslinking and immunoprecipitation (PAR-CLIP) approach, but its requirement for incorporating a photo-activatable nucleotide analog into RNA limits its use to *in vitro* systems that may not represent biologically meaningful binding sites or dynamic changes in response to stress (Lebedeva et al. 2011; Mukherjee et al. 2011). Thus, more stringent analysis of genome-wide targets is necessary in biologically relevant samples and in dynamic cellular responses.

Ago Regulation and microRNAs

MicroRNAs are small ~22-nucleotide RNAs that help direct Ago binding to mRNA to regulate target deadenylation, decay and translational status in diverse biologic processes such as proliferation, differentiation, and stress responses. The majority of microRNA genes in mammals are found in regions of the genome that were previously thought to be intergenic, although a number of microRNA are transcribed within the introns of coding genes. MicroRNAs are also found in genomic clusters that suggest joint transcriptional regulation. In all cases, the microRNAs are thought to begin as longer RNA molecules than their characteristic evolutionarily conserved stem loops. Generally, after the initial message known as the primary microRNA is transcribed, the first step in processing is the cleavage of the ~60-70 nucleotide stem loop from the rest of the message, by the

RNase III enzyme Drosha, to form the precursor microRNA. This cleavage event resolves one end of the mature microRNA duplex. The precursor microRNA is then actively exported from the nucleus by Ran-GTP and Exportin-5. The second cleavage is completed by another RNase III endonuclease Dicer at a fixed distance from the Drosha cleavage site. These cleavage products become incorporated into Ago proteins as single-stranded RNA molecules in ribonucleoprotein complexes, known as the RNA-induced silencing complex (RISC) (Ambros 2004; Bartel 2004).

MicroRNAs can mediate post-transcriptional regulation by targeting transcripts for mRNA cleavage and degradation or by modulating translation of their targets. These endpoints are decided by the complementarity of the microRNA sequence to the target and by the interaction of the Ago-microRNA complex with other RNA-binding proteins in response to cellular signaling and multiple stress responses (Bartel 2004; 2009; Leung and Sharp 2007; 2010). Thus, Ago regulation can be dynamically controlled. For example, the localization of Ago to stress granules is microRNA dependent and can be transient, with evidence that Ago can shuttle in and out of a stress granule in less than a minute (Leung, Calabrese, and Sharp 2006). Another example of rapid regulatory control involving microRNAs is in the light adaptation response of the retina where levels of microRNA were shown to change rapidly by decay and increased transcription to impact mRNA control (Krol et al. 2010). These and other regulatory systems, such as in interactions with other RNA-binding proteins, allow for rapid responses to external stimuli to influence the final stages of gene expression within a cell.

Some studies have indicated that microRNAs mediate repression of protein expression predominantly by decreasing target transcript levels (Baek et al. 2008; H. Guo et al. 2010; Hendrickson et al. 2009). Others have reported that translational control precedes corresponding changes in mRNA expression (Bazzini, Lee, and Giraldez 2012; Selbach et al. 2008). The mechanisms mediating Ago-mediated mRNA control are also varied including microRNA dependent deadenylation of transcripts leading to the degradation of target transcripts unrelated to translational control, or the inhibition of protein synthesis before or after the initiation of translation (Mathonnet et al. 2007; Olsen and Ambros 1999; Pillai et al. 2005; L. Wu, Fan, and Belasco 2006). While most studies of microRNA mediated translational control have focused on repression of translation, it has also been reported that Ago binding helps to mediate translational activation of some target mRNAs in certain biologic conditions (Henke et al. 2008; Jopling et al. 2005; Vasudevan and Steitz 2007; Vasudevan, Tong, and Steitz 2007; 2008; Ørom, Nielsen, and Lund 2008). In summary, Ago-microRNA regulation of targets has been linked to repression and enhancement of translation with and without changes in target abundance by influencing many mechanisms of translational control.

Ago Regulation in T cells

Ago regulation and microRNAs have been shown to be critical to the development of a healthy immune system and normal inflammatory responses. The differential abundance of microRNAs in distinct T cell lineages has been examined, but these studies have not considered the activation state of the lymphocytes or the mRNA regulation of Ago in

parallel (Landgraf et al. 2007; Monticelli et al. 2005; Salaun et al. 2011; H. Wu et al. 2007).

The Dicer enzyme is critical for generation of microRNAs by cleaving double stranded precursors. Mice lacking Dicer in the T cell lineage showed greatly impaired T cell differentiation, particularly for the development of CD8 T cells (Cobb 2005; Muljo et al. 2005). Furthermore, CD8 T cells conditionally deficient in Dicer after maturation were shown to have a heightened response to T cell activation. Lymphocytes stimulated *in vitro* showed quicker surface expression of CD69 and this activation marker persisted longer than in wild type T cells after the termination of the TCR stimulus. The T cells also showed quicker initiation of proliferation as seen by progression into the cell cycle. After *in vitro* stimulation of wild type T cells, microRNA-130/301, thought to be regulating CD69 expression, were increased as compared to resting cells (Zhang and Bevan 2010). Conditional deletion of Dicer in response to T cell activation with viral challenge led to a faulty expansion of antigen-specific T cells and poor viral clearance (T. Wu et al. 2012). Deletion of Ago2 in the bone marrow resulted in aberrant generation of B cells and cells of the erythroid lineage (O'Carroll et al. 2007).

T cell Differentiation and Responses Impacted by the Overexpression or Deletion of microRNAs in Mice

Regulatory T cells deficient in mir-146a showed a deficiency in their ability to control IFNG production themselves or in CD4 and CD8 cells due to loss of suppression of STAT1. This selective cytokine deregulation differed from Dicer deficient regulatory T cells that showed decreased suppression of multiple cytokines and general loss of

suppressive capacity (Liston et al. 2008; Lu et al. 2010). Macrophages from mice with a genetic deletion of miR-146a show an exaggerated response with intra-peritoneal lipopolysaccharide challenge, with elevated levels of serum TNF and decreased survival rate. The mice develop spontaneous autoimmunity with age, displaying enlarged spleens and lymph nodes, inflammation in peripheral organs, increased serum levels of IL-6, and expression of activation markers on T cells. This autoimmunity resulted in a decreased survival rate and the appearance of spontaneous tumors in secondary lymphoid organs (Boldin et al. 2011).

Mice lacking miR-155 showed deficiencies in both T and B cells. For example, CD4 T cells showed reduced expression of IFNG upon stimulation (Rodriguez et al. 2007; Thai et al. 2007). Additionally, mir-155 is necessary for the heightened responses of regulatory T cells to IL-2 even though most suppressor functions are maintained in its absence (Lu et al. 2009). Ago CLIP binding maps in WT and miR-155 deficient mouse regulatory CD4 T cells were recently published and help to establish that roughly forty percent of miR-155 binding sites do not display canonical seed matches (Loeb et al. 2012). These studies examine a different subset of T cells than is the focus of the work described here, but suggest a need to understand other mechanisms of transcript targeting for Ago binding aside from seed match pairing in lymphocytes.

Hematopoietic stem cells from the bone marrow were transduced with retrovirus to ectopically express miR-181a. When these cells reconstituted the bone marrow of sub-lethally irradiated hosts, while the percentage of mature B cells nearly doubled, the number of CD8 T cells was reduced more than ten-fold. Only small alterations were

observed in the CD4 T cell and myeloid compartments (Chen et al. 2004). miR-181a is highly expressed early in T cell development and decreases with maturation. CD4 T cells overexpressing miR-181a showed increased intracellular calcium fluctuations and IL-2 production with antigen stimulation, and required less peptide present on APCs to reach their maximal response, demonstrating that they were more sensitive to TCR stimulation. The opposite effect was seen in T cells with reduced miR-181a expression. These responses were shown to be mediated in part by the regulation of CD28 expression, but also by downstream components of the TCR signaling pathway (Li et al. 2007). Liu et al. utilized the increase in the development of double positive cells with overexpression of miR-181a-1 *in vitro* as a screen for functional microRNA activity. Sequential mutagenesis of the miR-181 stem loop demonstrated that while sequences in the mature microRNA were important for T cell development, the regulation of distinct miR-181 family members was dictated by their pre-microRNA loop sequences (G. Liu et al. 2008). Although the absolute expression levels of miR-181 are lower in double positive cells than other stages of development, it represents a larger percentage of the microRNA pool in these cells and this mediates the regulatory control of targets such as CD69 to regulate T cell development (Neilson et al. 2007).

Many studies have focused on the role of the miR-17-92 cluster in B cells due to its overexpression in human B cell lymphomas. This is due to transcriptional up-regulation of the cluster by c-MYC. The oncogenic capacity of these microRNAs is greatly due to the targeting effects of miR-19a and miR-19b (Mu et al. 2009). Mice deficient in the miR-17-92 cluster die shortly after birth. Wild type mice reconstituted with miR-17-92 deficient bone marrow showed drastic reductions in total lymphocyte counts due to

impaired B cell development, while the T cell compartment appeared grossly unaffected (Ventura et al. 2008). miR-17-92 is highly expressed during lymphocyte development and is decreased in mature cell populations including CD4 and CD8 single positive cells. Overexpression of miR-17-92 in lymphocytes led to lymphoproliferative disease, autoimmunity, and death. Interestingly, CD4 T cells overexpressing miR-17-92 proliferated with CD3 stimulation at similar levels to control CD4 T cells stimulated with both CD3 and CD28 indicating that the aberrant microRNA expression may have functionally mimicked CD28 co-stimulation (Xiao et al. 2008). miR-17-92 expression is temporally regulated with T cell activation and is needed for expansion of CD8 T cells after antigen encounter (T. Wu et al. 2012). By examining mice with T cells deficient for the miR-17-92 cluster, these microRNAs were shown to promote Th1 responses and suppression of tumor growth in melanoma challenged mice. Furthermore, miR-19b was demonstrated to rescue the production of IFNG in CD3/CD28 stimulated deficient cells with retroviral transduction of that microRNA (Jiang et al. 2011).

The Combinatorial Control of Ago and HuR

As reviewed above, HuR and Ago both positively and negatively regulate gene expression by transcriptional and translational control and are both critical to the regulation of healthy immune responses. We have previously demonstrated the ability to use high-throughput sequencing crosslinking immunoprecipitation (HITS-CLIP) to establish a precise and genome-wide map of Ago-microRNA-mRNA ternary interactions. Interestingly, this map showed that Ago binds to mRNA targets at very specific sites, on average only 2.6 regions per Ago regulated transcript. This specificity is hard to explain

solely by the reliance of a microRNA-mRNA interaction determined by a microRNA seed sequence of as few as six nucleotides of complementarity. Furthermore, Ago-mRNA binding sites did not appear to have a general sequence preference, suggesting that additional RNA-binding proteins may be required to determine mRNA accessibility to Ago (Chi et al. 2009). Many Ago binding sites have also been identified without exactly matching canonical microRNA seed sequences. While some of these regulatory sites represent microRNA mediated targeting through non-classical seed pairings, some cannot be explained by microRNA direction alone (Chi et al. 2009; Chi, Hannon, and Darnell 2012; Leung et al. 2011; Loeb et al. 2012).

3'UTRs are abundant in both microRNA binding sites and ARE. This creates a concentrated region for the possible combinatorial control of target mRNAs by Ago and other RNA-binding proteins. Ago and microRNA are important in the regulation of AU-rich elements (ARE) through their interactions with other RNA-binding proteins such as HuR (Meisner and Filipowicz 2010). Accordingly, a recent systematic analysis indicated that the efficacy of miRNA mediated silencing was attenuated by the presence of AREs near predicted miRNA target sites, suggesting that ARE-binding proteins may globally influence recruitment of Ago-miRNA complexes (Jacobsen et al. 2010). Much work studying the interactions of Ago and HuR have focused on specific target transcripts. While these may be informative for the specific examples, the differences in the outcome of their combinatorial control indicate the need for more systematic study of their co-regulation.

For example, CAT-1 protein levels increase in response to stress without a corresponding change in transcription. In normal cellular conditions, miR-122 mediates the subcellular localization of the CAT-1 mRNA to P-bodies. Upon activation of a stress response, HuR was demonstrated to bind to the 3'UTR of CAT-1 via ARE and reverse its microRNA-mediated repression. Binding by HuR led to the exit of CAT-1 from P-bodies and its association with active polysomes, resulting in an increase in CAT-1 translation. The mechanism mediating the interaction between Ago and HuR on the CAT-1 mRNA is unknown, but because the target sequence sites for each protein are not directly adjacent, the authors speculate that the proximity of their interaction may be enhanced by the RNA secondary structure, possibly bringing the sites closer together than indicated by their sequence, or by HuR oligomerization along the 3'UTR to disrupt Ago-miR-122 binding (Bhattacharyya, Habermacher, Martine, Closs, and Filipowicz 2006a; 2006b).

Conversely, HuR was shown to be necessary for the microRNA let-7 mediated repression of c-Myc. HuR associated with c-Myc in RNA-immunoprecipitation experiments. By diminishing levels of HuR in HeLa cells by siRNA or overexpressing recombinant HuR protein, HuR was observed to negatively correlate with c-Myc mRNA and protein levels suggesting repression of c-Myc by HuR. Using synthesized biotinylated mRNA fragments and chimeric GFP-reporter constructs, specific regions of the 3'UTR were identified as mediating the interaction between HuR and c-Myc. Let-7 was predicted to bind a region adjacent to the proposed HuR binding site. Decreasing functional let-7 with antagomiRs, or increasing its levels by transfection of synthesized precursor duplex RNA, increased or decreased c-Myc expression respectively. HuR was shown to be necessary for Ago2-let-7 binding to the c-Myc 3'UTR and the co-immunoprecipitation of

HuR with Ago was RNA dependent, although this immunoprecipitation did not utilize crosslinking and the interaction could have been formed after cell lysis (Kim et al. 2009). It is possible that the opposite affects of Ago and HuR interaction for this transcript are due to differences in the proximity of the binding sites for each protein, cell lines, cellular states, or that the interactions are more complex than only the involvement of these two regulators.

Although myeloid cell proliferation, survival, and differentiation were maintain in mice deficient in HuR in the myeloid compartment, steady state mRNA and microRNA levels were disrupted in these cells. The angiogenic pathway was implicated as being regulated by HuR expression and the strength of ARE in the 3'UTR correlated with the down regulation of these potential targets. In searching for regulated mRNA with ARE adjacent to putative microRNA binding sites, the Vegf-a mRNA was recognized as having reduced levels of both transcript and protein in the knock out cells, containing a previously identified binding site of HuR from PAR-CLIP, and a bioinformatics predicted ARE-adjacent site for miR-200b which was increased in the HuR deficient macrophages. Vegf-a mRNA was shown to immunoprecipitate with both Ago and HuR. In reporter systems, the intact miR-200b site was necessary to mediate reduction of luciferase expression with miR-200b transfection and concurrent HuR knockdown further mediated this repression. An antagomiR blocking miR-200b only de-repressed Vegf-a reporters if HuR was present and more Vegf-a mRNA was shown to associate with Ago2 in the absence of HuR. In a mouse tumor challenge, although wild type and myeloid HuR knock out mice had similar myeloid invasion of the tumor microenvironment, the tumors displayed defects in their vasculature and angiogenesis, and tumor growth was

attenuated due to tumor cell apoptosis. Morpholino knock down of *elavl1* zebrafish or miR-200b mimic injection resulted in severe vascular development in the subintestinal vein (SIV), while *elavl1* mRNA rescued the defects from miR-200b overexpression. Interestingly, using a suboptimal dose of either intervention resulted in fairly normal vasculature, but when both were applied simultaneously, the majority of zebrafish had defective SIV, supporting the antagonistic role of Ago and HuR in regulating *vegfaa* that had been demonstrated *in vitro* (Chang et al. 2012).

Utilizing *in vitro* systems and reporter constructs, Ago-miR-19 demonstrated repression of RhoB in an HuR dependent manner. This repression was relieved during UV-irradiation of keratinocytes leading to the apoptosis of these stressed cells (Glorian et al. 2011). In other cell culture studies using reporter constructs and recombinant protein expression, HuR binding sites were shown to be necessary to mitigate Ago-let-7 mediated cleavage of IL-1B mRNA. The transfection of oligonucleotides specific for the intervening sequences between the microRNA and HuR binding sites blocked Ago repression of this transcript suggesting that oligomerization of HuR may be necessary for its interaction in suppressing Ago cleavage (Kundu et al. 2012).

Previous Studies Using CLIP to Explore Co-Regulation of Ago and HuR Targets

Recent studies using Ago and HuR CLIP experiments have investigated the potential co-regulation of mRNA by these RNA-binding proteins on a genome-wide scale. HuR binding sites were recently identified in unstressed HeLa cells using PAR-CLIP. The largest group of target sites was found in the 3'UTRs of transcripts, but around a third of binding sites were in intronic regions of the message. These target sequences were

highly evolutionarily conserved. In comparing HuR binding sites with Ago regulation identified by PAR-CLIP in HEK293 cells, a preference for binding in areas of Ago targeting was not observed. With knockdown of HuR in the HeLa cells, miR-7 was shown to have increased expression levels that inversely correlated with the levels of HuR. HuR binding sites in the intron and surrounding exons containing the microRNA sequence were proposed to influence the levels of this microRNA, although no direct mechanism was explored (Lebedeva et al. 2011).

HuR PAR-CLIP was also done in HEK293 cells with epitope-tagged protein. Reproducible binding sites, determined by the crosslinking index of each sequenced tag, were found predominantly in the introns and 3'UTRs of target mRNAs, suggesting that pre-mRNA processing may be related to target stability. The authors suggest that the PAR-CLIP data reflects both stable and transient HuR-mRNA interactions and that targets identified by immunoprecipitation without crosslinking may reflect more stable binding events as evidenced by HuR knockdown leading to a more profound affect on identified targets' mRNA stability in targets identified in the RIP-chip method. In comparing data from Ago PAR-CLIP from the same cell line with HuR PAR-CLIP binding sites, significant overlapping patterns of regulation were observed for the two proteins, suggesting the potential for competition of these proteins for effective binding to targets and subsequent regulation. Still, the mRNA level changes seen with HuR knockdown could be explained with or without the presence of overlapping or adjacent microRNA binding sites. The authors suggest that this indicates a model of HuR using physical competition for access to binding sites to mitigate microRNA-mediated repression (Mukherjee et al. 2011).

Accordingly, previous CLIP experiments comparing Ago and HuR regulation have been completed in steady state cell culture systems and may not represent their binding patterns in biologic systems or in dynamic cellular state changes. While PAR-CLIP has been demonstrated to produce reliable binding site information for Ago and HuR proteins in addition to the HITS-CLIP methods, the necessity for incorporating a photo-activatable nucleotide analog into cells for PAR-CLIP analysis limits its utility in the study of biologic systems (Kishore et al. 2011). In only one of the two described studies, Ago and HuR binding maps were compared from the same type of cell line, nevertheless, they were not the same biologic samples and in one case used an epitope tagged version of HuR for immunoprecipitation in the HEK293 cells, which would not have been present in the previous Ago studies to which they compare their results (Mukherjee et al. 2011). Therefore, studying the dynamic regulation of Ago and HuR within a biologically meaningful context is critical to the understanding of these important RNA regulators.

Perspectives

The adaptive immune response has been studied in great mechanistic detail and many of the molecular processes involved T cell activation have been resolved. However, the regulatory mechanisms mediating these complex systems in the context of rapid cellular stress responses and disease are still not largely understood. Lymphocytes are required to respond quickly to rapid changes they confront within their host. When a T cell encounters its cognate antigen, cytokine production must be carefully regulated to instigate immediate induction of the inflammatory response, but also be transient to ensure the protection of surrounding tissue. Therefore, although nascent transcription is

large component of this response, it is logical that much of protein expression be controlled at a post-transcriptional level. The Ago and HuR RNA-binding proteins have been shown to be critical for normal lymphocyte development and the regulation of their phenotypes. While their mRNA targets and binding sites has been vastly explored in the literature, analysis of their regulation in biologic settings is limited. For these reasons, we have undertaken to study the role of Ago and HuR regulation during CD8 T cell activation by CD3 and CD28 stimulation in normal human donor CD8 lymphocytes. We accomplished this by overlaying genome-wide HITS-CLIP binding maps, for Ago and HuR, with translational profiles of the cells as they relate to transcriptional abundance. Using these dynamic regulatory maps, we gain insight into the mechanisms governing T cell stimulation.

CHAPTER 2. Experimental Procedures

Peripheral Blood Isolation

Blood cells were collected by peripheral blood draw or leukapheresis under a Rockefeller University IRB-approved protocol with informed consent. PBMC were isolated by density gradient centrifugation over Ficoll-Hypaque (Pharmacia).

Cell Culture

Cells were maintained at 37°C in 5% CO₂. Human T cells were maintained T cell Media (AIM V Medium (Invitrogen) supplemented with 1% pooled human sera). Mouse T cells and other non-adherent cells were maintained in R10 medium (RPMI 1640 medium (Mediatech) supplemented with 10% FBS (Hyclone), 2mM Glutamax (Gibco), sodium pyruvate, non-essential amino acids, 15 mM Hepes buffer, 50 µM β-mercaptoethanol, and gentimycin). Ascites cells were maintained in Growth Medium (equal volumes MCDB105 medium (Sigma) and M199 medium (Invitrogen) supplemented with 10% FBS, and penicillin-streptomycin). All adherent cell lines mentioned were maintained in D10 medium (DMEM high glucose (Mediatech) containing all of the same supplements as R10).

Negative Selection of CD8 T cells

Human PBMC were incubated with a cocktail of biotin-conjugated antibodies specific for markers on non-CD8 T cells from a CD8+ T cell Isolation Kit and then bound by anti-biotin magnetic beads supplemented with anti-CD19, anti-CD56, anti-CD4 and anti-

CD14 MACS beads (Miltenyi Biotech). Cells were washed and run through two magnetic columns collecting the flow through to isolate cells not bound by antibody.

Positive Selection of CD8 T cells

Human PBMC were incubated with anti-CD56 MACS beads (Miltenyi). These cells were washed and then were depleted by running the cells through two successive magnetic columns collecting the flow through to isolate cells not bound by CD56 antibody. The cells were then incubated with anti-CD8 MACS beads (Miltenyi), were washed, and loaded onto a magnetic column to isolate antibody bound cells. After washing the column, the positive cells were eluted by plunging the column. This selection process was repeated on a second column to ensure cell purity. Mouse positive selection uses the same protocol without the CD56 depletion. To rest human T cells, cells were resuspended at $2 \times 10^6/\text{ml}$ and 5-10 ml was put in a 50 ml conical tube (Denville Scientific) with loose caps at 37°C overnight. After the resting period, cells were harvested and filtered through a $70\ \mu\text{m}$ cell strainer to remove dead cells and any debris and the cells were collected by centrifugation.

CD3/CD28 Stimulation

T cells were plated at $\sim 18 \times 10^6/\text{ml}$ in R10 medium with $25\ \mu\text{l}/10^6$ T cells washed CD3/CD28 mouse or human T-Activator Dynabeads (Invitrogen). Cultures were agitated every 12 minutes to aid in the dispersal of stimulatory beads to each T cell. After one hour, cells were harvested and processed for future analysis.

Flow Cytometry Surface Staining

All surface antibodies were purchased from BD Biosciences. Cell surface expression of markers were measured using fluorescently-conjugated antibodies according to the manufacturer's instructions. Cells were resuspended in 100 μ l FACS buffer: PBS supplemented with 1% PHS, 1% FBS (HyClone), and for mouse cells 5% goat serum. Mouse cells were then Fc blocked for 10 minutes using 1 μ g of anti-CD16/CD32 (Fc γ RII/III). For both human and mouse cells, 1 μ g of each antibody was added directly to the cells. Human cells were incubated for 10 minutes at room temperature in the dark and mouse cells were incubated for 15 minutes at 4°C. Cells were washed twice with FACS buffer and collected immediately on a BD FACScaliber machine and analyzed using Flowjo software (Treestar).

Reverse Transcription and Quantitative PCR Analysis

Total RNA was extracted from CD8 T cells using an RNeasy Mini Kit with on-column DNase treatment (Qiagen) and eluted in 20 μ l of RT-grade H₂O. RNA was then reverse transcribed using the iScript cDNA Synthesis Kit (BioRad) as per manufacturer's instructions. cDNA was amplified by qPCR using iTaq SYBR Green Supermix with ROX (Biorad) on an iQ5 Multicolor Real-Time PCR Detection System (Biorad) using a 58°C annealing temperature and both melt curves and -RT controls were performed.

Primers

Human IFNG

Forward: TCAGCTCTGCATCGTTTTGGGTTC

Reverse: TCCGCTACATCTGAATGACCTGCAT

Human TNF

Forward: CTGCCTGCTGCACTTTGGAGTGAT

Reverse: TGGGCCAGAGGGCTGATTAGAG

Mouse Ifng

Forward: CAGCAACAGCAAGGCGAAAAAGG

Reverse: TTTCCGCTTCCTGAGGCTGGAT

Mouse Gapdh

Forward: TGAACGGGAAGCTCACTGGCAT

Reverse: TCAGATGCCTGCTTCACCACCT

Western Blot

T cells were lysed in PXL by three cycles of freezing and thawing. DNA was removed from lysate by DNase treatment at 37°C for 5 minutes. Samples were spun at 14,000rpm for 10 minutes at 4°C and the supernatant was harvested to a new tube. NuPAGE loading sample buffer and reducing agent (Invitrogen) were added to 1x concentrations in the lysate and samples were heated for 15 minutes at 70°C. Lysate was run on a 8% (Ago) or 10% (HuR) NuPAGE Bis-Tris gel (Invitrogen) in MOPS Buffer and transferred to Protran BA85 nitrocellulose (Whatman) or Immobilon-FL PVDF (Millipore) by standard methods. For nitrocellulose membranes, membranes were blocked for 1hr at room

temperature in 5% non-fat dry milk (Carnation) in PBS followed by addition of primary antibody for 1 hour at room temperature or overnight at 4°C. Blots were washed 3x10 minutes with Western blot wash buffer (23mM Tris, pH 8.0, 190mM NaCl, 0.1% w/v BSA, 1 mM EDTA, 0.5% Triton X-100, 0.02% SDS) after each antibody incubation. HRP-conjugated secondary antibodies (Jackson Immunochemicals) were used at 1:10,000 dilution in 5% milk/PBS for 1 hr at RT, washed as before, and HRP signal was detected by Enhanced ChemiLuminescence (Western Lightning detection kit, Perkin Elmer) and detected on film (Kodak MR). For Immobilon-FL membranes, membranes were blocked for 1 hour at room temperature in Odyssey Blocking Buffer (LI-COR) followed by the addition of primary antibody in LI-COR Antibody Buffer (50 mM Tris-HCl, pH 7.5, 150 mM NaCl, 0.1% Tween-20, 2% BSA and 0.02% Sodium Azide), for 1 hour at room temperature or overnight at 4°C. Blots were washed 4x5 minutes in TBST after each antibody incubation. Fluorescently-conjugated secondary antibody (Goat anti-mouse IgG IRDye, 827-08364, LI-COR) was used at 1:30,000 Dilution in LI-COR Antibody Buffer for 45 minutes rocking at room temperature shielded from light by foil. The blots were washed 3 times as before and then once with TBS without tween. Fluorescent signal was detected on the Odyssey LI-COR machine.

Ago and HuR HITS-CLIP

Bead Preparations for Immunoprecipitation

Protein A beads were vortexed and an aliquot was washed 3x in PBS with 0.02% Tween-20. Beads were pre-coated with rabbit anti-mouse IgG (Jackson ImmunoResearch, 315-005-008 at 2.3 mg/ml) as a bridging antibody (1 µl antibody per 2 µl beads for HuR or 1

μl antibody per 8 μl beads for Ago) for 35 minutes rotating at room temperature. Beads were washed 3x in PBS with 0.02% Tween-20. HuR or Ago antibody was then loaded to the beads. For HuR 1.7 μg/μl beads of 19F12 or 3A2 was added (Santa Cruz, (Gallouzi et al. 2000; Wang et al. 2000)). For Ago, 3 μl of 2A8 ascites (provided by Dr. Zissimos Mourelatos (Nelson et al. 2007)) is added per 400 μl beads. For irrelevant antibody controls, equivalent amounts of 7G1-1 antibody was added (Memorial Sloan-Kettering Cancer Center Monoclonal Antibody Core Facility, (Brown et al. 2001)). For Ago CLIP with Protein G beads, beads are washed in the same way, but no bridging antibody is needed and 3 μl 2A8 is added per 200 μl beads. Beads were rotated for 2 hours at 4°C to bind antibody. Generally, for HuR CLIP, we used roughly 20 μl of beads per 10 million CD8 T cells, and for Ago CLIP, 40 μl beads per 10 million CD8 T cells. After incubation with the antibodies for immunoprecipitation, the beads were washed once in PBS with 0.02% Tween-20 and three times in lysis buffer containing complete protease inhibitor mini EDTA free tablets (1 tablet/10 ml buffer) (Roche).

T cell Lysate Preparation

T cells were UV crosslinked as indicated on a bed of ice three times at 200 mJ/cm² (254 nm UV light) in a minimal volume of PBS with swirling between each irradiation, using a Stratalinker 2400 (Stratagene). Lymphocyte lysate was prepared by adding a volume of 1 ml PXL lysis buffer (1X PBS [tissue culture grade; no Mg²⁺, no Ca²⁺, GIBCO], 0.1% SDS, 0.5% Na-DOC, 0.5% NP-40) with complete protease inhibitor and the buffer was pipet multiple times to mix and resuspend cells in the buffer. T cells were rested on ice for ten minutes with vortexing 15 seconds every 2 minutes to ensure complete lysis. The

lysate was then DNase treated with RQ1 RNase-free DNase (Promega) for 5 minutes shaking in the Thermomixer R at 37°C. 5 µl of a 1:100 (high) or 1:10,1000 (low) RNase A solution was added to each sample as indicated and the lysate was incubated in the Thermomixer R for 5 minutes shaking at 37°C. The lysate was spun at 14,000 rpm for 30 minutes at 4°C to clear the lysate and the supernatant was harvested to a new tube for immunoprecipitation.

Samples were then rotated with primary antibody-loaded beads at 4°C for 2 hours. Following IP beads were washed sequentially (1 ml washes) twice with 1X PXL lysis buffer, twice with 5X PXL (5X PBS [tissue culture grade; no Mg²⁺, no Ca²⁺, GIBCO], 0.1% SDS, 0.5% Na-DOC, 0.5% NP-40), twice with high stringency buffer (15 mM Tris-HCl, pH 7.5, 5 mM EDTA, 2.5 mM EGTA, 1% Triton X-100, 1% Na-deoxycholate (DOC), 0.1% SDS, 120 mM NaCl, 25 mM KCl), high salt buffer (15 mM Tris-HCl, pH 7.5, 5 mM EDTA, 2.5 mM EGTA, 1% Triton X-100, 1% Na-DOC, 0.1% SDS, 1 M NaCl) and twice with low salt buffer (15 mM Tris-HCl, pH 7.5, 5 mM EDTA) followed by two washes with NT-2 buffer (50 mM Tris-HCl pH 7.4, 150 mM NaCl, 1 mM MgCl₂, and 0.05% NP-40) and two washes with PNK buffer (50mM Tris-HCl, pH 7.5, 10 mM MgCl₂, 0.5% NP-40). After each capture on the magnet beads, the beads were resuspended by end-over-end rotation. Throughout the washes tubes were treated in a random order to diminish the chance of artifacts. Throughout the CLIP protocol 1.5 ml SlickSeal microfuge tubes (National Diagnostics) were used to reduce non-crosslinked RNA binding to tubes.

Dephosphorylation of RNA, 3' Linker Ligation, and Rephosphorylation of 5' end of RNA Tags

Immunoprecipitations were treated with calf intestinal phosphatase to remove the 5' phosphate from RNA crosslinked to Ago and HuR (RNA tags) so that the RNA could not circularize during ligation, an otherwise predominant competing intramolecular reaction. Beads were resuspended in 60 μ l of 1X dephosphorylation buffer and 3 units of CIAP (Roche) with RNasin Plus RNase Inhibitor (Promega) and incubated in the Thermomixer R at 37°C for 20 min, programmed to shake at 1000rpm for 15 s every 2 min. This was followed 1 ml washes, once with PNK Buffer, twice with PNK buffer with EGTA (10mM Tris pH 7.5, 20mM EGTA, 0.5% NP-40) and twice again with with PNK buffer (no EGTA).

For Ago CLIP, to ligate a 32 P-labeled RNA linker to the 3' end of the RNA, the puromycin- blocked linker (L32, 5'-OH-GUGUCAGUCACUUCCAGCGG-3'-puromycin, Dharmacon) was first labeled using T4 phosphonucleotide kinase (PNK, New England Biolabs, NEB). 50 pmol of L32 RNA, 15 μ l 32 P- γ -ATP, 1 μ l RNasin and 2 μ l of T4 PNK in 1X PNK buffer were incubated at 37°C for 30 min, an additional 0.02 ml 1 mM ATP to drive the reaction to complete and was incubated 5 min. Radiolabeled linker was spun through a G-25 column (Amersham) to remove free ATP. 30 pmol of the labeled 3'RNA linker was added to a 60 μ l T4 RNA ligase reaction (Fermentas), according to kit instructions, and on-bead ligation reactions were incubated at 16°C for 1 hr in a thermomixer programmed to shake at 1000rpm for 15 sec every 4 min. After 1 hr, 80 pmol of cold L32 RNA linker with 5' phosphate was added to each tube and incubated

overnight. For HuR CLIP, only the cold L32 RNA linker with 5' phosphate was used for ligation overnight.

Following linker ligation, the beads were washed three times with PNK buffer. To rephosphorylate the 5' end of the RNA for 5' linker ligation, 80 ul of T4 PNK mix (6 ul of 1 mM ATP, 4 ul T4 PNK enzyme [NEB], 1 ul RNasin in 1X T4 PNK buffer [NEB], total volume 80ul) was added to each tube and incubated at 37°C in the Thermomixer R for 20 min at 1000 rpm shaking for 15 sec every 4 min. For HuR CLIP, this step was done in the presence of ^{32}P - γ -ATP for 20 minutes and then 1 mM cold ATP was added to drive the reaction to completion for 5 additional minutes at 37°C. Beads were washed three times with 1 ml PNK buffer.

SDS-PAGE Separation of RNA-binding Protein:RNA Complexes

After last PNK buffer wash, each tube of beads was resuspended in 30 ul NuPAGE loading buffer (LDS, Invitrogen) brought to 1x concentration with PNK buffer and containing reducing agent for Ago CLIP. The beads were incubated in the Thermomixer R at 70°C for 10min shaking at 1000 rpm. Supernatants were taken off the beads and run on Novex NuPAGE 10% Bis-Tris gels for HuR and 8% for Ago (Invitrogen) in MOPS running buffer (Invitrogen) for 2 hr at 175V and transferred to Protran BA85 nitrocellulose (Whatman) using a Novex wet transfer apparatus (Invitrogen). After transfer, the nitrocellulose was quickly rinsed with RNase-free PBS, blotted with Kimwipes, wrapped in plastic wrap and exposed to Biomax MR film (Kodak).

Recovery of Complexes, Protease Digestion, and 5' Linker Ligation

Nitrocellulose membranes were aligned carefully with the exposed film and filter excised from the low RNase immunoprecipitation lanes at a size directly above the overdigested band as indicated in Figure 4.3 and Figure 5.2 with a scalpel. Each band of nitrocellulose membrane was further cut into smaller pieces and proteinase K treated (0.2 ml of a 1:5 dilution of proteinase K (4 mg/ml, Roche) in PK buffer (100 mM Tris-Cl pH 7.5, 50 mM NaCl, 10 mM EDTA)) in the Thermomixer R at 37°C, shaking at 1100 rpm for 20 minutes. Then 0.2 ml of PK buffer with 7M urea solution was added and incubated for another 20 minutes at 37°C shaking at 1100 rpm. Finally, 0.4 ml of RNA phenol (pH 6.8, Applied Biosystems/Ambion) and 0.13 ml of 49:1 CHCl₃:isoamyl alcohol were added and incubated at 37°C, shaking at 1100 rpm for additional 20 min. Tubes were spun at 20,000g in a desktop microcentrifuge at room temperature. Glycogen (0.8 ul, Applied Biosystems/Ambion), 50 ul 3M NaOAc pH 5.2, and 1 ml of 1:1 ethanol:isopropanol were added to the aqueous phase in a fresh tube and RNA was precipitated overnight at -20°C.

RNA was pelleted, washed twice with 75% ethanol. The pellet dried and dissolved in 6 ul RNase-free H₂O. RNA ligation to add the 5' linker (RL5D: 5'-OH-AGGGAGGACGAUGCGGr(N)r(N)r(N)r(N)G3'-OH) was performed with 1 µl 10X T4 RNA ligase buffer (Fermentas), 1 µl BSA (0.2 µg/µl), 1 µl ATP (10mM), 0.1 µl T4 RNA ligase (3U, Fermentas), and 20 pmol of RL5D RNA linker in a total volume of 10 µl in the Thermomixer R at 16°C for 5 hrs. To the ligation reaction, 79 µl H₂O, 11 µl 10X RQ1 DNase buffer, 5 µl RQ1 DNase (Promega) and 5 ul RNasin (Promega) were added and incubated at 37°C for 20 min. 300 µl H₂O, 300 µl RNA phenol (Ambion) and 100 µl

CHCl₃ were added, vortexed, spun and the aqueous layer taken. RNA was precipitated with 50 µl 3M NaOAc pH 5.2, 0.5 µl glycogen (Ambion) and 1 ml 1:1 ethanol:isopropanol overnight at -20°C.

RT-PCR and High-Throughput Sequencing of PCR Products

RNA was pelleted, washed, dried as before, and resuspended in 10 µl of RNase-free H₂O. 2 µl of resuspended RNA was used as a –RT control and was brought to the same volume. The RNA was mixed with 2 µl of primer P32 (3' DNA primer 32, 5'-CTTCACTCACCTCGCAACCG-3', Operon) at 5 pmol/µl, and 3 µl 3mM dNTPs, and incubated at 65°C for 5 min in the Thermomixer R, chilled, and spun briefly. 1 µl 0.1M DTT, 4 µl 5X SuperScript RT buffer, 1 µl RNasin, and 1 µl SuperScript III (Invitrogen) were added and incubated at 50°C for 45 minutes, 55°C for 15 minutes, 90°C for 5 minutes and then moved onto ice. PCR reactions were performed immediately with 27 µl Accuprime Pfx Supermix (Invitrogen), 0.75 µl P51 (5' DNA primer 51, 5'-AGGGAGGACGATGCGG-3', Operon) at 20 pmol/µl, 0.75 µl P32 primer, 20 pmol/ul and 2 µl of the RT reaction, incubated at 95°C for 2 minutes and then cycled for 20-35 cycles using a program of 95°C for 20 seconds, 58°C for 30 seconds, and 68°C for 30 seconds. A 10% denaturing polyacrylamide was poured and the entire PCR reaction was loaded along with 3 µl of Amplisize Molecular Ruler (Biorad). To visualize DNA, the gel was immersed in a 1:10,000-fold dilution of SYBR Gold (Molecular Probes) in TBE for 10 minutes. Routinely, aliquots of the reaction were removed at various cycle numbers and product excised from the lowest cycle number giving visible product.

Remaining RT reaction was then brought up to this minimal cycle number, gel purified and the products were pooled with the smaller reactions. Acrylamide bands containing DNA of 60-100nts were excised and DNA purified by crushing in diffusion buffer (0.5M ammonium acetate, 10mM Mg acetate, 1mM EDTA, 0.1% SDS), incubating at 50°C for 30 min at 1200 rpm, and filtering through Whatman GF/D filters in Nanosep columns (VWR). DNA was recovered from filtrate using Qiaquick gel purification buffers and columns (Qiagen) and eluted in 30 µl TE. An additional PCR reaction was performed using the following fusion primers to permit sequencing on the Illumina platform.

SP5fusion:

5'AATGATACGGCGACCACCGACTATGGATACTTAGTCAGGGAGGACGATGC
GG3'

SP3fusion:

5'CAAGCAGAAGACGGCATAACGACCGCTGGAAGTGACTGACAC3'

PCR amplification was performed using Accuprime Pfx (Invitrogen) and ranged between 6 and 12 cycles. The product was then run on a 2% NuSieve agarose gel and purified using Qiaquick spin columns (Qiagen). A total of 10-30 µl of DNA (quantified using the Quant-IT kit (Invitrogen)) at 10 nM was submitted for sequencing. The sequencing of CLIP tags was performed using the sequencing primer SSP1 on an Illumina HiSeq.

SSP1:

5'CTATGGATACTTAGTCAGGGAGGACGATGCGG3'

Data analysis was done using the Galaxy platform (Hillman-Jackson et al. 2012) and using R Statistical Analysis Software (<http://www.R-project.org>).

Preparation of samples for RNA Sequencing analysis

RNA was prepared from CD8 T cells using the High Pure RNA extraction kit (Roche) as per manufacturer's instructions and the standard Illumina TruSeq protocol was followed to prepare samples for high-throughput sequencing.

Ribosomal Profiling and mRNA Sequencing

T cell Lysate Preparation and Sucrose Gradients

CD8 T cells were treated for 8 minutes with 100 µg/ml cycloheximide at 37°C. Treated cells were harvested and collected by centrifugation. Lysates were prepared in Lysis Buffer (10 mM Tris-HCl, pH 7.4, 5 mM MgCl₂, 100 mM KCl), which was supplemented freshly before lysis with 1% Triton X-100, 2 mM DTT, 100 µg/ml cycloheximide, 500 U/ml RNasin Plus (Promega), and complete protease inhibitor mini EDTA free tablets (1 tablet/10 ml buffer) (Roche). The lysate in a volume of 600 µl was homogenized gently four times with a 26-gauge needle at 4°C. The lysate was then clarified by centrifugation at 14,000 rpm for 10 minutes on a desktop microcentrifuge at 4°C. The supernatant was collected and 6 µl 10 mM CaCl₂ was added to a final concentration of 1 mM. 1000 U/ml micrococcal nuclease was added to T cell lysate and was incubated rotating at room temperature for 25 minutes. 9.6 µl 0.5 M EGTA was added and the lysate volume was adjusted to 1.1 ml with lysis buffer for layering on sucrose.

Equal volumes of supernatants were loaded onto a 10%–50% w/v linear density gradient of sucrose in Lysis Buffer without the added supplements and prepared using a Gradient Master 107 (BioComp), in 14x3x89 mm polyallomer ultracentrifuge tubes (Beckman 331372). Gradients were centrifuged at 35,000 rpm for 3 hours at 4°C in a Beckman SW41 rotor and sixteen fractions of 0.72 ml volume were collected with continuous monitoring at 254 nm using an ISCO UA-6 UV detector.

Isolation of Ribosomal Protected Fragment RNA

The pooled material from sucrose fractions 6-8 was spun through Ultra-4 centrifugal filters with Ultracel-100 membranes (Amicon) at 1900g for 30 minutes at 4°C. 1.2 ml ice-cold Release Buffer (20 mM HEPES-KOH, 100 mM KCl, 1 mM EDTA, 2 mM DTT, 20 U/ml SUPERaseIn (Ambion)) was added to the membrane and incubated on ice for 10 minutes. The filters were then spun again at 1900g for 15 minutes at 4°C with a new 15 ml collection tube. The filtrate was supplemented with SDS to 1% and treated with proteinase K (200 µg/ml) for 30 minutes at 42°C. The RNA was extracted by acid phenol:chloroform (pH 4.5, Ambion) with 360 µl Phenol, 120 µl 49:1 CHCl₃:isoamyl alcohol. The samples were vortexed and the aqueous layer was separated by spinning at 14,000 rpm in a desktop microcentrifuge for 10 minutes at room temperature. The aqueous layer (~400 µl) was supplemented with 40 µl 3M NaOAc pH 5.5, 1 µl Glycogen, and 1 ml 100% EtOH. The solution was inverted and left at -20°C overnight for the RNA to precipitate.

Isolation of Poly-A RNA and Partial Alkaline Hydrolysis

Matching aliquots of CD8 T cells also treated with cycloheximide as described above were resuspended in 1 ml Trizol and the RNA was chloroform extracted with 200 μ l 49:1 CHCl₃:isoamyl alcohol. The solution was mixed and incubated for 3 minutes at room temperature followed by centrifugation at 14,000 rpm in a desktop microcentrifuge for 15 minutes at room temperature. The aqueous layer was transferred to a new tube and supplemented with 1 μ l Glycogen and 500 μ l Isopropanol. The RNA was precipitated at -20°C for 2 hours. The RNA was pelleted by centrifugation at 14,000 rpm in a desktop microcentrifuge for 20 minutes at 4°C. RNA pellets were washed twice with 80% EtOH and then air dried for 10 minutes on the bench top. RNA was resuspended in 30 μ l H₂O and heated at 65°C for 2 minutes and placed on ice. The Dynabeads mRNA Purification Kit (Invitrogen) was used to select for poly-A RNA as per manufacturers instructions using (145 μ l Oligo (dT)₂₅ beads per RNA sample from 25x10⁶ T cells). Poly-A selected RNA was eluted from the beads in 75 μ l PBS heated at 80°C for 2 minutes and transferred to a new tube. 3.75 μ l 1M NaOH was added to the sample, mixed well and spun down. It was then incubated at 37°C for 30 minutes to fragment RNA shaking 15 seconds at 1250 rpm every 1.5 minutes in the Thermomixer R. 3.75 μ l 1M HCl was added to quench the base and 0.825 μ l 1M HEPES added to buffer the solution. 1 μ l Glycogen was added followed by 1 ml 100% EtOH. The solution was inverted and left at -20°C overnight for the RNA to precipitate.

PNK Treatment and Size Selection

Both the ribosomal protected fragment (RPF) and alkaline hydrolyzed poly-A selected (mRNA) were pelleted by centrifugation at 14,000 rpm in a desktop microcentrifuge for 20 minutes at 4°C. RNA pellets were washed twice with 80% EtOH and then air dried for 10 minutes on the bench top. RNA was resuspended in 30 µl H₂O supplemented. To rephosphorylate the 5' end of the RNA, the RNA was treated with PNK (4 µl PNK enzyme, 2 µl SUPERasin, 4 µl PNK Buffer) for 1 hour at 37°C, 75°C for 10 minutes and then moved to ice. 20% polyacrylamide Urea gel was poured and the entire RNA sample was loaded along with microRNA marker (New England Biolabs, N2102S), low range ssRNA Ladder (New England Biolabs, N0364S), and RNA 32-mer oligonucleotide (also PNK treated to match running conditions of sample). To visualize RNA, the gel was immersed in a 1:10,000-fold dilution of SYBR Gold (Molecular Probes) in TBE for 10 minutes. Gel fragments were cut from gel at ~35 nucleotides for RPFs and between ~35-55 nucleotides for mRNA, as indicated in Figure 7.8. 400 µl RNA gel Extraction Buffer (300 mM NaOAc, 1 mM EDTA, 0.1 U/ml SUPERasin) was added to each gel slice which was crushed in buffer with the plunger of a 1 ml syringe. Crushed slices were then frozen on dry ice for 30 minutes to help dissociation. The crushed gel was then rotated in buffer overnight at 4°C after which the RNA solution was filtered through Whatman GF/D filters in Nanosep columns (VWR). 2 µl Glycogen was added and 1 ml EtOH was used to precipitate RNA at -20°C for at least 2 hours or overnight.

Poly-A Tailing Reaction

Protein-G Dynabeads were prepared by washing three times in Antibody Binding Buffer (ABB) (1X PBS, pH 7.4 with 0.02% Tween-20). Beads were resuspended in 225 μ l/50 μ l beads ABB with 25 μ l/50 μ l beads Denhardt's Solution (Sigma). The beads were blocked rotating at room temperature for 45 minutes to 1 hour. RNA was pelleted by centrifugation at 14,000 rpm in a desktop microcentrifuge for 20 minutes at 4°C. RNA pellets were washed twice with 80% EtOH and then air dried for 10 minutes on the bench top. 6.25 μ l H₂O was added to RNA pellet and it was left on ice to go into solution aided by tapping of the tube and then the material was spun down. RNA was denatured at 65°C for 5 minutes and then placed immediately on ice. RNA was added to a reaction poly-A tail reaction mixture of 1 μ l 10X E-PAP Buffer (NEB), 1.5 μ l 1 mM ATP, 1.5 μ l RNAsin Plus (Promega), and 1 μ l 3U/ μ l E-PAP (NEB) in a PCR tube. The RNA was polyadenylated at 37°C for 10 minutes, 65°C for 20 minutes, and then moved to ice.

Reverse Transcription Reaction

Protein-G Dynabeads blocking in ABB and Denhardt's Solution were washed 3 times with ABB. For 250 μ l original bead volume, we added 100 μ l ABB, 25 μ l Denhardt's Solution, 125 μ l anti-BrdU antibody (Santa Cruz, sc-32323) and rotated at room temperature for a minimum of 45 minutes. The poly-A tailed RNA was spun down and 2.5 μ l of each sample was pooled together for a final volume of 10 μ l for -RT control. The RNA was supplemented with 1 μ l H₂O, 1 μ l 0.752 M Tris, 1 μ l each of dATP, dCTP, dGTP (8.2 mM, Invitrogen) and 1 μ l Br-dUTP (8.2 mM, Sigma). 1 μ l of 25 μ M primers

was added to each tube (NV20T-RT1 for RPF samples and NV20T-RT 2 for mRNA samples) and 0.5 µl of each were added to the –RT control.

NV20T-RT1:

5'pGACATCGTNNNNNNGATCGTCGGACTGTAGAACTCT/idSp/CAAGCAGAAG
ACGGCATAACGATTTTTTTTTTTTTTTTTTTTTTVN

NV20T-RT2:

5'pGCACTGTTNNNNNNGATCGTCGGACTGTAGAACTCT/idSp/CAAGCAGAAG
ACGGCATAACGATTTTTTTTTTTTTTTTTTTTTTVN

The samples were quickly spun down and incubated at 75°C for 3 minutes. A pre-warmed mixture of 1 µl 82 mM DTT, 1 µl 10U/µl RNAsin Plus (Promega) and 1 µl Superscript III (or H₂O for –RT control) were added to each sample and the reverse transcription reaction was incubated at 48°C for 45 minutes, 55°C for 15 minutes, 85°C for 5 minutes and then moved to ice.

cDNA Purification: Immunoprecipitation I

Protein-G Dynabeads labeled with anti-BrdU antibody were washed three times in IP Buffer (0.3x SSPE, 1mM EDTA, 0.5% Tween-20). 1 µl 2U/µl RNase H (Invitrogen) was added to each reverse transcription reaction and incubated at 37°C for 20 minutes to digest RNA and then placed on ice. 10 µl H₂O was added to the reaction and then it was spun through a G-25 column (Amersham) to remove free nucleotides. The flow through was adjusted to a final volume of 100 µl with H₂O and then incubated at 70°C for 5 minutes and at room temperature for 2 minutes. 25 µl of original slurry volume of

Protein-G beads in 100 μ l IP Buffer was added to fresh tubes and the supernatant was removed. cDNA was added to the beads and the beads were resuspended by tapping, trying to keep everything at the bottom of the tube. Beads were rotated for 30 minutes at room temperature to immunoprecipitate the cDNA via the incorporated Br-dUTP. The beads were then washed with 900 μ l of each buffer for 3 minutes at room temperature. First, they were washed once with IP Buffer with Denhardt's (4.5 ml IP Buffer/0.5 ml Denhardt's), then twice with low salt buffer (15 mM Tris- HCl, pH 7.5, 5 mM EDTA) with 2% Denhardt's, twice with high stringency buffer (15 mM Tris-HCl, pH 7.5, 5 mM EDTA, 2.5 mM EGTA, 1% Triton X-100, 1% Na-deoxycholate (DOC), 0.1% SDS, 120 mM NaCl, 25 mM KCl) with 2% Denhardt's, and twice with IP Buffer without Denhardt's. The last wash was completely removed from the beads and 50 μ l 100 μ M BrdU (Sigma) in IP Buffer was added to competitively elute the cDNA off of the beads. Beads were resuspended in solution by tapping and rotated for 30 minutes at room temperature. The beads were placed on the magnet and the eluate was collected and spun through a G-25 column. The flow through was adjusted to 150 μ l total volume with H₂O. This cDNA solution was stored overnight at 4°C.

cDNA Purification: Immunoprecipitation II

After leaving the samples overnight, the immunoprecipitation was repeated. The cDNA solution was quickly vortexed and spun down. It was incubated at 70°C for 5 minutes and at room temperature for 2 minutes. 25 μ l of original slurry volume of Protein-G beads in 100 μ l IP Buffer was added to fresh tubes and the supernatant was removed. cDNA was added to the beads and the beads were resuspended by tapping, trying to keep

everything at the bottom of the tube. Beads were rotated for 30 minutes at room temperature to immunoprecipitate the cDNA via the incorporated Br-dUTP. The beads were then washed with 900 µl of each buffer for 3 minutes at room temperature. First, they were washed once with IP Buffer with 10% Denhardt's, twice with low salt buffer with 2% Denhardt's, twice with high stringency buffer with 2% Denhardt's, and twice with IP Buffer without Denhardt's. The last wash was completely removed from the beads.

cDNA Circularization and Relinearization

20 µl CircLigase reaction mixture (2 µl CircLigase 10X Reaction buffer, 4 µl 5 M Betaine, 1 µl 50 mM MnCl₂, 0.5 µl (50U) CircLigase ssDNA Ligase II (Epicentre), and 12.5 µl H₂O) was added to the beads which were tapped into solution. This reaction was incubated at 60°C for 1 hour in the Thermomixer R to circularize the cDNA. The beads were collected and washed twice in low salt buffer with 2% Denhardt's, twice with high stringency buffer with 2% Denhardt's, and twice with APE1 wash buffer (50 mM Potassium Acetate, 20 mM Tris-Acetate, 10 mM Magnesium Acetate, pH 7.9). The last wash was removed from the beads completely and the cDNA was relinearized using an APE1 cut site with 2 µl 10X Reaction Buffer (NEB4), 1.25 µl 10U/µl APE1 (NEB), and 16.75 µl H₂O. This reaction was incubated for 1 hour at 37°C in Thermomixer R shaking at 1300 rpm for 15 seconds every 30 seconds. The beads were again washed twice in low salt buffer with 2% Denhardt's, twice with high stringency buffer with 2% Denhardt's, and twice in Phusion Wash Buffer (50 mM Tris pH 8.0).

PCR Amplification and High-Throughput Sequencing

To amplify the cDNA, PCR was done with Phusion Polymerase. First, 37.5 µl H₂O, 10 µl 5X Phusion HF Buffer, and 1 µl 10 mM dNTPs were added to the beads. This was incubated at 98°C for one minute shaking at 1200 rpm in the Thermomixer R to elute the cDNA from the beads. This was quickly placed on the magnet and the eluate was collected to a PCR tube with an optically clear cap. This solution was supplemented with PCR primers and DNA polymerase (0.5 µl 20 µM DP5 PAT, 0.5 µl 20 µM DP3 PAT, and 0.5 µl Phusion DNA Polymerase (NEB). SYBR Green I was diluted from 10,000X to 50X in Phusion Wash buffer and 0.5 µl was added to the PCR reaction and mixed by pipetting. Tubes were placed in the iQ5 Multicolor Real-Time PCR Detection System (Biorad) and pushed in place using a Kimwipe so as not to touch the lid. The tubes were incubated at 98°C for 30 seconds and then cycled at 98°C for 10 seconds, 60°C for 15 seconds, and 72°C for 20 seconds until the RFU signal reached ~800-1000. Note that the display is a cycle behind the detection so the tubes need to be removed when the display signals ~400-500 to account for doubling. 10 nM solution was submitted for sequencing and data analysis was done using the Galaxy platform (Hillman-Jackson et al. 2012) and using R Statistical Analysis Software (<http://www.R-project.org>).

DP5 PAT:

5'-AATGATACGGCGACCACCGACAGGTTCTAGAGTTCTACAGTCCGACG

DP3 PAT:

5'-CAAGCAGAAGACGGCATACGA

Illumina Small RNA Sequencing Primer:

5' -CGACAGGTTTCAGAGTTCTACAGTCCGACGATC

Mice

Wild-type C57BL/6 mice (stock number 000664), Lck-Cre mice (stock number 003802), and A2.1 transgenic AAD mice (stock number 003475) were purchased from The Jackson Laboratory. CD4-Cre mice (stock number 4196-F/M) were purchased from Taconic Farms. HuR^{fl/fl} mice were obtained from Dr. Dimitris Kontoyiannis (Katsanou et al. 2009). HuD knock out mice were obtained from Dr. Hideyuki Okano (Akamatsu et al. 2005).

Ocular Blood Draw

Mouse peripheral blood was obtained by ocular blood draw with heparinized capillary tubes. 5 drops were taken into 10 milliliters PBS.

Flow Cytometry Intracellular Staining

For intracellular staining, cells were incubated for 20 minutes at 4°C in the Fixation/Permeabilization solution from the Cytofix/Cytoperm kit (BD Biosciences). Cells were then permeabilized by washing in the BD Perm/Wash Buffer (PWB). Cells were stained in PWB with the indicated primary antibodies, for example HuR specific mouse monoclonal antibody 3A2, for 1 hour rocking on ice and covered in foil. Cells were washed twice and then incubated with anti-mouse IgG (Fc-specific) polyclonal goat F(ab')₂ fragment conjugated with DyLight 649 (Jackson ImmunoResearch) at a dilution of

1:1000 in PWB for 30 minutes rocking on ice and covered in foil. After this incubation, cells were washed twice in PWB and once in FACS Buffer. Cells were collected immediately on a BD FACScaliber machine and analyzed using Flowjo software (Treestar).

Single Linker Ligation CLIP

This protocol was used for Ago CLIP in HuR Wild-Type and cKO Mice. Samples were prepared as described in the standard CLIP methods starting with T cell lysate preparation through the recovery of protein-RNA complexes and protease digestion, except that a different 3' linker sequence was used which matches the Illumina small RNA sequencing primer.

SRA3:

5'-P UCGUAUGCCGUCUUCUGCUUG 3'-puromycin

No 5' linker ligation is used in this protocol and instead it follows the same cloning strategy as detailed in the ribosomal profiling and mRNA sequencing methods section starting at the reverse transcription step. The only modifications from the ribosomal profiling methods are that different reverse transcription primers were used matching the 3' linker sequence instead of the stretch of poly-A's and it was indexed as indicated for each sample. The PCR and sequencing primers were the same as for ribosomal profiling and mRNA sequencing.

Index 1a GCAT:

5'pGNNNNNNNNGATGCGATCGTCGGACTGTAGAACTCT/idSp/CAAGCAGAAG
ACGGCATACGA

Index 2a GTCA:

5'pGNNNNNNNNGTGACGATCGTCGGACTGTAGAACTCT/idSp/CAAGCAGAAG
ACGGCATACGA

Index 3a ACTG:

5'pGNNNNNNNNGCAGTGATCGTCGGACTGTAGAACTCT/idSp/CAAGCAGAAG
ACGGCATACGA

Index 4a AGCT:

5'pGNNNNNNNNGAGCTGATCGTCGGACTGTAGAACTCT/idSp/CAAGCAGAAG
ACGGCATACGA

Index 6a TCGA:

5'pGNNNNNNNNGTCGAGATCGTCGGACTGTAGAACTCT/idSp/CAAGCAGAAG
ACGGCATACGA

Adenovirus production

Recombinant adenoviruses expressing GFP, β -galactosidase, or HuD-GFP were produced by transduction of HEK293 cells (ATCC) and purified using the Adenopure Kit (Puresyn) according to the manufacturer's instructions. Viral titers were assessed by infection of HEK293 cells with serial dilutions of purified virus followed by determination of the number of virally infected cells after 20 hours by fluorescence or X-Gal staining.

Adenovirus Immunizations

6-8 week old mice were injected with 100 μ l purified adenovirus (10^9 PFU/ml) intradermally and treated with pertussis toxin (Sigma) intraperitoneally at days 0 and 2.

Mouse T cell in vitro Stimulation

Around 3×10^7 splenocytes, or half a spleen per flask, from adenovirus-immunized mice were incubated at 37°C in upright T25 culture flasks (Corning) in R10 with 0.5 μ M peptide for 7 days. For further rounds of re-stimulation, splenocytes were plated in 24 well plates ($2-6 \times 10^5$ splenocytes per well) with peptide-pulsed feeder cells in R10 with 50 CU/ml recombinant human IL-2 (Chiron). Feeder cells were prepared from spleens of naïve syngeneic mice by pulsing with 0.5 μ M peptide for 1 hour at room temperature and irradiating at 3,000 Rads before plating.

T cell Receptor Codon Optimization, Synthesis, and Cloning

Sequences of previously cloned T cell receptors were codon optimized and synthesized by GeneArt (Santomaso et al. 2007). Synthesized constructs contained restriction sites for insertion into pGEM4Z/GFP/A64 vector kindly provided by Dr. Eli Gilboa (Boczkowski et al. 1996).

In vitro Transcription of RNA for Electroporation

mRNA encoding GFP from pEGFP-N1 (Clontech) and mRNAs encoding TCR α and β chains were prepared from PCR products made using gene specific primer pairs

containing the T7 RNA polymerase promoter sequence. mMESSAGE mMACHINE High Yield Capped RNA transcription Kit (Ambion Inc. Austin, TX) was used to *in vitro* transcribe RNA according to the manufacturer's instructions. The RNA was then purified using an RNeasy Mini Kit (Qiagen) and purified RNA was resuspended in RNase free water at 1-3 mg/ml.

Electroporation of in vitro transcribed RNA

One vial of 10^8 PBMC was thawed into 100 ml of complete Stemline medium (CSM) (Stemline T cell Expansion Medium (Sigma) supplemented with 5% FBS (Hyclone), Glutamax (Invitrogen), and gentamycin). Upon thawing, PBMC were stimulated with IL-2 (300 IU/ml, Chiron Corp) with 50 ng/ml OKT3 for 3 to 4 days. After stimulation, CD8 T cells were isolated by positive selection. The purified CD8⁺ T cells were cultured in CSM with 300 IU/ml IL-2 without OKT3 for 10-17 days for expansion before electroporation and kept at a concentration of 10^6 /ml. The stimulated CD8 lymphocytes were resuspended in OPTI-MEM (Invitrogen) medium at a final concentration of 25×10^6 cells/ml. Cells and cuvettes were pre-chilled on ice for at least five minutes before electroporation. Lymphocytes were mixed at a concentration of 2 μ g in vitro transcribed RNA per 1×10^6 lymphocytes and electroporated in a 2 mm gap cuvette using an ECM830 Electro Square Wave Porator (Harvard Apparatus BTX) at 500 Volts/500 μ s. Warm media was added immediately to the cuvette and cells were transferred to fresh CSM with no IL-2 or OKT3 and rested for at least 6 hours.

Tetramer Staining

Human cells were stained in Human FACS buffer (PBS supplemented with 1% FBS (Hyclone), and 1% PHS). Mouse T cells were incubated for 10 minutes using 1 μ g of anti-CD16/CD32 (Fc γ RII/III) in Mouse FACS buffer (the same as for human cells but also supplemented with 5% goat serum). For tetramer staining, 10^5 - 10^6 human cells were incubated with 1:20 dilution of tetramer for 20 minutes at room temperature in the dark. Antibody to CD8 was then added for an additional 10 minutes. The cells were then washed twice in FACS buffer and collected immediately on a BD FACScaliber and analyzed using Flowjo software (Treestar).

Primary Ascites Cultures

Received freshly isolated ascited fluid in sterile containers from the operating room. The fluid was incubated with an equal volume of Growth Medium in a flask at 37°C with 5% CO₂ and not disturbed for 3-4 days. After this incubation period, the media was changed every 2-3 days until the flasks were confluent, which was typically between 7-10 days. To passage cells, the adherent cells were washed once in PBS and then trypsinized using a minimal volume of 0.06% w/v trypsin/EDTA (Cellgro) for 2-3 minutes at 37°C. Growth medium was then added to the disrupted cells and transferred to two new flasks. Stocks of ascites cells were frozen in RPMI (Mediatech) supplemented with 10% human serum albumin, and 10% DMSO (Sigma-Aldrich).

Preparation of Primary Murine Kidney Epithelial Cells (KECs)

Kidneys from adult mice were mashed using the back of a syringe and pipetted until a single cell suspension was obtained. The cell suspension was passed over a 70 μ m cell strainer and washed in D10 medium before plating in 10 cm dishes. Cultures were fed by replacing D-0 on days 4 and 7. On day 7, recombinant mouse IFNG (R&D Systems) was added at 10 units/ml medium. On day 8, 10 μ l recombinant adenovirus at 10^9 PFU/ml was added to each cell culture dish and the cells were harvested on day 9 for use in an IFNG ELISPOT assay.

Cell Lines

T2 cells are a human lymphoblast cell line deficient in TAP function containing abundant HLA-A2 molecules on the cell surface that can be loaded with exogenous peptide (Salter, Howell, and Cresswell 1985). EL4 cells are a murine lymphoblast cell line. Other cell lines used include: Adenovirus (Ad)-5 transformed cell line HEK293 (CRC 1573; ATCC), the cervical carcinoma cell line HeLa (CCL- 2, ATTC), the ovarian carcinoma cell line COV413 provided by Dr. Victor Engelhard. For IFNG treatments, recombinant mouse IFNG (R&D Systems) was added at 10 units/ml medium for 48 hours prior to use in assay.

Peptides

All peptides for cdr2, HuD, β -gal and Ova were purchased from American Peptide Company.

Tumor Killing Assay

T cells were resuspended at 1×10^6 cells/ml and target cells were resuspended at 1×10^5 cells/ml. 1 ml of T cells and target cells were plated together in a 6-well dish. The cells were co-cultured overnight. Cells were then harvested and TO-PRO 3 Iodide (Invitrogen) was used to stain dead cells as per manufacturer's instructions. Blank calibration beads (BD Biosciences) were added to the tube before flow cytometry collection to normalize acquisition between samples. Cells were collected immediately on a BD FACScaliber and analyzed using Flowjo software (Treestar).

Murine and Human IFNG ELISPOT Assays

Enzyme-linked immunospot (ELISPOT) assay was used to quantify the number of antigen-specific IFNG producing lymphocytes in response to different target cells. Briefly, nitrocellulose-bottomed 96-well plates (MultiScreen HA, Millipore) were coated overnight at 4°C with anti-IFNG monoclonal antibody (clone AN18 at $5 \mu\text{g/ml}$ for mouse, clone 1-DIK at $10 \mu\text{g/ml}$ for human; both from Mabtech). Wells were washed three times with PBS and blocked for 2 hours with R10 medium at 37°C . For direct ex vivo mouse ELISPOTs, CD8 T cells were isolated by positive selection from spleens using MACS purification (Miltenyi Biotec) and 2×10^5 CD8 T cells were co-cultured with 5×10^4 target cells. For ELISPOTs with T cell clones or otherwise *in vitro* stimulated cells, 1×10^4 CD8 T cells were cocultured with 5×10^4 target cells. For human ELISPOTs with RNA electroporated human lymphocytes, 1×10^5 CD8 T cells were co-cultured with 5×10^4 target cells. All co-culture conditions were performed in triplicate wells. After incubation for 20 hours at 37°C , the plates were washed 6 times with PBS supplemented

with 0.05% Tween-20. Biotinylated IFN- γ mAb (clone R4-6A2 for mouse, Pharmingen; clone 7-B6-1 for human, Mabtech), the conjugate (avidin-peroxidase complex; Vectastain avidin-biotin complex method Elite Kit; Vector Laboratories) and AEC substrate (Sigma) were then used for spot development according to the manufacturer's instructions. After development, red spots on the membrane represent IFNG released by individual T cells and are reported as spot-forming-cells per 10^6 cells. The ELISPOT plate quantification was performed in a blinded fashion by an independent evaluation service (Zellnet Consulting) using an automated ELISPOT reader (Carl Zeiss) with KS Elispot 4.8 software.

CD107a assay

10^5 tumor cells were placed into one well of a 24-well plate along with an equal number of TCR-electroporated or mock-electroporated CD8⁺ T cells in a total volume of 1 milliliter R10. 20 μ l of FITC-conjugated CD107a antibody and 1 μ l of GolgiStop (Beckton Dickinson, San Jose, CA) were added to the well according to the manufacturer's instructions. The co-culture was incubated for 4 h at 37°C followed by washing and flow cytometry.

HuD peptide 321 specific CD8 T cell Cloning

6-8 week old mice were injected with 100 μ l purified adenovirus-HuD at 10^9 PFU/ml intradermally and treated with pertussis toxin (Sigma) intraperitoneally at days 0 and 2. On day 13 spleens were removed. The red blood cells were lysed with ACK buffer (Biofluids) and splenocytes were plated for in vitro stimulation as described. CD8

isolated T cells from IVS cultures were plated in an entire 96 well plate at a concentration of 3, 1 and 0.3 cells per well with 5×10^6 HuD peptide 321 pulsed irradiated feeder cells and 10 U/ml recombinant human IL-2 (Chiron) in a final volume of 200 μ l R10. After one week, plates with less than 33% positive wells were expanded by transferring each well into a separate well of a 24-well plate containing 10^6 HuD peptide 321 pulsed irradiated splenocytes and 10 U/ml recombinant human IL-2 in a final volume of 1 ml. Clones were maintained by weekly stimulations with irradiated feeders and expanded 6 fold. Adapted from (Galfrè and Milstein 1981).

In Vitro CTL Chromium Release Assay

For target cell preparation, 10^6 EL4 cells in 100 μ l R10 were labeled with 10 μ M peptide plus 100uCi ^{51}Cr for 1 hour at 37°C, shaking every 10 minutes. EL4 cells were then washed 3 times in 1 ml R10 and resuspended at 10^5 /ml. 5×10^3 EL4 cells were plated per well in a round bottom plate with serial dilutions of T cells. Plates were spun at 300 rpm for 5 minutes to sediment cells and incubated at 37°C for 4.5 hours. To harvest and measure radioactivity from the CTL assay, 100ul of supernatant from each well was pipetted into a sample plate for gamma measurement with 100 μ l gamma scintillation fluid.

Titermax Immunization

C57BL/6 mice were injected in the footpad with a single peptide emulsified in Titermax adjuvant. To form the peptide emulsion, 75 μ l of peptide at 10 mg/ml in 50% DMSO was added to 75ul ddH₂O. This solution was then added to a sterile eppendorf tube

containing 150ul Titermax adjuvant. The tube was then vortexed for 30 minutes on high to form an emulsion of Titermax and peptide. The peptide emulsion was drawn into an insulin syringe and 50 μ l (approximately 125 μ g of peptide) was injected per animal. After 7 days, the animal was sacrificed and the right popliteal and inguinal lymph nodes were removed. Lymph nodes were ground between two sterile frosted glass slides to obtain a single cell suspension.

Bone Marrow Chimeras

Bone marrow recipient mice were given two doses of 450 Rads whole body gamma-irradiation to sub-lethally deplete bone marrow. Bone marrow was collected from donor mice by extracting cells from the tibia and femur. Red blood cells were lysed with ACK buffer (Biofluids) and the bone marrow cells were depleted of CD90.2 positive mature lymphocytes by MACS selection. 5×10^6 bone marrow cells were transferred into the irradiated hosts in the retro-orbital cavity and then were left to rest for two months to allow for bone marrow reconstitution before challenge.

CHAPTER 3. The Efficiency and Activation of Purified Lymphocytes Using Different Isolation Techniques

Introduction

Cluster of differentiation eight (CD8) T cells are circulating lymphocytes that monitor and selectively kill infected, transformed, or damaged cells. Generally, in virtually all cells, intracellular proteins are presented as peptides extracellularly to the immune system in major histocompatibility complex (MHC) I molecule complexes. Each T cell expresses a unique T cell receptor that can bind a particular peptide-MHC complex. In this way, T cells can initiate an immune response in an epitope and MHC-restricted manner. Typically, non-self proteins that indicate that a cell has been compromised, such as viral proteins, will be detected on the cell surface by CD8 T cells and targeted for killing.

In order to study the impact of the dynamic stimulus of T cell activation on RNA regulation within the T cell, we developed a system to analyze T cells in a resting state as well as after stimulation. Our plan, as discussed in Chapter I and in subsequent chapters, was to compare and contrast HuR and Argonaute (Ago)-microRNA regulation in these cells. To activate a polyclonal population of T cells without antigen dependency, antibody coated beads were used to mimic the signaling that a CD8 T cell would encounter from a cognate antigen-presenting cell (APC). The first signal from the APC is directed towards the T cell receptor-CD3 complex that can be mimicked with an anti-CD3 antibody. Second, for complete activation and proliferative responses, co-stimulation is needed through the CD28 co-receptor molecule on the surface of lymphocytes. By using beads coated with antibodies against CD3 and CD28 the T cells

encounter both signals on a surface approximately the size of an APC, resulting in T cell activation.

We developed a quantitative RNA-based assay as a surrogate to monitor the activation response of the lymphocytes. In this assay, we measured the induction of two cytokine transcripts, IFNG and TNF, by isolating T cell RNA and performing reverse transcription for quantitative PCR (qPCR) analysis. Stimulation of CD8 T cells with CD3 and CD28 agonists leads to a dramatic increase in the expression of IFNG and TNF mRNA (Lindstein et al. 1989; Thompson et al. 1989; Wang et al. 2006). These cytokines are critical to the activation response because both help to mediate effector functions of CD8 lymphocytes. For example, IFNG produced after T cell activation stimulates Janus Tyrosine Kinase (JAK) signaling and can directly inhibit viral replication and induce the starvation of intracellular pathogens. IFNG can also induce the production of antigen processing machinery, which in turn increases the presentation of pathogenic antigen to the lymphocytes (Levy and Darnell 2002; Shuai and Liu 2003; Stark et al. 1998). TNF stimulates the transcription of a wide array of cytokines and chemokines by cells in the local environment of the activated T cell. In this way, IFNG synergizes with TNF to activate and recruit white blood cells to propagate the inflammatory response and aid in the clearance and killing of infected material (Boehm et al. 1997; Janeway and Medzhitov 2002; Rock and Goldberg 1999). Therefore, these two transcripts were analyzed because of their early transcriptional induction with T cell activation and because they had been previously shown to be regulatory targets of HuR (Brennan and Steitz 2001; Mazan-Mamczarz et al. 2003; Wang et al. 2006).

Several prior studies were used to support this activation method and chosen time of one hour of stimulation. For instance, the RNA binding protein HuR translocates from the nucleus to the cytoplasm in peripheral T cells by 45 minutes of *in vitro* stimulation with CD28 monoclonal antibodies. One hour of activation also showed a consistently measurable change in the cellular status of lymphocytes by a detectable induction of immediate early genes (Lindstein et al. 1989; Thompson et al. 1989; Wang et al. 2006). Ago and HuR have also been shown to mediate rapid effects on mRNA localization and stability. For example, these proteins can rapidly shuttle in and out of stress granules, to mediate translational silencing and potentially degradation of bound mRNAs (Bhattacharyya, Habermacher, Martine, Closs, and Filipowicz 2006a; 2006b; Leung and Sharp 2007; 2010). Therefore, we chose to examine this early time point of T cell activation to investigate the direct dynamic regulatory control of RNA by Ago and HuR.

In this chapter we develop methods to purify a sufficient quantity and quality of human lymphocytes for subsequent HuR, Ago and RNA profiling experiments. We explore and optimize two main methodological issues: the yield and purity of T cells from isolation procedures, and the impact of the isolation procedures themselves on T cell activation. Purification of sufficient T cell numbers for these studies depended upon the requirements for RNA analyses. As will be detailed in subsequent chapters, high-throughput sequencing of RNA isolated by crosslinking immunoprecipitation (HITS-CLIP) studies and ribosomal profiling studies are variable in their sensitivity, depending on the abundance and avidity of RNA-protein interactions and RNA levels in polyribosomes. Hence one variable we explore in this chapter is the impact of T cell activation on the levels of Ago.

In general, these studies suggest that sufficient numbers of cells for analysis may require isolation of 20 million peripheral lymphocytes for each activation state of a paired sample for HITS-CLIP analysis and additional material for other RNA profiling experiments. Achieving such yields from a peripheral human blood draw would be difficult. Therefore, we turned to leukapheresis, a protocol we have utilized within the laboratory to purify PMBCs from patients with paraneoplastic neurologic disorders (Albert et al. 1998). This protocol yields large numbers of peripheral blood mononuclear cells (PBMC), returning the remainder of the blood back to the donor. For the purposes of the current study, we were approved by the Rockefeller University Hospital Institutional Review Board to obtain leukapheresates from normal healthy human volunteers.

In these studies, it was important to assess whether our protocol to isolate peripheral blood lymphocytes for analysis perturbed their activation state. Hence we compared different isolation protocols for purifying T cells from PBMC. Typically, these protocols use antibodies against cell surface markers to isolate different cellular populations. Two different approaches were assessed. In one, T cells of interest were directly purified with antibodies to the T cell co-receptor CD8 molecule. One concern here is that such purification might crosslink the receptors and initiate downstream signaling and activation of the T cells. Therefore we compared this protocol with ones in which we isolated CD8 T cells by negative selection, using a mix of depleting antibodies specific for other cell surface markers present on all unwanted peripheral lymphocytes. We assessed whether using negative selection could produce sufficient yield and purity of CD8 T cells while leaving the T cells naïve.

Results

Purification of CD8 T cells by Negative Selection

We first examined whether negative selection of CD8 T cells could be efficiently accomplished from 100-250 milliliters of peripheral blood collected from normal volunteers. Heparinized and phosphate buffered saline (PBS)-diluted blood was purified over a Ficoll gradient to separate the PBMC from plasma and from a pellet of erythrocytes and granulocytes. The number of circulating peripheral cells per unit volume was dependent on the donor but 240-960 million PBMC were isolated in each case. T cells were then isolated by negative selection, by incubating the PBMC with a biotin-conjugated antibody mixture directed at non-CD8⁺ cells for depletion. To ensure maximal purity of this isolation, we depleted cells using additional antibodies specific to B cells (CD19), NK cells (CD56), CD4 T cells, monocytes and macrophages (CD14). Using anti-biotin magnetic beads, non-CD8⁺ cells were bound to a magnetic column and CD8 lymphocytes were collected as the flow-through of the column. This yielded between 7 and 40 million freshly purified CD8 T cells per donor.

The isolated cells were analyzed for purity by flow cytometry. Between 90% and 95% of the isolated cells were CD8 T cells based on expression of CD8 and the T cell lineage marker CD3. By forward and side scatter profiles we determined the viability of these cells to be greater than 95% (Figure 3.1). We concluded that purification of CD8 lymphocytes by negative selection is effective for purifying small numbers of cells from peripheral blood and allowed isolation of a population of at least 90% pure CD8 T cells.

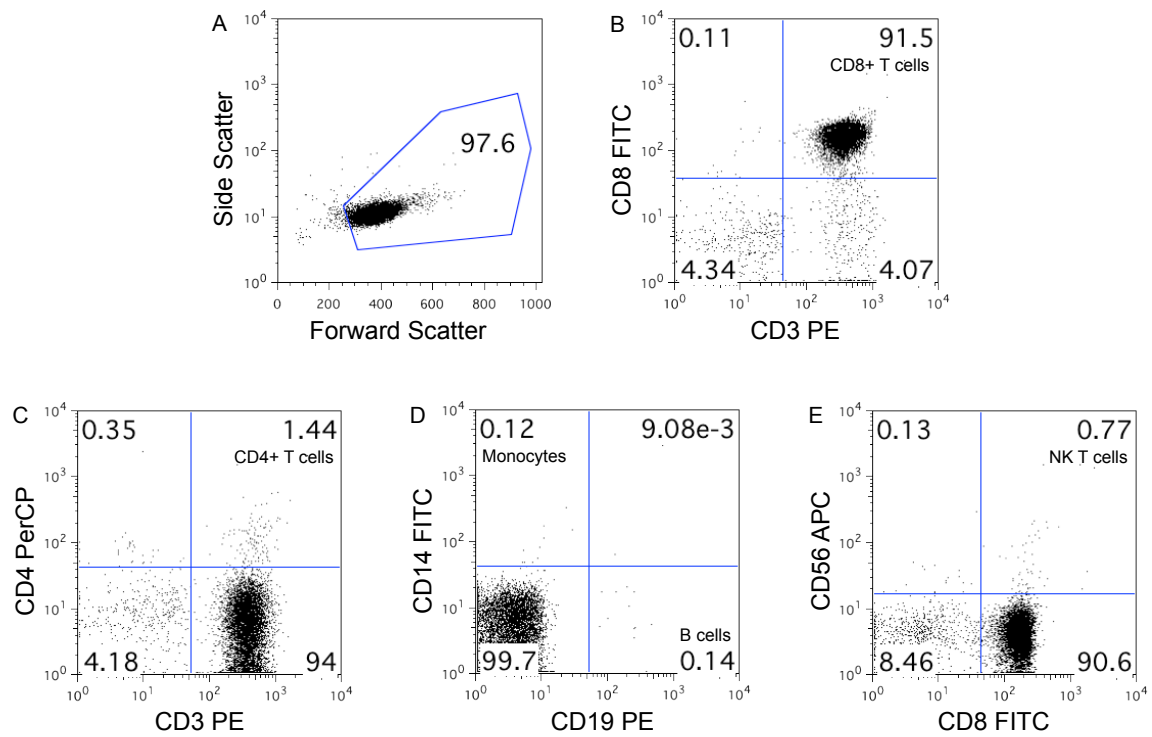


Figure 3.1 Purity of CD8 T Cells Purified by Negative Selection. Representative CD8 T cells purified from PBMC of normal human donors by negative selection. **(A)** Forward and side scatter determined by flow cytometry. The percentage of live cells (97.6%) is noted in the gated population. **(B-E)** Stains indicated on each axis and percentages of cells for the indicated lineages are noted for each quadrant.

Purification of CD8 T cells by CD56 Depletion followed by CD8 Positive Selection

To purify larger numbers of CD8 lymphocytes more efficiently, we explored the purification of CD8 T cells from PBMC by positive selection. When isolating the cells by positive selection of the CD8 marker on the cell-surface of T cells, we found that the resulting lymphocytes contained a significant percentage of CD8+ CD56+ Natural Killer (NK) T cells. Therefore, to remove this population of cells in subsequent purifications, we first depleted NK T cells using CD56 antibody-conjugated magnetic beads.

We found that depletion of CD56+ cells followed by positive selection of CD8+ cells yielded enhanced purity of CD8 T cells as compared to negative selection (Figure 3.2). The average purity determined from five preparations of normal donor cells from leukapheresis and screened by flow cytometry was 97% CD8 T cells. The non-CD8+ cells contaminating the preparation typically correspond to 2% each of CD4 T cells and CD8+ CD56+ NK T cells. There is typically less than 0.5% contamination by CD14+ monocytes or macrophages, and by CD19+ B cells (Table 3.1).

Furthermore, we found that this purity was preserved when processing larger amounts of cells from leukapheresis of normal healthy volunteers rather than relying on peripheral blood draw. We collected between 120 and 150 milliliters of leukapheresate from normal donors and layered and centrifuged this material through a Ficoll gradient. From this volume of material we were able to isolate 2-6 billion PBMC from each donor, which was roughly one hundred times more material than from a standard peripheral blood draw. After depletion of CD56 positive cells and selection of CD8 positive cells as described above, we were able to elute 400-800 million CD8 T cells. After resting the cells

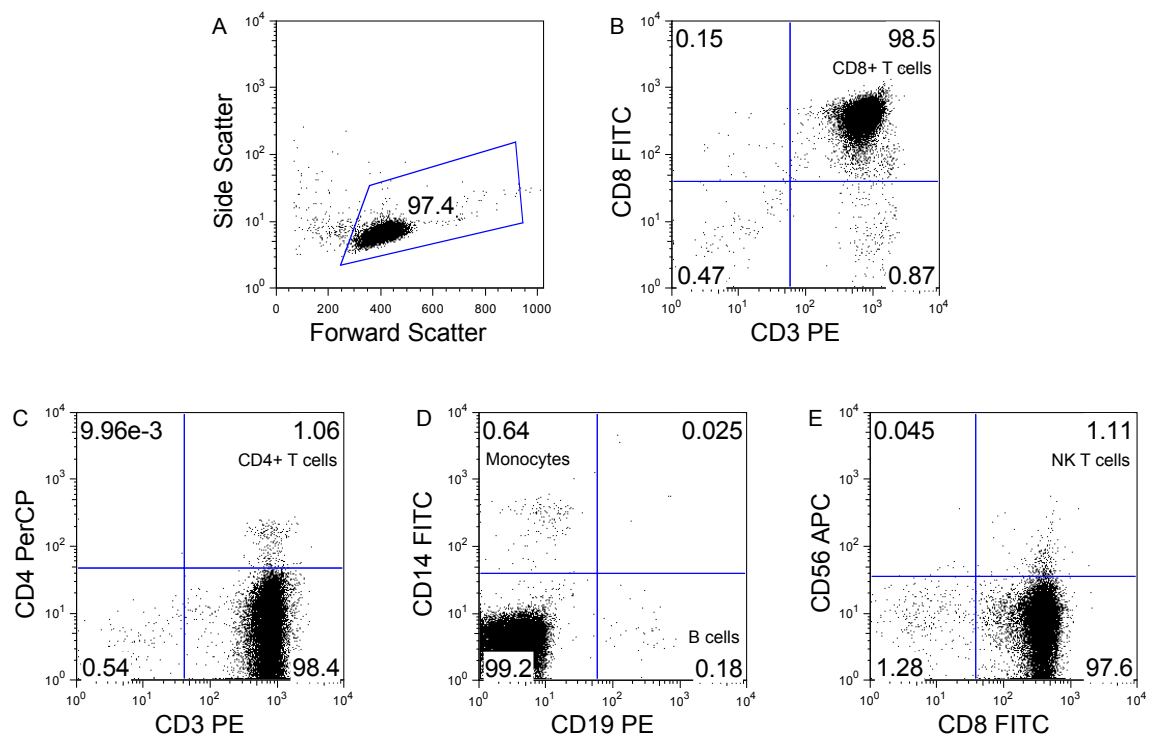


Figure 3.2 Purity of CD8 T Cells Purified by CD56 Depletion and CD8 Positive Selection. Representative CD8 T cells purified from PBMC of normal human donors by CD56 depletion and CD8 positive selection. **(A)** Forward and side scatter determined by flow cytometry. The percentage of live cells (97.4%) is noted in the gated population. **(B-E)** Stains indicated on each axis and percentages of cells for the indicated lineages are noted for each quadrant.

Table 3.1 Purification of CD8 T cells from Normal Human Donor Leukapheresis. Five normal healthy donors were leukapheresed. CD8 T cells were purified by CD56 depletion and CD8 positive selection. Leukapheresates collected and resulting cell populations isolated are described. Abbreviations: leukapheresate (Leuk.), peripheral blood mononuclear cells (PBMC).

| | Leukapheresate Volume (ml) | Total PBMC (x 10 ⁹) | Selected CD8 (x 10 ⁶) | Rested CD8 (x 10 ⁶) | Live Cells (%) | CD8+ T cells (%) | CD4+ T cells (%) | CD56+ NK T cells (%) | CD19+ B cells (%) | CD14+ Monocytes (%) |
|--------------------------------|----------------------------|---------------------------------|-----------------------------------|---------------------------------|----------------|------------------|------------------|----------------------|-------------------|---------------------|
| Donor 1 | 150 | 3.5 | 560 | 410 | 96.2 | 97.4 | 3.19 | 1.39 | 0.19 | 0.20 |
| Donor 2 | 150 | 2.0 | 420 | 277 | 97.4 | 98.5 | 1.06 | 1.11 | 0.18 | 0.64 |
| Donor 3 | 140 | 6.0 | 780 | 560 | 95.8 | 97.6 | 3.24 | 2.49 | 0.29 | 0.54 |
| Donor 4 | 120 | 3.0 | 496 | 261 | 97.1 | 96.9 | 1.39 | 2.00 | 0.31 | 0.37 |
| Donor 5 | 140 | 2.6 | 595 | 455 | 95.6 | 92.7 | 1.87 | 0.39 | 0.11 | 0.03 |
| Average +/- Standard Deviation | 140 +/- 12 | 3.4 +/- 1.5 | 570 +/- 140 | 393 +/- 125 | 96.4 +/- 0.8 | 96.6 +/- 2.3 | 2.15 +/- 1.01 | 1.48 +/- 0.81 | 0.22 +/- 0.08 | 0.36 +/- 0.25 |

overnight in media, we recovered 250-600 million live CD8 T cells. Therefore, we concluded that purifying lymphocytes by positive selection followed by resting them overnight was an efficient method to isolate large numbers of pure populations of normal human CD8 lymphocytes.

Assessment of CD8 T cell Activation

We assessed the degree to which the two isolation protocols activated the CD8 T cells. The lymphocytes were analyzed for activation by isolation of total RNA from the cells and assessing levels of TNF and IFNG mRNA, two transcripts that are rapidly induced from low baseline levels to high levels within one hour of T cell activation (Lindstein et al. 1989; Thompson et al. 1989; Wang et al. 2006). To address whether T cell activation occurred during the process of cell isolation, normal donor samples were processed by either positive or negative selection in parallel and then evaluated immediately for their activation status, or after resting the cells overnight. CD8 T cell RNA was isolated and reverse transcribed. cDNA was used to measure the abundance of TNF and IFNG normalized to levels of GAPDH by qPCR, as a surrogate for the level of T cell activation. GAPDH mRNA levels did not vary significantly between resting and activated T cells.

Cells that had been isolated by positive selection had increased levels of TNF and IFNG mRNA as compared to those isolated by negative selection (data not shown). Interestingly, the levels of T cell activation in cells that had been positively selected and rested overnight returned to the low baseline levels seen in T cells isolated by negative selection without resting (Figure 3.3). It is likely that cells isolated by positive selection either revert to a resting state overnight or die overnight and are lost from analysis. We

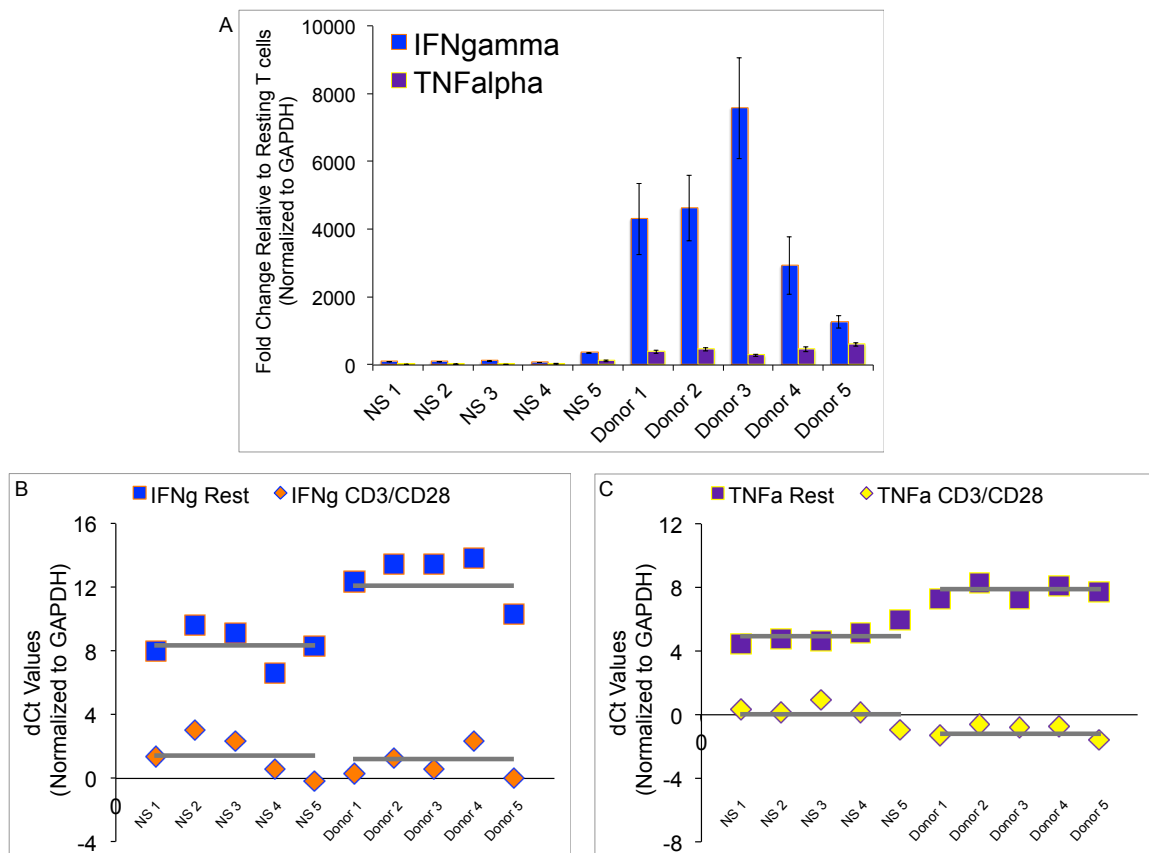


Figure 3.3 CD8 T Cell Activation qPCR Analysis. IFNG and TNF mRNA in resting and activated CD8 T cells was analyzed by qRT-PCR. (A) IFNG or TNF mRNA levels were normalized to GAPDH. Plotted is the fold change of these transcripts in CD3/CD28 stimulated CD8 T cells relative to resting CD8 T cells mRNA for five normal human donor samples prepared either by negative selection (NS) or positive selection (Donor). (B) Ct values for GAPDH mRNA were subtracted from the Ct values for IFNG mRNA (dCt) for resting or CD3/CD28 stimulated CD8 T cells for each donor. Gray bars indicate the average dCt value for each group of T cells. (C) Ct values for GAPDH mRNA were subtracted from the Ct values for TNF mRNA (dCt) for resting or CD3/CD28 stimulated CD8 T cells for each donor. Gray bars indicate the average dCt value for each group of T cells.

conclude that where large numbers of cells are needed, it is preferred to take advantage of the increased efficiency and purity of the positive selection process and rest the cells overnight to return them to a quiescent state. We observed that processing the cells for plating and harvesting them for one hour in media without CD3/CD28 stimulus after resting the cells also induced small but measurable amounts of cytokine production (data not shown). Thus, to maximize the signal seen by activating the cells with the CD3/CD28 stimulus, 'resting' cells were collected and processed for the subsequent assays without any further manipulation or incubation.

We also examined whether the level of activation with CD3 and CD28 stimulation would be altered by either isolation method or by resting the lymphocytes overnight. We found that the cells reached a similar level of activation after an hour stimulus with the CD3/CD28 beads if they had been isolated by either negative selection or positive selection with resting overnight (Figure 3.3). We concluded that the cells were able to achieve a maximal activation state with CD3/CD28 stimulation after either method of purification. Consequently, the large difference in the fold change seen with activation of negatively selected or positively selected and rested CD8 T cells was due to a difference in the amount of TNF and IFNG transcript present in the resting T cells rather than a marked difference in the absolute amount of activation of the cells with one hour of stimulation.

To maximize the purity of the isolated sample while preserving the resting state of the cells, we concluded that the T cells should be isolated by CD56 depletion and positive CD8 selection and then rested overnight. Following the resting period, non-stimulated

cells would be immediately processed and frozen for subsequent assays while another aliquot of cells would first be stimulated for an hour in culture with CD3/CD28 beads.

Ago protein levels with T cell activation

To determine if the levels of Ago increase during T cell activation, a pilot experiment of a stimulation time course was done for a series of time-points ranging from no stimulation to 72 hours of activation with CD3/CD28 beads. We separated lysates by SDS-PAGE and visualized Ago protein by western blot. We analyzed a fixed number of cells after different periods of time in culture with or without activation. This showed that while there was no significant induction of Ago with one hour of stimulation, the levels of Ago protein per cell did increase with time in culture as noted at the 16-hour time point. This induction stayed constant for cells grown in media alone, but continued to increase with time when stimulated with CD3/CD28 beads. It was also seen that the Ago signal on a western blot of 300,000 T cells was comparable to that of less than 2% of a mouse cortex (Figure 3.4). From this observation we estimate that the amount of Ago in a mouse cortex is roughly equivalent to that in 20 million human CD8 T cells. We conclude that on the order of 10-100 million lymphocytes may be necessary for subsequent Ago HITS-CLIP assays and that activation of T cells for one hour does not significantly change the amount of Ago material available for analysis.

Discussion

In this chapter, we established a system for analysis of the effects of T cell activation on RNA regulation. This entailed several aspects of investigation beginning with the

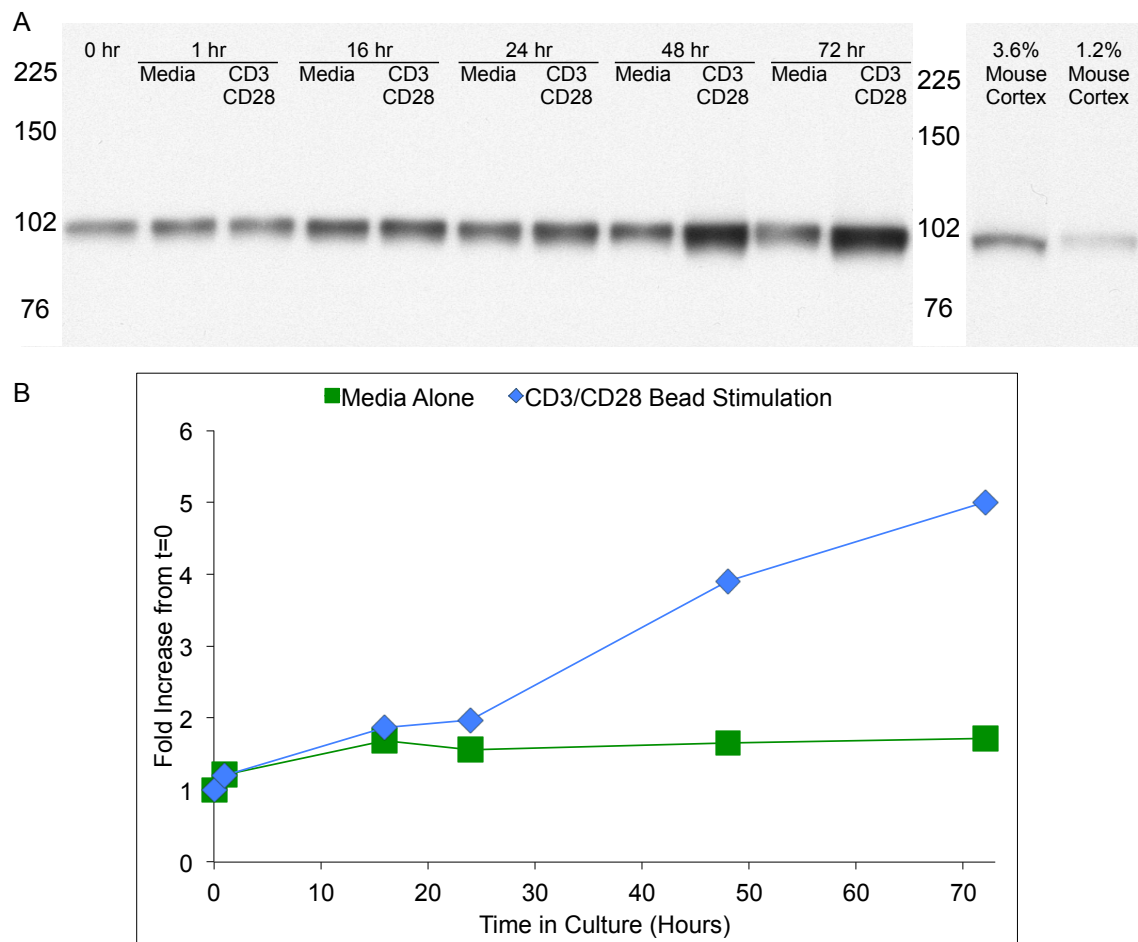


Figure 3.4 Ago Protein Levels with CD8 T Cell Activation in vitro. (A) Cell-equivalent aliquots of CD8 T cells were analyzed by western blotting for Ago (with Rabbit polyclonal Ago2/eIF2C2 specific ab32381) after the time in culture in media alone or with stimulation by CD3/CD28 beads as indicated above each lane. Percentage of C57BL/6 wild-type cortex lysate analyzed as indicated. (B) Quantitation of Ago levels by phosphorimager analysis of (A) normalized against time=0 hours (n=1).

establishment of methods to reproducibly obtain purified populations of CD8 lymphocytes from normal human donors. We examined the effects of these T cell purification methods on the activation state of the resulting lymphocyte populations using the qPCR assay we developed to compare levels of activation with and without stimulation. Finally, we examined the corresponding abundance of Ago proteins after CD3/CD28 interrogation of the T cells.

One hour of stimulation with CD3/CD28 beads was chosen for our assays because at this time point there was a dramatic increase in both TNF and IFNG mRNA and by this time it has been shown that HuR has already partially shuttled from the nucleus to the cytoplasm with stimulation (Lindstein et al. 1989; Thompson et al. 1989; Wang et al. 2006). Because Ago and HuR have been implicated in regulating rapid changes in mRNA localization and stability, such as the movement of targeted transcripts in or out of stress granules or active polysomes, we chose to investigate an early time point in the lymphocyte activation process (Bhattacharyya, Habermacher, Martine, Closs, and Filipowicz 2006a; 2006b; Leung and Sharp 2007; 2010). It was hypothesized that at one hour of stimulation, a sufficient number of cells would be present in the activated status and that the regulation of the HuR and Ago could be determined during the initiation of the activation response and induction of the new transcriptional program.

It would be interesting to examine the regulation by HuR and Ago at even earlier time points in this signaling cascade. However, since each cell may not be activated simultaneously, the status evaluated biochemically at one hour can be seen as the sum of events leading up until this time. Later time points could also be interesting to study, but

we thought it might be more straight forward to see direct effects of these regulators at an earlier time rather than a later one. Hao and Baltimore described that the inflammatory response of macrophages in response to TNF α could be grouped into three sets of genes. Those that peaked in expression at half an hour after activation, after two hours of activation, and genes that increased more steadily with the stimulus and peaked at 12 hours after activation (Hao and Baltimore 2009). We thought that looking at the regulation of RNA at one-hour post T cell activation might provide interesting insight into the regulation of these rapidly changing transcripts as different groups of genes are being simultaneously induced and silenced during the inflammatory sequence (Hao and Baltimore 2009; Hargreaves, Horng, and Medzhitov 2009; Ramirez-Carrozzi et al. 2009; Smale et al. 2012).

We examined the efficiency of purifying CD8 T cells using different protocols. We found that we could generally achieve greater purity of the cell populations with positive selection than negative selection and could expect roughly 95% purity of CD8 lymphocytes. Interestingly, we found that the T cell purification process had a significant impact on cell activation. Positive selection of CD8 lymphocytes left the cells in a more activated state than by negative selection as determined by our assay measuring TNF and IFNG transcription by qPCR. We hypothesize that binding of antibody to the CD8 co-receptor may have led to crosslinking of other cell surface receptors that mediate downstream signaling in the lymphocytes leading to the induction of immediate early genes. Fortunately, we found that this activation during the purification process could be overcome by resting the cells in culture overnight. This achieved a reversal of the activation of these transcripts that was seen with purification. Furthermore, cells could

be activated to comparable levels with stimulation by CD3/CD28 beads after the resting period as seen with the stimulation of freshly negatively selected lymphocytes.

It was important to first establish general mechanisms of regulation with T cell stimulation as described in this work to understand any processes unique to specific responses. Nevertheless, the protocol we established suggests that this purification method could be extended to study more specific populations of T cells. Antigen-specific cells can be purified by fluorescent-activated cell sorting using labeled synthetic MHC-tetramers. Our data suggest that if this extended isolation process led to activation of the cells, it is possible that they could be rested to return them to a quieter state *in vitro* prior to stimulation. In this way, the molecular processes mediating such responses such as anti-viral, anti-tumor, or autoimmune reactions and the differences in signaling mediating them could be studied. In these systems, using an APC could introduce difficulties distinguishing the responses of stimulators and responders in the subsequent assays. Thus, we thought using a cell-autonomous method for stimulation might decrease background and allow for analysis of earlier time points of cellular regulation without further purification of the lymphocytes from stimulators. Nevertheless, we understand that stimulation with CD3/CD28 beads is a very strong agonist and that it can activate different subsets of cells simultaneously, which may be pre-programmed for different responses, confusing the subsequent results.

Because Ago HITS-CLIP is less efficient than HuR in yield of the radiolabeled RNA co-precipitated with each protein (data not shown), it was thought that stimulating the cells might increase this signal and help to decrease the number of cells needed for analysis.

The levels of Ago did increase with T cell stimulation in culture, but not within the timeline that was pursued for further experiments. The size of the cells in culture also increased with activation and expansion and this difference in cellular volume could explain the increase in Ago with stimulation. HuR expression has also been shown to increase with T cell stimulation and the induction of the cell cycle, still as in the case of Ago expression, it is unlikely that this would have a significant effect on these experiments due to the short time course of stimulation (Atasoy et al. 1998; Sakai et al. 2003).

CHAPTER 4. Determination of HuR *in vivo* Binding Sites in Resting and Activated T cells

Introduction

Lymphocytes are required to rapidly respond to changes within their host, such as during an encounter with antigen. Therefore, it is logical that much of their protein expression be regulated at the translational level. RNA-binding proteins can help to regulate mRNA translation in a number of ways. These include the regulation of mRNA turnover, localization, and access to ribosomes, mechanisms that are not mutually exclusive. For example, RNA-binding proteins can harbor latent transcripts in cytoplasmic granules as a means regulating their stability and ability to be translated. In this state, transcripts can be translated almost instantaneously, which is congruous with the rapid responses seen from lymphocytes. Alternatively, RNA-binding proteins can also rapidly shuttle in and out of stress granules, presumably in conjunction with bound mRNAs, to mediate translational silencing and potentially degradation (Anderson 2010).

Within T cells, rapid changes in the production of proteins such as cytokines is known to involve RNA-binding proteins. The expression of cytokines in T cells needs to be transient in order to avoid damage to cells in the surrounding microenvironment after an antigen-specific response. RNA-binding proteins can ensure this by targeting cytokine mRNA transcripts for rapid degradation or repressing cytokine translation (Anderson 2008). To better understand the immune response in lymphocytes, and as a surrogate system for understanding general principles of dynamic RNA-binding protein regulation

of mRNA translation, we have undertaken a large-scale approach to analyze the post-transcriptional regulation of T cell cytokines.

We hypothesize that HuR plays a critical role in shaping the immune response with cluster of differentiation eight (CD8) T cell activation. HuR has been shown to regulate cytokine production in T cells, including regulating interleukin (IL)-13, IL-4, interferon gamma (IFNG), and tumor necrosis factor (TNF) (Brennan and Steitz 2001; J. G. Wang et al. 2006; Yarovinsky et al. 2006). HuR is thought to promote stabilization of cytokine mRNA transcripts upon T cell activation by binding to AU-rich elements (ARE) in the 3' untranslated region. HuR binding can either promote or inhibit translation due to cooperative and competitive interactions with other RNA-binding proteins. Together the bound proteins determine the fate of the transcript (Anderson 2008; Casolaro et al. 2008; Fan and Steitz 1998; Myer, Fan, and Steitz 1997). Most research to date investigating the targets and effects of HuR binding has been studied *in vitro* with reporter constructs or by over expressing HuR, leading to non-physiologic conditions. Furthermore, there is evidence that RNA-binding proteins can associate with transcripts after a cell has been lysed for immunoprecipitation leading to false targets of regulation (Mili and Steitz 2004). Thus, previous studies examining HuR function during T cell activation using RNA immunoprecipitation without crosslinking may not represent *in vivo* interactions between HuR and RNA and do not point to discrete binding sites within the RNA molecule. Moreover, HuR binding sites have been mapped using the photoactivatable ribonucleoside crosslinking and immunoprecipitation (PAR-CLIP) approach, but its requirement for incorporating a photo-activatable nucleotide analog into RNA limits is

use to cell culture systems that may not preserve biologically meaningful binding sites or dynamic changes in cellular states (Mukherjee et al. 2011).

Here we have employed more rigorous biochemical techniques for analyzing RNA-protein interactions in live cells to the study of lymphocyte dynamics. We have used a powerful platform technology developed in the lab, high-throughput crosslinking immunoprecipitation (HITS-CLIP) (Figure 4.1). In this procedure, live cells are ultraviolet (UV) irradiated to crosslink protein to bound RNA. Crosslinking allows us to harshly wash immunoprecipitated RNA-protein complexes to remove cross-reacting or co-precipitating contaminants. The RNA is partially digested so that full transcripts will not be bound to the protein, but rather only RNA “tags” which are radioactively labeled. After gel-purifying the RNA-protein complexes, the protein can be digested and ligated RNA linkers are used to reverse transcribe the CLIP tags. High-throughput sequencing enables us to identify genome-wide targets of the protein of interest (Licatalosi et al. 2008; Ule et al. 2003; 2005). In this chapter we develop HITS-CLIP to examine HuR-RNA interactions in resting and activated CD8 T cells from normal human donors.

Results

Immunoprecipitation of HuR from T cell Lysate

In order to begin an experiment utilizing HITS-CLIP, it is necessary to develop a means of purifying the RNA binding protein of interest after crosslinking it to its RNA targets in cells. Most commonly used such purifications consist of immunoprecipitation. To examine whether HuR could be efficiently immunoprecipitated from normal human

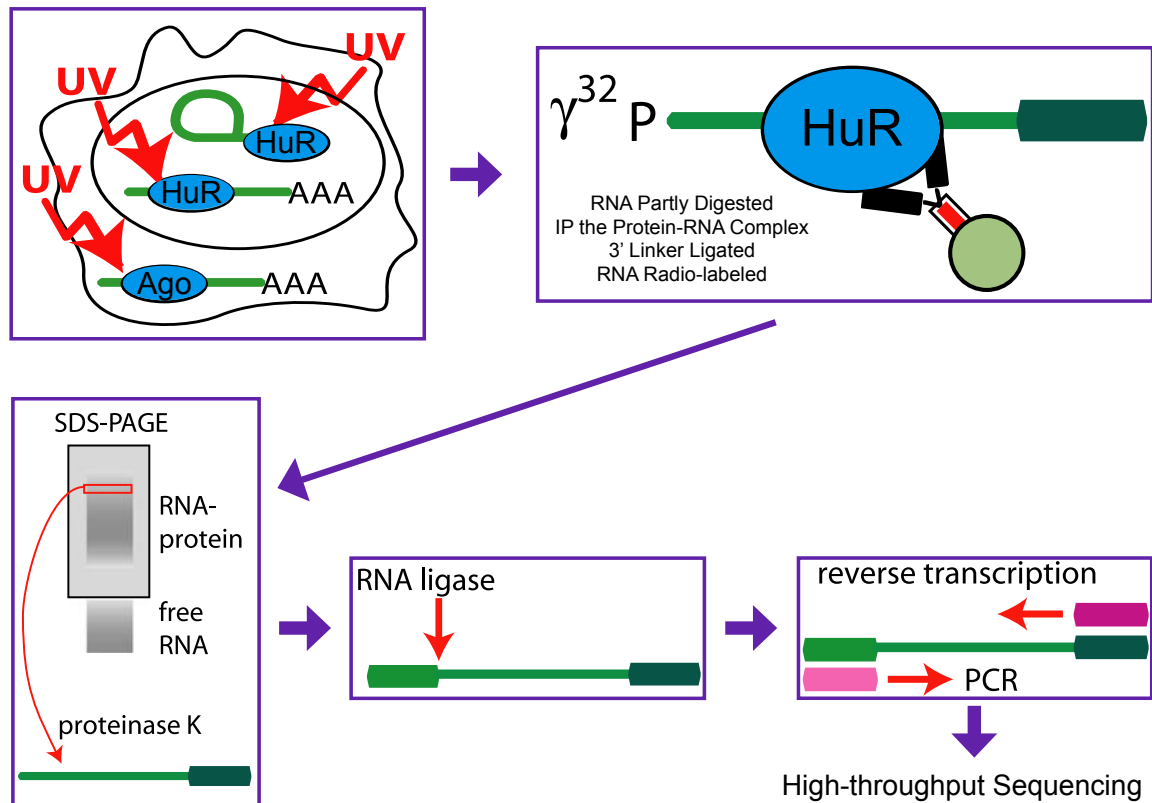


Figure 4.1 HuR HITS-CLIP Methods Schematic. UV-B irradiation penetrates live cells to induce covalent crosslinks between RNA and bound proteins that are within ~ 1 Å distance. Cells are lysed and treated with DNase to remove DNA and partially RNase digested to reduce RNA to small fragments. Once covalently bound, protein-RNA complexes can be purified under harsh conditions to remove interactions with non-crosslinked RNA and potential contaminating proteins. SDS-PAGE and transfer to nitrocellulose purify these complexes and radiolabeled RNA is visualized by autoradiogram. After size selection, the protein-RNA complexes are isolated from the membrane and proteinase K digestion removes the RNA-binding protein. The cloning method utilizes linker ligations, reverse transcription, and PCR to amplify bound targets which are analyzed by high-throughput sequencing.

donor T cells, we developed an IP protocol using a mix of two mouse monoclonal antibodies (mAbs) to HuR to increase avidity to the protein (Harlow and Lane 1988). We first bound a bridging rabbit anti-mouse mAb to protein A Dynabeads and then mixed the beads with two mouse HuR mAbs, clones 3A2 and 19F12 (Gallouzi et al. 2000; W. Wang et al. 2000). As a negative control, an aliquot of protein A Dynabeads was bound with the same bridging antibody and an irrelevant mAb to a mouse protein. The antibody-bead complexes were incubated with the isolated primary T cell lysate, and, after a series of washes in different stringency buffers, the immunoprecipitated proteins were eluted from the beads. The eluted proteins were separated on a sodium dodecyl sulfate polyacrylamide gel electrophoresis (SDS PAGE) gel and transferred to a nitrocellulose membrane. The membrane was blotted with HuR mAb 3A2 and a secondary HRP-conjugated donkey anti-mouse antibody (Figure 4.2).

A strong immunoreactive band was evident in the HuR mAb immunoprecipitation at the molecular weight of HuR (~36 kD; Figure 4.2, Lane 5). Moreover, we observed a reduction of protein at this molecular weight in the supernatant of the immunoprecipitation (Figure 4.2, Lane 3) relative to the input sample (Figure 4.2, Lane 1). As expected, we did not see an immunoreactive band in the irrelevant mAb immunoprecipitation (Figure 4.2, Lane 4) and the quantity of HuR was not significantly depleted in that supernatant (Figure 4.2, Lane 2). Together, these data indicated that the HuR antibody specifically immunoprecipitates a protein of the size expected of HuR.

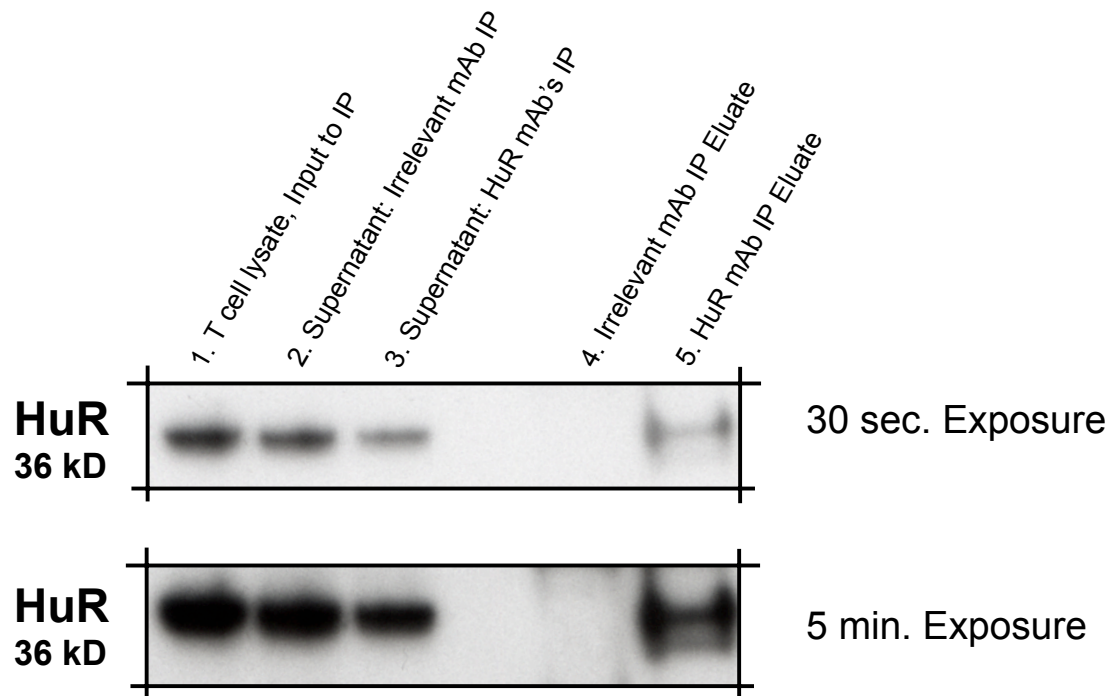


Figure 4.2 HuR Immunoprecipitation. Human CD8 T cell lysate was immunoprecipitated for HuR (with monoclonal HuR specific 3A2) or using irrelevant antibody (mouse monoclonal FMRP specific 7G1) and analyzed by western blotting for HuR (with monoclonal HuR specific 3A2). Equivalent aliquots of T cell lysate input to immunoprecipitation, supernatant from immunoprecipitation, or immunoprecipitated and eluted material were analyzed as indicated. Film exposures for 30 seconds or 5 minutes are shown.

Pilot HuR HITS-CLIP Experiment on Human T cells expanded in Culture with IL-2

The HITS-CLIP methods were used to investigate what RNA targets HuR binds in activated T cells. In preliminary experiments, we assessed whether HuR could be immunoprecipitated with crosslinked RNA in CD8 T cells expanded and growing in culture with IL-2. The T cells were crosslinked, lysed, and the RNA was partially digested prior to the immunoprecipitation to shorten the RNA “tags” that would be bound to HuR. HuR crosslinked to RNA targets was immunoprecipitated using the mixture of monoclonal antibodies specific to HuR bound to protein A Dynabeads. To optimize the stringency of the assay, IPs were washed with a series of high stringency buffers containing differing amounts of detergents and salt concentrations. RNA tags were then ligated to 3' linkers for later PCR amplification and labeled with polynucleotide kinase-mediated incorporation of radioactive ATP. The material was separated by SDS-PAGE and transferred to a nitrocellulose membrane (Figure 4.3A, Lanes 2,4). Protein-RNA complexes were cut from the membrane, the protein was digested and the RNA extracted. After adding 5' linkers and performing an RNase-free DNA digestion to remove any contaminating DNA, RNA tags were reverse transcribed, PCR amplified, and high-throughput sequenced (Figure 4.3B,C).

This first HuR CLIP pilot experiment produced nearly 9 million pre-filtered CLIP tags, of which roughly 6 million could be mapped to the human genome unambiguously. More than 300,000 were determined to be unique binding events, which is a large data set of mapped HuR regulation. Approximately half of the tags mapped to deep intergenic regions and a third were intronic sequences. Only 1% of the tags mapped to coding

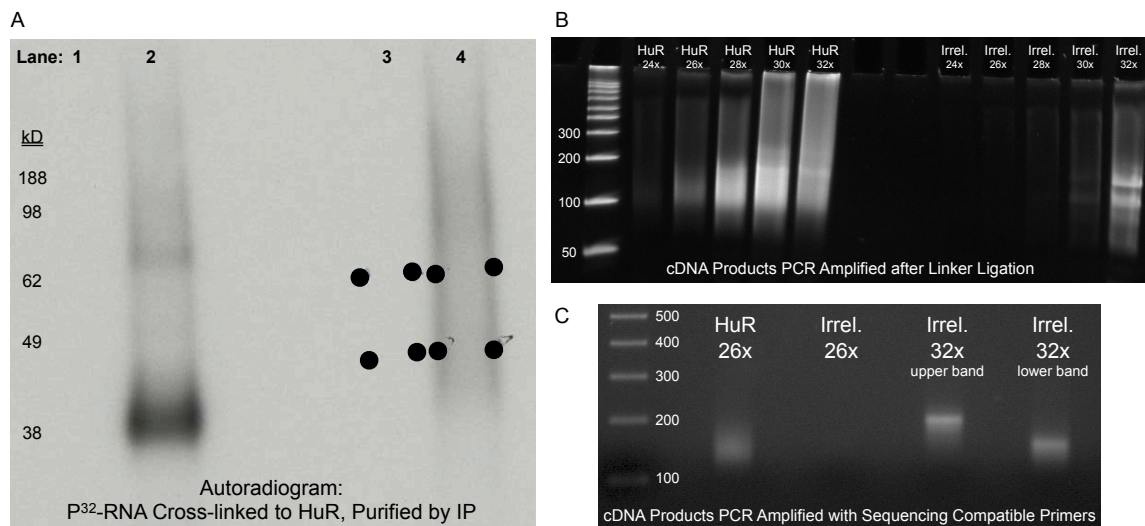


Figure 4.3 HuR CLIP: mAb Specific to HuR. (A) Autoradiogram of immunoprecipitation results from human CD8 T cells expanded in culture in IL-2 and crosslinked. Lysate was immunoprecipitated with irrelevant antibody (mouse monoclonal FMRP specific 7G1-1) in lanes 1 and 3, or with HuR antibodies (mouse monoclonal HuR specific 3A2 and 19F12) in lanes 2 and 4. Lysate treated with high RNase A concentrations in lanes 1 and 2, and low RNase A concentrations in lanes 3 and 4. 3'linker was added to RNA and then labeled by PNK with ³²P-γ-ATP, protein-RNA complexes were separated on SDS-PAGE, transferred to nitrocellulose and imaged by autoradiography. ³²P-labeled RNA was evident in HuR immunoprecipitation but not in irrelevant control immunoprecipitation. Dots indicate regions of nitrocellulose processed for RNA purification. (B) After protease digestion of the radioactive RNA-protein complexes, 5' linker was added and products amplified by RT-PCR; products of the expected size, 100-150 nucleotides, were seen after 26 cycles from HuR CLIP. (C) Final PCR products after amplification of CLIP tags with high-throughput sequencing compatible primers.

sequence with the remaining tags falling in the region surrounding the genes and in the 5' and 3' untranslated regions of genes (data not shown).

Although these data only represent one experiment, a large proportion of the genes that had the most tags in this data set matched CLIP tag maps from other neuronal Hu protein family members in the mouse brain that are being studied by other members of the laboratory in other systems, suggesting that the data are robust and that HuR targets are evolutionarily conserved.

Radioactive RNA Signal on the Autoradiogram is Specific to the HuR Antibodies

To ensure that the labeled RNA signal seen on the autoradiogram was specific to HuR and not due to an artifact of the protein A beads or the bridging antibody used to bind the monoclonal antibodies for HuR. In addition to labeling protein A beads with the bridging antibody and the two HuR monoclonal antibodies, we had prepared another aliquot of the protein A beads with bridging antibody and used another mouse monoclonal antibody that was specific to a mouse protein and should not specifically recognize any proteins in human T cell lysate.

Following immunoprecipitation with the irrelevant antibody bound beads, there was no radioactive signal from the lysate prepared with either high RNase concentration (Figure 4.3, Lane 1) or low RNase concentration (Figure 4.3A, Lane 3). As a control, we cut from the membrane at the same molecular weight as in the HuR immunoprecipitation and continued to prepare the two RNA samples in parallel. The amplified cDNA products from the HuR immunoprecipitation were visible on the gel beginning around 24 PCR

cycles. In the control sample, the cDNA was not visible until later cycle numbers and the characteristic smearing pattern of the RNase treated samples was not apparent from the irrelevant immunoprecipitation (Figure 4.3B). We isolated DNA from the lane containing products from 26 PCR cycles for both the HuR and the irrelevant antibody immunoprecipitation. Additionally we prepared DNA from the upper and lower bands in the irrelevant immunoprecipitation that were visible at 32 PCR cycles.

In the control PCR reactions with the irrelevant antibody purification material from 26 cycles of the first PCR, we were not able to amplify products to add the sequencing compatible sequences. The contaminating bands that had been visible with later PCR cycles from the irrelevant immunoprecipitation were not overlapping in size with the smear seen from the HuR immunoprecipitation (Figure 4.3C). Thus, we concluded that the RNA material isolated with the HuR immunoprecipitation was specific to the mix of HuR monoclonal antibodies.

Radioactive signal on the Autoradiogram is Sensitive to RNase A Digestion

During the CLIP experiment, we rely on radiolabeling of the RNA to visualize the material associated with the protein during immunoprecipitation. To ensure that the signal is from RNA, we treated the cellular lysate prior to immunoprecipitation with different concentrations of RNase A to show sensitivity to this digestion. With a high concentration of RNase, the RNA should be almost entirely degraded and the signal seen on the autoradiogram should be roughly that of the protein alone.

A discrete signal at around 38 kDa was visible on the autoradiogram with over digestion of the sample (Figure 4.3, Lane 2). In this lane, there are other bands at higher molecular weights, such as near 80 kDa, which is not present in the irrelevant antibody control, so is therefore specific to immunoprecipitation with the HuR monoclonal antibodies. We speculate that this could represent a dimer of HuR because it is running at double the molecular weight of the protein alone. However, it is also possible the band represents a contaminating RNA-binding protein. To ensure that these complexes do not contaminate the samples, we were careful to cut below this size when purifying RNA for cloning.

Digestion of the T cell lysate with a lower concentration of RNase A trims HuR-bound transcripts to RNA fragments. The small length of the RNA fragments will allow for precise determination of the RNA-binding site footprint of HuR rather than identifying the entire transcript as a target of regulation. These digested fragments will not be uniform in size and will therefore appear as a smear of RNA signal above the expected size of the protein. In Figure 4.3, lane 4, we observed the labeled signal initiating above the size of the collapsed band in the over digested sample in lane 2. Thus, the radioactive labeling pattern on the membrane is RNase A sensitive, demonstrating that the labeled material immunoprecipitated with HuR is RNA.

Radioactive RNA Signal on the Autoradiogram is Dependent on Crosslinking

In order to study native *in vivo* binding interactions between HuR and RNA, we rely on crosslinking live cells to covalently link the RNA binding protein to its targets. The UV irradiation should only crosslink interactions that are on the order of a single angstrom in distance. With sufficiently stringent washing protocols, we can dissociate non-

crosslinked RNA from immunoprecipitating with the protein of interest and deplete re-association artifacts of the protein with RNA during the immunoprecipitation.

To confirm that radiolabeled protein-RNA complexes are UV-dependent, we used both crosslinked and non-crosslinked samples as the input to immunoprecipitation. Using crosslinked samples, we were able to see labeled signal in both the high and low RNase treated samples at the expected size of HuR or a smear above that size respectively. But, without crosslinking, we were unable to detect an RNA signal (Figure 4.4). Therefore, the RNA signal is dependent on the *in vivo* crosslinking and not due to random association of the protein and RNA available during immunoprecipitation. Furthermore, the lysis and washing conditions are sufficient to dissociate all measureable RNA signal from immunoprecipitated HuR.

HuR CLIP in Mouse CD8 T cells

The HuR protein is highly conserved between human and mouse. In addition to the human lymphocytes, we crosslinked mouse T cells to determine if we could detect an RNA signal from immunoprecipitation of murine HuR. We purified CD8 T cells from mouse spleen by negative selection similarly to the protocol outlined for human peripheral blood cells. Briefly, spleens were quickly extracted from sacrificed C57BL/6 mice. The spleens were mashed with the back of a syringe in ice cold PBS until a single cell suspension was achieved. These cells were harvested into a tube and spun down. The cells were then incubated in a suspension of PBS, fetal bovine serum, and magnetic beads with antibodies conjugated to a mix of non-CD8 T cell surface markers. Non-

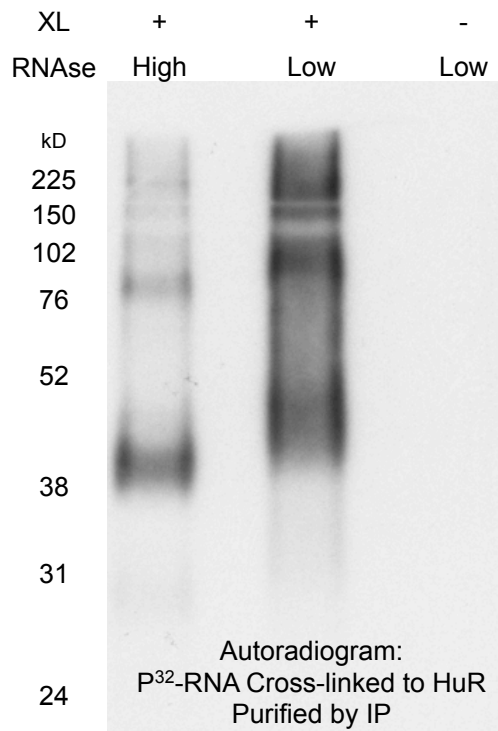


Figure 4.4 HuR-RNA Complexes are Crosslinking Dependent. Autoradiogram of immunoprecipitation results from human CD8 T cells expanded in culture in IL-2 and prepared with or without crosslinking. Lysate was immunoprecipitated with HuR antibodies (mouse monoclonal HuR specific 3A2 and 19F12). ^{32}P -labeled RNA was evident in HuR immunoprecipitation with crosslinked lysate, but not from non-crosslinked lysate.

CD8+ cells were bound to a magnetic column and CD8+ cells were collected as flow-through, with roughly 90% purity (Figure 4.5).

Cross-linked and non-cross-linked cells were processed for HuR CLIP as described above. As seen with the material from the human immunoprecipitation, with a high concentration of RNase A treatment of the lysate, the labeled RNA bound to HuR collapsed to a band at the expected size of the protein. With lower amounts of RNase added to the lysate, a smear of RNA was seen above the expected size. Unfortunately, in this experiment, even the low concentration of RNase yielded products that appeared slightly over digested, although there was still ample signal for subsequent cloning. Importantly, the RNA signal was crosslinking dependent, as no signal was observed in the lane on the membrane that derived from non-crosslinked T cell lysate (Figure 4.5). We were encouraged that the results we were able to see in the human samples were not species specific.

Numbers of T Cells Necessary for HuR CLIP

The first human HuR T cell CLIP experiment previously described was performed on cells that had been expanded in culture. Although this is a valid method to produce large numbers of T cells, prolonged activation *in vitro* is likely to undermine the physiologic relevance of the system. To assess the number of lymphocytes required for HuR CLIP, we titrated the amount of crosslinked T cell lysate that was used as input for HuR immunoprecipitation. The RNA bound to HuR was radiolabeled and visualized by autoradiogram after being separated by SDS-PAGE and transferred to nitrocellulose. We could visualize a strong signal from immunoprecipitated RNA from the lysate of 0.5

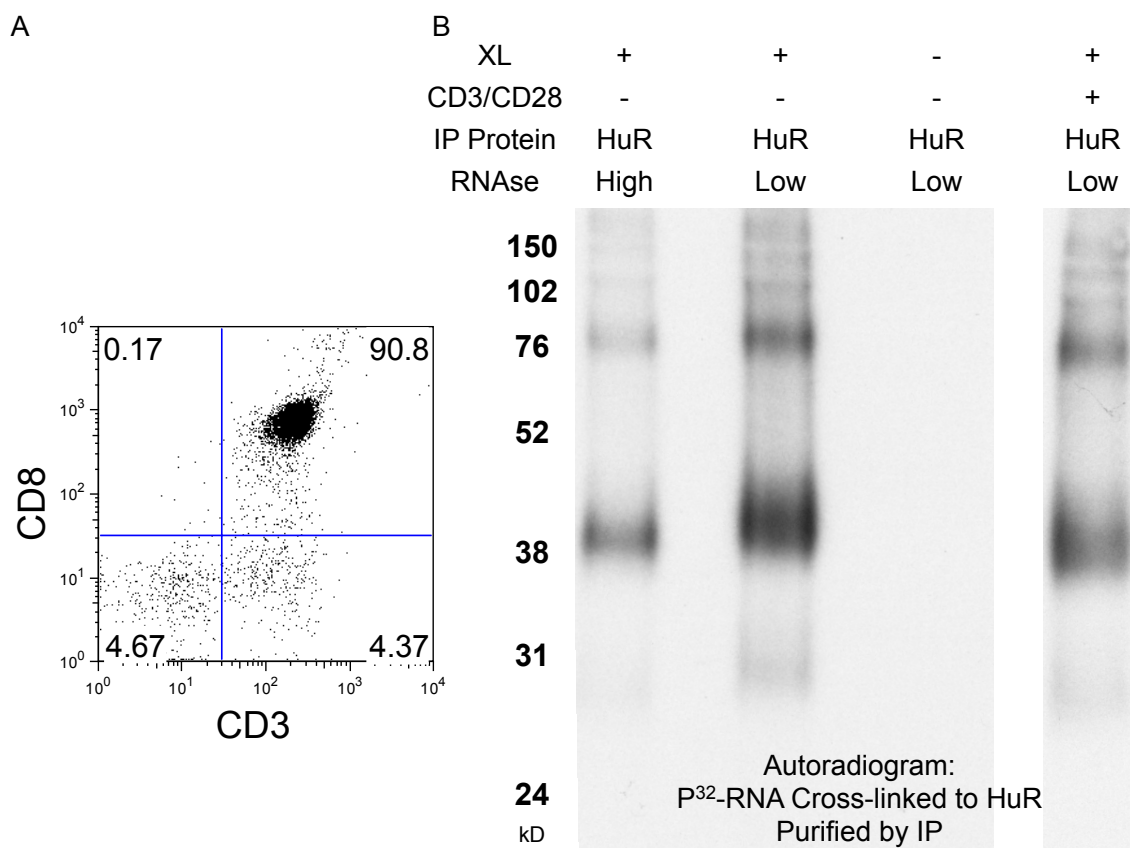


Figure 4.5 HuR Mouse CD8+ T Cell CLIP. (A) CD8 T cells purified from splenocytes of wild-type C57BL/6 mice and purified by negative selection. CD3 and CD8 staining determined by flow cytometry. Percentages of cells are noted in each quadrant. (B) Autoradiogram of immunoprecipitation results from resting and CD3/CD28 stimulated mouse CD8 T cells prepared with or without crosslinking. Lysate was immunoprecipitated with HuR antibodies (mouse monoclonal HuR specific 3A2 and 19F12). ³²P-labeled RNA was evident in HuR immunoprecipitation with crosslinked lysate from resting and activated mouse lymphocytes, but not from non-crosslinked lysate

million normal human T cells, almost twenty-fold less than we used for the pilot experiment described above (Figure 4.6). This will allow for the use of fresh samples that have not been distorted by cell culture conditions. With the ability to use low numbers of cells for the identification of HuR-bound RNA, these methods may be applied to the investigation of antigen-specific lymphocyte responses from patient samples or other cellular populations of interest. Still, the complexity of the pool of sequenced RNA may be proportional to the amount of starting material due to our current dependence on PCR amplification of cloned tags, so the initiation of the protocol from larger cell numbers would be preferred.

HuR HITS-CLIP from Five Normal Donor Resting and Activated CD8 T cells

As described in the previous chapter, CD8 lymphocytes were isolated from normal human donors and prepared for analysis by HITS-CLIP. Briefly, five healthy normal donors were leukapheresed and the material was layered onto and spun through a Ficoll gradient. The resulting layers of collected PBMCs were depleted of CD56+ cells and then positively selected for CD8+ cells. The eluted CD8 lymphocytes were rested overnight in media. The following morning, T cells were harvested and aliquots of lymphocytes were crosslinked immediately or after being stimulated in culture for one hour with CD3/CD28 beads. The T cells were crosslinked with UV-B irradiation. The purity of the cells was determined by flow cytometry to be greater than 90% CD8 lymphocytes, and analyzing TNF and IFNG mRNA levels by RT-qPCR confirmed the activation status (Table 3.1). The cells displayed between roughly 300 and 600 fold inductions of TNF mRNA and 1000 to 8000 fold inductions of IFNG mRNA (Figure 3.3).

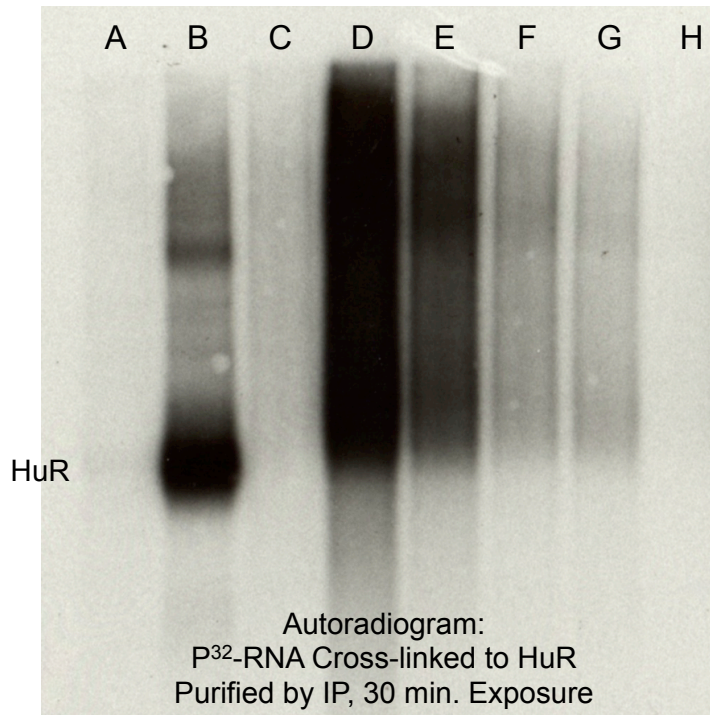


Figure 4.6 HuR CLIP CD8+ T Cell Titration. Autoradiogram of immunoprecipitation results from human CD8 T cells expanded in culture in IL-2 and crosslinked. Aliquots of lysate corresponding to 10 million (C,D), 5 million (A,B,E), 1 million (F), 0.5 million (G) or 0.1 million T cells (H), were immunoprecipitated with HuR antibodies (mouse monoclonal HuR specific 3A2 and 19F12) (B, D-H) and irrelevant antibody (mouse monoclonal FMRP specific 7G1-1) (A,C). ^{32}P -labeled RNA was evident in HuR immunoprecipitation from lysate starting at 0.5 million T cells.

For three of the five donors, the T cell lysates were prepared and used first for Ago HITS-CLIP experiments described in the Chapter 5. HuR was then immunoprecipitated from the same lysates to perform comparisons with identical starting material. However, this approach raised the potential concern that carry-over from the Ago experiment could contaminate HuR HITS-CLIP data. To address this possibility, HuR HITS-CLIP for the other two donor samples was performed without prior Ago depletion. Additionally, different, uniquely indexed RNA linkers were used for these two additional donors so that potential contamination of sequenced RNA tags with tags from previous experiments could be unambiguously assessed. HuR HITS-CLIP was performed as described above.

Overview of RNA Tag Statistics

In total, we sequenced material from five normal donor CD8 T cell samples activated for one hour with CD3/CD28 beads and from four paired resting samples. From each sample we were able to get between 9 and 38 million sequencing reads from each high-throughput sequencing run. Because of the PCR amplification and saturation of sequencing of samples, the number of total reads did not necessarily dictate the final counts of unique mappable reads. For example, the largest number of processed usable RNA tags came from a sample that had a starting number of only 13.6 million total reads, while the smallest number of unique mappable reads, from a sample sequenced in its own lane, started with 28 million total reads. To process this large amount of data, first we removed all duplicate copies of reads, leaving only one of each exact sequence. This reduced the total number of reads to between 1.8 to 10.4 million sequences. These sequencing reads were then mapped to the hg18 build of the human genome. The

percentages of sequences mapping to unique positions within the genome ranged from 41 to 70% (Table 4.1).

In preparing the sequencing libraries, we used ligated RNA linkers to clone and amplify the RNA bound to HuR. Within the sequence of the 5' RNA linker, we included a four base random degenerate code, which can consist of 256 different possible sequences. Different degenerate barcodes would therefore be ligated to each individual piece of RNA to be cloned from the same genomic location. This barcode is meant to distinguish between identical cross-linked tags that were independently isolated and ligated to linker, which are biologically informative, from likely PCR amplified duplicates, which are not. This also gives us the ability to monitor contamination between the preparations of different sequencing libraries. These barcodes allowed us to collapse sequences that mapped to exactly the same start and stop site in the genome and also contained the identical barcode; we term these collapsed products unique mappable reads or CLIP tags. Each sample produced between 400,000 and 1.2 million unique mappable reads (Table 4.1).

In addition to the four nucleotide degenerative barcode, for the three samples prepared from fresh T cell lysate, we used an additional two-nucleotide index within the 5' linker. These additional bases allowed us to distinguish the sequences from each sample when the final material was pooled and sequenced together. For these samples, together the sequencing produced over 500,000 unique mappable reads which then collapsed to roughly 150,000 unique reads per sample (Table 4.1). In Table 4.1, the colors highlighting each individual donor sample will be used to indicate sequencing reads from

Table 4.1 HuR CLIP Tag Statistics.

| Resting HuR | Total Reads | Total Reads (One Copy) | Mappable Reads (One Copy) | Unique Mappable Reads | % Total Reads (One Copy) |
|-------------------|-------------|---------------------------|---------------------------------|-----------------------------|-----------------------------|
| Donor 1 | 34,680,120 | 8,423,102 | 3,934,897 | 658,968 | 7.82 |
| Donor 2 | 37,475,646 | 10,390,637 | 4,593,807 | 706,821 | 6.80 |
| Donor 3 | 28,162,328 | 5,254,520 | 2,538,822 | 400,103 | 7.61 |
| Multiplex: | 30,671,330 | 1,914,692 | 1,190,522 | 515,861 | |
| Donor 4 | --- | --- | --- | 143,101 | |

| Activated HuR | Total Reads | Total Reads (One Copy) | Mappable Reads (One Copy) | Unique Mappable Reads | % Total Reads (One Copy) |
|------------------|-------------|---------------------------|---------------------------------|-----------------------------|-----------------------------|
| Donor 1 | 13,595,577 | 3,029,521 | 2,093,555 | 1,154,523 | 38.11 |
| Donor 2 | 11,851,138 | 2,297,658 | 1,412,266 | 587,257 | 25.56 |
| Donor 3 | 9,047,999 | 1,848,374 | 1,105,861 | 539,178 | 29.17 |
| Donor 4 | --- | --- | --- | 175,523 | |
| Donor 5 | --- | --- | --- | 141,819 | |

that donor in the CLIP tag representations in subsequent figures from the genome browser. This enables us to distinguish the results between the donors and compare the binding events between activation states for each donor.

In total, we cloned 1.9 million unique tag reads for the resting T cells and 2.6 million in the activated state. These CLIP experiments were the first to produce such large numbers of data and represent an expansive network of HuR regulation of RNA in the resting and activated states of CD8 lymphocytes.

Reproducibility of Binding between Biologic Replicate Samples

We were interested in focusing on sites of regulation where the binding events were abundant and reproducible between the different donor samples. To do this, we developed a program to cluster CLIP tags. We designated tags as belonging to a cluster if their genomic locations overlapped by at least 5 nucleotides. Next we specified that within each cluster there must be 5 tags overlapping in at least one nucleotide genomic position, termed a peak height of at least 5. For this analysis, we excluded nine clusters that had over 1,000 reads because they seemed to skew the correlations to be higher and we were not sure if these were specific binding events. To determine the reproducibility of binding between the data sets produced from the different samples, we calculated the absolute value of the Pearson correlation coefficient of the number of tags per cluster between each donor in both the resting and activated states shown in Figure 4.7.

We found very high correlations, r of greater than 0.9 between the datasets for the donors processed from the same activation state and prepared from the same kind of lysate

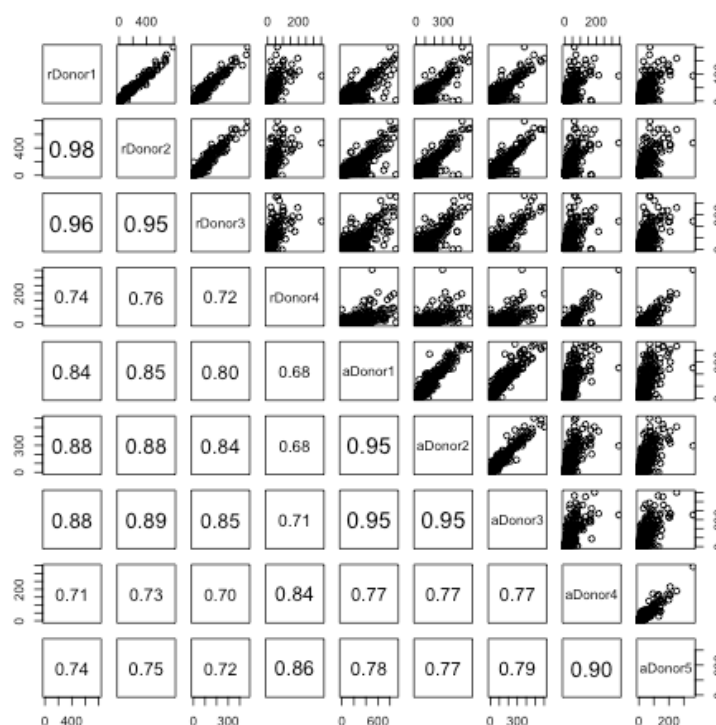


Figure 4.7 Pairwise Correlation of HuR CLIP Clusters. Upper half of table: Pair-wise scatter plots displaying the number of tags per cluster of HuR CLIP tags contributed to the cluster by each resting (r) or activated (a) donor sample as indicated. Lower half of table: absolute value of the pair-wise Pearson correlation coefficient of the number of tags contributed to each cluster by each resting or activated donor sample. The size of text is scaled to the correlation value. Clusters needed to contain a minimum of 5 overlapping tags at one nucleotide position to be included in either analysis.

(either supernatant from prior Ago immunoprecipitation or fresh T cell lysate). There was slightly lower correlations between samples processed from the same kind of lysate but in different activation states, ranging from $r=0.84-0.89$ which may represent the differences in HuR binding with and without T cell activation. The correlations were a little lower still for comparing samples processed from Ago supernatant to those from fresh T cell lysate. This may represent some difference in the lysates due to the Ago immunoprecipitation in one and not the other, but we think it is more likely that the differences are due to the sequencing depths between these samples. Because we started with lysate from a larger number of cells for those prepared from the Ago supernatant, we were able to clone a larger number of unique reads (ranging from 400,000 to over 1 million reads). The samples from fresh T cell lysate were not only just from smaller numbers of starting material, but were also multiplexed and sequenced on in the same lane of the sequencer which resulted in less than 200,000 unique reads for those samples. Moreover, as the sequencing depth was lower, it is more likely that a tag from those experiments will not be represented in any given cluster, lowering the correlation coefficient. Even with these caveats, the correlation coefficient between any two samples was at least $r=0.68$ which represents great reproducibility of binding.

For further analysis, we also specified that there be at least three of the five donor samples represented in each cluster in either the resting or the activated state to demand biologic reproducibility in each binding site. Additionally, for each cluster we required that at least one tag be present from the multiplexed barcoding experiment to ensure that the cluster was not due to an artifact of the Ago immunoprecipitation. With these criteria, we determined over 24,000 sites of robust and reproducible HuR binding. Nearly 6,000

of these clusters showed reproducible binding of at least biologic complexity of 3 and a peak height of 5 in both the resting and the activated states. Interestingly, there were a lot of clusters that changed dynamically with activation and were only present at this stringency in either the resting state (3,481 clusters) or the activated state (14,657 clusters) (Figure 4.8). We were surprised to find more than 4-fold the number of robust binding sites exclusively in the activated state as compared to the resting state with only a third more unique reads. These results began to demonstrate the dynamic changes in HuR binding that quickly occur with T cell activation.

Genomic Distribution of HuR Binding Sites

In order to gain a global view of HuR regulation, we determined the location of HuR Clusters of biologic complexity 3 (including a tag from the indexed experiment) and peak height of 5. We were surprised to find that half to two-thirds of reproducible HuR binding sites fell in the intronic regions of target RNA molecules. The next most represented region of RNA was the 3' untranslated region (3'UTR) or within 10 kilobases of stop codons, which most likely denote un-annotated 3'UTR regions of transcripts (Licatalosi et al. 2008). These regions at the 3' end of transcripts represented 21-30% of HuR clusters. Less than 10 percent of clusters fell within the 5'UTR, coding sequence, or deep intergenic regions of the genome. These intergenic clusters may represent un-annotated RNAs. The distribution of HuR binding along target transcripts was not altered greatly between the data sets of regulation seen in resting T cells or activated T cells. In clusters present in both the resting and the activated states, we saw a

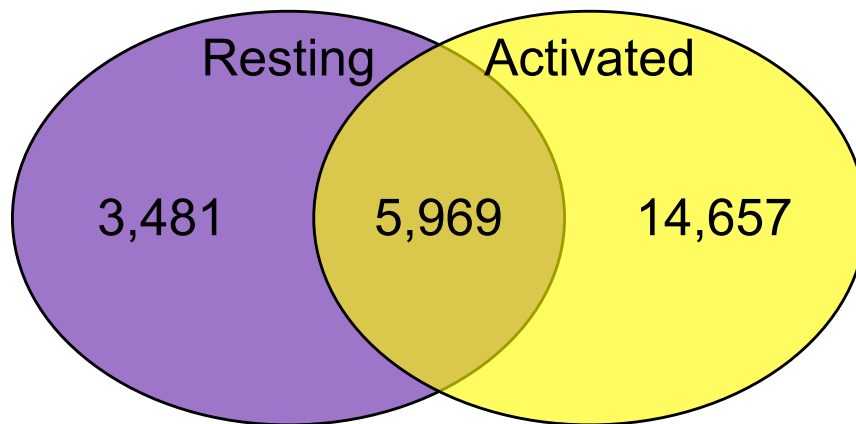


Figure 4.8 HuR Clusters Activation State Distributions. Venn diagrams show the overlap between HuR target clusters in the indicated activation states with the number of clusters including 3 biologic donor samples and a peak height of at least 5 CLIP tags shown.

larger proportion of binding in the 3'UTRs of transcripts than in either state alone (Figure 4.9).

Top Hexameric Sequences Represented in HuR Binding Dataset

To investigate whether there was a conserved motif in the binding sites across different clusters that were biological complexity of 3 and had a peak height of 5, we calculated the number of times each hexameric sequence appeared within the HuR binding sites. We compared the counts for all of the HuR binding sites together, for resting and activated sites separately, and also for binding sites that were reproducible in both the resting and activated state. For all cases, the top hexamer seen in the data sets was UUUUUU (Table 4.2). One interesting observation was the high frequency of both GUGUCA and UGUCAG in the data. These overlapping sequences were the third and fourth highest ranked hexamers in clusters present in both the resting and activated state. It was also interesting that these were less represented in the resting alone dataset and even more so in the activated dataset. This may represent different binding preferences of the protein in different cellular states. As expected, uracil was the most frequently represented base followed closely by adenine and then cytosine and guanine at a lower rate (Figure 4.10). These data correlate well with previously reported binding preferences for Hu proteins. HuR has been shown to bind U-rich elements in previously reported targets of regulation and previous work from our laboratory showed similar binding sites for the neuronal Hu family members (de Silanes et al. 2004; Ince-Dunn et al. 2012; Kishore et al. 2011; Mukherjee et al. 2011).

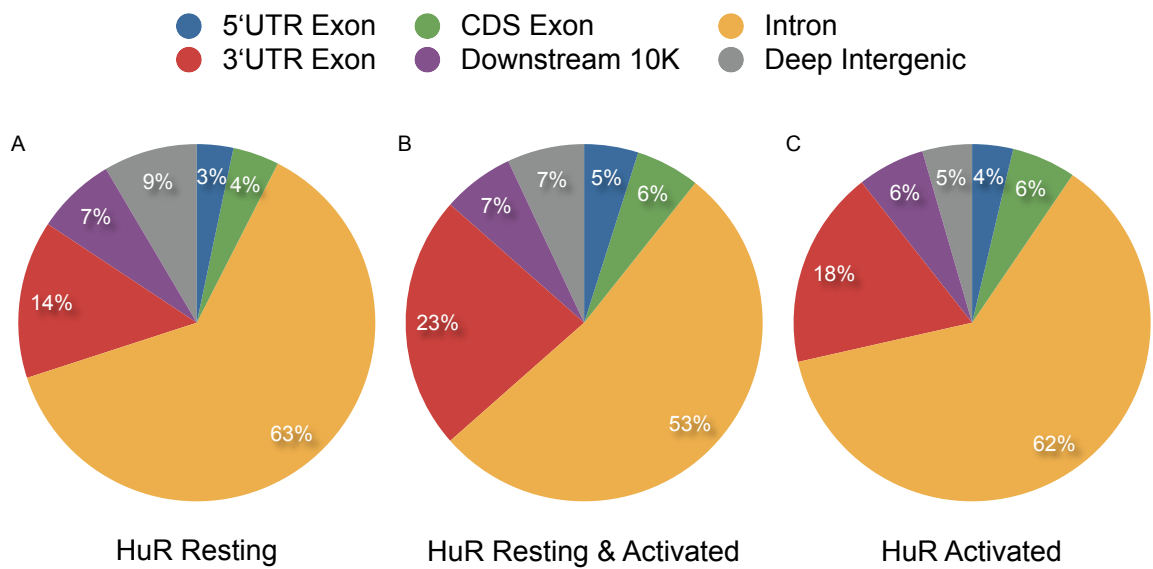


Figure 4.9 HuR Clusters Genomic Distribution. Distribution of clusters, comprised of at least 3 biologic donor samples in the resting and or activated state and a peak height of at least 5 CLIP tags, among HuR target transcripts represented by pie chart.

Table 4.2 Top Hexameric Sequences in HuR Clusters. Listed are the top 25 hexamers found in all HuR clusters representing at least three biologic donors in one activation state (biologic complexity three: BC3) and having at least five tags in the peak position of binding (peak height five: ph5). Hexamers were sorted by comparing the ratio of the observed to the expected frequency of each hexamer within CLIP tags. The ranking and absolute count of each hexamer within subsets of clusters BC3 and ph5 for the resting, activated state, or both are shown.

| Overall Rank | Hexamer | Observed Count | Observed Frequency | Observed/Expected Frequency | Resting: Rank (Count) | Activated: Rank (Count) | Both: Rank (Count) |
|--------------|---------|----------------|--------------------|-----------------------------|-----------------------|-------------------------|--------------------|
| 1 | UUUUUU | 18006 | 0.00699 | 28.6 | 1 (2166) | 1 (10191) | 1 (5649) |
| 2 | AAAAAA | 8875 | 0.00344 | 14.1 | 2 (1233) | 2 (5016) | 2 (2626) |
| 3 | UUAUUU | 6912 | 0.00268 | 11.0 | 3 (857) | 3 (4030) | 5 (2025) |
| 4 | UAUUUU | 6663 | 0.00259 | 10.6 | 5 (765) | 4 (3884) | 6 (2014) |
| 5 | UUUAUU | 6433 | 0.00250 | 10.2 | 4 (788) | 5 (3711) | 8 (1934) |
| 6 | AUUUUU | 6303 | 0.00245 | 10.0 | 7 (672) | 6 (3673) | 7 (1958) |
| 7 | UUUUUA | 5967 | 0.00232 | 9.5 | 6 (681) | 7 (3383) | 9 (1903) |
| 8 | UGUUUU | 5388 | 0.00209 | 8.6 | 10 (606) | 8 (3177) | 12 (1605) |
| 9 | UUUUAU | 5375 | 0.00209 | 8.5 | 9 (613) | 9 (3114) | 11 (1648) |
| 10 | UUUUAA | 5362 | 0.00208 | 8.5 | 12 (602) | 10 (3033) | 10 (1727) |
| 11 | UUUUCU | 5087 | 0.00197 | 8.1 | 8 (628) | 12 (2937) | 15 (1522) |
| 12 | UUUGUU | 5047 | 0.00196 | 8.0 | 15 (580) | 13 (2903) | 14 (1564) |
| 13 | UUGUUU | 5007 | 0.00194 | 8.0 | 17 (567) | 11 (2966) | 17 (1474) |
| 14 | UUUUGU | 4981 | 0.00193 | 7.9 | 16 (572) | 14 (2828) | 13 (1581) |
| 15 | UUUCUU | 4747 | 0.00184 | 7.5 | 11 (603) | 15 (2705) | 18 (1439) |
| 16 | UUUAAA | 4614 | 0.00179 | 7.3 | 20 (504) | 16 (2623) | 16 (1487) |
| 17 | GUGUCA | 4561 | 0.00177 | 7.3 | 13 (595) | 46 (1676) | 3 (2290) |
| 18 | UUUUUC | 4477 | 0.00174 | 7.1 | 22 (499) | 17 (2613) | 20 (1365) |
| 19 | UUCUUU | 4387 | 0.00170 | 7.0 | 14 (589) | 18 (2433) | 21 (1365) |
| 20 | AUUUUU | 4281 | 0.00166 | 6.8 | 21 (501) | 20 (2430) | 22 (1350) |
| 21 | UUUUUG | 4246 | 0.00165 | 6.7 | 24 (459) | 18 (2472) | 23 (1315) |
| 22 | CUUUUU | 4245 | 0.00165 | 6.7 | 23 (490) | 22 (2381) | 19 (1374) |
| 23 | UGUCAG | 4231 | 0.00164 | 6.7 | 18 (536) | 52 (1551) | 4 (2144) |
| 24 | UUAAAA | 4143 | 0.00161 | 6.6 | 26 (438) | 21 (2400) | 24 (1305) |
| 25 | UCUUUU | 3936 | 0.00153 | 6.3 | 19 (506) | 24 (2238) | 27 (1192) |

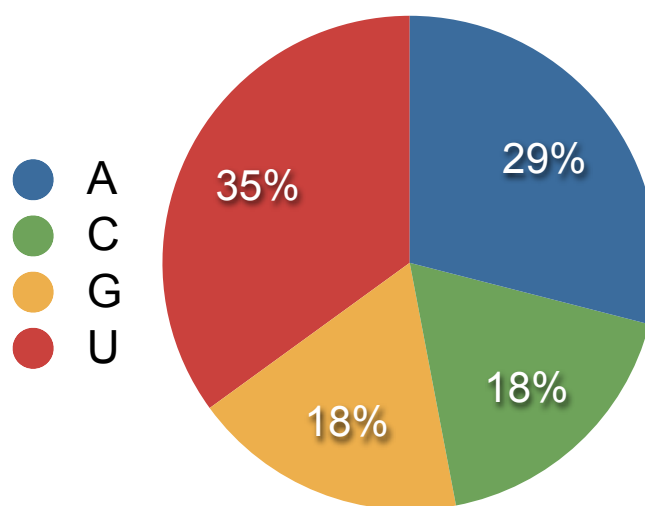


Figure 4.10 Nucleotide Frequency in HuR Clusters. The percentage of each nucleotide (adenine, cytosine, guanine, uracil) present in HuR CLIP clusters comprised of at least 3 biologic donor samples in the resting and or activated state and a peak height of at least 5 CLIP tags, represented by pie chart.

HuR Binding Changes with Activation

To help give context to HuR binding patterns and changes with activation, we did RNAseq on other aliquots of resting and activated T cells from the same pools of lymphocytes used for HITS-CLIP, absent UV-crosslinking. This allowed us to overlay HuR regulation with the expression levels of target transcripts using calculated values of reads per kilobase per million (RPKM) for each RNA transcript. Then, for each cluster we assigned a score for the relative HuR binding and transcript abundance in the resting and activated states.

As diagramed in Figure 4.11, we pooled the HuR CLIP tags from both the resting and activated state together and required that the tags overlapped at least 5 nucleotide positions to be included in a cluster. For this analysis, we specified that clusters had to be at least of biologic complexity 4 in the resting and or activated state and have a minimum combined peak height of 10 tags between the resting and activated states together. For each cluster we calculated the percentage of tags that originated from the activated state out of the total number of resting and activated tags in that cluster. Finally, we grouped binding sites into bins of whether the HuR binding and transcript expression in the activated state was greater than, roughly equal to, or less than the resting state based on cutoffs at 40 and 60 percent. We required that transcripts have a minimum of an RPKM of 15 in either the resting or activated state for inclusion in this analysis to ensure that the read depth changes for each transcript with activation was evaluable.

Interestingly, more than two-thirds of HuR binding sites shifted in binding intensity dramatically with T cell activation, with about 28% of these binding changes mirroring

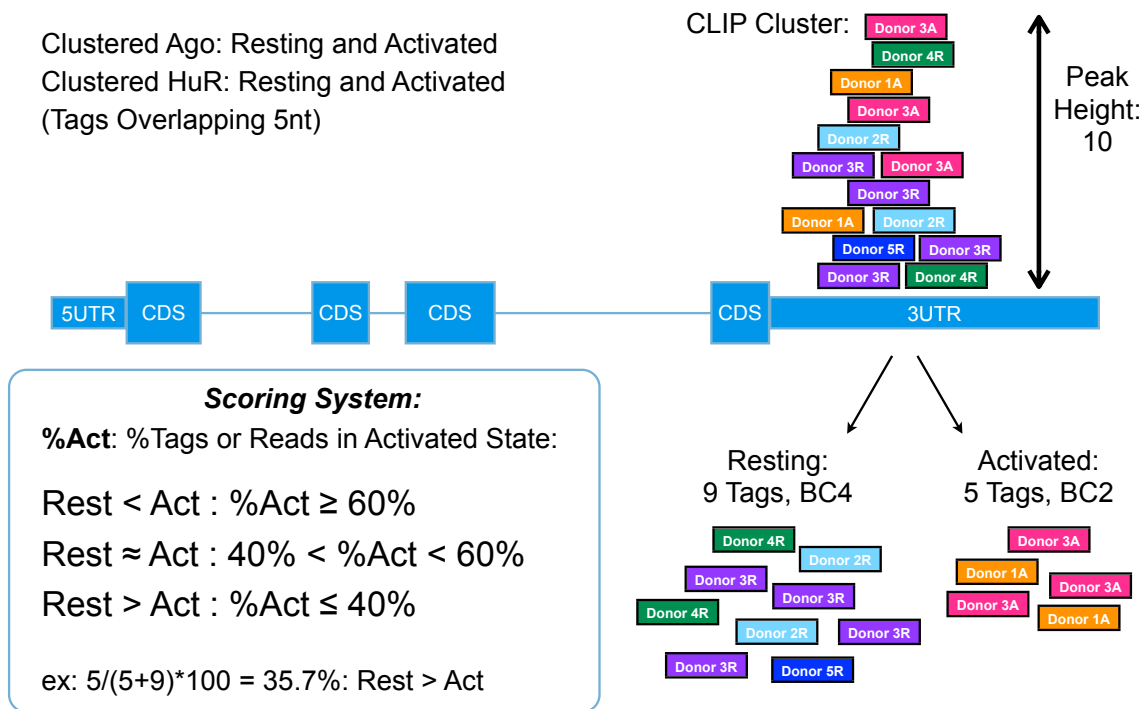


Figure 4.11 Cluster Scoring System. Schematic representing the cluster scoring system CLIP tags for each protein were clustered based on overlapping genomic positions of at least 5 nucleotides. Clusters were included in the analysis if they were comprised of at least 4 donor samples in the resting and or activated state and had a peak height of at least 10 tags between both activation states. The number of tags in each state was calculated and the percentage of tags in the activated state out of the total number of tags in that cluster from both states was calculated. Clusters were binned into whether the binding increased (>60% activated tags), decreased (<40% activated tags), or showed little to no significant change (between 40% and 60% activated tags) with T cell activation.

changes in transcript abundance. Overall, 45% of the binding distribution of HuR between the resting and activated state for the cluster could be explained by parallel distributions in gene expression for that transcript. In only 7% of clusters did the transcript abundance shift between activation states without a dramatic change in HuR binding, although HuR binding was seen to shift in 45% of clusters without a substantial change in gene expression. Interestingly, it was a small minority of clusters, less than 3%, in which HuR binding and transcript abundance changed dramatically in opposite directions (Table 4.3A). The transcripts with the top changes in cluster binding between resting and activated lymphocytes are listed in Table 4.3B.

The most impressive changes in HuR regulation were seen in the activated state of early activation genes and markers. While these transcripts had very low transcript expression in the resting state and very weak levels of HuR binding, within the one hour of stimulation, HuR appeared to coat these transcripts. One example of this is the EGR3 transcript that showed the most striking HuR change with CD3/CD28 stimulation. As shown in Figure 4.12, there are only a few HuR tags at the end of the annotated 3'UTR in the resting state, the coding region and UTRs of EGR3 are littered with robust clusters with activation. It was unexpected that these changes would be seen so dynamically with only an hour of stimulation of the lymphocytes. We also see that the binding extends beyond the annotated 3'UTR for EGR3 and may represent a longer isoform than is represented in the RefSeq database.

Another top HuR target with T cell activation is the IFNG transcript. As seen in Figure 4.13, there are only a few HuR binding sites mapped to IFNG in the resting state in

Table 4.3 Combining HuR CLIP with RNAseq. (A) This table shows the number of clusters binned in each category based on the scoring system outlined in Figure 4.11. (B) This table lists the transcripts with the largest changes in cluster binding between resting and activated states. First are HuR clusters with the largest decreases in binding with T cell activation, then the largest increases in binding, and finally clusters where HuR binding most opposes the changes in transcript abundance.

A

679

1591

2742

5112

HuR

Rest > Act

HuR

Rest ≈ Act

HuR

Rest < Act

598

RPKM

Rest > Act

187

284

127

3670

RPKM

Rest ≈ Act

488

1337

1845

844

RPKM

Rest < Act

4

70

770

B

Clusters: HuR ↓
with CD3/CD28

Clusters: HuR ↑
with CD3/CD28

Clusters: HuR
Opposing RPKM

HSF2

EGR3

SP140

WDR22

NR4A3

ZHX2

PDE4D

FOSB

MAP3K7IP2

MAPK14

IFNG

ATF7IP

DARS

EGR1

ARL4C

INSIG2

CCL4

ARGLU1

ASH1L

NFKBID

N4BP2L2

NAP1L4

EGR2

ZEB1

MGAT4A

CD69

WAC

BCL11B

FOS

RASGRP1

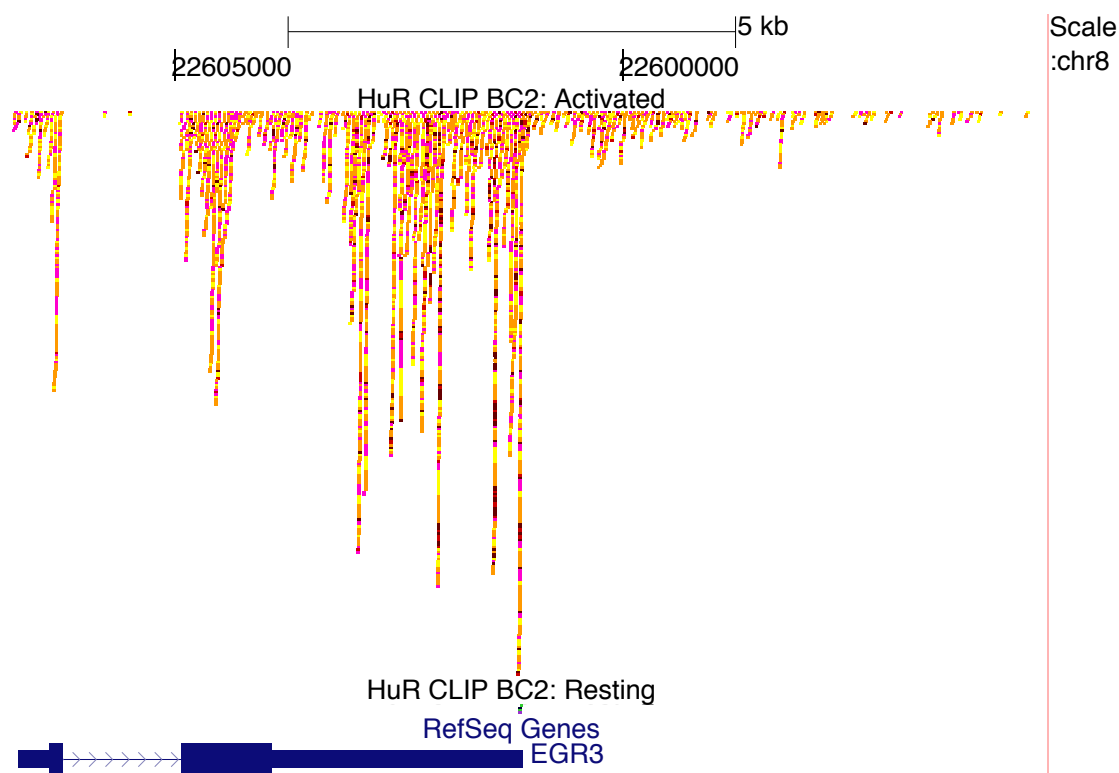


Figure 4.12 HuR Binding on Human EGR3. The position of individual HuR unique CLIP tags in biologic complexity two clusters plotted relative to their mapped position on the human EGR3 transcript. From top to bottom: chromosomal location, HuR CLIP tags from activated CD8 T cells (colors represent each donor sample as shown in Table 4.1), HuR CLIP tags from resting CD8 T cells, Gene diagram from RefSeq.

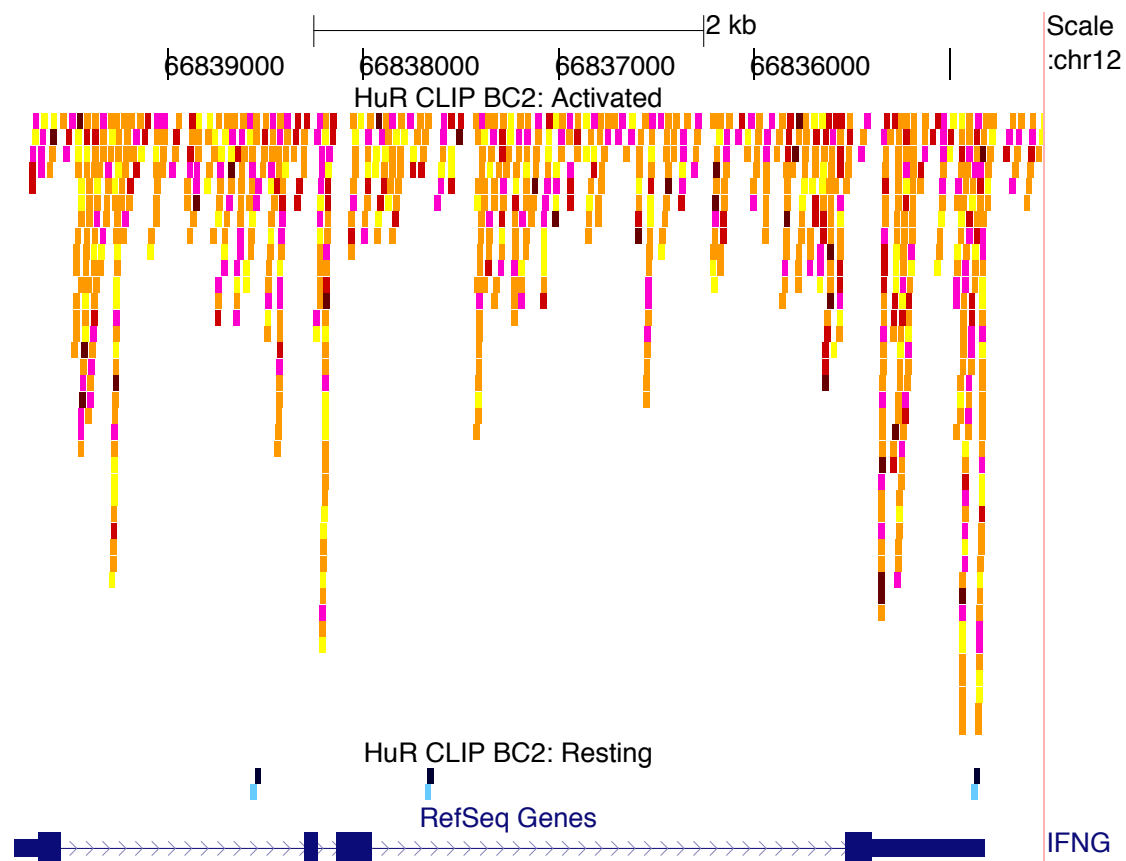


Figure 4.13 HuR Binding on Human IFNG. The position of individual HuR unique CLIP tags in biologic complexity two clusters plotted relative to their mapped position on the human IFNG transcript. From top to bottom: chromosomal location, HuR CLIP tags from activated CD8 T cells (colors represent each donor sample as shown in Table 4.1), HuR CLIP tags from resting CD8 T cells, Gene diagram from RefSeq.

intronic regions and in the 3'UTR, but not more than biologic complexity of 2 or peak height of 2. In contrast, almost the entire IFNG transcript is coated with robust HuR binding clusters after an hour with CD3/CD28 stimulation. Most surprisingly, it appears that HuR binds to the unprocessed pre-mRNA. This suggests that HuR may deposit on the immature IFNG RNA co-transcriptionally and may accompany it from the nucleus to the cytosol for processing.

Discussion

In this chapter we explored the regulation of RNA by HuR in CD8 T cells in the resting and activated states from five normal human donors. We were able to establish conditions to effectively immunoprecipitate HuR from lymphocyte lysate and demonstrated that the isolated RNA during CLIP was HuR monoclonal antibody specific, crosslinking-dependent, and also achievable in mouse T cells. Using HITS-CLIP we were able to define robust and reproducible binding sites across different human donors samples that represented regulation in the resting and activated states of CD8 lymphocytes. We uncovered large sets of HuR regulatory sites that dynamically changed within one hour of T cell stimulation.

We also demonstrated that only small numbers of T cells were needed to clone RNA bound to HuR, therefore, this methodology may be easily applied to study more specific populations of T cells. It could be possible to isolate antigen-specific T cells or other small subsets of cellular populations and apply the HuR HITS-CLIP methods without expansion of these cells in culture. This would allow for the molecular mechanisms of

HuR control to be elucidated in physiologically relevant human donor cells for the study of different disease states and for lymphocytes in an antigen specific manner.

We found that a majority of HuR binding sites was located in intronic regions of targeted transcripts, followed by between 21 and 30 percent of binding falling in 3'UTR regions of genes (Figure 4.9). Our finding that the vast majority of binding occurring in intronic and 3'UTR regions of targeted genes corresponded to studies reporting HuR binding sites determined by PAR-CLIP (Mukherjee et al. 2011). Interestingly, these binding patterns contrast from those of the neuronal Hu proteins, which showed a binding preference to the 3'UTR in nearly three quarters of highly reproducible clusters. This previous result was seen for clusters of biologic complexity of 5 out of 6 sequenced samples, while lower biologic complexity clusters showed a reduced preference towards the 3'UTR (Ince-Dunn et al. 2012). It is therefore possible that the increased percentage of 3'UTR clusters in T cells that were reproducible in both the resting and activated states is a reflection of the enhanced robustness of these clusters as being at least a total of biologic complexity of 6 and total peak height of 10 rather than a difference in the biology of this dataset.

Still, it is clear that the genomic distribution of binding appears to be different between HuR and its neuronal family members. These binding patterns could represent multiple possibilities. If the binding patterns are determined by the RNA sequence, then the distribution of Hu binding sites might be different in the brain and T cells. Or there could be other variables that influence HuR binding preferences such as the cooperative or antagonistic interactions with other RNA-binding proteins, which might differ in repertoire, abundance, and regulation in the two systems. Furthermore, differences

between the regulation of RNA in the steady state of the brain from the acutely activated and proliferating T cells could account for differences seen in the proportion of intronic binding. Comparatively, there is more active transcription in these lymphocyte populations and therefore likely more mRNA, leaving the possibility for increased co-transcriptional and intronic associations of HuR.

While we found that more than two-thirds of HuR binding clusters shifted in their dominance between the resting and activated state, by combining this data with RNAseq transcript abundance levels, we determined that much of the binding patterns can be explained by gene expression levels. We saw that 45% of binding distribution between the resting and activated states mirrored transcript abundance levels in these cells. Still, in an additional 45% of clusters, HuR binding changes with activation were more dramatic than changes in transcript abundance. This differs greatly from the reciprocal scenario, where only 7% of genes that changed dramatically with T cell activation showed roughly equivalent HuR binding in both states. It was very rare, in 3 percent of clusters, for HuR binding to change in the opposite direction of a significant change in transcript abundance (Table 4.3).

The largest changes in HuR binding were seen in early activation genes and markers of T cell activation. Some of the largest differences in HuR tags between the resting and activated states were seen in the EGR3 and IFNG mRNA. While robust binding was seen along both of the transcripts, it was notable that for EGR3 while it appeared that HuR bound solely exonic and UTRs, for IFNG it appeared to bind in intronic regions as well. We were interested to find such robust HuR binding on the pre-processed transcript

and consider that HuR appears to be deposited co-transcriptionally. Still, the largest binding sites for both of these genes were seen in the 3'UTR. It would be interesting to investigate the binding patterns of these and other genes at additional time points following T cell stimulation. For example, it would be interesting to see if the HuR binding resolved at later time points to include only processed mRNA sites or to the 3'UTR alone. Similarly it could be informative to study earlier time points to gain insight into how these binding sites accumulate along the transcript. Nevertheless, at one hour of activation, the view we are given of HuR regulation is most likely the population average of activation time points leading up to one hour because it is unlikely that all of the T cells encounter CD3 and CD28 antibody at time zero.

In this study, the activation and crosslinking was done at a short time point, so it would be interesting in future studies to observe the binding of HuR to targets affects transcript stability and translation at subsequent time points. It is possible that while HuR mirrors transcript abundance with the new burst of transcriptional changes with CD3/CD28 stimulation that the presence or absence of HuR binding sites may help dictate the fate of these transcripts as the activated biology resolves.

CHAPTER 5. Determination of Ago *in vivo* Binding Sites in Resting and Activated T cells

Introduction

As described in previous chapters, T cells must transition very quickly from a quiescent state to an active state to perform various functions to maintain immunity within a host, such as when they encounter cognate antigen and transmit signals through their T cell receptors. Because of the rapid nature of these encounters, while they utilize regulated gene expression at every level, the regulation of protein expression from pre-synthesized mRNA provides the most rapid means of response. Such translational regulation occurs in many ways, but a common feature is regulation by RNA-binding proteins that help control the localization and stability of target transcripts, keep them poised for quick translation into proteins, or help them be swiftly degraded to begin, reshape, or terminate an immune response. Transcripts encoding cytokines are good examples of such remodeling because they are needed to initiate antigen-specific responses but need to be terminated just as abruptly so that lymphocytes do not harm surrounding cells after antigen encounter (Anderson, 2008). Understanding the post-transcriptional control of RNA is essential to understanding the biology of the dynamic regulation of lymphocyte activation.

Argonaute (Ago)-microRNA complexes provide one well-studied mechanism to regulate translation of extant mRNAs, and there is emerging evidence that they may do so in a dynamic manner. For example, the CAT-1 mRNA has been showed to localize to stress granules by microRNA mediated repression. Upon amino acid starvation, HuR mediates

de-repression from Ago by mobilization of this transcript from stress granules and into active polysomes (Bhattacharyya, Habermacher, Martine, Closs, & Filipowicz, 2006a; 2006b). Vasudevan and Steitz showed that Ago and FXR1 associate together with the TNF 3' untranslated region (3'UTR) during serum starvation and recruit bound mRNA to actively translating polysomes during the induction of cell cycle arrest (Vasudevan & Steitz, 2007; Vasudevan, Tong, & Steitz, 2007). The localization of Ago to stress granules upon the induction of stress conditions is microRNA mediated and rapidly reversible in less than one minute. It appears that Ago helps to exchange mRNA localization between these cytoplasmic foci and actively translating ribosomes (Leung, Calabrese, & Sharp, 2006). Work from other groups has also demonstrated that microRNA can be regulated to impact rapid changes within the retina and other neuronal systems (Krol et al., 2010).

The abundance of microRNAs in different T cell lineages has also been studied extensively, but has not taken into account the activation state of these cells or the binding preferences of Ago therein (Landgraf et al., 2007; Monticelli et al., 2005; Salaun et al., 2011; Wu et al., 2007). The genetic manipulation of specific microRNAs in mice has demonstrated that many are necessary for the maintenance of a healthy immune system, with ablation or overexpression of microRNAs showing various deleterious results such as aberrant cell death, the induction of multiple autoimmune disorders, and cancer (Xiao & Rajewsky, 2009). Mice lacking Ago2 in bone marrow derived cells showed deficiencies in the development of the B cell and erythroid cell compartments (O'Carroll et al., 2007). Dicer is essential for the production of mature microRNA and mice deficient for this enzyme in the T cell lineage showed greatly impaired lymphocyte

differentiation, with heightened defects in the development of CD8 T cells (Cobb, 2005; Muljo et al., 2005). Zhang and Bevan examined the role of Dicer in mature mouse cluster of differentiation eight (CD8) T cells and found that cells lacking Dicer were able to respond more quickly to T cell activation *in vitro* including quicker expression of CD69 and prolonged expression of this marker following withdrawal from the T cell receptor stimulus. They also found that certain microRNAs were increased after stimulation in culture (Zhang & Bevan, 2010). Still, these analyses were on the order of days in culture and did not represent the potential dynamic changes of Ago regulation immediately following T cell stimulation *ex vivo* or the identification directly mapped binding events.

We have previously demonstrated the ability to use high-throughput sequencing cross-linking immunoprecipitation (HITS-CLIP) to establish a precise and genome-wide map of Ago-microRNA-mRNA ternary interactions (Chi, Zang, Mele, & Darnell, 2009). This work examined Ago binding in the mouse brain in a steady state and did not explore the dynamics of Ago regulation. Ago binding maps in WT and miR-155 deficient mouse regulatory CD4 T cells were recently published, but these studies focus on a different subset of T cells in mice and represent data from cells stimulated in culture for four days (Loeb et al., 2012). Thus, to our knowledge studying the regulation of Ago in normal human CD8 lymphocytes and with acute T cell stimulation has not been previously examined. In this work we aim to map RNA-binding patterns of Ago in resting and activated normal human CD8 T cells to decipher the mechanics of T cell activation and probe the dynamic regulation of RNA.

Results

Ago HITS-CLIP from Five Normal Donor Resting and Activated CD8 T cells

Five healthy normal volunteers were leukapheresed and the collected material was used to purify CD8 T cells for HITS-CLIP, as described in previous chapters. Briefly, We used a Ficoll gradient to isolate the PBMC from leukapheresate that were then depleted of CD56+ cells using antibody bound magnetic beads and magnetic columns. The CD56 depleted PBMC were then subjected to CD8 positive selection and the resulting lymphocytes were rested in media overnight. After resting, T cells were UV-B irradiated to crosslink RNA to protein either immediately or after stimulation for one hour with CD3/CD28 beads. As shown in Chapter 3, the cells were analyzed by flow cytometry to confirm that their purity was greater than 90 percent (Table 3.1). Their activation status was confirmed by analyzing RNA from a non-crosslinked aliquot of the T cells by RT-qPCR for levels of TNF and IFNG (Figure 3.3). Each sample had between a 280 to 610-fold induction of TNF mRNA and between 1250 to 7600-fold induction of IFNG mRNA.

For three of the donors, Ago immunoprecipitation was performed using protein A beads with bound rabbit anti-mouse antibodies supporting a broader net of Ago specific monoclonal antibody 2A8 (Harlow & Lane, 1988). For the other two, we used protein G beads bound directly to the Ago antibody 2A8. We saw a reduced RNA signal in the protein G immunoprecipitation as compared to with protein A. In pilot experiments, we compared the signal to noise from both immunoprecipitation methods and found that protein A samples contributed more unique CLIP reads than protein G samples, but that CLIP tags from both methods clustered in many of the same genomic locations (data not

shown). The correlations between the protein A and G immunoprecipitation methods used in the lymphocyte Ago CLIP described in this chapter will be discussed below. Thus, although the resulting data from the two methods produced differing amounts of data, we included both in the analysis moving forward.

The HITS-CLIP protocol is schematized in Figure 4.1. Ago was immunoprecipitated from CD8 T cell lysate that had been DNase treated, to degrade DNA, and partially RNase digested to reduce the size of RNA molecules in the samples to clonable fragments and to determine the exact binding position of Ago on its target transcripts. The protein-RNA complexes captured on the Ago antibody coated protein A beads or protein G beads were then thoroughly washed on bead. The samples were heated to remove the Ago-RNA complexes from the beads and dissociate free RNA. Next these complexes underwent size selection after being run on an SDS-PAGE gel and being transferred to a nitrocellulose membrane. As in HuR CLIP, free RNA not crosslinked to Ago would not be expected to co-migrate with Ago on the gel and then subsequently to the nitrocellulose and should have been removed during these rigorous processes. Because of these purifications, there was no signal seen at the size of Ago bound to RNA on the autoradiogram in non-crosslinked samples (Figure 5.1A). Thus, we concluded that the isolation of mRNA was cross-linking dependent. Also, the signal seen from the Ago-RNA complexes collapsed to the expected size of Ago bound to microRNA with over digestion of the sample with a high concentration of RNase A (Figure 5.1A). This showed that the signal seen above the molecular weight of RNA was RNase sensitive.

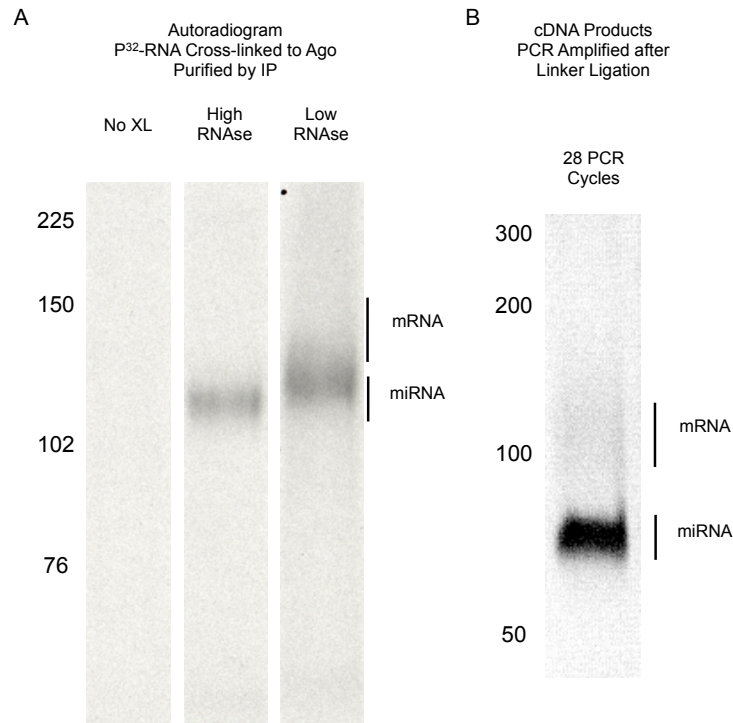


Figure 5.1 Ago HITS-CLIP. (A) Autoradiogram of immunoprecipitation results from human CD8 T cells prepared with or without crosslinking. Lysate was immunoprecipitated with HuR antibodies (mouse monoclonal Ago specific 2A8). ^{32}P -labeled RNA was evident in Ago immunoprecipitation with crosslinked lysate, but not from non-crosslinked lysate. With high RNase treatment, the size of the RNA-protein complexes approach the modal size of Ago. With a lower RNase treatment, RNA-protein complexes of ~110 kD are visible, corresponding to the size of Ago-microRNA complexes, and also ~130 kD, corresponding to the size of Ago bound predominantly to partially digested mRNA. (B) PCR products amplified after linker ligation of microRNA and mRNA products excised from the membrane shown in A.

We isolated protein-RNA complexes from the nitrocellulose membrane at the size of Ago bound to microRNA and also at a higher molecular weight of Ago bound to larger fragments of mRNA. After this size selection, we digested Ago with Proteinase K and cloned the RNA by ligating RNA linkers to either end of the isolated RNA. Then we utilized reverse transcription and amplified the resulting cDNA samples by PCR for high-throughput sequencing (Figure 5.1B). During the PCR for the samples prepared from protein A immunoprecipitation, we used small aliquots of the total sample to determine the minimum number of cycles needed to visualize the resulting products on a Urea-PAGE gel with SYBR gold staining without over amplification. Ideally, we want to amplify these products for a minimum number of cycles to isolate enough material for high-throughput sequencing, but to preserve the complexity of the cloned RNA sequences. Once the minimal cycle numbers were established for each sample, those PCR cycles were performed on the remaining aliquot of the sample and they were gel purified. The products from each donor were pooled together to increase the complexity of the samples to be sequenced.

Overview of RNA Tag Statistics

We sequenced samples produced from the CD8 lymphocytes of five healthy normal donors in both a resting state and after being stimulated for an hour with CD3/CD28 beads. Each Ago associated mRNA sample produced between 21 and 35 million sequencing reads. We collapsed duplicate reads, to minimize the bias introduced from PCR amplification. With only one representation of each sequence in the library, we had between 4 and 10 million reads for each sample. This dramatic decrease is most likely

due to both over sequencing of the sample and PCR duplication of CLIP tags. Each sample was then mapped to its location in the hg18 build of the human genome (Table 5.1), yielding between 800,000 to 4.5 million uniquely mapping RNA CLIP tags.

The 5' RNA linker contained a four nucleotide degenerative sequence. Comparing the four-nucleotide barcodes allowed us to distinguish between unique Ago binding events that occur on different mRNA molecules at the same position and yielded identical RNA sequences and PCR duplications of a single Ago interaction. We removed duplicates that had the same starting and ending genomic coordinates and the same four-nucleotide code in the linker sequence. After this computation, the samples were reduced to under 100,000 reads for the protein G samples and between 300,000 and 1.25 million unique CLIP tags for the protein A samples. The colors used to highlight each donor sample in the table correspond to the colors of the tag representations in subsequent analyses on the genome browser (Table 5.1). In this way, we can compare the data in each state from matching donor samples and relate binding changes to the sequencing depth of each sample. The Ago sample coloring also matches HuR CLIP data from the same donors, presented in Chapter IV. These Ago HITS-CLIP analyses in lymphocytes in the resting and activated state from five normal donors resulted in the generation of an extensive dataset of Ago bound RNA.

Reproducibility of Binding between Biologic Replicate Samples

As with our analysis of HuR binding, we wanted to focus on Ago sites of regulation where the cloned binding events were robust and reproducible between different donors. To begin this exploration, we used a program to group CLIP tags that mapped to regions

Table 5.1 Ago CLIP mRNA Tag Statistics.

| Resting Ago | Total Reads | Total Reads (One Copy) | Mappable Reads (One Copy) | Unique Mappable Reads | % Total Reads (One Copy) |
|----------------|-------------|------------------------|---------------------------|-----------------------|--------------------------|
| Donor 1 | 32,542,843 | 8,079,941 | 3,655,774 | 556,098 | 6.88 |
| Donor 2 | 26,822,766 | 6,789,815 | 3,525,705 | 690,355 | 10.17 |
| Donor 3 | 29,655,003 | 9,280,766 | 4,407,580 | 1,009,902 | 10.88 |
| Donor 4 | 34,142,134 | 6,983,614 | 1,671,612 | 75,346 | 1.08 |
| Donor 5 | 31,620,159 | 4,443,870 | 791,461 | 24,852 | 0.56 |

| Activated Ago | Total Reads | Total Reads (One Copy) | Mappable Reads (One Copy) | Unique Mappable Reads | % Total Reads (One Copy) |
|----------------|-------------|------------------------|---------------------------|-----------------------|--------------------------|
| Donor 1 | 32,467,147 | 8,807,525 | 4,026,449 | 1,301,022 | 14.77 |
| Donor 2 | 21,768,315 | 4,433,931 | 1,699,750 | 305,414 | 6.89 |
| Donor 3 | 21,658,925 | 4,930,455 | 2,425,804 | 1,218,059 | 24.70 |
| Donor 4 | 30,981,793 | 4,959,913 | 1,147,922 | 50,879 | 1.03 |
| Donor 5 | 28,363,457 | 4,605,741 | 965,624 | 46,980 | 1.02 |

of the genome that overlapped at least 5 nucleotides. Within each cluster of tags, we designated that in at least one position there be at least 5 tags overlapping the same nucleotide. We calculated the number of tags overlapping at the peak nucleotide position of each cluster and call this the peak height. To look at the correlation between the ten samples, we excluded 8 clusters that had a sum of over 1,000 CLIP tags grouped together. We did this to have a more conservative estimation of the correlation, because these clusters improved the correlations and we were concerned that these were not accurate depictions of Ago regulation.

To assess the reproducibility of our HITS-CLIP assay, we then calculated the absolute value of the Pearson correlation coefficient between the numbers of tags per cluster that originated from each normal donor from either resting or activated T cells (Figure 5.2). For the samples prepared from protein A immunoprecipitation, we saw at least a correlation of $r=0.88$ between samples from different donors in the same activation state. These high correlations were slightly reduced, but very robust of at least $r=0.77$, comparing protein A samples derived from activated T cells compared to resting T cells. Because of the low read depth in the protein G prepared samples, the correlations between them was lower than those from protein A, between 0.65 and 0.84. And they are even lower when comparing protein G samples to protein A. These lower correlations are most likely due to the lower probability of a unique read from the protein G samples being present in a cluster formed by the larger numbers of reads from the protein A samples. Still, there is the possibility that the different immunoprecipitation protocols introduce bias into the samples.

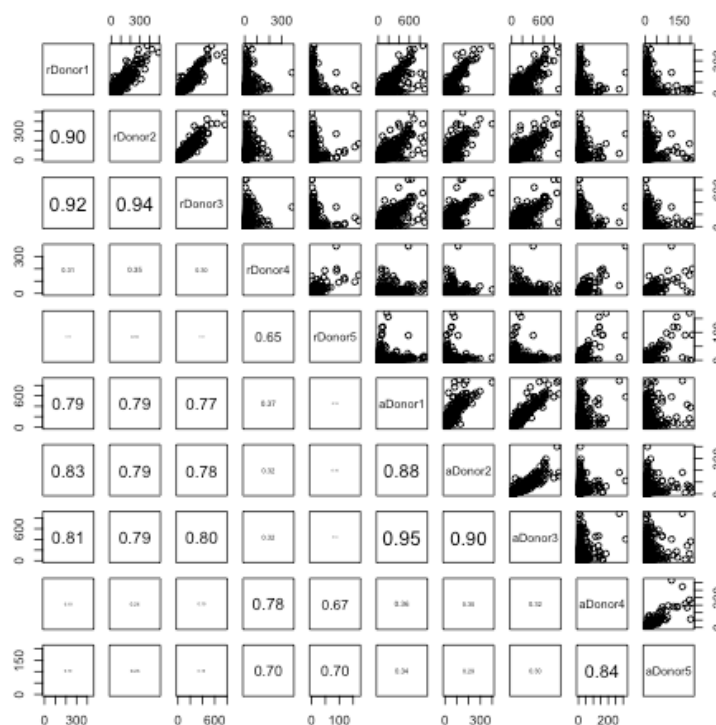


Figure 5.2 Pairwise Correlation of Ago CLIP Clusters. Upper half of table: Pair-wise scatter plots displaying the number of tags per cluster of Ago CLIP tags contributed to the cluster by each resting (r) or activated (a) donor sample as indicated. Lower half of table: absolute value of the pair-wise Pearson correlation coefficient of the number of tags contributed to each cluster by each resting or activated donor sample. The size of text is scaled to the correlation value. Clusters needed to contain a minimum of 5 overlapping tags at one nucleotide position to be included in either analysis.

For more stringent analysis, we also specified that there be at least three of the five donor samples represented in each cluster in either the resting or the activated state to demand biologic reproducibility in each putative Ago binding site. With these conditions, we defined over 38,000 sites of robust Ago mRNA binding. More than 40 percent of these clusters had robust binding in both the resting and activated states. 28 percent of clusters were present at this stringency level only in the resting state (10,839 clusters) and 41 percent of clusters were in the activated state alone (15,740 clusters) (Figure 5.3). Interestingly, while there were more clusters with Ago binding sites in the activated state, we saw less of a difference in the percentages of clusters distributed between resting and activated states with Ago regulation than with HuR (Figure 4.8). In summary, these data demonstrate the reproducibility of the Ago HITS-CLIP method between different normal human donor samples.

Genomic Distribution of Ago Binding Sites

To examine the role of Ago in regulating mRNA in T cells, we next determined which regions of target transcripts were represented by the Ago binding sites. We mapped clusters that represented tags from at least three of the five donors and a peak height of 5 in either the resting state (Figure 5.4A), activated state (Figure 5.4C), or both (Figure 5.4B). As in the HuR dataset, we were surprised at the large number of robust clusters that mapped to intronic regions of target transcripts. In all three groups we saw more than two thirds of clusters mapping to intronic regions of regulation, while 3'UTR binding represented a smaller, but significant portion of Ago regulation (13-15%). An even smaller proportion of clusters mapped to the coding region and 5'UTR of genes.

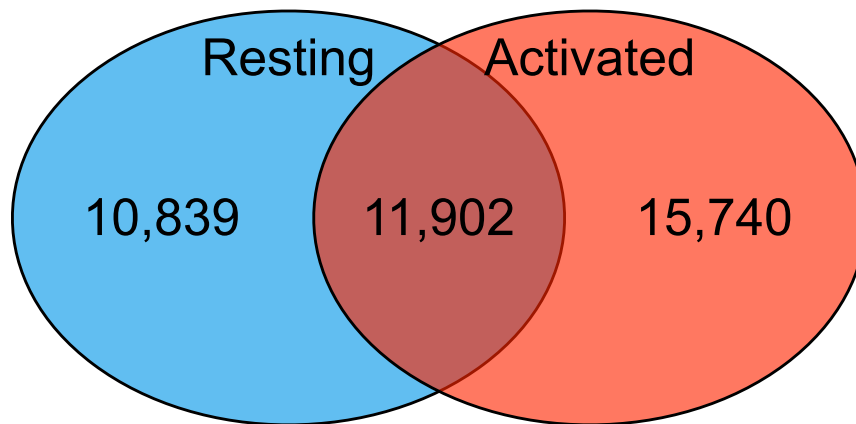


Figure 5.3 Ago Clusters Activation State Distributions. Venn diagrams show the overlap between Ago target clusters in the indicated activation states with the number of clusters representing 3 biologic donor samples and a peak height of at least 5 CLIP tags shown.

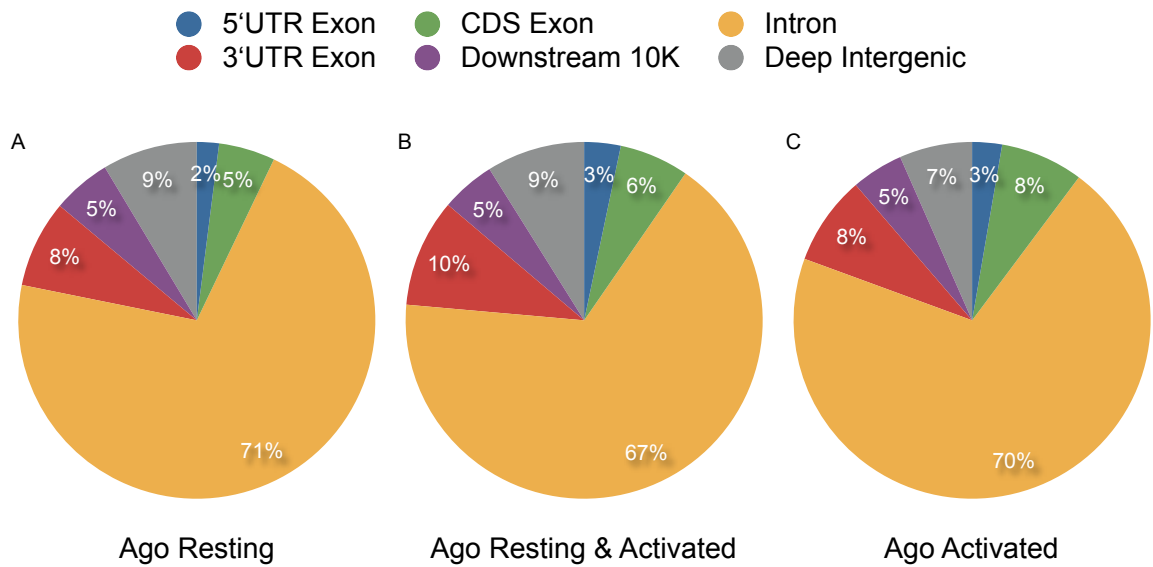


Figure 5.4 Ago Clusters Genomic Distribution. Distribution of clusters, comprised of at least 3 biologic donor samples in the resting and or activated state and a peak height of at least 5 CLIP tags, among Ago target transcripts represented by pie chart.

Thus, the binding regions of Ago on target transcripts were reproducible between binding states and lymphocytes may provide a strong model system to study the roles of Ago in intronic RNA binding.

Ago bound MicroRNA Analysis

In addition to mapping Ago-binding events in mRNA target transcripts, we also cloned and sequenced bound microRNA molecules from two donors in both the resting and activated states. From these samples we mapped between 21 and 35 million microRNA tags (Table 5.2). We identified 271 microRNA that were present in at least one of the four sequenced samples, but the top 35 sequenced microRNAs represented over 98% of the sequencing reads. These top microRNAs are listed in order of total sequencing frequency in Table 5.3. The top microRNA found in the CD8 lymphocytes was miR-142-3p. miR-142 is specific to the hematopoietic lineage and was shown previously to be the most represented microRNA in T cells, confirming that our data correlates well with previous findings (Landgraf et al., 2007).

To examine whether microRNAs changed in their binding status to Ago during T cell activation we calculated the number of tags sequenced for each microRNA normalized to the total read depth so that they could be compared between samples. We determined the ratio of tags in the activated and resting state for each microRNA for both of the two donors. We included microRNAs that were more than 1.5 fold changed in either direction but in the same direction with CD3/CD28 stimulation in both of the donor samples. We included these small changes in microRNA fluctuations because these were shown to be potentially biologically meaningful in many contexts, for instance, the light

Table 5.2 Ago CLIP microRNA Tag Statistics.

| Mappable miRNA Reads | |
|-------------------------|------------|
| Resting Ago | |
| Donor 3 | 29,655,003 |
| Donor 4 | 34,142,134 |
| Activated Ago | |
| Donor 3 | 21,658,925 |
| Donor 4 | 30,981,793 |

Table 5.3 Ago CLIP: Top 35 microRNAs. Listed are the top 35 microRNAs represented in the Ago CLIP microRNA dataset ranked by the total number of CLIP reads for each microRNA from all four sequencing experiments pooled together.

| Top 35 miRNA | Donor 3 Resting | Donor 3 Activated | Donor 4 Resting | Donor 4 Activated | Total Reads | % Total Reads |
|-----------------|-----------------|-------------------|-----------------|-------------------|-------------|---------------|
| hsa-miR-142-3p | 8,515,220 | 6,696,915 | 8,817,909 | 8,332,644 | 32,362,688 | 34.122 |
| hsa-miR-30e | 1,392,825 | 1,487,372 | 3,909,695 | 4,685,356 | 11,475,248 | 12.099 |
| hsa-miR-27a | 1,650,403 | 1,935,439 | 4,046,307 | 2,875,217 | 10,507,366 | 11.079 |
| hsa-miR-26a | 1,145,899 | 1,169,916 | 2,823,385 | 3,565,442 | 8,704,642 | 9.178 |
| hsa-miR-146b-5p | 609,620 | 567,185 | 2,054,043 | 1,937,224 | 5,168,072 | 5.449 |
| hsa-miR-374a | 603,602 | 754,739 | 1,834,183 | 1,845,924 | 5,038,448 | 5.312 |
| hsa-miR-30d | 553,358 | 714,481 | 1,490,311 | 1,700,847 | 4,458,997 | 4.701 |
| hsa-miR-150 | 515,547 | 532,214 | 998,918 | 966,580 | 3,013,259 | 3.177 |
| hsa-miR-19b | 358,778 | 290,837 | 303,262 | 608,323 | 1,561,200 | 1.646 |
| hsa-miR-181a | 146,886 | 156,775 | 470,628 | 595,160 | 1,369,449 | 1.444 |
| hsa-miR-374b | 157,360 | 186,928 | 435,675 | 449,082 | 1,229,045 | 1.296 |
| hsa-miR-101 | 236,535 | 245,996 | 333,864 | 400,586 | 1,216,981 | 1.283 |
| hsa-miR-21 | 314,130 | 318,429 | 239,254 | 273,519 | 1,145,332 | 1.208 |
| hsa-miR-20a | 116,350 | 126,002 | 207,719 | 195,158 | 645,229 | 0.680 |
| hsa-miR-16 | 118,932 | 117,031 | 189,527 | 193,081 | 618,571 | 0.652 |
| hsa-miR-186 | 143,883 | 120,637 | 169,311 | 157,836 | 591,667 | 0.624 |
| hsa-let-7i | 121,066 | 116,858 | 115,255 | 140,371 | 493,550 | 0.520 |
| hsa-miR-222 | 115,497 | 134,916 | 80,877 | 127,151 | 458,441 | 0.483 |
| hsa-miR-29b | 155,622 | 109,587 | 96,612 | 92,757 | 454,578 | 0.479 |
| hsa-miR-17 | 68,345 | 72,967 | 124,358 | 127,512 | 393,182 | 0.415 |
| hsa-miR-19a | 92,935 | 74,627 | 56,256 | 106,223 | 330,041 | 0.348 |
| hsa-miR-26b | 67,407 | 61,673 | 67,048 | 88,771 | 284,899 | 0.300 |
| hsa-miR-31 | 74,834 | 64,612 | 48,024 | 58,200 | 245,670 | 0.259 |
| hsa-let-7g | 70,368 | 63,330 | 45,329 | 48,572 | 227,599 | 0.240 |
| hsa-miR-30b | 48,111 | 62,490 | 53,251 | 62,742 | 226,594 | 0.239 |
| hsa-miR-92a | 51,946 | 48,263 | 45,599 | 64,291 | 210,099 | 0.222 |
| hsa-miR-142-5p | 59,166 | 58,643 | 39,219 | 44,112 | 201,140 | 0.212 |
| hsa-miR-30a | 29,167 | 25,415 | 39,905 | 46,708 | 141,195 | 0.149 |
| hsa-miR-155 | 27,260 | 25,858 | 33,528 | 37,810 | 124,456 | 0.131 |
| hsa-miR-181b | 15,069 | 14,618 | 32,433 | 51,007 | 113,127 | 0.119 |
| hsa-miR-30c | 30,893 | 30,747 | 25,484 | 25,953 | 113,077 | 0.119 |
| hsa-miR-106b | 14,344 | 20,174 | 39,123 | 28,142 | 101,783 | 0.107 |
| hsa-miR-140-5p | 29,568 | 21,862 | 20,733 | 26,551 | 98,714 | 0.104 |
| hsa-miR-146a | 23,109 | 21,528 | 22,782 | 21,337 | 88,756 | 0.094 |
| hsa-let-7a | 25,371 | 23,861 | 15,695 | 16,880 | 81,807 | 0.086 |

and dark adaptation of the retina (Krol et al., 2010). Finally, we ranked these changes by taking the ratio of the sum of normalized reads in the activated and resting state for the two donors together. As enumerated in Table 5.4, there were 33 microRNA with reproducible changes in Ago binding with T cell activation of at least 1.5 fold change. Still, it is unclear whether these changes are biologically significant, because the most highly abundantly sequenced microRNA in this list, miR-32, had a normalized rank of 68th out of the 271 sequenced microRNAs. As mentioned above, a very small number of microRNAs represented the vast majority of sequencing reads and the microRNAs ranked above miR-32 accounted for 99.7% of the total reads sequenced. While the largest changes were among microRNAs with low levels of Ago binding, it is possible that the identified fluctuations could represent the dynamic control of lymphocyte activation acutely at one hour of CD3/CD28 stimulation.

Ago mRNA Binding Changes with Activation

As described in the previous chapter, RNAseq was done on non-crosslinked aliquots of the same pools of cells that were prepared for HITS-CLIP. Using this data, we can give context to the regulation by Ago and HuR by considering the transcript abundance of target and non-target RNAs. In this manner we were able to compare the dynamic changes in both transcript binding by Ago and HuR with the dynamic changes in gene expression seen with lymphocyte activation.

Using the same criteria as for HuR tags outlined in Figure 4.11, we clustered Ago CLIP tags together from the resting and activated states of the five donors sequenced. For each cluster we specified that the CLIP tags overlap at least 5 nucleotides in their genomic loci,

Table 5.4 MicroRNAs Shifting More than 1.5 Fold with Activation. MicroRNAs are ranked by the total number of CLIP reads for each microRNA from all four sequencing experiments pooled together.

| | | Donor 3 Resting Tags | Donor 3 Activate d Tags | Donor 4 Resting Tags | Donor 4 Activate d Tags | Total Reads | Donor 3 Resting Norm. | Donor 3 Activate d Norm. | Donor 4 Resting Norm. | Donor 4 Activate d Norm. | Act/ Rest (Norm.) |
|----------------|----------------|----------------------------|----------------------------------|----------------------------|----------------------------------|----------------|-----------------------------|-----------------------------------|-----------------------------|-----------------------------------|-------------------------|
| Act ↑ | hsa-miR-365 | 0 | 24 | 0 | 46 | 70 | 0.00 | 0.79 | 0.00 | 2.74 | --- |
| | hsa-miR-941 | 0 | 36 | 0 | 18 | 54 | 0.00 | 1.19 | 0.00 | 1.07 | --- |
| | hsa-miR-151-5p | 0 | 1 | 0 | 4 | 5 | 0.00 | 0.03 | 0.00 | 0.24 | --- |
| | hsa-miR-769-3p | 1 | 37 | 3 | 43 | 84 | 0.03 | 1.22 | 0.17 | 2.56 | 18.90 |
| | hsa-miR-99b | 10 | 63 | 20 | 72 | 165 | 0.34 | 2.07 | 1.11 | 4.29 | 4.40 |
| | hsa-miR-548e | 0 | 363 | 58 | 35 | 456 | 0.00 | 11.95 | 3.21 | 2.09 | 4.37 |
| | hsa-miR-1977 | 4 | 80 | 23 | 38 | 145 | 0.13 | 2.63 | 1.27 | 2.26 | 3.47 |
| | hsa-miR-132 | 97 | 761 | 201 | 360 | 1,419 | 3.27 | 25.05 | 11.14 | 21.45 | 3.23 |
| | hsa-miR-98 | 74 | 271 | 80 | 162 | 587 | 2.50 | 8.92 | 4.43 | 9.65 | 2.68 |
| | hsa-miR-200b | 630 | 2,306 | 330 | 504 | 3,770 | 21.25 | 75.92 | 18.29 | 30.03 | 2.68 |
| Rest ↓ | hsa-miR-192 | 611 | 1,718 | 1,135 | 1,701 | 5,165 | 20.61 | 56.56 | 62.90 | 101.36 | 1.89 |
| | hsa-miR-874 | 105 | 498 | 733 | 1,118 | 2,454 | 3.54 | 16.39 | 40.62 | 66.62 | 1.88 |
| | hsa-miR-503 | 35 | 55 | 31 | 58 | 179 | 1.18 | 1.81 | 1.72 | 3.46 | 1.82 |
| | hsa-miR-320b | 184 | 287 | 82 | 143 | 696 | 6.21 | 9.45 | 4.54 | 8.52 | 1.67 |
| | hsa-miR-182 | 0 | 255 | 112 | 11 | 378 | 0.00 | 8.39 | 6.21 | 0.66 | 1.46 |
| | hsa-miR-940 | 0 | 41 | 23 | 1 | 65 | 0.00 | 1.35 | 1.27 | 0.06 | 1.11 |
| | hsa-miR-579 | 0 | 46 | 43 | 13 | 102 | 0.00 | 1.51 | 2.38 | 0.77 | 0.96 |
| | hsa-miR-32 | 4,459 | 2,594 | 3,872 | 2,383 | 13,308 | 150.43 | 85.40 | 214.59 | 142.00 | 0.62 |
| | hsa-miR-338-3p | 217 | 46 | 503 | 258 | 1,024 | 7.32 | 1.51 | 27.88 | 15.37 | 0.48 |
| | hsa-miR-339-3p | 149 | 62 | 169 | 74 | 454 | 5.03 | 2.04 | 9.37 | 4.41 | 0.45 |
| | hsa-miR-100 | 47 | 0 | 68 | 36 | 151 | 1.59 | 0.00 | 3.77 | 2.15 | 0.40 |
| | hsa-miR-1277 | 5 | 0 | 75 | 24 | 104 | 0.17 | 0.00 | 4.16 | 1.43 | 0.33 |
| | hsa-miR-135b | 131 | 1 | 465 | 154 | 751 | 4.42 | 0.03 | 25.77 | 9.18 | 0.31 |
| | hsa-miR-130b | 144 | 35 | 95 | 25 | 299 | 4.86 | 1.15 | 5.26 | 1.49 | 0.26 |
| | hsa-miR-548n | 2 | 0 | 3 | 1 | 6 | 0.07 | 0.00 | 0.17 | 0.06 | 0.25 |
| | hsa-miR-548i | 3 | 1 | 1 | 0 | 5 | 0.10 | 0.03 | 0.06 | 0.00 | 0.21 |
| | hsa-miR-362-3p | 56 | 0 | 27 | 10 | 93 | 1.89 | 0.00 | 1.50 | 0.60 | 0.18 |
| | hsa-miR-1972 | 0 | 1 | 74 | 11 | 86 | 0.00 | 0.03 | 4.10 | 0.66 | 0.17 |
| | hsa-miR-331-5p | 2 | 1 | 31 | 0 | 34 | 0.07 | 0.03 | 1.72 | 0.00 | 0.02 |
| | hsa-miR-212 | 112 | 0 | 43 | 0 | 155 | 3.78 | 0.00 | 2.38 | 0.00 | 0.00 |
| hsa-miR-545 | 2 | 0 | 16 | 0 | 18 | 0.07 | 0.00 | 0.89 | 0.00 | 0.00 | |
| hsa-miR-744 | 3 | 0 | 14 | 0 | 17 | 0.10 | 0.00 | 0.78 | 0.00 | 0.00 | |
| hsa-miR-499-3p | 1 | 0 | 15 | 0 | 16 | 0.03 | 0.00 | 0.83 | 0.00 | 0.00 | |

that there be four of five donors represented in the resting and or activated state, and that there be a position in the cluster where at least 10 tags from either activation state overlap. We calculated the percentage of tags in each cluster that originated from activated cells and then binned the clusters into whether the binding increased (>60 % activated tags), decreased (<40% activated tags), or showed little to no significant change (between 40% and 60% activated tags) with T cell activation. For the gene expression for each cluster, we binned the RNAseq values into the same three groups with the same cutoffs depending on the percentage of RPKM values from sequencing the activated T cells for each gene. Furthermore, to ensure that the RNAseq data was interpretable, we specified that the transcript have a minimum of an RPKM of 15 for inclusion in the subsequent analysis.

As shown in the summarized results in Table 5.5A, nearly two thirds of robust Ago clusters showed dramatic changes in binding patterns with T cell activation. Of these dynamically changing Ago clusters, 37% reflected parallel changes in transcript abundance in the cells. Globally, more than half of Ago clusters had paired gene expression changes with their binding changes. It was in only 7% of robust Ago binding sites that gene expression changed between the resting and activated state without a dynamic change in Ago binding and in less than 2% of clusters in which Ago binding and gene expression shifted in opposite directions. Thus, we can conclude that while Ago binding clearly shifts dramatically and dynamically with lymphocyte activation, much of these differences at one hour of CD3/CD28 stimulation can be explained by changes in transcript abundance.

Table 5.5 Combining Ago CLIP with RNAseq. (A) This table shows the number of clusters binned in each category based on the scoring system outlined in Figure 4.11. (B) This table lists the transcripts with the largest changes in cluster binding between resting and activated states. First are Ago clusters with the largest decreases in binding with T cell activation, then the largest increases in binding, and finally clusters where Ago binding most opposes the changes in transcript abundance.

| A | | 351 | 625 | 861 | B | | |
|------|--------------------|-------------------|-------------------|-------------------|----------------------------------|----------------------------------|--------------------------------|
| | | Ago Rest > Act | Ago Rest ≈ Act | Ago Rest < Act | Clusters: Ago ↓ with CD3/CD28 | Clusters: Ago ↑ with CD3/CD28 | Clusters: Ago Opposing RPKM |
| 1837 | | | | | WDR68 | EGR2 | IFI16 |
| 251 | RPKM Rest > Act | 108 | 111 | 32 | STX2 | NR4A3 | TAF15 |
| 1215 | RPKM Rest ≈ Act | 241 | 488 | 486 | BRWD1 | EGR3 | PLEC1 |
| 371 | RPKM Rest < Act | 2 | 26 | 343 | C6orf190 | EGR1 | ZC3H18 |
| | | | | | ENO2 | NR4A2 | SFRS8 |
| | | | | | MGAT4A | CD69 | SRRM1 |
| | | | | | SLC4A7 | IFNG | SESN3 |
| | | | | | FYB | MYC | ARGLU1 |
| | | | | | ARRDC3 | IL2 | NFATC2 |
| | | | | | UBQLN1 | NR4A1 | ANKRD10 |

Similarly to HuR, the biggest changes in Ago binding occurred with T cell activation in early activation genes and markers (Table 5.5B). These transcripts had very minimal expression in the resting state and virtually no Ago binding. After an hour of T cell activation, Ago crosslinked throughout these transcripts in high abundance. Using the same examples as for HuR binding, in Figure 5.5 we see Ago coating the coding region, UTRs and downstream of the 3'UTR of the EGR3 transcript. We did not expect to see such dynamic changes in binding within one hour of stimulation with CD3/CD28 antagonists. Similarly, Ago binding on the IFNG transcript increased dramatically with lymphocyte activation (Figure 5.6).

Finally, Ago binding in some clusters decreased dramatically with lymphocyte activation. One of the more dynamic examples of such changes was in the intronic region of FYB (Figure 5.7). This example illustrates robust binding in the resting state that has less than biologic complexity of two binding in the activated state. While the FYB gene decreases slightly with T cell activation, it is binned with the group of genes that do not show dramatic shifts in transcript abundance and shows more dynamic binding preferences by Ago. As seen in Figure 5.4 the intronic regulation by Ago as seen in the IFNG transcript is not limited to the activated state and is not necessarily linked to dramatic induction of transcription within the T cell. In summary, we identified reproducible Ago binding clusters in lymphocytes in both the resting and activated states. Many of these clusters show dramatic quantitative changes in binding events with T cell stimulation and generally the majority of binding patterns in each state mirror the RNA level of that target.

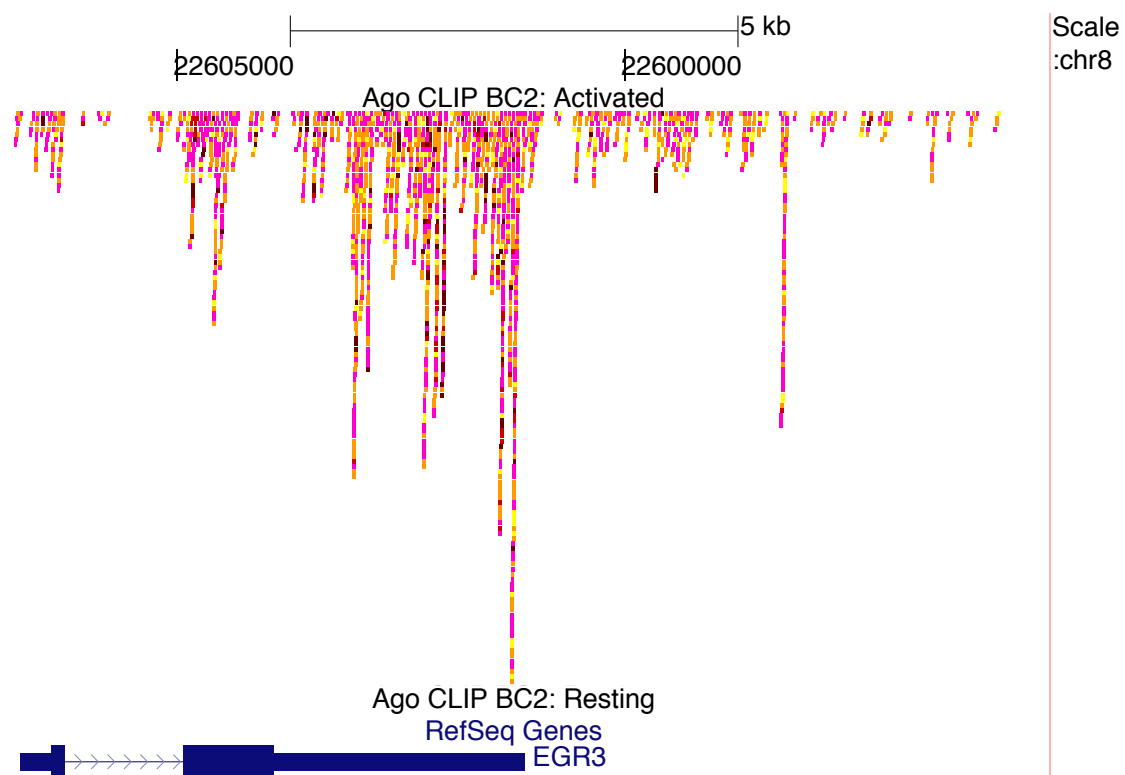


Figure 5.5 Ago Binding on Human EGR3. The position of individual Ago unique CLIP tags in biologic complexity two clusters plotted relative to their mapped position on the human EGR3 transcript. From top to bottom: chromosomal location, Ago CLIP tags from activated CD8 T cells (colors represent each donor sample as shown in Table 5.1), Ago CLIP tags from resting CD8 T cells, Gene diagram from RefSeq.

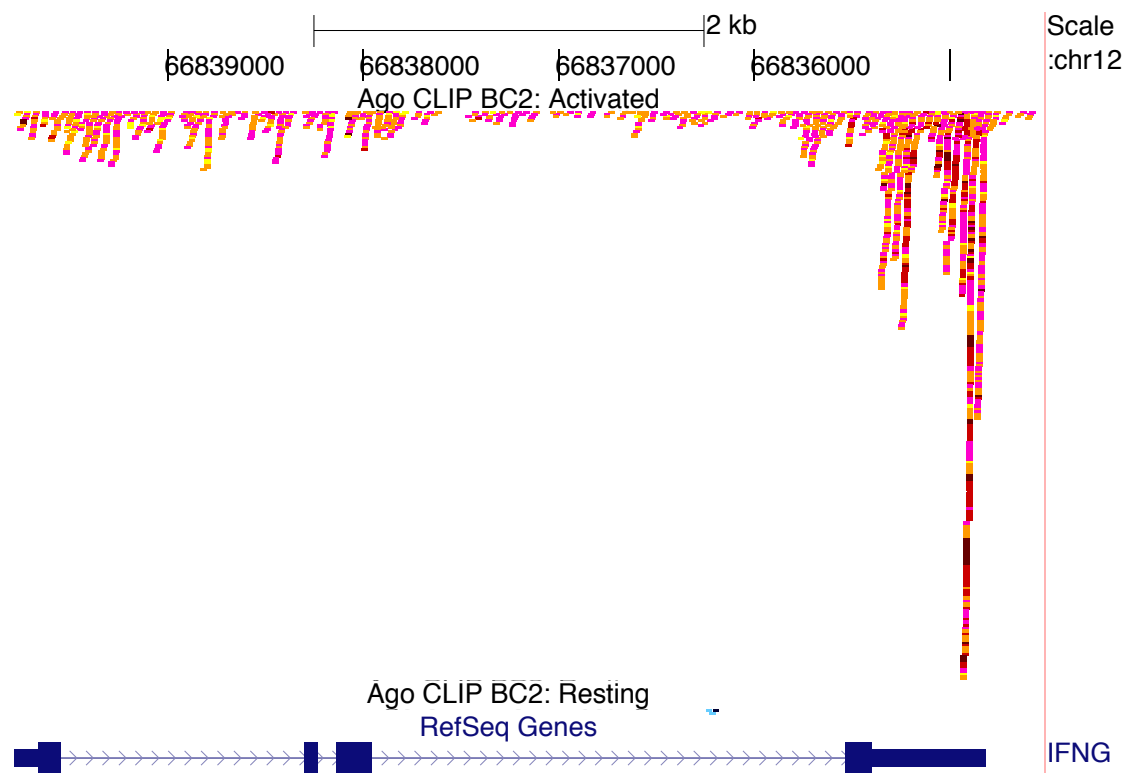


Figure 5.6 Ago Binding on Human IFNG. The position of individual Ago unique CLIP tags in biologic complexity two clusters plotted relative to their mapped position on the human IFNG transcript. From top to bottom: chromosomal location, Ago CLIP tags from activated CD8 T cells (colors represent each donor sample as shown in Table 5.1), Ago CLIP tags from resting CD8 T cells, Gene diagram from RefSeq.

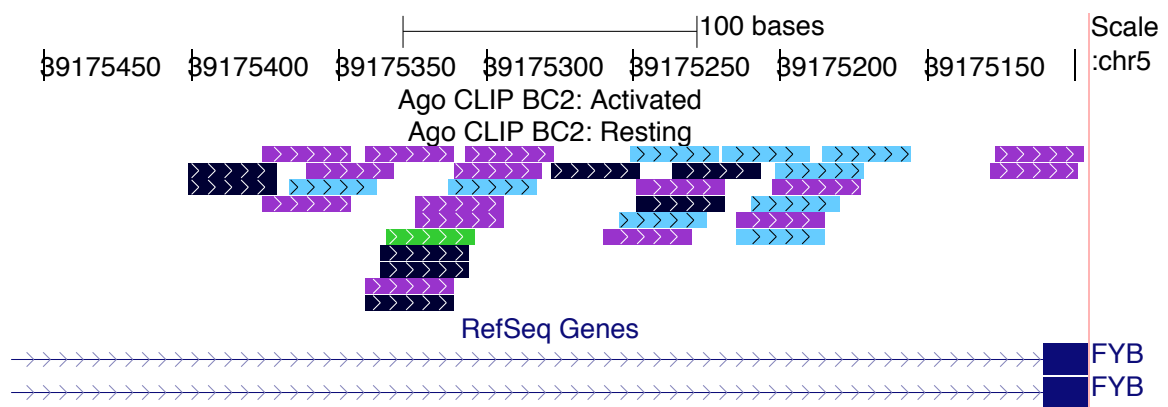


Figure 5.7 Ago Binding in Human FYB Intron. The position of individual Ago unique CLIP tags in biologic complexity two clusters plotted relative to their mapped position on an intron of the human FYB transcript. From top to bottom: chromosomal location, Ago CLIP tags from activated CD8 T cells (colors represent each donor sample as shown in Table 5.1), Ago CLIP tags from resting CD8 T cells, Gene diagram from RefSeq.

Discussion

In this chapter we examined the binding patterns of Ago in the resting and activated states of CD8 lymphocytes from five normal human donors. Using two different immunoprecipitation configurations with protein A or protein G beads, we were able to amass a large dataset of reproducible binding sites for Ago in T cells on mRNA and microRNA. As alluded to above, we think the difference in complexity between the protein G and protein A samples is due to a increased efficiency of the immunoprecipitation using protein A and a bridging antibody to maximize the antigen binding surface of the Ago monoclonal antibody. Also, using a larger proportion of the isolated cDNA to be amplified and pooled from lower cycle numbers in the PCR reactions helped increase the overall complexity of the sequenced material during the protein A sample preparations.

We found many clusters of Ago binding in the resting state alone, both states, and a slightly larger number of clusters in the activated state alone. This represents the first *in vivo* dataset of mapped Ago regulation in human T cells with a physiologic biologic state change and it was interesting to discover that Ago binding changes quite dramatically within one hour of CD3/CD28 stimulation in CD8 lymphocytes. While the distribution of binding within clusters and between transcripts did shift dramatically with T cell activation, we did not see a global shift in the regions of transcripts that are bound by Ago in the different states. We were surprised to find that, while 3'UTR binding represented a significant portion of Ago regulation (13-15%), the majority of robust Ago clusters were found in intronic regions of transcripts. This contrasts with the maps

previously determined in the lab for Ago function in the mouse brain, where only 12% of clusters biologic complexity greater than or equal to two mapped to intronic sequences. In the Ago brain map, about one third of clusters mapped to the 3'UTR regions of transcripts and a quarter to coding regions, while less than half of those percentages did in T cells (Chi et al., 2009). This may represent differences in the biology of lymphocytes, which unlike the brain are actively dividing cellular populations. Loeb et al. also reported a lower percentage of Ago CLIP tags mapping to 3'UTR regions within T cells. These studies used a polyclonal antibody specific to Ago2 for immunoprecipitation and not a pan-Ago antibody as we did (Loeb et al., 2012). Thus we speculate that it is possible that some of the increased intronic binding seen in our samples could be due to regulation by the other Ago proteins in T cells or other binding preferences of the antibodies in isolating populations of Ago within the T cells.

Similar to other studies measuring microRNA abundance in lymphocyte populations, we found that miR-142 was the most represented in our CD8 T cells (Landgraf et al., 2007; Salaun et al., 2011; Wu et al., 2007). While we were able to identify almost 300 microRNA bound to Ago in either the resting and activated states, similar to previous work, we found that a small number of microRNA represented the vast majority of Ago-bound sequencing reads (Chi et al., 2009). The top 35 microRNA found in our T cell dataset represented over 98% of the total reads. We identified 33 microRNAs that changed in their Ago binding status between the resting and activated state and more than 1.5 fold with activation. Although these may be robust differences, it is unclear whether these shifts in microRNAs that are representative of far less than 0.5% of Ago binding could greatly influence the biology of T cells. Further analysis and studies are needed to

determine if these shifts in these Ago bound microRNA help define the biology of the resting and activated T cell phenotypes.

While we did not observe large differences in Ago-bound mature microRNAs cloned in our CLIP experiments, we did observe an increase in binding in many microRNA host genes and pre-microRNA transcripts (data not shown). Previous studies have demonstrated that the levels of many microRNAs can be regulated in the reaction to different stress responses (Leung & Sharp, 2007). It would therefore be informative to consider the Ago-bound microRNA repertoire with respect to the cellular pool of microRNAs at later time points with activation to examine the kinetics of Ago-microRNA interactions and determine if and when there is a shift to reflect this changing population of small RNAs in the cell.

As observed in HuR binding pattern changes with activation, although nearly two thirds of Ago binding sites shift quantitatively with CD3/CD28 stimulation, the majority of Ago binding changes are parallel to variations in transcript abundance. It was surprising to find that Ago binding correlated well with transcript expression levels, because it is typically assumed that increased Ago binding leads to decreased expression of its targets (Bartel, 2009). One possible interpretation is that the dynamic Ago binding map determined here after one hour of T cell stimulation may be too short of a time course to see the downstream effects of Ago binding in terms of transcript abundance. It would therefore be informative to look at RNA levels, ribosomal occupancy, and protein levels at later time points to elucidate the ultimate effects of Ago regulation during T cell activation.

With one hour of stimulation, the most dramatic shifts in Ago-binding patterns were in early activation gene transcripts and T cell activation markers. Although in the EGR3 and IFNG transcripts, the largest clusters of Ago binding could be seen in the 3'UTR, like for HuR, we observed binding throughout the entire transcript including intronic regions. This was even more unexpected for Ago than HuR because it was assumed that a majority of Ago regulation was occurring in the cytoplasm and on processed mRNA transcripts rather than pre-mRNA. It was also surprising for these and other transcripts that Ago coated the newly transcribed RNAs in a manner that does not appear to be microRNA specific but rather that Ago may be deposited co-transcriptionally. This differs from the binding seen by Ago in the brain where intronic clusters are less represented. This may reflect differences between these two biologic systems (Chi et al., 2009). These top Ago transcript targets overlapped impressively with HuR targets and led us to investigate the potential combinatorial control of Ago and HuR in resting and activated lymphocytes.

CHAPTER 6. Exploring the Combinatorial Control of Ago and HuR RNA Regulation During T cell Activation

Introduction

The instruction of transcriptional and translational control by (Argonaute) Ago and HuR are both critical for immune function. As described in the previous two chapters, we have used high-throughput sequencing crosslinking immunoprecipitation (HITS-CLIP) to establish regulatory maps for both of these RNA-binding proteins in the resting and activated states of cluster of differentiation eight (CD8) lymphocytes. Interestingly, we saw similar binding changes in key Ago and HuR target mRNAs. Therefore, we undertook to study the combined regulation of these proteins during lymphocyte activation.

The pronounced specificity of Ago targeting mRNA sites cannot be explained solely by the presence of target sequences complementary to the six-nucleotide microRNA seed region, because potential target sites far outnumber true Ago binding sites in the transcriptome. Additionally, many Ago binding sites have been identified without having clear microRNA pairings (Bhattacharyya, Habermacher, Martine, Closs, & Filipowicz, 2006a; 2006b; Chi, Hannon, & Darnell, 2012; Chi, Zang, Mele, & Darnell, 2009; Leung et al., 2011; Loeb et al., 2012). Predicted microRNA target sites are abundant in AU-rich elements (ARE), creating the possibility for combinatorial regulation of mRNA by Ago and other RNA-binding proteins, such as HuR (Chang et al., 2012; Meisner & Filipowicz, 2010). Studies investigating the control of joint mRNA targets of both Ago and HuR have signaled the importance of these interactions, but their focus on specific transcripts

and varied outcomes on the regulation of these messages has indicated the need for more systematic study of their combinatorial regulation.

For instance, CAT-1 protein levels can increase during stress responses without a corresponding change in transcription. While the translational repression of this message is mediated by Ago-miR-122 sequestration of CAT-1 to P-bodies, upon the activation of a stress response, HuR binds this 3'UTR in ARE and allows for the association of CAT-1 with active polysomes. Thus, upon the induction of cellular stress, HuR mitigates Ago repression of CAT-1 (Bhattacharyya, Habermacher, Martine, Closs, & Filipowicz, 2006a; 2006b; Kim et al., 2009). Furthermore, Ago and HuR were shown to compete for regulation of Vegf-a and the balance of this regulation influenced the development of angiogenesis in mice and zebrafish (Chang et al., 2012; Glorian et al., 2011; Kundu, Fabian, Sonenberg, Bhattacharyya, & Filipowicz, 2012). Conversely, HuR was shown to be necessary for microRNA let-7 mediated repression of c-Myc. Manipulation of HuR and let-7 levels within HeLa cells showed that each negatively correlated with c-Myc mRNA and protein levels. The binding region in the 3'UTR for HuR was shown to be adjacent to a let-7 site and HuR was necessary for Ago binding to the 3'UTR to mediate down regulation of c-Myc (Kim et al., 2009; Lebedeva et al., 2011). Other work investigating the combinatorial control of Ago and HuR utilizing *in vitro* systems has also elucidated further examples of Ago and HuR interdependence for the regulation of RhoB and IL-1B mRNA (Glorian et al., 2011; Kundu et al., 2012; Mukherjee et al., 2011).

Recent work integrating Ago and HuR binding maps produced by PAR-CLIP has produced conflicting results on whether their binding patterns are similar. In comparing genome-wide HuR binding sites in HeLa cells with Ago maps identified in HEK293 cells, a preference for binding in areas of Ago targeting was not observed (Lebedeva et al., 2011; Mukherjee et al., 2011). These differences may represent differences in the regulation of these proteins between the cell lines explored. Mukherjee et al. compared this same HEK293 cell Ago PAR-CLIP data with HuR PAR-CLIP binding sites from HEK293 cells expressing a tagged HuR protein. This group reported significant overlapping patterns of regulation for the two proteins, suggesting a potential for competition of these proteins for regulatory binding of target transcripts. Still, the mRNA level changes observed in these cells with HuR knockdown could be explained with or without the presence of overlapping or adjacent microRNA binding sites. The authors suggest that HuR may physically compete with Ago for access to binding sites to regulate the fate of targets (Levy & Darnell, 2002; Mukherjee et al., 2011). Therefore, more work is needed to understand the relationship of these RNA-binding proteins, especially in the context of physiologic systems and dynamic cellular state changes. In this section we study the Ago and HuR HITS-CLIP binding maps from resting and stimulated human CD8 T cells to determine their roles in combinatorial regulation of target mRNAs.

Results

Ago and HuR HITS-CLIP Summary

As previously described, we purified CD8 lymphocytes from five healthy normal volunteers. We crosslinked both rested cells and T cells that were stimulated for one hour with CD3/CD28 beads. The purity of the cells was established to be over 90% CD8 T cells by flow cytometry and RT-qPCR analysis of TNF and IFNG levels confirmed the activation state of non-crosslinked aliquots of the lymphocytes. The T cells showed a 280 to 610-fold induction of TNF mRNA and 1250 to 7600-fold induction of IFNG mRNA. Using these CD8 T cells, we have amassed datasets from paired samples for Ago and HuR CLIP and the summarized sequencing results are found in Table 6.1. As in previous chapters, the color highlighting each donor for Ago and HuR sequencing statistics in the table corresponds to the color of the tags represented on the tracks of the genome browser. This allows us to compare the Ago and HuR tags from each donor easily and relate the binding maps to the overall read depth of each sample as we examine the regulatory patterns of the proteins on each target transcript.

Ago and HuR Bind EGR3 and IFNG

Because the transcripts with the largest dynamic changes in binding patterns for Ago and HuR with T cell activation appeared to be very similar, we compared the binding maps of the two proteins. We began by examining the binding patterns on the previously discussed EGR3 (Figure 6.1) and IFNG (Figure 6.2) transcripts. We found that the binding patterns of Ago and HuR on these transcripts appeared very similar although they

Table 6.1 HITS-CLIP Sequencing Summary. Abbreviations: Ago immunoprecipitation supernatant (Ago Sup), CLIP reads containing an additional 2-nucleotide sequence in the linker region to identify them as coming from unique experimental replicates (2 nt Index).

| A | | |
|---------------------------------------|----------------|-----------------------|
| RESTING | | Unique Mappable Reads |
| Ago | Donor 1 | 556,098 |
| | Donor 2 | 690,355 |
| | Donor 3 | 1,009,902 |
| | Donor 4 | 75,346 |
| | Donor 5 | 24,852 |
| HuR (Ago Sup) | Donor 1 | 658,968 |
| | Donor 2 | 706,821 |
| | Donor 3 | 400,103 |
| HuR (Not Sup) 2 nt Index | Donor 4 | 143,101 |
| B | | |
| ACTIVATED | | Unique Mappable Reads |
| Ago | Donor 1 | 1,301,022 |
| | Donor 2 | 305,414 |
| | Donor 3 | 1,218,059 |
| | Donor 4 | 50,879 |
| | Donor 5 | 46,980 |
| HuR (Ago Sup) | Donor 1 | 1,154,523 |
| | Donor 2 | 587,257 |
| | Donor 3 | 539,178 |
| HuR (Not Sup) 2 nt Index | Donor 4 | 175,523 |
| | Donor 5 | 141,819 |

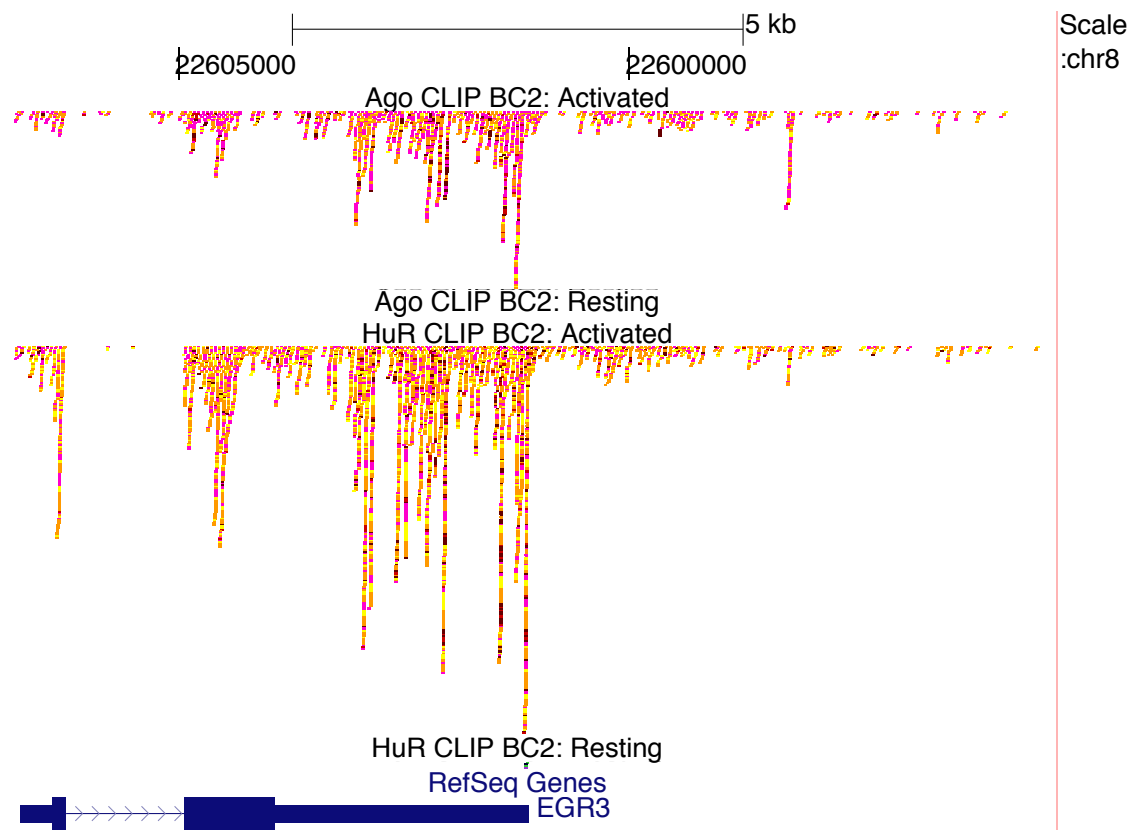


Figure 6.1 Ago and HuR bind Human EGR3. The position of individual Ago and HuR unique CLIP tags in biologic complexity two clusters plotted relative to their mapped position on the human EGR3 transcript. From top to bottom: chromosomal location, Ago CLIP tags from activated CD8 T cells (colors represent each donor sample as shown in Table 6.1), Ago CLIP tags from resting CD8 T cells, HuR CLIP tags from activated CD8 T cells, HuR CLIP tags from resting CD8 T cells, Gene diagram from RefSeq.

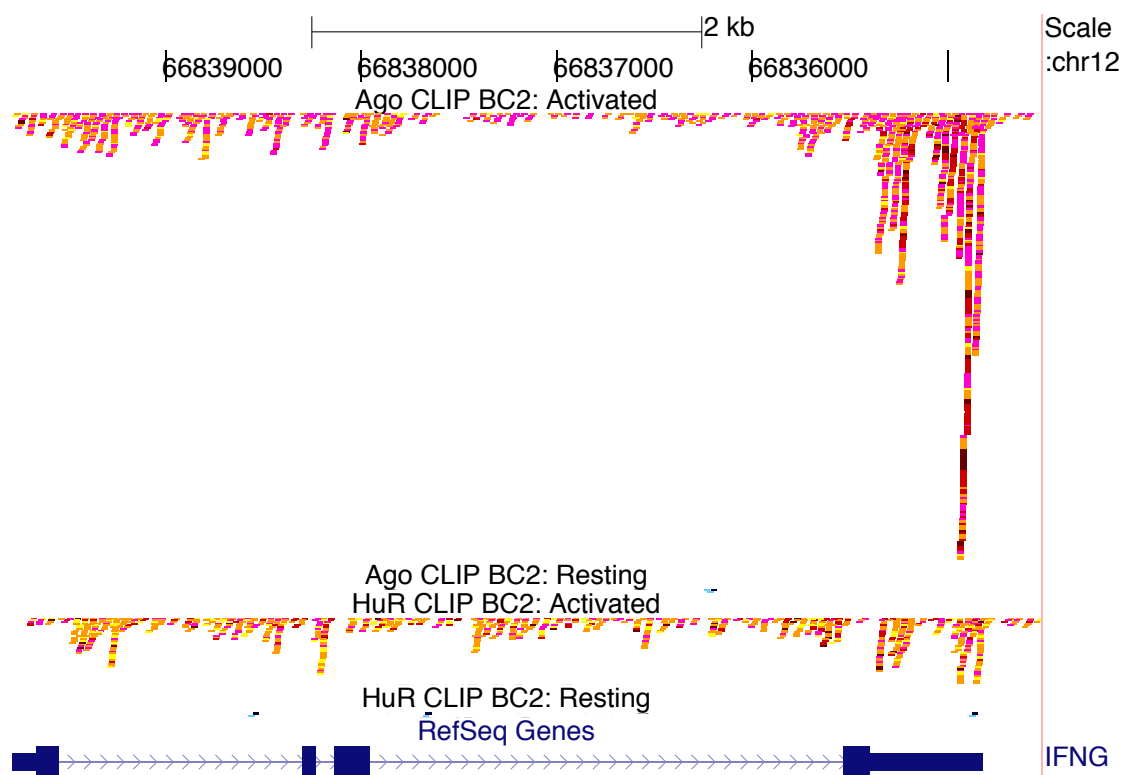


Figure 6.2 Ago and HuR bind Human IFNG. The position of individual Ago and HuR unique CLIP tags in biologic complexity two clusters plotted relative to their mapped position on the human IFNG transcript. From top to bottom: chromosomal location, Ago CLIP tags from activated CD8 T cells (colors represent each donor sample as shown in Table 6.1), Ago CLIP tags from resting CD8 T cells, HuR CLIP tags from activated CD8 T cells, HuR CLIP tags from resting CD8 T cells, Gene diagram from RefSeq.

were not identical. Interestingly, while the amount of HuR binding exceeded that of Ago on EGR3, the opposite was true for IFNG, where there was much more binding of Ago. Because we were able to observe both patterns, and some of the HuR samples were not prepared from Ago supernatant and with different RNA linkers, we were able to rule out the concern that Ago depleted target sites from being clonable for HuR or that there was contamination between samples. Additionally, Ago and HuR bind with different stoichiometry on individual target transcripts.

For both transcripts, the largest clusters of binding were found on the 3' untranslated regions (3'UTRs) and their binding sites overlap between the two proteins. As mentioned previously, it was interesting to observe the binding pattern of both Ago and HuR on the IFNG transcript in both the intronic and coding regions. This suggested that the two proteins might be deposited throughout the newly transcribed message either co-transcriptionally or at least prior to being processed to become a mature transcript. Although HuR and Ago proteins are found in the nucleus, it was unexpected to find robust binding events at such early stages of mRNA processing.

Overlapping Binding of Ago and HuR

In order to study the intersection of regulatory regions of Ago and HuR in more depth, we computed the overlap of CLIP tag clusters on a genome-wide scale. The calculations are diagrammed in Figure 6.3. To begin, we clustered together all of the resting and activated tags for Ago and separately for HuR. We then specified that each Ago or HuR cluster needed to contain reads from four out of five samples in the resting and or activated states and that at least 10 tags from either state must overlap in one genomic

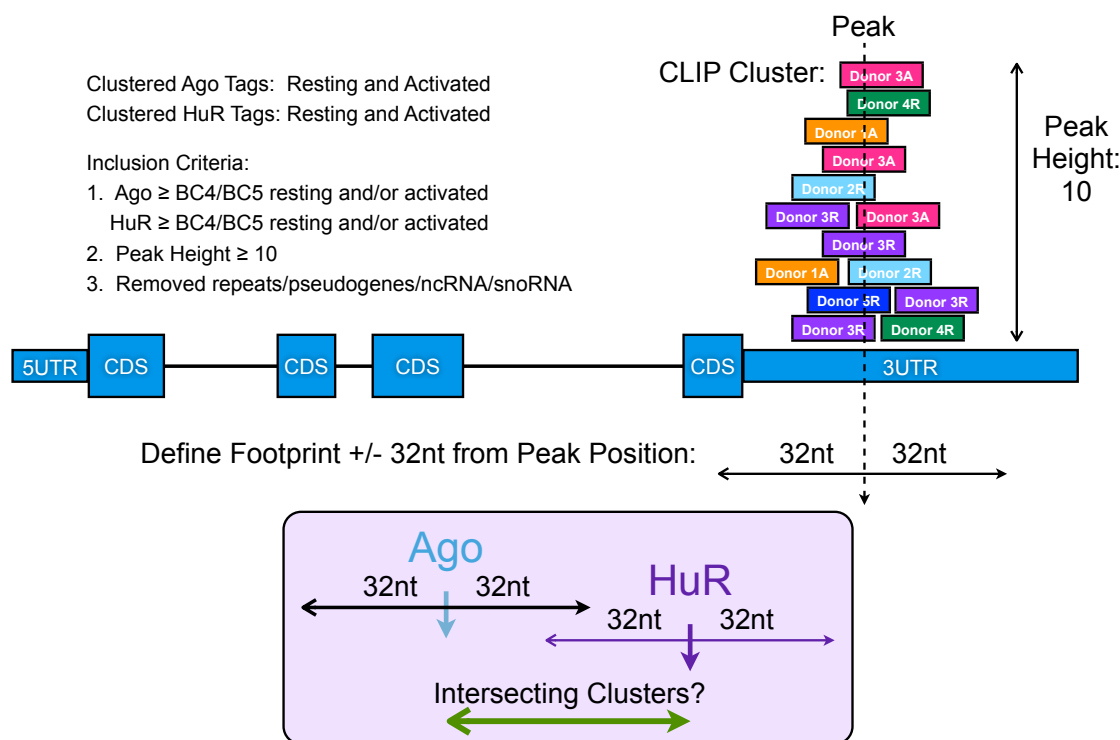


Figure 6.3 Ago and HuR Cluster Overlap Parameters. Schematic representing cluster and binding footprint definitions used as input into cluster overlap analysis. CLIP tags for each protein were clustered based on overlapping genomic positions of at least 5 nucleotides. Clusters were included in the analysis if they were comprised of at least 4 donor samples in the resting and or activated state and had a peak height of at least 10 tags between both activation states. Cluster regions overlapping genomic repeats, pseudogenes, ncRNA, or snoRNA were removed from analysis. The binding footprint of each cluster was defined as including 32-nucleotides 5' and 3' of the peak position. Ago and HuR clusters were designated as overlapping if their binding footprints overlapped at least 1 nucleotide.

position. To make the analysis more stringent, we also removed clusters in low complexity repeat regions, pseudogenes, non-coding RNAs and snoRNAs. We calculated the peak binding position of each cluster, where the most tags overlapped, and defined a footprint for each cluster of 32 nucleotides up and downstream of the peak location. Finally, we identified clusters from Ago where the footprint of binding overlapped with the footprint of HuR clusters. It was possible for more than one Ago cluster to overlap an HuR cluster and vice versa.

We had roughly 2,500 Ago clusters and 7,500 HuR clusters of biologic complexity of 4 and peak height of 10 as input into the intersection analysis. Remarkably, we defined over 1,000 intersecting regions that represented over 40% of Ago clusters and 14% of HuR clusters. Figure 6.4 shows a histogram of the distance between the peak positions of overlapping Ago and HuR clusters. Interestingly, not only do large numbers of Ago and HuR clusters overlap within a small distance, but their peak positions are also highly superimposable suggesting that in many cases Ago and HuR are binding in the exact same positions on many transcripts. Our HuR CLIP samples processed from separate lysate from Ago and with distinguishing indexing linker sequences provided a control that these binding similarities were not an artifact of having done the immunoprecipitation from the same lysate or due to contamination from previous experiments. Similar results were recently published showing a high degree of overlap between Ago clusters in HEK293 cells and HuR clusters in HEK293 cells expressing an epitope-tagged HuR, providing further support for our finding (Mukherjee et al., 2011).

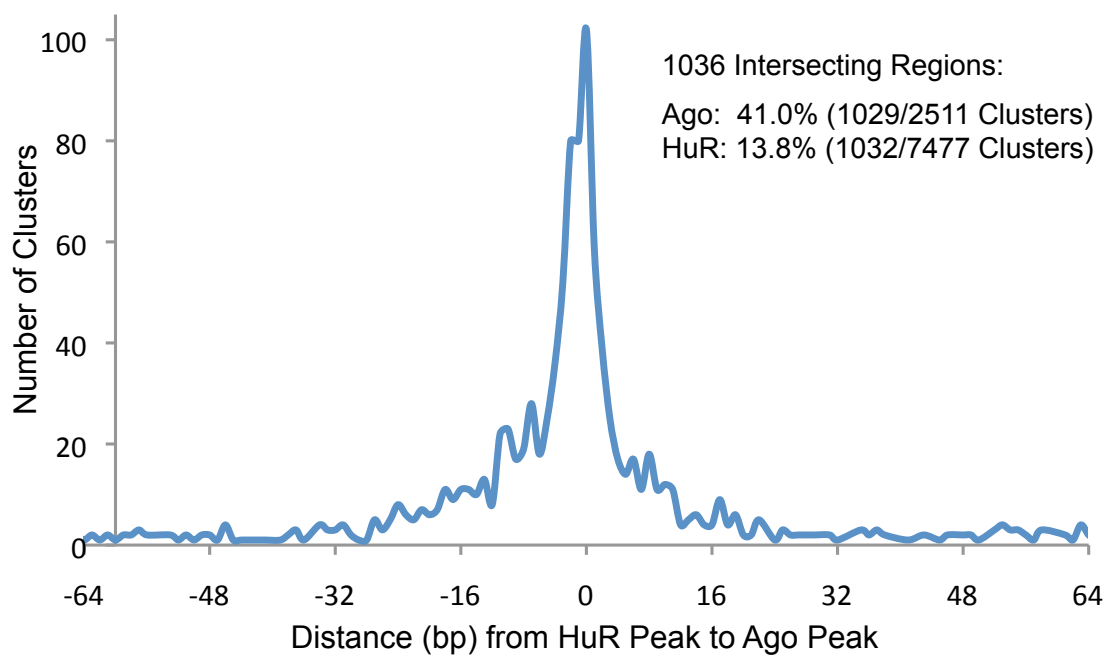


Figure 6.4 Histogram of Ago and HuR Cluster Overlap. Histogram of the number of overlapping cluster footprints with a given distance from the peak position of the HuR cluster to the peak position of the Ago cluster.

To see whether the overlap of Ago and HuR regulation differed between activation states, we repeated the cluster intersection calculations using HuR or Ago clusters that had biologic complexity of 4 for each state without consideration of the biologic complexity in the opposing state for that protein. In Figure 6.5, we demonstrate that Ago and HuR clusters have high levels of overlap regardless of which states they originated from. We see the same distribution pattern for individual T cell activations states as with all clusters together; the most represented position of overlap is at the peak position of the clusters of Ago and HuR. As in the previous analysis, we find that a higher proportion of Ago clusters were found to overlap than HuR, but in both cases, this is most likely due to the differences in the starting numbers of clusters for each protein as HuR had roughly three-fold more clusters as input into the analysis.

Examining Dynamic Changes in Ago and HuR Binding within Overlapping Transcript Regions

In order to understand the interactions between Ago and HuR in overlapping clusters, we examined the binding changes in these intersecting regions with lymphocyte stimulation. For each cluster, we calculated the \log_2 ratio of CLIP tags in the activated state to the resting state. In Figure 6.6 these ratios are plotted for intersecting clusters of Ago versus HuR. As shown in Chapters 4 and 5, the majority of Ago or HuR binding changes with T cell activation mirror transcriptional changes in these levels. Consistent with this observation, the binding changes with activation were often in the same direction for Ago and HuR. This could suggest agonism between Ago and HuR binding. For example, on the IFNG transcript discussed previously, there is more binding seen in the activated state

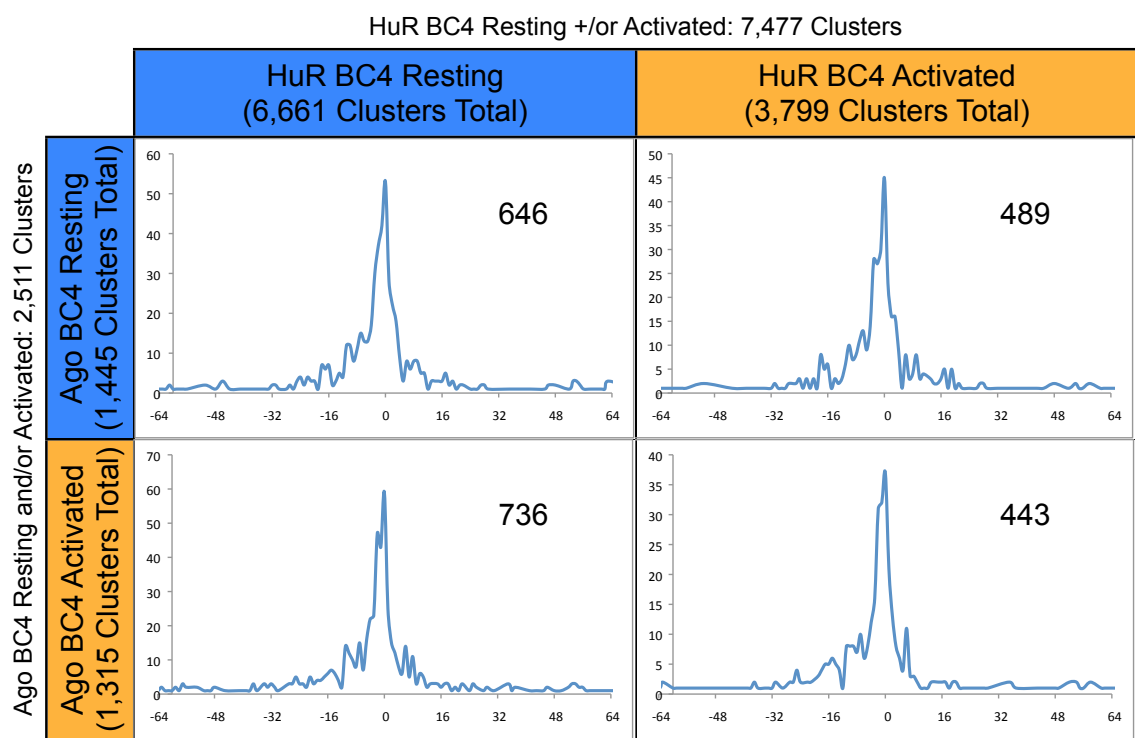


Figure 6.5 Ago and HuR Cluster Overlap in Resting and Activated States. Clusters were defined as described in Figure 6.3, with the addition of each cluster being designated as resting or activated if there was biologic complexity of four (BC4) in that state. Histograms of the number of overlapping cluster footprints with a given distance from the peak position of the resting or activated HuR cluster to the peak position of the resting or activated Ago cluster. The number of intersecting clusters is indicated in each panel. Y-axis denotes the number of clusters. X-axis is the distance (bp) from HuR peak to Ago peak.

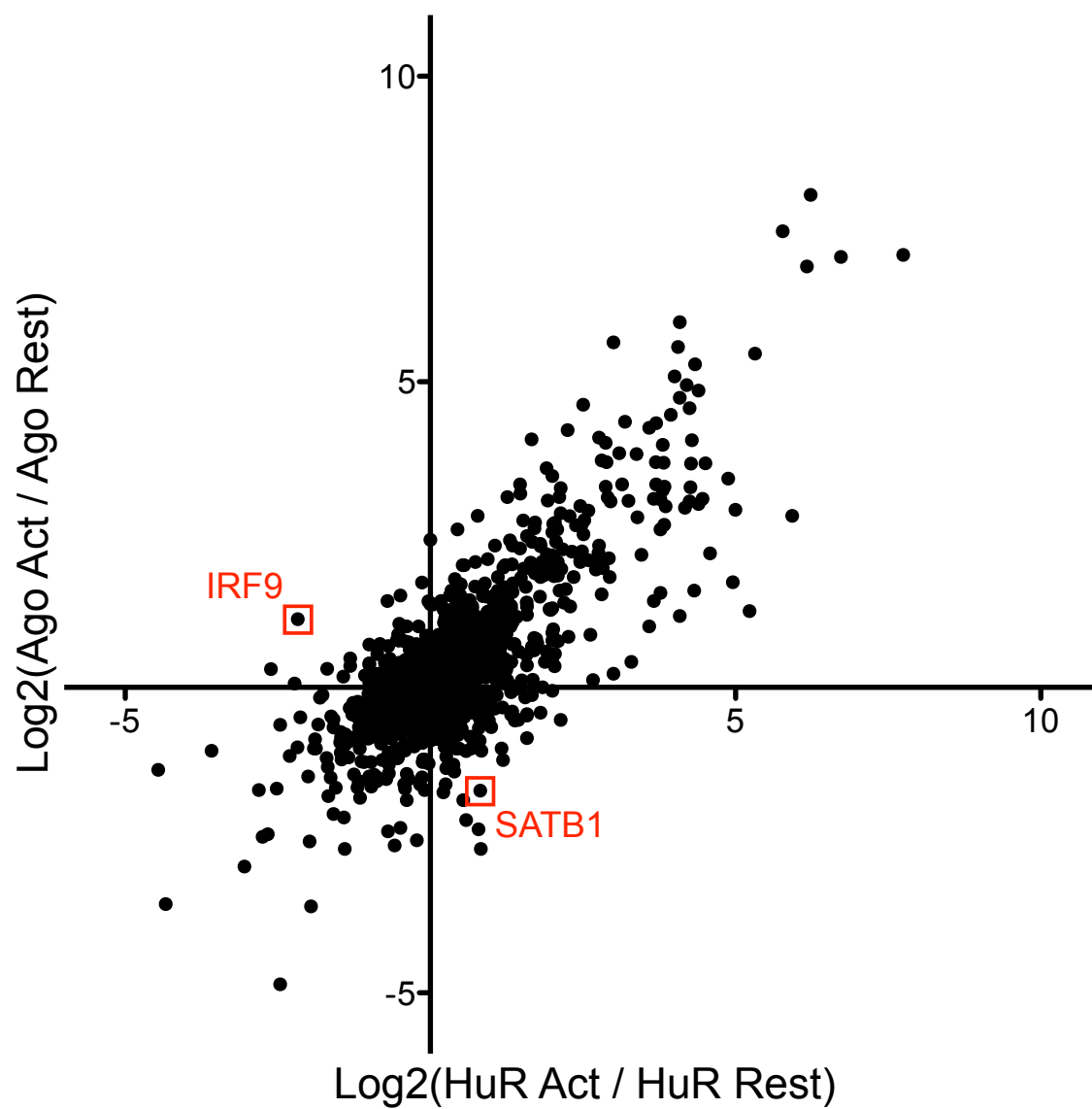


Figure 6.6 Dynamic Ago and HuR Changes in Overlapping Clusters. Scatter plot of the Log_2 ratio of the number of activated tags and resting tags in an Ago cluster versus the Log_2 ratio of the number of activated tags and resting tags in an HuR cluster with a footprint intersecting the Ago footprint.

for both Ago and HuR than in the resting state, which reflects the levels of IFNG mRNA in each T cell state. Still, although the changes on IFNG and other transcripts were shifting in the same directions, there were many overlapping regions where Ago or HuR binding changes were not directly proportional to each other with CD3/CD28 stimulation. In the example of IFNG, Ago binding was increased more at one hour than HuR and the opposite was observed for EGR3.

There were also many clusters represented in the upper left and lower right quadrants of the graph where Ago and HuR binding changes were in opposite directions, suggesting that the proteins could function antagonistically. For example, a region of overlapping Ago and HuR regulation in the 3'UTR of IRF9 is highlighted in the upper left quadrant of Figure 6.6. For these overlapping clusters, the amount of Ago binding increased with activation, while the HuR binding decreased. This cluster is highlighted in the genome browser representation of IRF9 in Figure 6.7. Interferon Regulatory Factor 9 (IRF9) is part of the transcriptional regulatory machinery that activates gene expression through Tyrosine Kinase (JAK) signaling in response to type I interferon interrogation of cell surface receptors. IRF9 has been demonstrated to increase in response to IFNG which is induced substantially with CD3/CD28 activation (Levy & Darnell, 2002). Thus, IRF9 might need to be dynamically controlled with T cell stimulation, although transcript levels do not shift drastically. In this example it appears that while both proteins bind robustly in both states, that the reduction of HuR binding with activation corresponds with the induction of Ago binding. This suggests that the two proteins may be competing for this site of regulation.

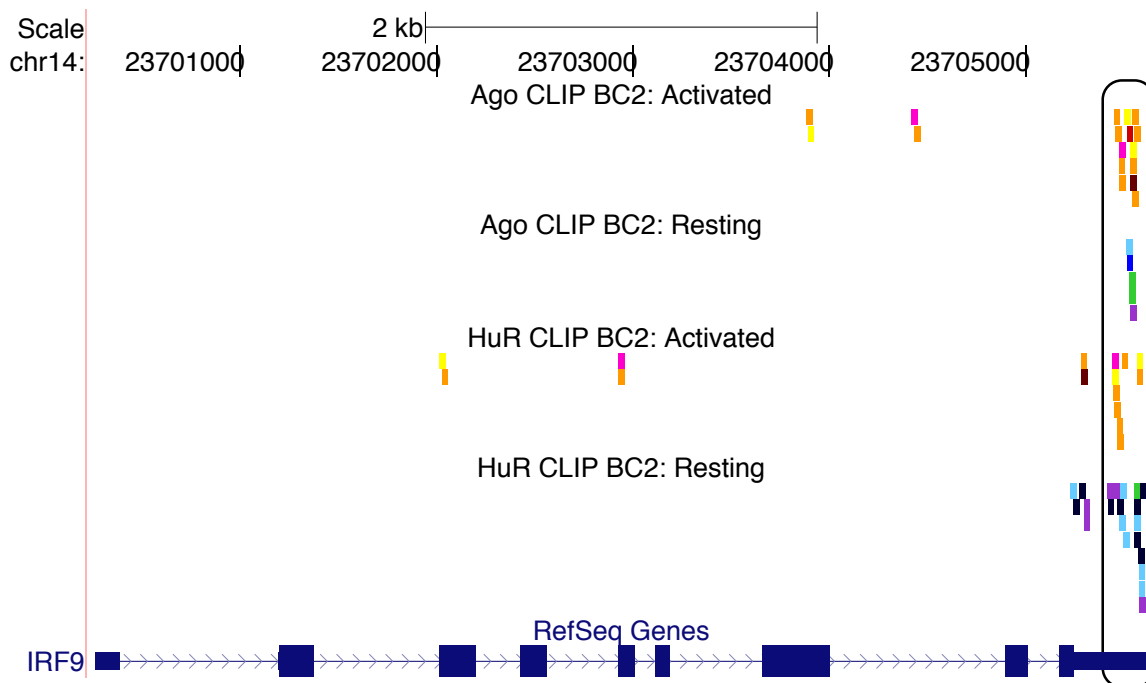


Figure 6.7 Reciprocal Changes in Ago and HuR Binding in the Human IRF9 3'UTR

The position of individual Ago and HuR unique CLIP tags in biologic complexity two clusters plotted relative to their mapped position on the human IRF9 transcript. The CLIP cluster showing dynamic reciprocal Ago and HuR binding changes is outlined in the 3'UTR. From top to bottom: chromosomal location, Ago CLIP tags from activated CD8 T cells (colors represent each donor sample as shown in Table 6.1), Ago CLIP tags from resting CD8 T cells, HuR CLIP tags from activated CD8 T cells, HuR CLIP tags from resting CD8 T cells, Gene diagram from RefSeq.

Another example of where the binding pattern shifted between T cell activation states in an opposing manner for each protein is in the SATB1 transcript. This cluster is highlighted in the scatter plot in Figure 6.6 and the binding map is displayed in Figure 6.8. The SATB1 protein regulates chromatin structure organization by recruiting histone modifiers to its targets' genomic loci and its gene regulation has been shown to be important in T cell differentiation and proliferation (Burute, Gottimukkala, & Galande, 2012). While the binding sites for both Ago and HuR are robustly represented in both activation states in this overlapping cluster, the number of HuR tags increases with T cell activation while Ago binding decreases, indicating that they may compete for regulation at this binding position.

Examining Ago and HuR Binding in the Context of Transcriptional Levels of Target RNA

In previous chapters, we examined the binding changes of HuR and Ago in the context of the levels of target transcripts as determined by RNAseq. By comparing binding maps with transcript abundance, we can begin to understand the cellular context for the regulation by these RNA binding proteins and the dynamic state changes that occur quickly with T cell stimulation.

As diagrammed in Figure 4.11, we designated each Ago or HuR binding site and each transcript as being more represented in the resting state, more represented in the activated state, or relatively unchanged between the two. This was accomplished by tabulating the percentage of reads for each feature in the activated state as a proportion of the total number of reads for that cluster or transcript. We applied cutoffs at 40 or 60 percent representation in the activated state to bin each one into a category, as previously

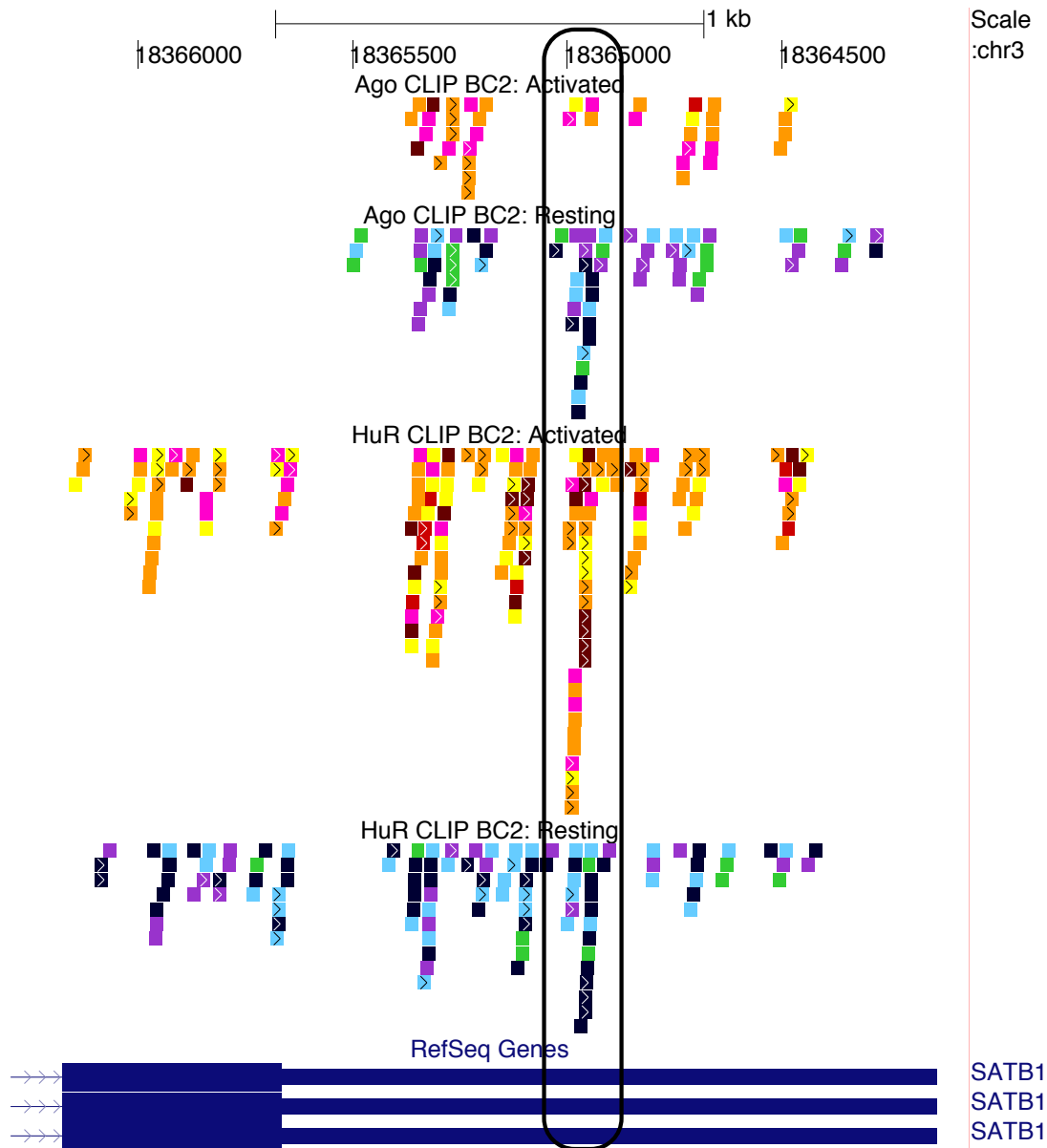


Figure 6.8 Reciprocal Changes in Ago and HuR Binding in the Human SATB1 3'UTR. The position of individual Ago and HuR unique CLIP tags in biologic complexity two clusters plotted relative to their mapped position on the human SATB1 3'UTR. The CLIP cluster showing dynamic reciprocal Ago and HuR binding changes is outlined. From top to bottom: chromosomal location, Ago CLIP tags from activated CD8 T cells (colors represent each donor sample as shown in Table 6.1), Ago CLIP tags from resting CD8 T cells, HuR CLIP tags from activated CD8 T cells, HuR CLIP tags from resting CD8 T cells, Gene diagram from RefSeq.

described. Therefore, for each overlapping Ago and HuR cluster, the site is scored on the relative amount of binding in the activated state compared to the total binding at that site for both Ago and HuR, and the relative amount of transcript abundance in the activated state compared to both states together. As in the other chapters, we also specified that the RPKM of target transcripts be at least 15 in either the resting or activated state for inclusion in this analysis. This ensured that there was robustly measured transcript abundance for the targeted message in at least one of the states for it to be considered. This reduced the number of clusters being analyzed to roughly 700 intersecting regions out of the 1,000 regions defined above.

The results of this combinatorial analysis are summarized in Table 6.2. In more than 60% of clusters, Ago and HuR follow a similar pattern of binding with CD3/CD28 stimulation. In 60% of those clusters, Ago and HuR both follow the same trend as their target transcript levels. More than one fifth of Ago and HuR overlapping clusters are synchronized in having a more exaggerated change than that of the transcript level. In a little over a quarter of clusters, while transcript abundance does not shift with T cell activation, the binding of either Ago or HuR does dramatically shift binding patterns with CD3/CD28 stimulation. These findings suggest that much of the dynamic change seen in binding patterns for Ago and HuR are reflective of the transcriptional changes in the cell, although in some cases the RNA-binding map may be even more responsive than changes in steady state levels of transcript within the cell. It is rare that there is a change in transcript level without some dynamic change in the binding of Ago and or HuR. Interestingly, when transcript abundance increases with T cell activation, there are no Ago and HuR intersecting clusters where either protein has more tags in the resting state.

Table 6.2 Combining Overlapping Ago and HuR CLIP with RNAseq. (A) This table shows the number of overlapping Ago and HuR clusters binned in each category based on the scoring system outlined in Figure 4.11. **(B)** This table lists the transcripts with the largest changes in cluster binding in the resting and activated states between Ago and HuR.

A

| | HuR Rest > Act | | | HuR Rest ≈ Act | | | HuR Rest < Act | | |
|-------------------|-----------------------|-----------------------|-----------------------|-----------------------|-----------------------|-----------------------|-----------------------|-----------------------|-----------------------|
| Ago Rest > Act | 21 | 40 | 0 | 25 | 33 | 0 | 4 | 10 | 0 |
| Ago Rest ≈ Act | 13 | 21 | 0 | 32 | 124 | 4 | 4 | 69 | 11 |
| Ago Rest < Act | 1 | 0 | 0 | 6 | 63 | 7 | 1 | 111 | 125 |
| | RPKM Rest > Act | RPKM Rest ≈ Act | RPKM Rest < Act | RPKM Rest > Act | RPKM Rest ≈ Act | RPKM Rest < Act | RPKM Rest > Act | RPKM Rest ≈ Act | RPKM Rest < Act |

B

| Clusters with Ago Opposing HuR Binding |
|--|
| ARGLU1 |
| C2orf64 |
| FYB |
| GLS |
| HECA |
| IKZF1 |
| RAP1A |
| SATB1 |
| TBC1D1 |
| TRAM1 |
| TXNIP |
| USP25 |
| WIPF1 |
| ZBTB38 |

This might reflect that lymphocyte stimulation induced increases in gene expression of transcripts that are not present in the steady state of a quiescent T cell.

The FYB transcript was among the top clusters with opposing changes in overlapping Ago and HuR binding. FYB mRNA abundance was scored as relatively unchanged with T cell stimulation. Therefore the dynamic shifts in Ago and HuR binding are not due to a dramatic change in transcript level. While this is the same gene as discussed in Figure 5.6, the previously analyzed region only contained a robust binding site for Ago and therefore was not included in the overlap analysis here. For all of the clusters of FYB identified in either analysis, the binding of Ago was either relatively unchanged or decreased with activation. Here we see overlapping HuR clusters where the binding pattern is increased with T cell stimulation. In the two examples in Figure 6.9, there are biologically reproducible binding sites for Ago and HuR in both the resting and activated state that overlap. The quantitative direction of the binding changes, increased HuR binding in the activated state with a decrease in Ago binding, suggest that although robust binding is present in both states, the two proteins may compete for regulation between the resting and activated states and seem to shift the predominantly bound protein in those sites with stimulation.

Ago and HuR and microRNAs

To begin to probe whether the co-regulation of Ago and HuR was microRNA dependent, we examined whether HuR associated with specific Ago-microRNA complexes. To do this, we searched each Ago binding footprint for a microRNA seed match from the top microRNAs sequenced in our Ago CLIP samples. In Figure 6.10A we plotted the

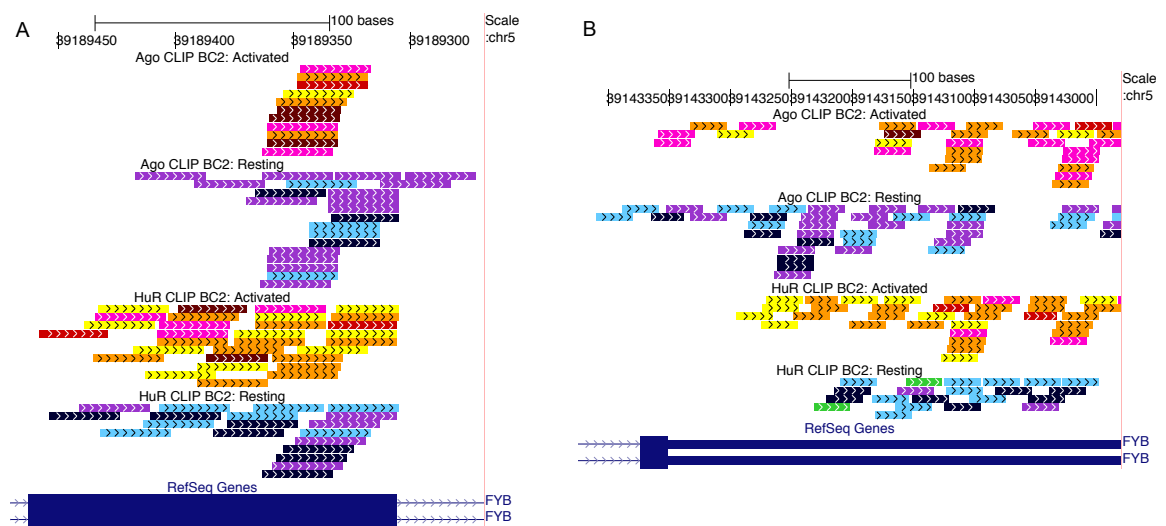


Figure 6.9 Reciprocal Changes in Ago and HuR Binding in the Human FYB Gene. The position of individual Ago and HuR unique CLIP tags in biologic complexity two clusters plotted relative to their mapped position on the human FYB transcript in a coding exon (A) or 3'UTR (B). From top to bottom: chromosomal location, Ago CLIP tags from activated CD8 T cells (colors represent each donor sample as shown in Table 6.1), Ago CLIP tags from resting CD8 T cells, HuR CLIP tags from activated CD8 T cells, HuR CLIP tags from resting CD8 T cells, Gene diagram from RefSeq.

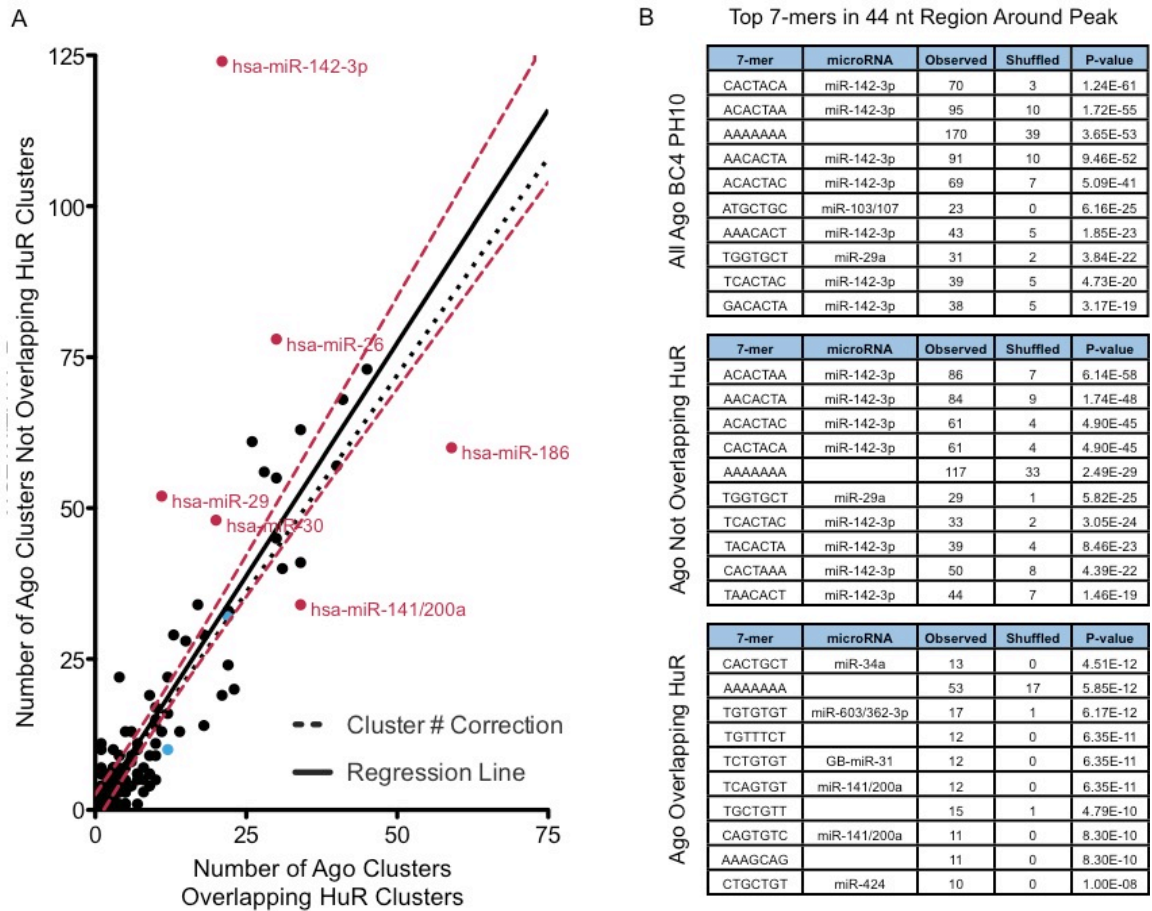


Figure 6.10 Ago Clusters with Matches in each Seed Family. (A) Scatter plot of the number of Ago clusters containing a seed family match for clusters with footprints not overlapping HuR binding footprints versus clusters with footprints overlapping HuR binding footprints. Overlaid is a solid line representing the linear regression of the points with ninety-five percent confidence intervals in red. Additionally, a black dotted line is displayed with a slope that corresponds to the ratio of the number of Ago clusters not overlapping HuR to the number of Ago clusters overlapping HuR. (B) Top 7-mers identified in the 22-nucleotide region 5' and 3' of Ago peak positions for clusters including at least four biologic replicate samples (biologic complexity 4: BC4) and at least ten nucleotides in the peak position of the cluster (peak height 10: ph10). Each 7-mer was ranked by the p-value of the binomial test comparing the frequency of each 7-mer (observed) as compared to the frequency of a shuffled sequence of that 7-mer (shuffled). The 7-mers with the ten highest p-values and matching microRNA seed sites are listed. (Top) All Ago clusters of BC4 ph10. (Middle) Ago clusters BC4 ph10 not overlapping an HuR cluster. (Bottom) Ago clusters BC4 ph10 overlapping an HuR cluster.

number of Ago clusters with or without overlapping HuR binding sites that matched each seed family. The solid regression line with 95% confidence intervals in red is overlaid on top of the plotted points. Additionally, a dotted line is shown displaying the ratio between the number of Ago clusters without HuR to the number of Ago clusters that intersect HuR clusters. We found that a lot of seed matches seemed to hover near the cluster number corrected line, but that there were seed families which showed preference for binding with or without HuR. The top microRNA cloned in the Ago CLIP sample was miR-142-3p, which represented about a third of the total number of reads in the sequenced material. This microRNA showed a strong preference for binding in Ago clusters that did not overlap HuR. There were roughly five-fold more Ago clusters that contained miR-142-3p seed sequences than in sites that overlapped with HuR binding.

Next we identified the top 7-mer sequences that were most significantly represented within 22 nucleotides up or downstream from the peak position of the Ago cluster. We began with Ago clusters of biologic complexity 4 and peak height 10 and also split these into two groups whether the Ago cluster was alone or overlapped with an HuR cluster. We ranked each sequence by the p-value of the binomial test comparison of the frequency of each 7-mer as compared to the frequency of the 7-mer within shuffled sequences of the same nucleotide composition of the Ago footprint regions (Figure 6.10B).

We see in the top table in Figure 6.10B that permutations of the 8mer targeting sequence of miR-142-3p is found in seven out of ten of the most significantly enriched 7-mers surrounding the peak of robust Ago clusters. The other sequences consisted of a stretch

of adenine, which may represent sequencing error, or the presence of AU-rich elements in these footprints. The other sequences matched seeds of miR-103/miR-107 and miR-29a. These matches were more unexpected because they did not represent microRNAs that were highly cloned from our Ago CLIP microRNA dataset (Table 5.3). Consistent with the plot in Figure 6.11A, almost all of the 7-mers from Ago clusters not overlapping with HuR clusters, listed in the middle table, represented matches with miR-142-3p. This microRNA was absent in the list of top microRNA matches for Ago clusters overlapping HuR. Of the other top enriched 7-mers in Ago clusters overlapping HuR, the only microRNA that was highly cloned in Ago CLIP was miR-31. We also note that miR-362-3p was listed in the previous chapter as being potentially down regulated with T cell activation, while it had a very low level of sequencing in Ago CLIP.

Another interesting result was found in examining Ago and HuR binding at primary microRNA loci, especially in regions that represent microRNA clusters that are independently transcribed, as opposed to processed from pre-mRNA introns. We did a closer examination at the miR-17-92 locus because five of the six microRNA encoded on the same primary transcript, miR-7, miR-19a, miR-19b, miR-20a, and miR-92a, were in the top 35 sequenced Ago CLIP microRNA (Table 5.3). Only miR-18a was not represented as frequently and was ranked 87th overall. The Ago tags shown in Figure 6.11 map to sites that will become mature microRNA, but do not represent binding to mature microRNA because the cloned sequences were longer than processed microRNA sequences, with each tag being at least 27 nucleotides in length. We have observed this affinity for Ago binding to preprocessed microRNA stem loops in previous Ago CLIP datasets derived in the lab.

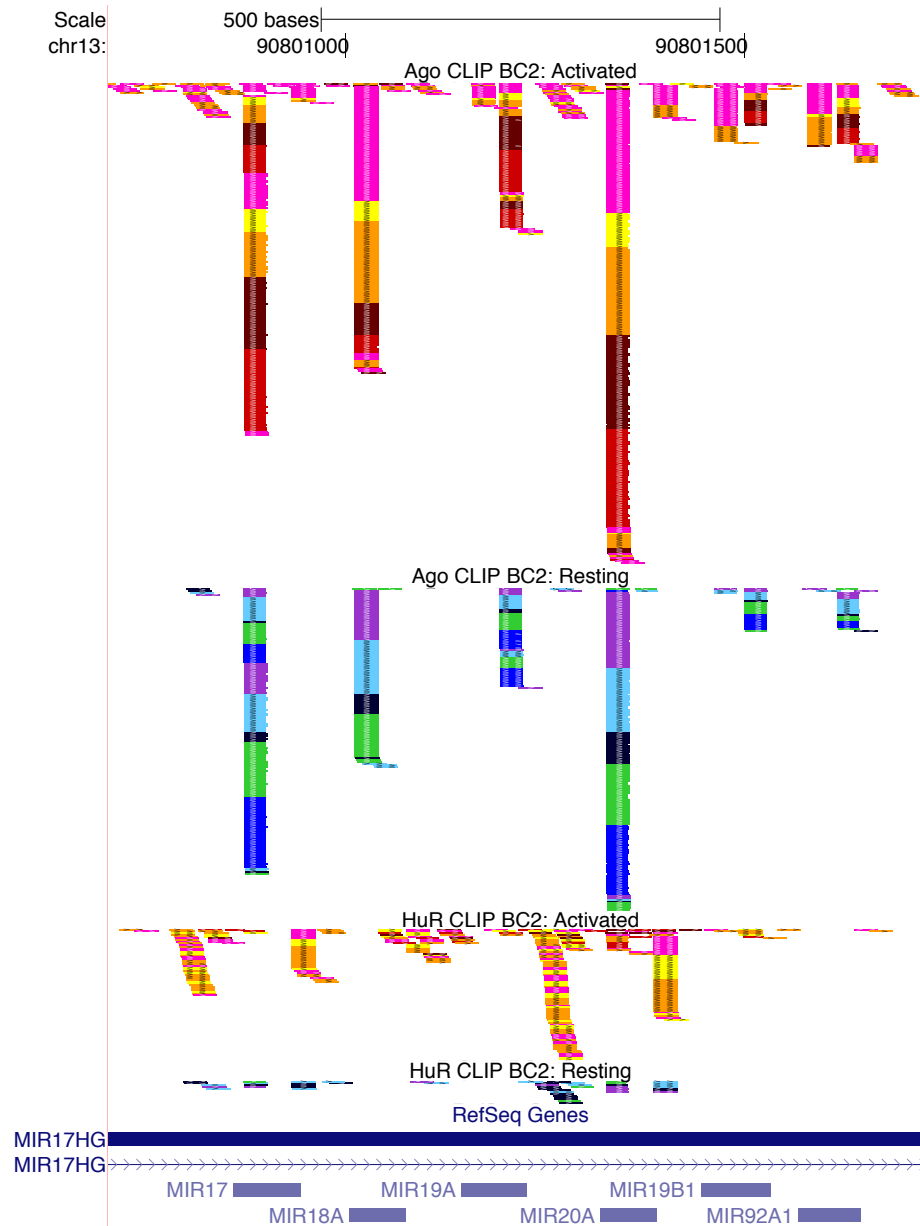


Figure 6.11 Ago and HuR bind the Human microRNA-17-92 Locus. The position of individual Ago and HuR unique CLIP tags in biologic complexity two clusters plotted relative to their mapped position on the human microRNA-17-92 locus. From top to bottom: chromosomal location, Ago CLIP tags from activated CD8 T cells (colors represent each donor sample as shown in Table 6.1), Ago CLIP tags from resting CD8 T cells, HuR CLIP tags from activated CD8 T cells, HuR CLIP tags from resting CD8 T cells, Gene and microRNA diagram from RefSeq.

It was interesting to see that HuR bound robustly in the miR-17-92 locus and that the binding appeared to map to regions either between the inferred structure of microRNA stem loops or mostly excluding what would become the mature sequences. We found this same pattern of Ago binding to eventual mature microRNA sequences and HuR binding surrounding these sequences in many other microRNA loci (data not shown). The HuR cluster binding sites from the miR-17-92 cluster are highlighted in orange in Figure 6.12, adapted from (Chaulk et al., 2011). The exceptions to this binding pattern of HuR being limited to between the microRNAs in this region were binding sites coating the entire miR-20a stem loop, and minor binding sites not highlighted in the figure on miR-17 and miR-19b which each contained less than 10 tags between the resting and activated state.

Discussion

We have defined reproducible genome-wide maps of Ago and HuR RNA binding sites before and after T cell activation and have identified differences in the binding maps of both Ago and HuR in resting and activated T cells. Both Ago and HuR rapidly assemble on newly transcribed RNA such as EGR3 and IFNG. In the latter case these proteins were found to bind pre-processed message as determined by the coating of binding sites along intronic regions in addition to coding sequence and UTRs. The inclusion of RNA-binding events on intronic regions suggest that Ago and HuR may play a role in the regulation of processing of these and other nascent transcripts. While Ago and HuR proteins are present in the nucleus of the cell, their role there is less defined. We speculate that shuttling of HuR out of the nucleus with T cell activation may involve the

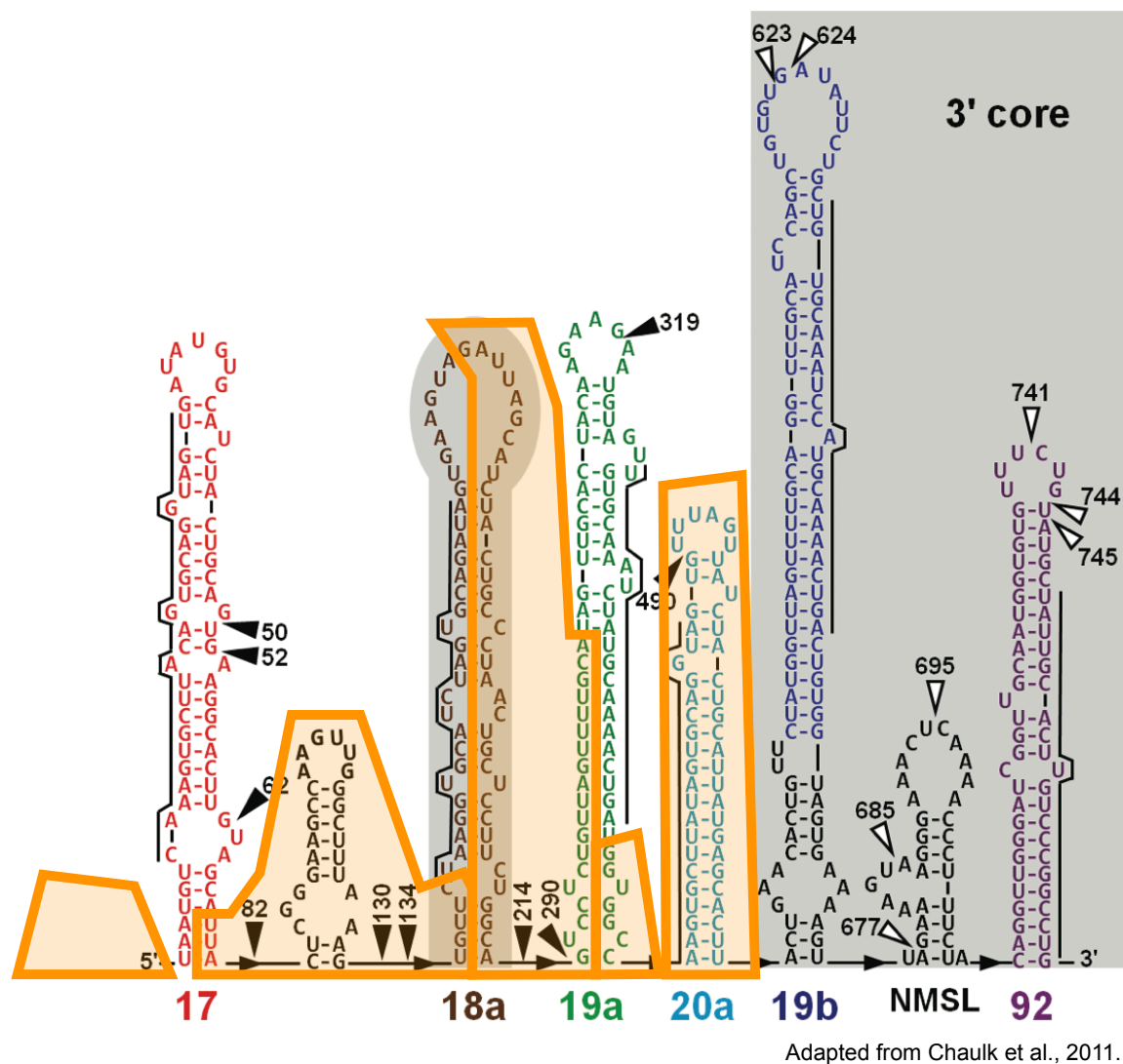


Figure 6.12 HuR binding sites mapped onto miR-17-92 Locus. Predicted secondary structure of microRNA-17-92 locus with RNase T1 cleavage sites indicated with arrows from Chaulk et al. 2011. Highlighted in orange are the sequences found in robust human HuR binding sites. The mature microRNA sequences are indicated with black lines.

transport of RNA molecules poising them for post-transcriptional regulation. This would allow quick association of targets with active polysomes or the combination of Ago and HuR binding might lead to the competition of these transcripts for active translation or storage in stress granules. As mentioned in previous chapters, while the binding maps at one hour of activation most likely represent not only an hour of stimulation but a combination of earlier time points, it would be interesting to see how these binding maps resolve at earlier and later time points and if intronic binding persists with increased time after stimulation.

Interestingly, the stoichiometry of Ago and HuR binding in the activated states differs for these two examples. While there is more binding of HuR on the EGR3 transcript, Ago binding predominates in the IFNG transcript. We hypothesize that these differences may help determine the fate of these transcripts with time after stimulation. While both transcripts are greatly induced with CD3/CD28 activation, the ultimate fate of these transcripts is most likely determined by RNA-binding protein regulation. We speculate that the dominant Ago binding on the IFNG transcript may help to temper the induction of translation of the cytokine while the HuR predominance on EGR3 may be transiently increasing the stability of this transcript. It would be interesting to study the Ago and HuR binding events at earlier and later time points to examine whether these ratios shift over time to help mediate the fluctuations in the availability of these transcripts and their necessity in different sequential points of the inflammatory response. Also, studying the translational status of these transcripts over time with paired binding maps would help elucidate these regulatory mechanisms.

Many Ago-binding footprints on a given transcript overlap with those of HuR, and our results suggest that in these clusters the peak position of Ago and HuR are quite superimposed. We also observed the overlapping of Ago and HuR binding events in both resting and activated T cell states suggesting that the coincident binding is not solely a function of T cell stimulation or the rapid increases in transcription therein. One interpretation of these observations is that Ago and HuR are directly competing for binding interactions on the same transcript in the same cell. However, since HITS-CLIP data represent cellular population averages, it is also possible that Ago and HuR bind to the same sites on distinct transcript populations. In both cases, it is interesting that the two proteins share so many sites of regulation. Because the binding patterns of both proteins often reflect changes in transcript abundance, it appears that the binding status is very much reflective of the abundance of targets within the cell. Also, because these binding changes with T cell stimulation are so similar, it appears that Ago and HuR could be binding to these transcripts cooperatively to regulate post-transcriptional control. This would lead to the determination of the fate of the transcripts in terms of its translational status, stability, and cellular localization. It will be interesting to study whether this combinatorial control results in competition between these pathways mediated by each individual protein or whether they work in concert to determine the outcome of the target.

While overlapping Ago and HuR binding patterns are often mirrored with T cell activation, we were able to identify examples of binding sites where the two proteins change dynamically in opposite directions with CD3/CD28 stimulation. We highlighted the IRF9 and SATB1 3'UTRs and the FYB transcript which show robust overlapping binding of both proteins in both T cell states, but have opposite dynamic quantitative

shifts for Ago and HuR with T cell stimulation. These binding interactions may represent competition between Ago and HuR for binding sites on these transcripts. These shifts may act to quickly change the processing of these targets during the initiation of T cell activation. Still, the biologically reproducible binding sites in both activation states for both of these targets indicate that the binding may not be as simple as a complete switch between the two with T cell stimulation. These sites could in fact represent a dependence on one protein for recruitment of the other or could represent antagonistic binding where one protein blocks binding sites from the other in opposing stimulation states. Furthermore, since the data represent the population average of the T cells, it is possible that while the two proteins may compete for these binding sites that only one protein occupies the 3'UTR in any one, or the two could be regulating the same individual transcripts.

The microRNA seed matches and top 7-mers represented in Ago binding footprints differ between the group of clusters that overlap with HuR or do not. We found that the most highly cloned microRNA in Ago CLIP, miR-142-3p was overrepresented in clusters of Ago regulation that did not overlap with HuR binding sites. Interestingly, most of the highly represented microRNAs predicted to be in Ago clusters that overlap HuR were not highly abundant in Ago CLIP cloning of microRNAs. In other words, there may be enrichment of Ago to binding sites for rare microRNAs by HuR, perhaps acting as a chaperone. At this point, it is unclear whether these microRNAs were underrepresented in the CLIP results, or whether in clusters where Ago and HuR both bind, if the microRNA is less critical to the specificity of Ago binding at those sites. It would be

interesting if HuR helped recruit Ago to binding sites in a non-microRNA specific manner to help regulate transcript ability and protein abundance.

We also considered Ago and HuR binding in primary microRNA regions. While we saw very large and reproducible Ago clusters on transcript sites that would be processed to become mature microRNAs, we saw reduced HuR binding there. This is consistent with our finding that we did not see microRNAs being amplified from HuR immunoprecipitation even when we cut at lower molecular weights from CLIP nitrocellulose membranes (data not shown). Surprisingly, we saw very robust HuR binding directly adjacent to and between the sequences that would become mature microRNAs in many regions. The stem loops and tertiary structures of these transcripts are important for the regulation of the mature sequences and the primary microRNAs can be involved in transcript targeting in the absence of processing (Chaulk et al., 2011; Liu, Min, Yue, & Chen, 2008; Meisner & Filipowicz, 2010; Trujillo, Yue, Tang, O'Gorman, & Chen, 2010; S.-B. Yue, Trujillo, Tang, O'Gorman, & Chen, 2011). Thus, it will be interesting to examine the implications of HuR binding on the regulation of microRNA processing and targeting.

Comparing the Ago and HuR HITS-CLIP genome-wide maps suggests agonistic and antagonistic actions of these two proteins to confer microRNA-mediated regulation of mRNA transcripts. Our results suggest that differences in RNA interactions occur quickly after T cell activation and provide important insight into the specificity of how microRNA translational regulation may mediate the inflammatory response.

CHAPTER 7. Characterization of Ribosomal Profiling of Resting and Activated T cells

Introduction

It has been demonstrated that the levels of mRNA expression are not perfectly correlated with protein levels in a mammalian cell. In a study by Vogel et al. combining microarray and shotgun proteomic analysis, it was described that only roughly two thirds of protein expression can be modeled by mRNA levels and sequence properties such as transcript length, amino acid usage and secondary structure (Vogel et al., 2010). Another study estimated that less than half of protein expression could be explained by mRNA levels and that translational efficiency was the best predictor of protein abundance (Schwanhäusser et al., 2011). Therefore, in order to understand the biological implications of dynamic changes in the RNA binding sites of HuR and (Argonaute) Ago, it is important to consider factors beyond steady state RNA levels.

HuR and Ago have been shown to positively and negatively regulate gene expression at transcriptional and translational levels. Although much work studying HuR has focused on transcript stability, HuR has also been linked to dynamic control of translation such as in the study of UV-C irradiation of cancer cell lines (Lal et al., 2004; Mazan-Mamczarz et al., 2003). HuR was also shown to promote translation of cytochrome c, as evidenced by levels and synthesis of cytochrome c being directly correlated to levels of HuR as determined by knockdown and overexpression experiments without observable changes in cytochrome c mRNA expression (Kawai et al., 2006). HuR overexpression studies in macrophages, in an inducible mouse model, displayed a reduction in TNF protein levels

with increased HuR expression. This was despite augmented levels and stability of TNF mRNA, showing that stabilization of transcripts by HuR can be uncoupled from translational increases (Katsanou, Dimitriou, & Kontoyiannis, 2006). This work and that by Sureban et al., describe competition between HuR and other RNA binding proteins for regulation of RNA targets. For example, *in vitro* studies showed that CUGBP2 competes with HuR to mitigate the effect of HuR promoting increased translation of COX-2 mRNA (Sureban et al., 2007). Additionally, HuR has also been shown to relieve microRNA localization of CAT-1 mRNA to P-bodies within the cell upon amino acid starvation and linked to the subsequent translational de-repression of CAT-1 (Bhattacharyya, Habermacher, Martine, Closs, & Filipowicz, 2006a; 2006b).

There is evidence that microRNAs can mediate changes in protein expression without affecting steady state levels of mRNA targets, poly-A tail length, or polysome association of the transcript (Olsen & Ambros, 1999). Still, others have found that decreases in mRNA levels by microRNA mediated repression can predominantly account for the protein expression changes of their targets (Baek et al., 2008; Guo, Ingolia, Weissman, & Bartel, 2010; Hendrickson et al., 2009). It has also been reported that the timing for translational control may precede the corresponding changes in mRNA expression (Bazzini, Lee, & Giraldez, 2012; Selbach et al., 2008). Other mechanisms of translational control by Ago have been proposed as well, such as the microRNA mediated deadenylation of mRNA targets leading to degradation of target transcripts but uncoupled from translational control, or microRNA interaction with targets inhibiting initiation of translation (Pillai et al., 2005; Wu, Fan, & Belasco, 2006). While most studies have focused on microRNA mediated repression of translation, it has also been reported that

there are cases where Ago binding helps to mediate translational activation of its targets (Henke et al., 2008; Jopling, Yi, Lancaster, Lemon, & Sarnow, 2005; Vasudevan & Steitz, 2007; Vasudevan, Tong, & Steitz, 2007; 2008; Ørom, Nielsen, & Lund, 2008).

In summary, microRNA mediated targeting of mRNA targets has been implicated in enhancing or repressing translation of those targets both with and without effecting changes in target abundance and by interfering with multiple other mechanisms of translational control. The majority of these studies of Ago and HuR function have been performed in cell lines with overexpression or knockdown of microRNAs or with reporter constructs. It is therefore important to study RNA regulation and translational control in a biologically meaningful dynamic setting of primary cells in the context of the combinatorial control of Ago and HuR regulation.

To accomplish this, we sought to use a technique that measures the steady state translational profile of the cell via a high-throughput sequencing approach. As proteins are being synthesized, ribosomes translocate along transcripts to determine the ultimate amino acid sequence to be produced. These ribosomes are able to protect around 30 nucleotides of bound RNA from nuclease digestion. After digesting surrounding and unbound message in a cell, ribosomes and their protected RNA can be isolated and cloned (Guo et al., 2010; Ingolia, Brar, Rouskin, McGeachy, & Weissman, 2012; Ingolia, Ghaemmaghami, Newman, & Weissman, 2009). By sequencing fragments of ribosomal protected material, we can gain quantitative insight into which transcripts are actively being translated into protein at any point in time in a living cell.

In order to determine a global view of the translational profile of the cells as it relates to the transcriptional setting, cells were treated with cycloheximide to arrest ribosomal complexes from translocating and thereby blocking translational elongation. The resting and activated cluster of differentiation eight (CD8) T cells were each split into two aliquots for analysis of the ribosomal footprints in the cells and the levels of mRNA. From one aliquot, the cells were lysed and the RNA was digested with micrococcal nuclease to reduce the RNA into fragments that were protected by the ribosome. The lysate was spun over a sucrose gradient and then fractions were collected to separate the monosomes from the remaining material. The ribosomal protected fragments (RPFs) were purified from the monosome fraction. In parallel, total RNA was isolated from the second aliquot of cells. The poly-A RNA was selected using Oligo (dT)₂₅ beads to enrich for mRNA from the lymphocytes. The poly-A RNA was alkaline hydrolyzed to reduce the mRNA into small fragments. Both the RPFs and poly-A RNA fragments were then cloned, amplified, and were used for high-throughput sequencing to determine the ribosomal and transcriptional profiles of the cells (Figure 7.1).

Results

Nuclease Titration of CD8 T cells for Sucrose Gradients

To isolate fragments of RNA protected by the ribosomal complex, it was necessary to determine an optimal nuclease digestion protocol to sufficiently degrade non-protected RNA, but also to leave the ribosomal complexes intact so that they could be purified on the sucrose gradient. We found that multiple cell types responded very differently to nuclease treatment, presumably because of their endogenous nuclease activities, so a

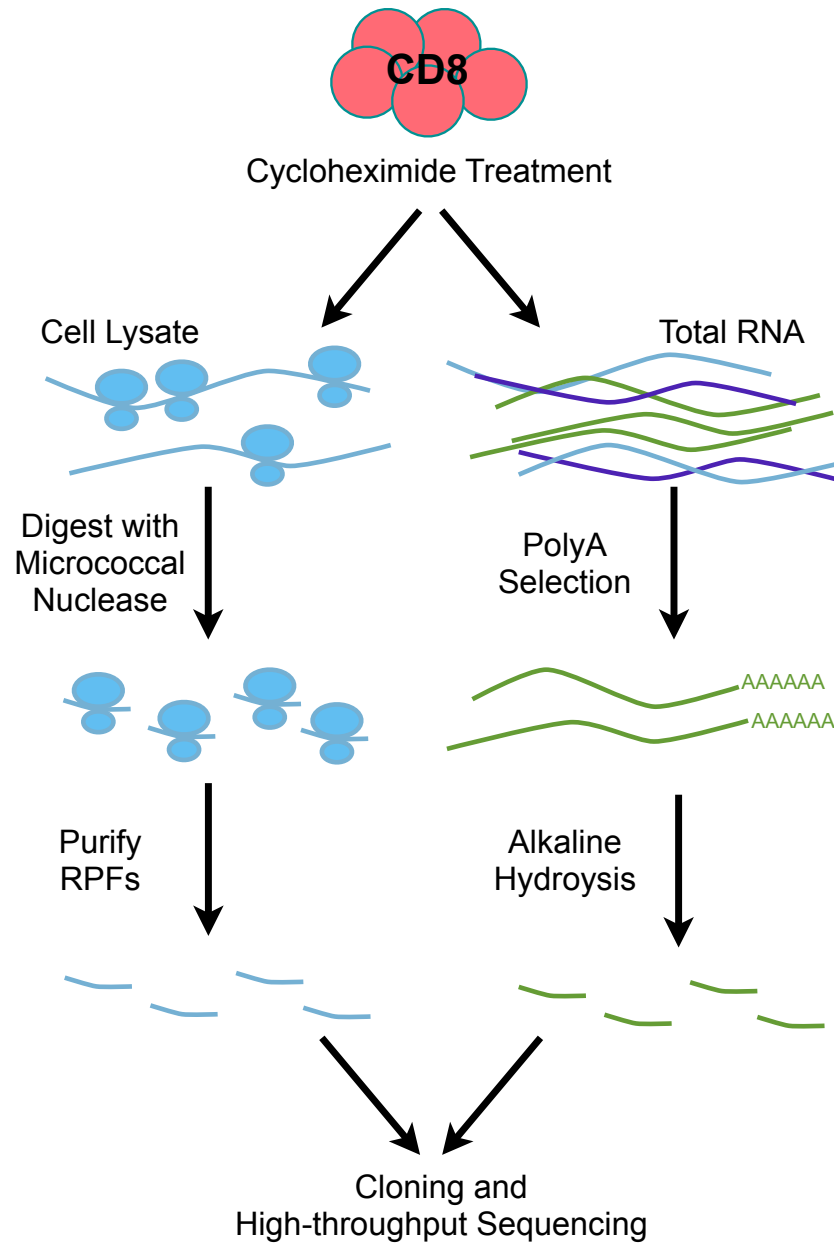


Figure 7.1 Ribosomal Profiling and RNA Sequencing Schematic. CD8 T cells were treated with cycloheximide and snap frozen. (Left) Aliquots of CD8 T cells were lysed and treated with micrococcal nuclease to digest RNA to ribosomal protected fragments (RPFs). (Right) Total RNA was extracted from aliquots of CD8 T cells and poly-A selected. Poly-A RNA was alkaline hydrolyzed to reduce RNA to fragments of similar length to RPFs. RNA fragments were purified, size selected, cloned, and amplified for high-throughput sequencing. (Adapted from Guo et al. 2010).

titration with comparable starting material to the experimental cells was necessary. To determine the optimal nuclease digestion protocol, we subjected equivalent aliquots of CD8 T cells to different nucleases at varying concentrations and for different periods of time. Next we spun the lysate through a 10%-50% linear sucrose gradient and examined the profile of the resulting ribosomes.

When the cells were lysed, but not treated with any nuclease, a large monosomal peak was present and then smaller peaks to the right of the monosome peak represented the presence of polysomes within the sample (Figure 7.2.A). For ribosomal profiling, it would be ideal to digest the RNA so that the polysomes are reduced to monosomes so that all ribosomes would be present in the same sucrose fractions protecting RNA of uniform size.

When we digested the lysate with RNase I, we found that although the presence of polysomes may have decreased, we saw a drastic reduction of the monosome peak that was further diminished with increased digestion time and or increased RNase I concentration (Figure 7.2B,C,D). We concluded that the RNase I was not only digesting mRNA, but also breaking apart the ribosome itself. This is not the desired outcome, as we intended to clone all the ribosomal protected material.

We also digested T cell lysate with micrococcal nuclease. When we treated the cells with 1,000 units of the nuclease per milliliter of lysate for 25 minutes at room temperature, the size of the monosome peak was greatly increased as compared to the non-digested sample and the polysome peaks smoothed out slightly (Figure 7.2E). When we increased the digestion to 20,000 units for the same time period, the monosome peak decreased

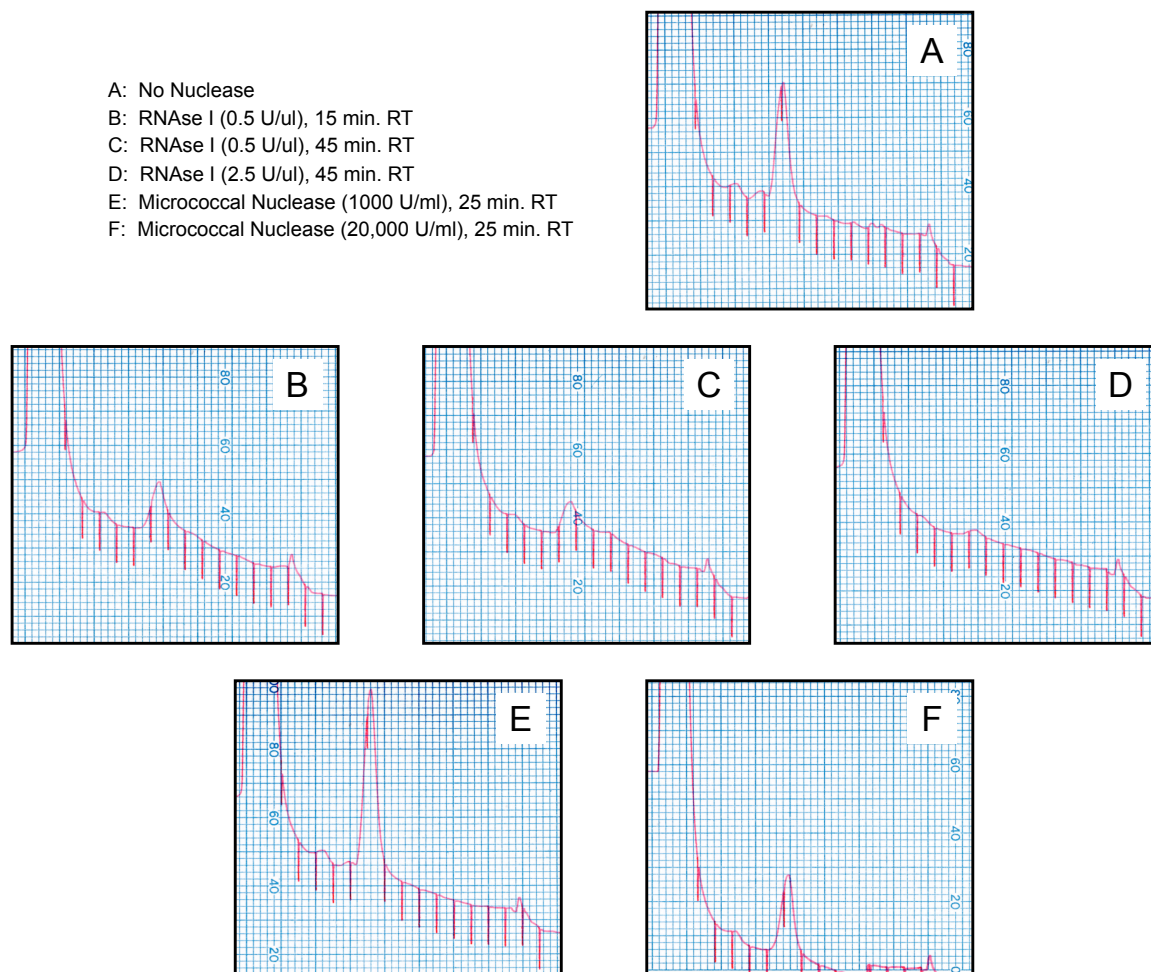


Figure 7.2 Sucrose Gradients After Nuclease Titration. Cell-equivalent aliquots of CD8 T cells were nuclease digested with the indicated protocols and applied to 10%–50% sucrose gradients. A₂₅₄ traces of total RNA distribution are shown.

dramatically (Figure 7.2F). Therefore we determined that using 1,000 units per milliliter lysate micrococcal nuclease would be optimal to maximize the number of monosomes collected during sucrose fractionation.

Poly-A mRNA selection and Alkaline Hydrolysis Titration

In order to clone poly-A RNA in parallel with the RPFs, we fragmented the RNA into smaller pieces so that the ribosomal protected and total RNA could be processed and sequencing in the same manner. To determine the optimal amount of hydrolysis, total RNA was Trizol extracted and ethanol precipitated from lymphocytes. The resulting RNA was then poly-A selected using Oligo (dT)₂₅ beads. Next, sodium hydroxide was added to the RNA sample to increase the pH and hydrolyze the RNA into smaller fragments. We incubated the samples at 37°C for different amounts of time ranging from 5 to 90 minutes and then quenched the base with hydrochloric acid and added buffer to help stabilize the pH of the sample. The RNA was precipitated and analyzed on a Urea Acrylamide gel (Figure 7.3). After only 5 minutes of digestion, the RNA remained in large pieces and much of the sample did not enter the gel, remaining in the well at the top of the lane. With increasing time the modal size of the RNA decreased in a stepwise fashion. We determined that digestion for 30 minutes would hydrolyze the RNA sufficiently so that much of the sample would be between 30 and 50 nucleotides.

Preparation of CD8 T cells for Ribosomal Profiling and RNA Sequencing

We asked one of our normal donors (donor 1) from our CLIP experiments to return for a repeat leukapheresis. This allowed us to acquire enough starting material to perform the

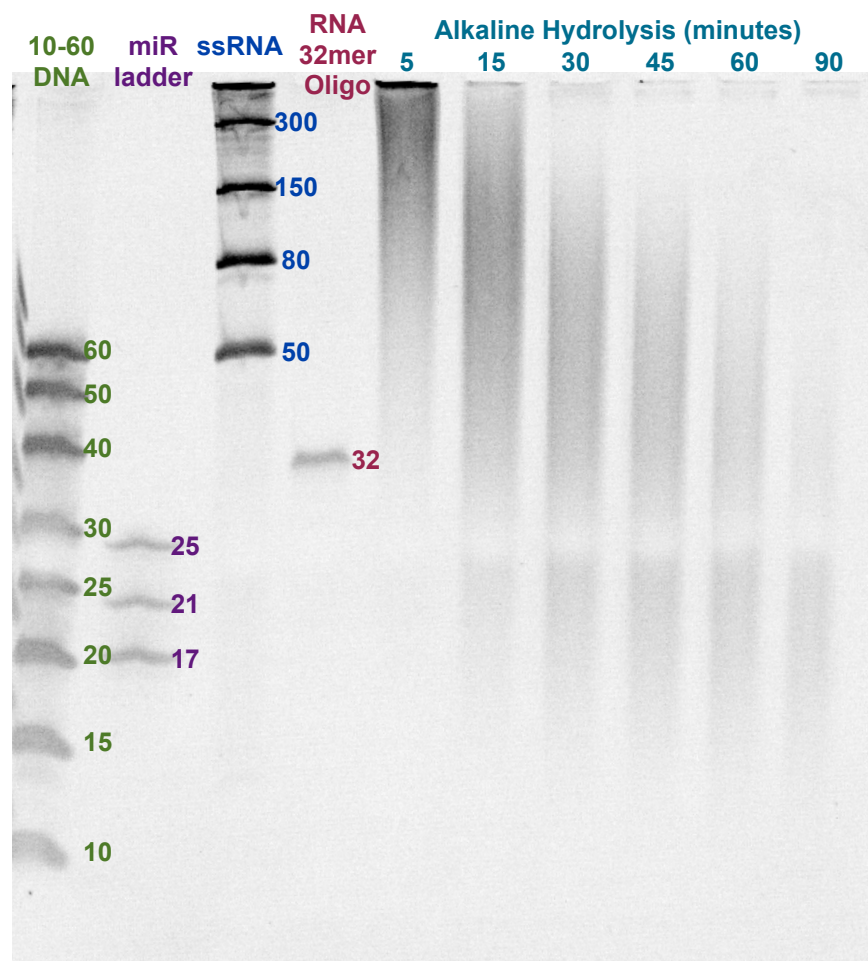


Figure 7.3 Urea gel of Alkaline Hydrolysis Duration Titration. Poly-A RNA from lymphocytes was alkaline hydrolyzed with sodium hydroxide. At the indicated amounts of time, the basic solution was quenched with hydrochloric acid. 20% Urea-Acrylamide gel with separated RNA fragments is shown. MicroRNA Marker (New England Biolabs, N2102S), Low Range ssRNA Ladder (New England Biolabs, N0364S), and RNA 32-mer oligonucleotides are shown with indicated sizes.

ribosomal profiling and RNA sequencing experiment while genetically matching the samples used to create our previous datasets. To isolate CD8 lymphocytes using the same protocol as for CLIP, the leukapheresate was layered and spun through a Ficoll gradient to collect PBMCs. The PBMCs were depleted of CD56+ cells and then selected for CD8 T cells. After resting the sample overnight, the resulting sample was 97% live cells and 94% CD8 T cells. In this preparation there were about 4% contaminating CD4 T cells and less than 1% each of B cells, monocytes, and NK cells present in the sample (Figure 7.4A and data not shown). After the over night resting period, an aliquot was stimulated for one hour with CD3/CD28 beads. The resting and activated T cells were cycloheximide treated and frozen for ribosomal profiling and RNA sequencing analysis. The cells were determined to be sufficiently activated with an almost 4,000 fold induction of IFNG and close to 200-fold induction of TNF RNA in the activated T cells compared to the resting ones (Figure 7.4B). This activation profile is within the range of the activation seen in the lymphocytes prepared for HuR and Ago CLIP.

Sucrose Gradient Profile of Resting and Activated Lymphocytes

To isolate ribosomal protected fragments of RNA, an aliquot of resting and activated CD8 lymphocytes were lysed and treated with micrococcal nuclease to digest RNA to the size of protected pieces by ribosomes. The digested lysate was layered and spun through a 10%-50% linear sucrose gradient. This material was run by upward displacement through a gradient fractionator and sucrose fractions were collected. The A254 traces showed the monosome peak was in fractions 6 through 8 and the relatively smooth trace following the monosome peak showed a decrease in polysomes in the sample (Figure

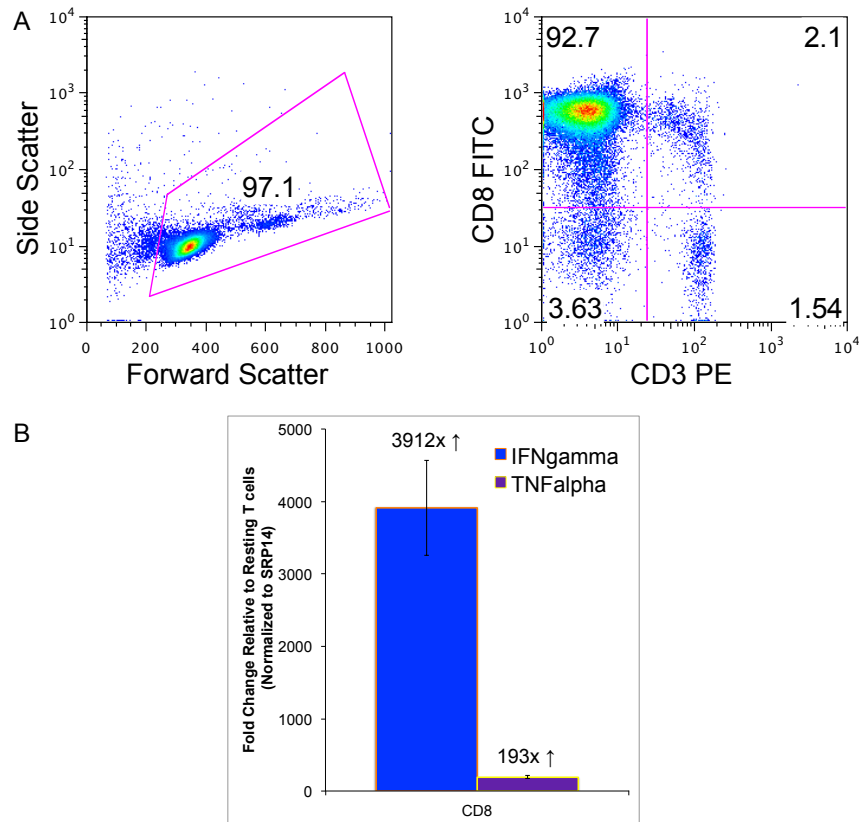


Figure 7.4 CD8+ T Cell Characteristics of Donor 1 for Ribosomal Profiling Experiment. CD8 T cells purified from PBMC of normal human donors by CD56 depletion and CD8 positive selection. **(A)** Forward and side scatter determined by flow cytometry. The percentage of live cells (97.4%) is noted in the gated population (left panel). CD3 and CD8 staining determined by flow cytometry. Percentages of cells are noted in each quadrant (right panel). **(B)** IFNG and TNF mRNA in resting and activated CD8 T cells was analyzed by qRT-PCR. Plotted is the fold change of these transcripts in CD3/CD28 stimulated CD8 T cells relative to resting CD8 T cells mRNA. Fold increase for each transcript is noted above each bar.

7.5A). To be sure that the peak in the A254 trace represented the monosomes, we spotted a nitrocellulose membrane with 2 microliters of each sucrose fraction and probed the membrane with RPL7 antibody. This confirmed that the bulk of ribosomal material resided in fraction 7 for both the resting and activated cells (Figure 7.5B). We therefore pooled the material from fractions 6 through 8 for the resting and activated T cell samples.

Ribosomal Protected Fragments and Poly-A RNA Isolation, Size Selection, and Amplification

We isolated RPFs from the material pooled from sucrose fractions 6, 7, and 8. Smaller aliquots of resting and activated T cells were lysed for mRNA sequencing and poly-A RNA was prepared for cloning after a Trizol extraction, oligo (dT)₂₅ selection, and alkaline hydrolysis. Both the RPFs and fragmented poly-A RNA from resting and activated T cells were run on a Urea Acrylamide gel. Fragments of roughly 35 nucleotides in length from the ribosomal fractions and poly-A RNA fragments of roughly 35 to 55 nucleotides were isolated from the gel (Figure 7.6).

The RNA fragments were polyadenylated to create an anchor for reverse transcription. The polyadenylated RNA was reverse transcribed using primers specific to the poly-A tail and containing sequences necessary for PCR amplification and high-throughput sequencing. PCR was done in the presence of SYBR green and amplification was monitored on a real time PCR machine to bring the products to an optimal concentration for sequencing. The products were purified and quantified for high-throughput sequencing (Figure 7.7). We saw a distinct band at the size of the RPFs with the additional poly-A and primer sequences and a smear of the expected size from the

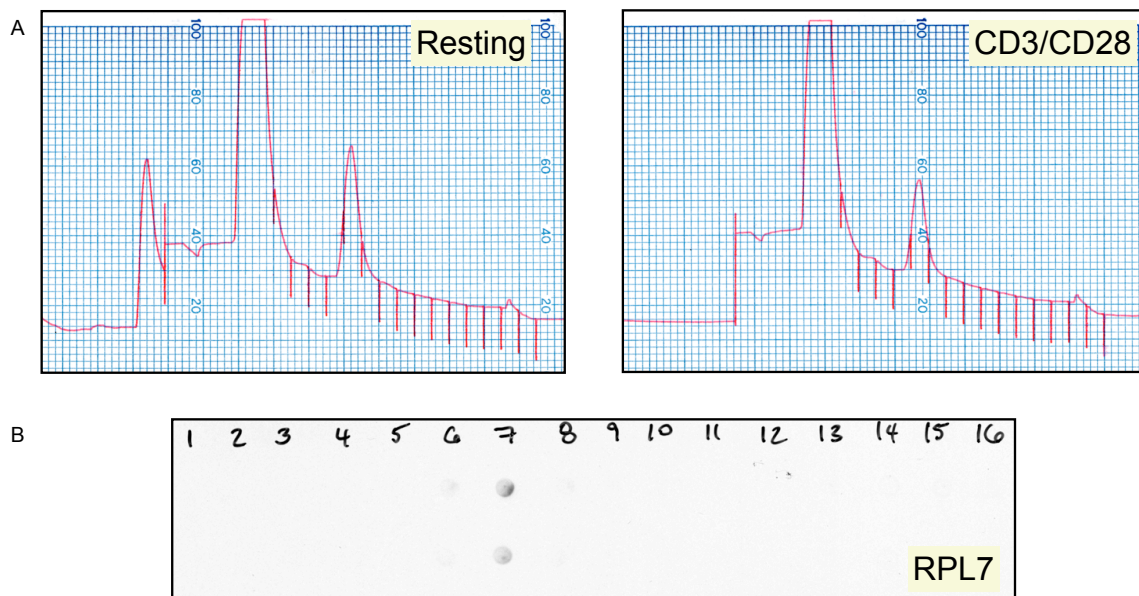


Figure 7.5 Sucrose Gradient Profile of Resting and CD3/CD28 Stimulated CD8+ T Cells. (A) Cell-equivalent aliquots of resting or CD3/CD28 Stimulated normal human donor 1 CD8 T cells were micrococcal nuclease digested (1000U/ml) for 25 minutes at room temperature and applied to 10%–50% sucrose gradients. A₂₅₄ traces of total RNA distribution are shown. (B) 2 μ l aliquots of gradient fractions were dotted onto nitrocellulose and were analyzed by western blotting for RPL7 (with Rabbit polyclonal RPL7 specific ab72550) to determine the distribution of ribosomes.

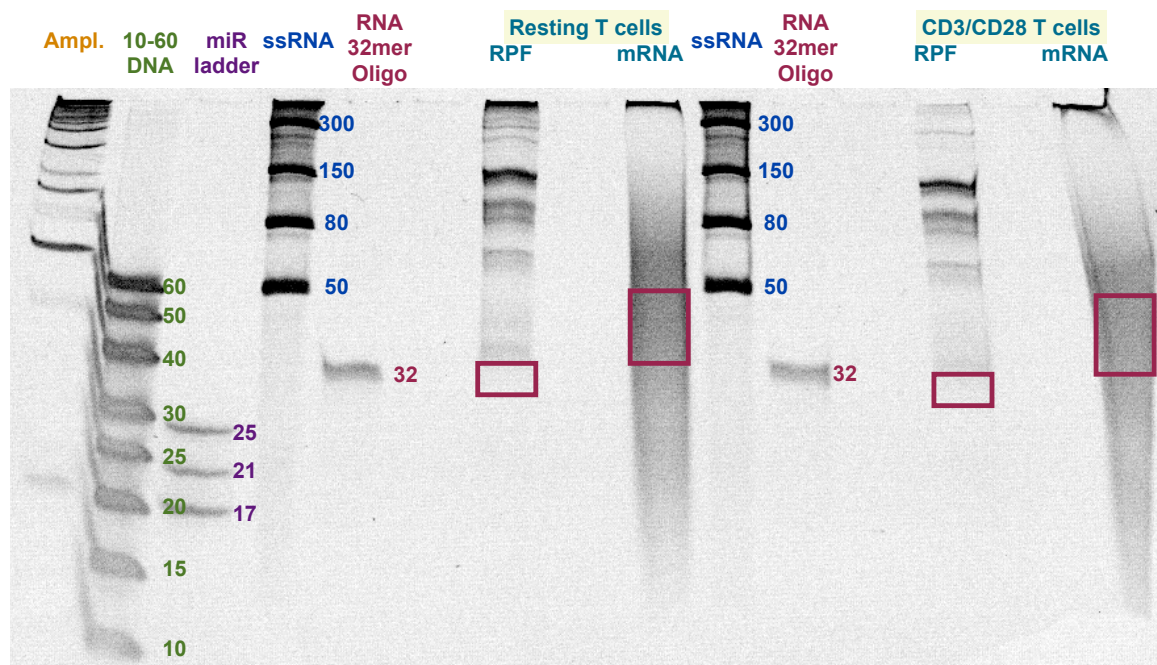


Figure 7.6 Urea Acrylamide Gel of RPFs and PolyA RNA. 20% Urea-Acrylamide gel with separated RNA fragments is shown. Isolated ribosomal protected fragments (RPFs) and poly-A mRNA (mRNA) from resting and CD3/CD28 activated CD8 T cells are indicated. MicroRNA Marker (New England Biolabs, N2102S), Low Range ssRNA Ladder (New England Biolabs, N0364S), and RNA 32-mer oligonucleotides are shown with indicated sizes.

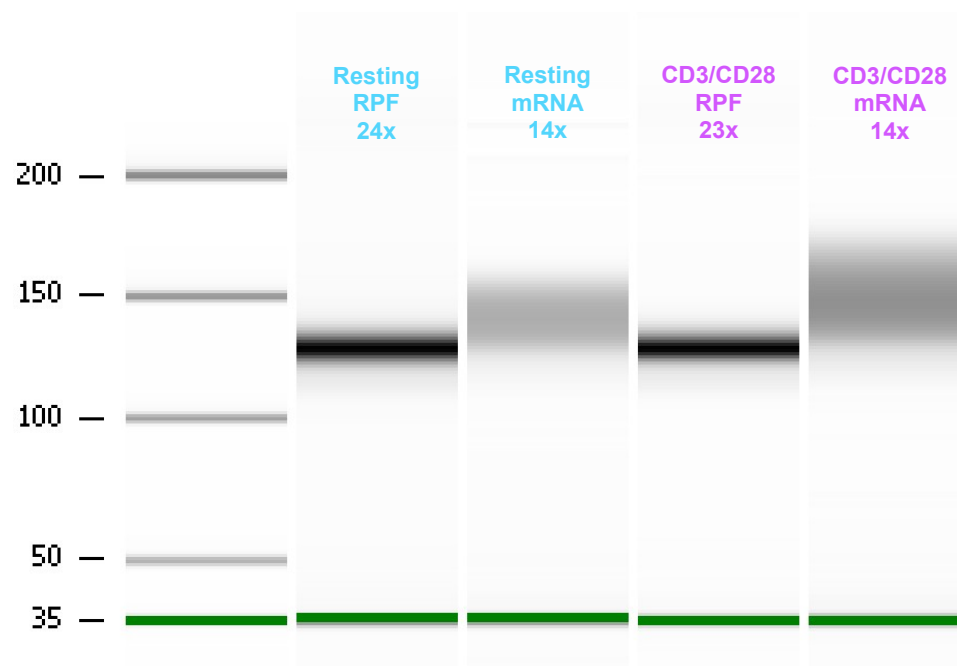


Figure 7.7 RPFs and mRNA PCR Products for High-Throughput Sequencing. High sensitivity DNA assay bioanalyzer results for ribosomal protected fragments (RPFs) and poly-A mRNA (mRNA) for resting and CD3/CD28 activated T cells as indicated. PCR cycle numbers for each sample are shown (#x).

hydrolyzed mRNA fragments. We used different RT primer sequences for the mRNA and RPFs so that the two samples could be pooled for sequencing for the resting and activated samples.

Ribosomal Profiling Read Statistics and Genomic Distribution of Binding

The high-throughput sequencing produced over 200 million total reads for both the resting and the activated samples. After filtering the raw data and collapsing it to contain only one copy of each sequence there were between 55 and a little over 70 million unique sequencing reads. Next we stripped the reads of the linker sequences to distinguish whether the tags came from RPFs or mRNA. We retrieved 6 to 10 times as many raw reads from the mRNA as from the RPF samples (Table 7.1). This may be in part due to the differences in the amounts of starting material for each of these samples. We started cloning from a greater amount of RNA as seen by the levels stained on the Urea Acrylamide gel in Figure 7.6, which led to the requirement for around 10 fewer PCR cycles to bring them to a concentration necessary for sequencing. This would lead to many less duplicate reads being created during the amplification process, many of which were already eliminated in the proceeding step. Furthermore, it is possible that the initial complexity of the RNA pools was different for the RPFs and the mRNA samples. The poly-A samples should represent the mRNA in the cell whether or not it is being translated. It also would include all regions of the molecule, while coding regions should predominate the translating population of RNA. Therefore, the expected complexity of these samples would be very different.

Table 7.1 RPFs and mRNA Sequencing Read Statistics.

| | Resting | | Activated | |
|----------------------------|-------------|------------|-------------|------------|
| Total Reads | 220,007,550 | | 215,585,970 | |
| After Quality Filtering | 192,965,617 | | 200,798,983 | |
| Exact Duplicates Collapsed | 70,033,114 | | 55,768,748 | |
| | RPF | mRNA | RPF | mRNA |
| Linker Stripped | 8,537,955 | 51,405,429 | 4,646,999 | 43,333,499 |
| CLIP Adaptor Removed | 8,409,472 | 50,369,268 | 4,568,050 | 42,476,315 |
| Poly-A Sequences Removed | 8,290,118 | 49,351,320 | 4,486,767 | 41,310,320 |
| hg18 Mapping | 3,903,433 | 33,254,982 | 2,582,273 | 29,964,273 |
| Not Mapped to rRNA | 3,822,809 | 31,746,326 | 2,504,216 | 28,938,339 |
| CDS Only | 3,214,813 | 6,995,210 | 2,201,969 | 5,976,530 |
| PCR Duplicates Collapsed | 128,780 | 5,251,323 | 218,095 | 5,186,994 |
| | | | | |
| rRNA Mapping | 347,403 | 4,212,912 | 177,901 | 2,974,432 |
| PCR Duplicates Collapsed | 23,666 | 1,085,502 | 21,479 | 1,144,789 |

Next, the adapter and poly-A sequences were removed from the ends of the sequences and reads that contained only these sequences or had less than 5 nucleotides left after their clipping were removed from the dataset. The resulting reads were mapped to the hg18 build of the human genome. Between 2.5 million and 4 million RPF reads and around 30 million mRNA reads mapped to the genome per sample. Next, reads that mapped to rRNA were subtracted from the samples to remove these contaminating sequences. We then specified that the reads must map to coding sequence or untranslated region (UTR) exonic regions of the genome which only slightly reduced the number of RPF reads but reduced the reads from the mRNA dataset to between 20 and 22 percent of the mapped reads (Table 7.1). This removed the potential for contamination from non-mRNA species. As seen in Figure 7.8, the great majority of RPF reads mapping to the human genome were either in the coding sequence or exonic regions of the 5'UTR and 3'UTR of transcripts. Still, 37 percent of the mapped RPF reads from resting T cells and 17 percent of the mapped RPF reads from activated T cells fell in intronic regions of transcripts, deep intergenic regions of the genome or mapped to rRNA (Figure 7.8). We removed these data from subsequent analyses from both the RPF and mRNA datasets so that they would accurately represent material likely to be present on ribosomes.

Degenerate barcode sequences added to the RNA during the RT reaction allowed us to collapse for PCR duplicates in the same manner as with our CLIP data. This allows us to reduce sequences to one copy that may have mismatches but map to the identical genomic locus and have the same barcode sequence. This again was more impactful for the RPFs than the mRNAs because they required more PCR cycles of amplification and therefore many more replicates of uniquely cloned events. These resulting collapsed

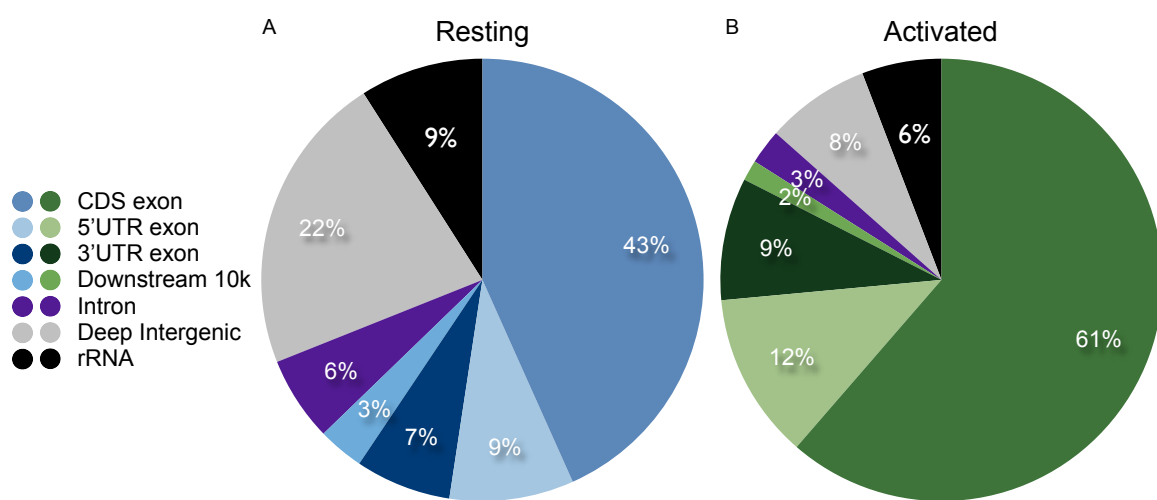


Figure 7.8 Mapped RPFs Read Genomic Distribution. Distribution of human genome (hg18 build) mapped ribosomal protected fragments (RPFs) represented by pie chart for resting and CD3/CD28 activated CD8 lymphocytes.

reads served as the basis for subsequent analyses. We were able to identify 130,000 RPFs from resting CD8 T cells and 220,000 RPFs from activated CD8 T cells. We also over 5 million mRNA reads for each sample (Table 7.1).

Ribosomal Profiling Changes with T cell Activation

With the RPF and mRNA reads aligned to the genome, we calculated an RPKM (reads per kilobase per million mapped reads) value for each transcript. This allows us to compare a normalized value for RPF and mRNA for the resting and activated states. By comparing the RPF RPKM value for each transcript to its mRNA RPKM we can examine the translational efficiency (TE) of the transcript (Ingolia et al., 2009). Figure 7.9A compares the activated T cell TE with the resting T cell TE. In this figure we demonstrate that the general tendency for most transcripts is that the TE does not shift dramatically between the resting and activated state because the plot seems to resemble the trend of $y=x$. Still, for many transcripts the TE does change with activation. We have highlighted in red transcripts that have the biggest increases in TE in the activated state and are robust 3'UTR targets of either HuR and/or Ago. 3'UTR CLIP targets are highlighted in blue that have decreased TE in the activated state. These same transcript targets are highlighted in Figure 7.9B where the change in RPF between the activated and resting state is plotted against the change in mRNA tags for each transcript. For most of the highlighted transcripts, we saw a greater change in RPF than mRNA with T cell activation, suggesting that while the steady state levels of these transcripts may be changing, the translational status is changing even more rapidly.

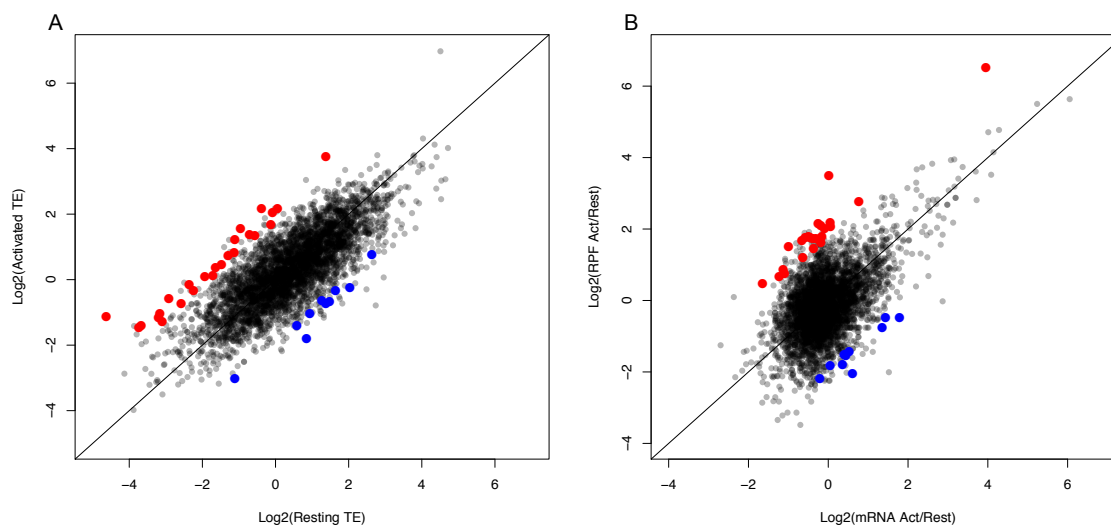


Figure 7.9 RPFs and mRNA Changes with T Cell Activation. (A) Scatter plot of the activated T cell versus resting T cell Log_2 ratio of ribosomal protected fragments (RPFs) reads per kilobase per million mapped reads (RPKM) to the mRNA RPKM (This ratio is called the translational efficiency: TE). Line shown is $y=x$. (B) Scatter plot of the Log_2 ratio of RPF RPKM in the activated to the resting state versus the Log_2 ratio of mRNA RPKM in the activated to the resting state. Line shown is $y=x$. Highlighted in red are transcripts with the largest increases in TE in the activated state compared to the resting state with robust 3'UTR binding targets of Ago and/or HuR. Highlighted in blue are transcripts with the largest decreases in TE in the activated state compared to the resting state with robust 3'UTR binding targets of Ago and/or HuR.

To examine this in more depth, we plotted the RPKM values of RPF versus the mRNA for both the resting and activated states for the red and blue highlighted transcripts from Figure 7.9 in Figure 7.10A. This is further teased apart by highlighting the transcripts with increased TE with activation in Figure 7.10C and decreased TE with activation in Figure 7.10B. In the background a gray point represents the mRNA and RPF data from the resting state and a purple point the data from the activated state. A line connects the two points from each state for each transcript. In this figure the highlighted data from the resting state is represented in the lighter color red or blue and the activated state in the darker color. Looking at the highlighted data of the 3'UTR CLIP target transcripts with the most dynamic changes in TE, we found some targets that have large changes in mRNA abundance between the two states represented by connected points being dispersed laterally. However, most of the large changes in TE are found from targets having dynamic changes in RPF between the resting and activated states, or are represented graphically by shifting vertically. We hypothesize that changes in regulation and binding by HuR and Ago help mediate these changes in translation and occupancy by the ribosomes.

Combining CLIP, Ribosomal Profiling and RNA Sequencing

In Figure 7.11 we combined the dynamic changes seen in CLIP binding with the dynamic changes in ribosomal profiling graphically. To do this, we plotted the Log2 ratio of activated to resting RPKM values of RPF compared to the ratio of activated to resting RPKM values of mRNA for transcripts containing an HuR binding site of biologic complexity of 3 and peak height of 5, but not containing an Ago CLIP cluster of that

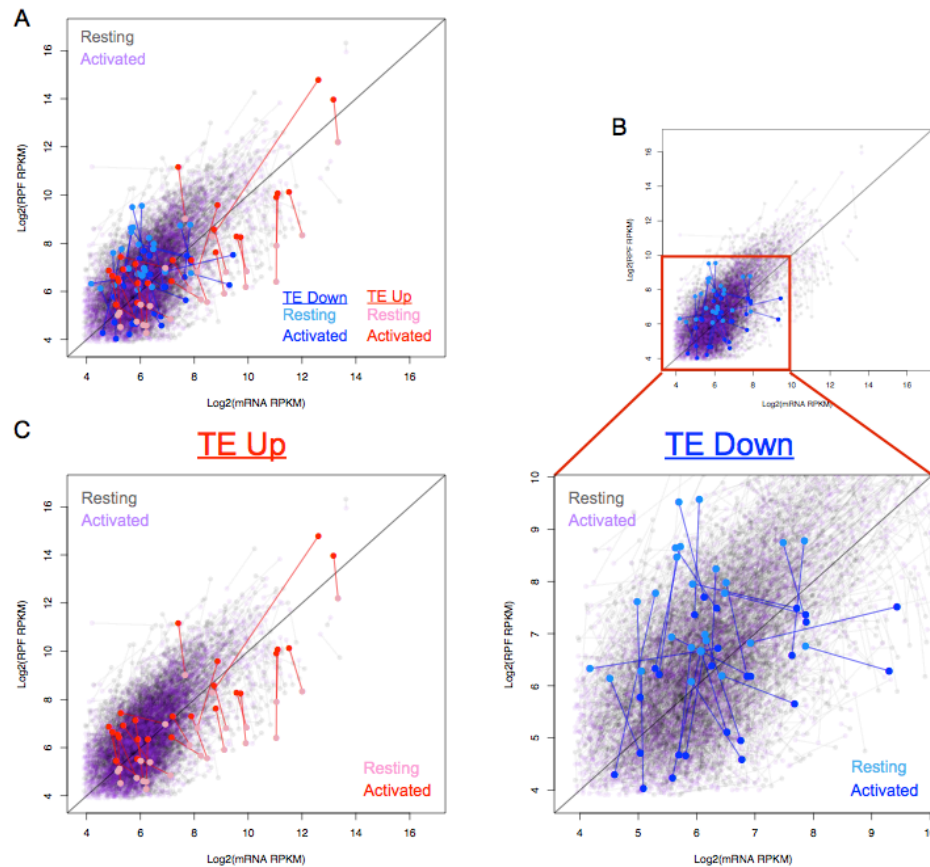


Figure 7.10 T Cell RPFs and mRNA in the Resting and Activated State. (A) Scatter plot of the Log₂ ribosomal protected fragment reads per kilobase per million mapped reads (RPF RPKM) versus the Log₂ mRNA RPKM. In the background, gray points represent data from the resting state and purple points from the activated state. A line connects the two points from each state for each transcript. Highlighted in red are transcripts with the largest increases in translational efficiency (TE, RPF/mRNA) in the activated state compared to the resting state with robust 3'UTR binding targets of Ago and/or HuR (light red points represent data from the resting state and dark red points represent data from the activated state, a red line connects the two points from each state for each transcript). Highlighted in blue are transcripts with the largest decreases in TE in the activated state compared to the resting state with robust 3'UTR binding targets of Ago and/or HuR (light blue points represent data from the resting state and dark blue points represent data from the activated state, a blue line connects the two points from each state for each transcript). Line shown is y=x. (B) Larger view highlighting transcripts with the largest decreases in TE in the activated state compared to the resting state with robust 3'UTR binding targets of Ago and/or HuR. (C) Larger view highlighting transcripts with the largest increases in TE in the activated state compared to the resting state with robust 3'UTR binding targets of Ago and/or HuR.

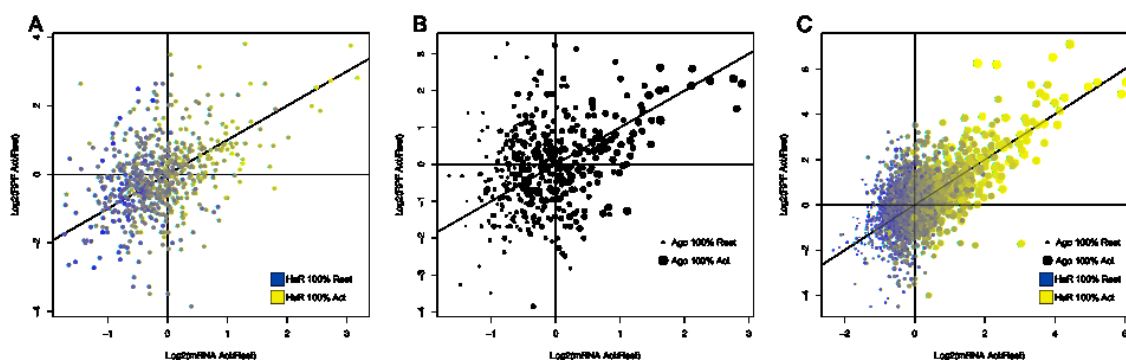


Figure 7.11 Combining Ribosomal Profiling, mRNA Sequencing, and CLIP Data.

Scatter plots of the Log_2 ratio of ribosomal protected fragment reads per kilobase per million mapped reads (RPF RPKM) in the activated state to the resting state versus the Log_2 ratio of mRNA RPKM in the activated state to the resting state. (A) Transcripts with HuR clusters of biologic complexity of three (BC3) and peak height five (ph5) and no Ago clusters of those criteria. Points are colored based upon the percentage of HuR CLIP tags in the cluster from each activation state. The color scale gradient ranges from blue (100% of HuR tags in the resting state) to yellow (100% of HuR tags in the activated state). (B) Transcripts with Ago clusters of BC3 and ph5 and no HuR clusters of those criteria. Points are sized based upon the percentage of Ago CLIP tags in the cluster from each activation state. The scale ranges from the smallest point (100% of Ago tags in the resting state) to the largest point (100% of Ago tags in the activated state). (C) Transcripts with both Ago and HuR clusters of BC3 and ph5. Points are colored based upon the percentage of HuR CLIP tags in the cluster from each activation state. The color scale gradient ranges from blue (100% of HuR tags in the resting state) to yellow (100% of HuR tags in the activated state). Points are sized based upon the percentage of Ago CLIP tags in the cluster from each activation state. The scale ranges from the smallest point (100% of Ago tags in the resting state) to the largest point (100% of Ago tags in the activated state).

robustness. To overlay the changes in HuR binding between the resting and activated states, the points were colored with a gradient of colors to represent the percentage of HuR binding in the resting state (in blue) or activated state (in yellow). There are exceptions to the general pattern, but as described in earlier chapters, the changes in CLIP binding are most directly reflective of changes in mRNA expression levels between the two states. Or more specifically, as transcripts are positioned from left to right on the x-axis representing more mRNA in the resting state to more mRNA in the activated state, the colors of the points shift from dark blue to bright yellow representing a dominance in HuR binding in proportion to the levels of RNA. The translational profile as represented on the y-axis seems to be more scattered without a clear pattern dictating the relationship between HuR binding with the RPF levels as they relate to mRNA expression (Figure 7.11A). This indicates that while HuR binding may impact changes in translational control, there is not an overall rule that governs these dynamics. The role of HuR binding is part of a complex set of interactions with other regulatory RNA-binding proteins and may serve different functions depending on the target transcript.

These same patterns are seen for targets of Ago alone in Figure 7.11B. In this component of the figure, the amount of Ago CLIP binding is represented in the size of the data point on the graph for transcripts where there is a cluster of biologic complexity of at least 3 and minimum peak height of 5 tags, without an HuR cluster at that level of binding on the transcript. If all of the Ago binding is in the resting state, the point is of the smallest size, and would be the largest if the binding were exclusively in the activated state. As seen in HuR binding, the amount of Ago binding in clusters in the activated state increases for transcripts that are more highly expressed in the activated state. Graphically, this is seen

as an increase in the size of the plotted points as transcripts are positioned with increasing mRNA levels in the activated state from left to right. Additionally, it is difficult to decipher a pattern of Ago regulation as it relates to the ribosomal profile of the transcripts with an hour of activation. Similar to HuR, the consequences of Ago binding are often dictated by the sum of interactions of the transcript not solely with Ago but also with other RNA-binding proteins. Thus, even without being able to determine a general rule relating Ago binding to translational status of its targets, it is important to consider the role of Ago on individual transcripts in the context of other regulatory factors.

For transcripts that are robust targets of both HuR and Ago regulation, the correlations between binding and transcript expression are even more apparent. The color gradient representing HuR binding levels in Figure 7.11C clearly shift from blue (resting) to yellow (activated) as transcript expression shifts from left to right representing more binding in the activated state. The dot size representing Ago binding also shift from small to large in this direction showing a strong correlation between the binding proteins and transcript expression level. Still, there are outliers from this pattern where large blue dots are seen or small yellow ones showing a shift in binding between the resting and activated state of the two proteins. This is consistent with previously discussed results in Chapter 6. While the majority of targets regulated by both proteins display binding patterns for each that match gene expression, there are exceptions where the binding patterns fluctuate in opposite directions with T cell stimulation.

Additionally, while Ago and HuR binding patterns seem to mirror transcript expression as seen in their patterns with respect to the x-axis, there are many points that do not

follow a $y=x$ trend. In fact, it appears that there is a large density of transcripts that are represented vertically near the origin of the plot. In this region, these vertical shifts indicate that while gene expression has not changed dramatically, that the TE has increased or decreased with T cell stimulation. This indicates that Ago and HuR targets are being dynamical regulated with respect to translation without synchronous changes in transcript abundance.

We narrowed this analysis to HuR and Ago binding in the 3'UTR region of target transcripts and the resulting plots are shown in Figure 7.12. Generally, the same patterns noted above are still apparent, but with this smaller subset of target transcripts it is easier to visualize outliers. For example, for 3'UTR targets of both proteins there are notable points in the upper right quadrant where the RPF and Ago binding is increased in the activated state, but HuR binding is decreased in the activated state as represented by large blue spots above the plotted $y=x$ line (Figure 7.12C). These points represent transcripts where the transcript abundance and Ago binding is increasing with T cell activation, but the amount of HuR binding decreases. These points seem to go against examples in the literature whereby increased Ago binding and decreased HuR binding would be expected to result in a decrease in ribosomal occupancy (Bazzini et al., 2012; Bhattacharyya, Habermacher, Martine, Closs, & Filipowicz, 2006a; 2006b; Guo et al., 2010). It is possible that these transcripts represent breaks with this thought or they represent dynamic changes in RNA binding that will have the expected effects on RNA regulation at later time points.

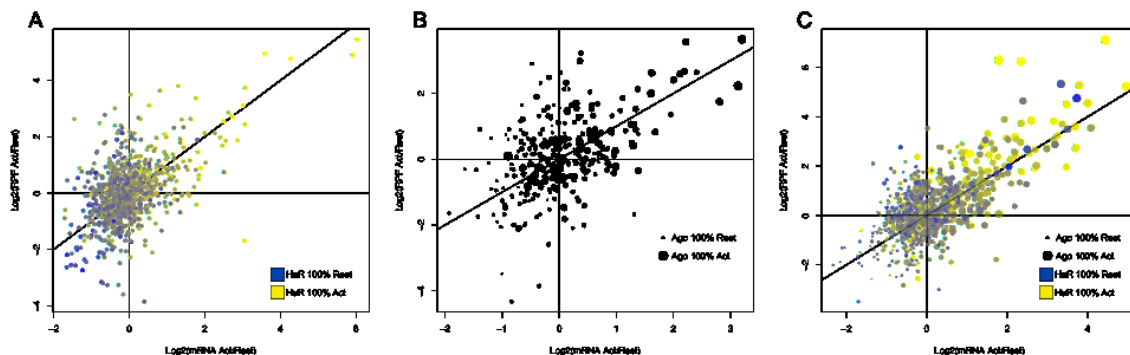


Figure 7.12 3'UTR CLIP Targets: Combining Ribosomal Profiling, mRNA Sequencing, and CLIP Data. Scatter plots of the Log_2 ratio of ribosomal protected fragment reads per kilobase per million mapped reads (RPF RPKM) in the activated state versus the Log_2 ratio of mRNA RPKM in the activated state to the resting state. **(A)** Transcripts with 3' untranslated region (3'UTR) HuR clusters of biologic complexity of three (BC3) and peak height five (ph5) and no 3'UTR Ago clusters of those criteria. Points are colored based upon the percentage of HuR CLIP tags in the cluster from each activation state. The color scale gradient ranges from blue (100% of HuR tags in the resting state) to yellow (100% of HuR tags in the activated state). **(B)** Transcripts with 3'UTR Ago clusters of BC3 and ph5 and no 3'UTR HuR clusters of those criteria. Points are sized based upon the percentage of Ago CLIP tags in the cluster from each activation state. The scale ranges from the smallest point (100% of Ago tags in the resting state) to the largest point (100% of Ago tags in the activated state). **(C)** Transcripts with both Ago and HuR 3'UTR clusters of BC3 and ph5. Points are colored based upon the percentage of HuR CLIP tags in the cluster from each activation state. The color scale gradient ranges from blue (100% of HuR tags in the resting state) to yellow (100% of HuR tags in the activated state). Points are sized based upon the percentage of Ago CLIP tags in the cluster from each activation state. The scale ranges from the smallest point (100% of Ago tags in the resting state) to the largest point (100% of Ago tags in the activated state).

Discussion

In this section we explored the dynamic changes in translation that occur with T cell activation by comparing the deep sequencing of ribosome protected RNA fragments and mRNA. By measuring the levels of transcripts protected by ribosomes, we were able to directly measure the amount of protein synthesis per transcript in the resting and activated states of a CD8 lymphocyte. Comparing this information with the parallel RNA sequencing data generated from these same groups of cells, we intended to identify sites of translational regulation and to extract biologically meaningful insights into changes in HuR and Ago binding by overlaying their CLIP maps with the transcriptional and translational cellular states.

One possible caveat to the ribosomal profiling dataset is that to date it only represents one biologic experiment. To ensure that the dynamic changes we see in translation are reproducible, we will repeat this experiment with other normal donors and are currently recruiting donors to do so. If possible, we will start with a larger number of cells to improve upon the complexity of the resulting cloned RPF dataset. In these ways, we will define robust sites of translational changes with T cell activation. Still, we believe these data represent biologically meaningful information and we plan to pursue interesting targets to validate our findings by other means such as by flow cytometry and performing quantitative western blot of resting and activated CD8 lymphocytes to investigate protein expression changes with different time points of T cell activation.

The ribosomal profiling data combined with mRNA sequencing gives us insight into the rapid changes that occur with T cell activation both translationally and transcriptionally.

With only one hour stimulation with CD3/CD28 beads, it is remarkable how distinctly the global profiles of the cells change. While many alterations in ribosomal occupancy correlate with changes in transcript expression, we were able to identify sites that did not match these variations in abundance and we believe these represent sites of translational control. We were able to identify transcripts with robust HuR and Ago binding sites that had RPF values deviating from the patterns of transcript expression.

Still, we did not uncover simple rules of translational regulation by the RNA binding proteins. We can identify individual cases where protein binding increases or decreases correlating with both increases and decreases in RPF abundance. This may represent the complex dynamics of multiple layers of combinatorial control that are necessary to dictate cellular function. Even so, for individual candidate transcripts, we can learn much from this data about the dynamics of lymphocyte activation and the importance of tightly regulated transcriptional and translational control.

CHAPTER 8. Studying T cell Regulation in HuR Deficient CD8 Lymphocytes

Introduction

In Chapter 6 we introduced the necessity for understanding the combinatorial control of Ago and HuR regulation of mRNA. In summary, previous studies have indicated that (Argonaute) Ago and HuR may compete for regulatory function on target transcripts (Chang et al. 2012). HuR binding may alleviate repression of microRNA-mediated inhibition of targets by altering a transcript's subcellular localization and targeting it for translation upon the induction of stress (Bhattacharyya, Habermacher, Martine, Closs, and Filipowicz 2006a; 2006b). Alternatively, HuR has been shown to work in concert with Ago to mediate repression of other mRNA (Glorian et al. 2011; Kim et al. 2009; Kundu et al. 2012).

We have already described the impressive overlapping binding patterns of Ago and HuR in human cluster of differentiation eight (CD8) lymphocytes during T cell activation. In order to further study the combinatorial control of HuR and Argonaute (Ago), we sought to investigate the binding patterns of Ago in T cells lacking HuR. While HuR deficient mice are embryonic lethal, mice with HuR deficient T cells are viable throughout development. HuR null lymphocytes, due to floxed excision of HuR exon 2 from Lck promoter driven Cre expression, have altered phenotypes in T cell maturation. These T cells show decreased exiting of the thymus and reduced chemotaxis towards cytokines that alter the intracellular localization of HuR. Single positive cells lacking HuR also have a reduced proliferative response after CD3/CD28 stimulation and show defects in intracellular signaling downstream of the T cell receptor. HuR negative T cells also

avoided an apoptotic response when stimulated with CD3/CD28 as compared to HuR positive T cells. The authors also found increased mRNA levels of Tnf with activation of HuR deficient cells as compared to HuR expressing T cells (Katsanou et al. 2009; Papadaki et al. 2009). Thus, examining Ago binding maps upon CD3/CD28 activation of CD8 T cells with and without HuR provides a means to probe their possible synergistic and antagonistic regulatory functions in an important biological context.

Results

Lck-Cre⁺ HuR^{fl/fl} CD8 Lymphocyte Characterization

We characterized the levels of HuR in the T cells of conditional knock out (cKO) mice for potential use in CLIP, RNAseq, and ribosomal profiling experiments. Three mice were chosen that were Lck-Cre⁺ and had both alleles of the second exon of HuR floxed and three mice that had a wild type HuR locus. The PCR products confirming these genotypes are shown in Figure 8.1A. For this experiment, splenic CD4 T cells were selected and their purity of nearly 99% was confirmed by flow cytometry (Figure 8.1B). Aliquots of the T cells were run on an SDS-PAGE gel and probed for HuR using the 3A2 monoclonal antibody and also for Hsp90 as a loading control. As seen in Figure 8.1C and quantified in Figure 8.1D, two of the three mice showed greatly reduced levels of HuR expression in their T cells, with expression levels around 5 percent of that of a wild type mouse. However, in the third HuR cKO mouse, the expression of HuR was equivalent to that of a wild type mouse.

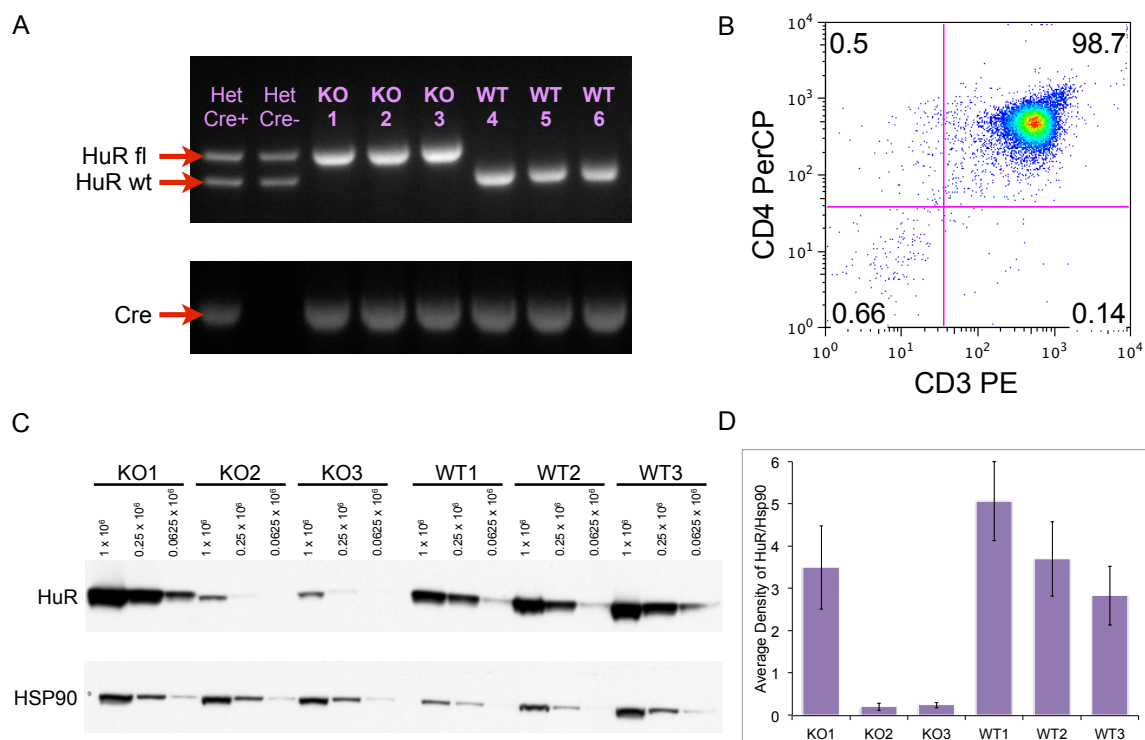


Fig 8.1 Lck-Cre HuRfl/fl Characterization. (A) Genotyping PCR analysis of eight mice with determined genotypes as indicated for Lck-Cre⁺ HuR^{fl/+} (Het Cre⁺), Lck-Cre⁻ HuR^{fl/+} (Het Cre⁻), Lck-Cre⁺ HuR^{fl/fl} (KO), and Lck-Cre⁺ HuR^{+/+} (WT). (B) T cell purity determined by CD3 and CD8 staining and flow cytometry. Percentages of cells are noted in each quadrant. (C) Mouse CD4 T cell lysate from the indicated number of cells was analyzed by western blotting for HuR (with monoclonal HuR specific 3A2) and HSP90 (with monoclonal HSP90 specific BA86). (D) Quantitation by phosphoimager analysis of HuR levels in (C) normalized against levels of HSP90. Plotted are the averages of the three lanes for each mouse with standard deviations in error bars.

To screen the mice in the colony, we evaluated the level of HuR expression in lymphocytes by intracellular staining for HuR and flow cytometry. This allowed us to determine HuR expression in an ocular blood sample prior to sacrificing the animals for an experiment. Briefly, mice were bled from the ocular vein and after red blood cell lysis, the cells were permeablized and intracellularly stained for HuR and analyzed by flow cytometry. We found that the amount of HuR in Lck-Cre⁺ HuR^{fl/fl} mouse T cells showed a continuous spectrum of expression levels. These expression patterns varied for each individual mouse and ranged from levels at overlapping the isotype control, indicating virtually no HuR expression, to levels mimicking wild type protein expression (data not shown).

To ensure that the levels of HuR identified by flow cytometry matched the levels detected by western blot, we sacrificed one wild type mouse and four animals that had been screened by HuR staining of blood cells to have HuR expression levels ranging from very low to wild type levels of protein. T cells were isolated from these five mice and analyzed by both flow cytometry and western blot. The intracellular HuR staining showed that the HuR expression patterns seen in peripheral blood were equivalent to those from splenic T cells ranging from low expression of HuR in KO1 to wild type expression in KO4 (Figure 8.2A). These protein levels were confirmed by western blot (Figure 8.2B). We concluded that the Lck-Cre⁺ HuR^{fl/fl} mouse system was unreliable for consistently obtaining HuR deficient T cells, although it was possible to control for the phenotype of the mice by screening them by intracellular staining of T cells for HuR using flow cytometry.

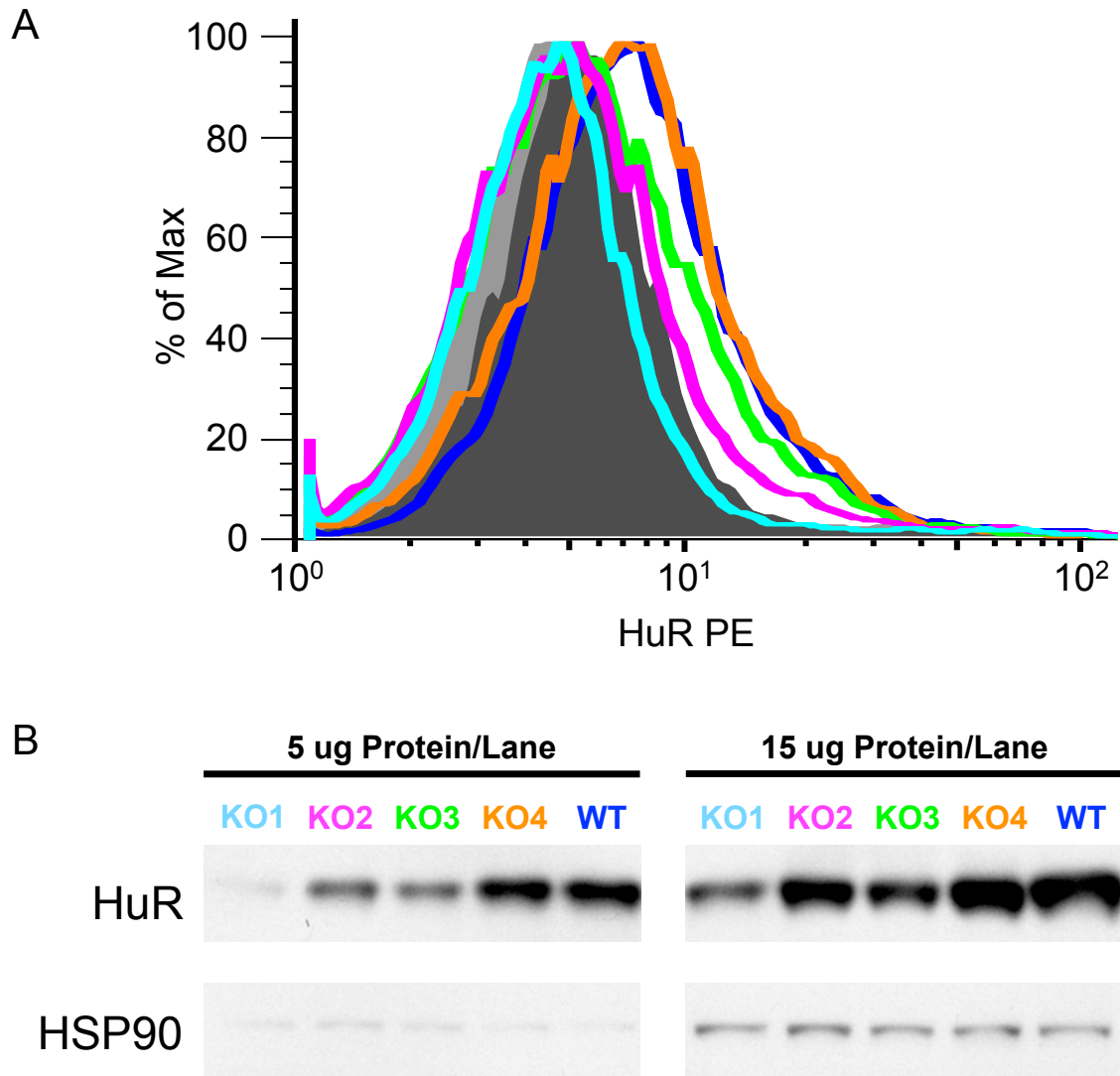


Figure 8.2 HuR Intracellular Stain and Western Blot. Analysis of CD4⁺ T cells from four Lck-Cre⁺ HuR^{fl/fl} (KO) mice and one Lck-Cre⁺ HuR^{+/+} (WT) mouse. **(A)** Intracellular stain for HuR (with monoclonal HuR specific 3A2) in colored lines and mouse IgG control antibody in gray shaded plot with secondary anti-mouse PE antibody as analyzed by flow cytometry. Color of plotted lines match mice indicated in **(B)**. **(B)** Mouse CD4 T cell lysate was analyzed by western blotting for HuR (with monoclonal HuR specific 3A2) and HSP90 (with monoclonal HSP90 specific BA86).

CD4-Cre⁺ HuR^{fl/fl} Mouse Characterization

In order to have a more reliable system for studying T cells lacking the HuR protein, we began breeding the HuR^{fl/fl} mice onto a CD4-Cre background. All T cells express both CD4 and CD8 before they differentiate into single positive cells. Therefore, CD4-driven Cre expression should delete HuR in all mature T cell subsets. To screen the mice in the colony, we evaluated the level of HuR expression in the lymphocytes by flow cytometry as described above. The HuR profiles of these cells clearly segregated by genotype. Both CD8 and CD4 lymphocytes from CD4-Cre⁺ HuR^{fl/fl} showed consistently reduced levels of HuR as compared to wild type lymphocytes. In the HuR cKO samples, there was a small peak of cells at expression levels comparable to the wild type mice (Figure 8.3A,B). This signal was seen with irrelevant mouse IgG and secondary alone, so we do not believe that it is a population of HuR expressing T cells in the HuR cKO mice, but rather background staining in the assay. When we gated on CD3 negative cells, which should not have Cre expression from the CD4 locus and therefore should retain full-length HuR even in HuR^{fl/fl} cells, we did not see a difference in HuR expression between the HuR cKO and wild type mice (Figure 8.3C). We concluded that HuR protein levels were robustly depleted in the HuR cKO mice and that the conditional excision of exon 2 of HuR was specific to T cells.

Preparation of Mouse CD8 T cells for Ago CLIP

We prepared wild type and HuR cKO T cells for analysis by Ago CLIP. Originally, we intended to prepare both resting and activated cells to match the datasets collected for the human cells. As in human cells, we observed that freshly isolated mouse T cells had

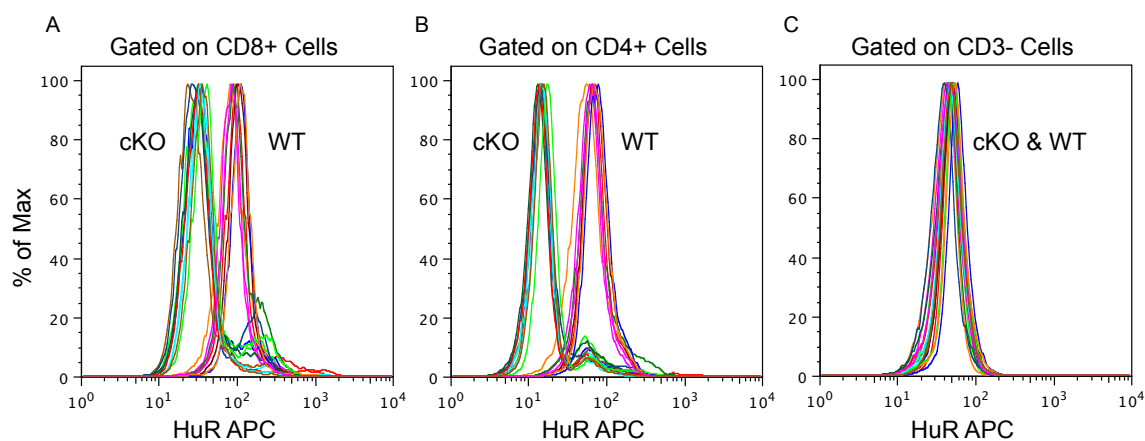


Figure 8.3 CD4-Cre HuR^{fl/fl} Intracellular FACS from Blood. Analysis of lymphocytes from CD4-Cre+ HuR^{fl/fl} (cKO) mice or CD4-Cre+ HuR^{+/+} (WT) mice. Intracellular stain for HuR (with monoclonal HuR specific 3A2) with secondary anti-mouse APC antibody as analyzed by flow cytometry. **(A)** HuR stain of CD8+ T cells. **(B)** HuR stain of CD4+ T cells. **(C)** HuR stain of CD3- cells.

elevated levels of *Ifng* mRNA, indicating that the isolation procedure caused low levels of activation. However, unlike with human cells, resting the mouse cells overnight in media did not permit recovery of healthy T cells the next day (data not shown). Therefore, we decided to utilize the T cells immediately after isolation by activating them in culture with CD3/CD28 beads.

We processed three groups of four CD4-Cre⁺ HuR^{fl/fl} mice, and three groups of four littermate wild type or CD4-Cre⁺ mice, to obtain six biologic samples for analysis. These pooled T cells were determined to be more than 95% pure by flow cytometry (Figure 8.4A). The isolated T cells were stimulated for one hour in culture with CD3/CD28 beads. The activation states of the resulting lymphocytes were analyzed by isolation of total RNA from the cells. The RNA was reverse transcribed into cDNA and the abundance of *Ifng* mRNA assayed by qPCR. The delta Ct values for *Ifng* normalized to levels of GAPDH are plotted in Figure 8.4B in comparison to other mouse T cell sample qPCR data. We saw very good stimulation of the T cells being prepared for CLIP regardless of genotype as compared to previously isolated samples.

Furthermore, it was important to ensure that the levels of HuR in the T cell samples were significantly reduced in the CD4-Cre⁺ HuR^{fl/fl} lymphocytes compared to the wild type T cells. We ran lysate from an aliquot of the T cell samples on an SDS-PAGE gel and blotted for HuR and also for Hsp90 as a loading control. We saw an average of roughly 10 percent HuR expression in the HuR cKO T cells compared to matched littermate wild type cells. In summary we were able to isolate a pure population of CD8 T cells from wild type and HuR cKO mice. These cells had appropriate levels of HuR expression

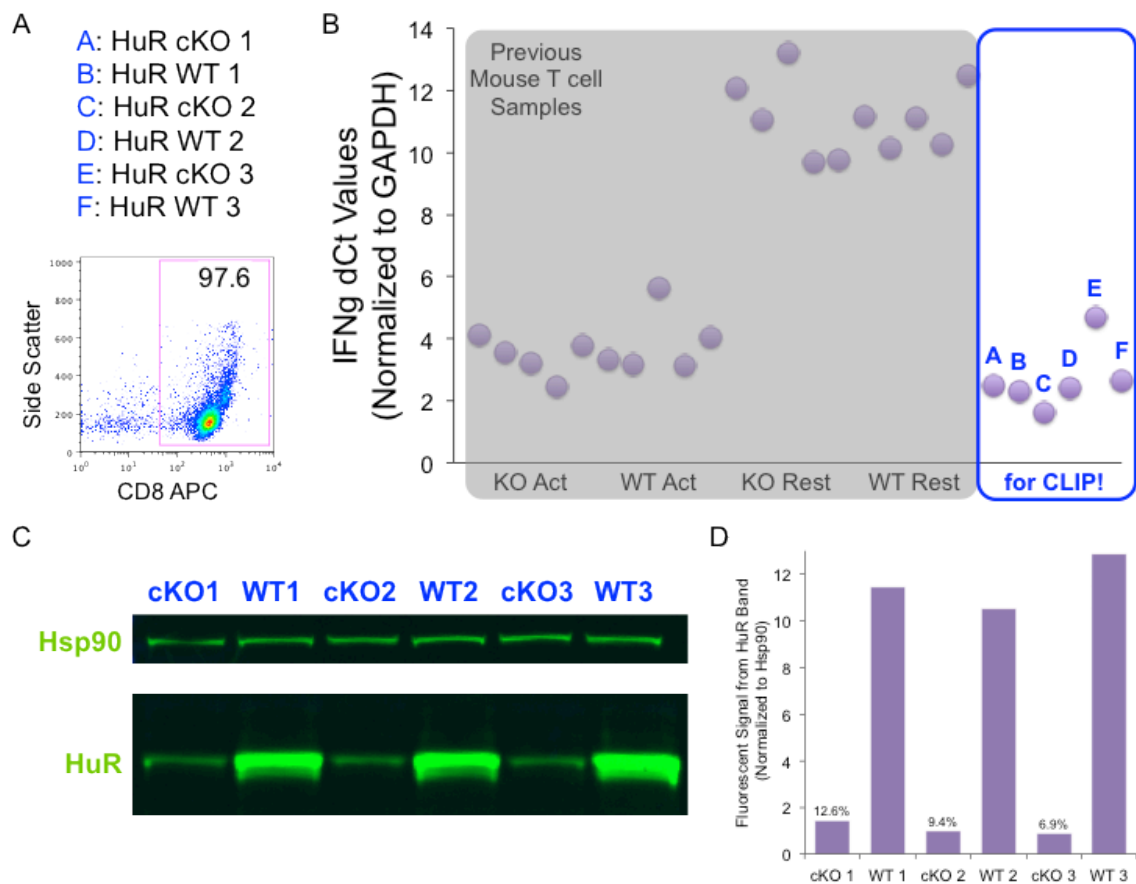


Figure 8.4 Mouse CD8 T Cells: Characterization for Ago CLIP. Analysis of 6 pools of purified mouse CD8+ T cells from CD4-Cre+ HuR^{fl/fl} (cKO) mice (Pools A, C, E) or CD4-Cre+ HuR^{+/+} (WT) mice (Pools B, D, F). **(A)** Representative T cell purity determined by CD8 staining and flow cytometry. Percentages of CD8+ cells are noted in the box. **(B)** Ct values for Gapdh mRNA were subtracted from the Ct values for Ifng mRNA (dCt) for resting or CD3/CD28 stimulated CD8 T cells. dCt values from each pool of mouse cells prepared for CLIP (A to F) is compared to previous resting and activated KO and WT mouse cells. **(C)** Equivalent aliquots of mouse CD8 T cell lysate from the indicated samples were analyzed by western blotting for HuR (with monoclonal HuR specific 3A2) and HSP90 (with monoclonal HSP90 specific BA86). **(D)** Quantitation by fluorescent signal analysis of HuR levels in (C).

corresponding to their genotype and were activated *in vitro* for one hour before crosslinking. Both wild type and HuR cKO mouse CD8 T cells were applied in Ago CLIP analysis and high-throughput sequencing. For these samples, we used the same crosslinking immunoprecipitation protocol as for human cells, but utilized a different cloning strategy of the CLIP tags with only one linker ligation step as described in Chapter 2.

Tag Statistics

We performed HITS-CLIP on CD8 lymphocytes of three biologic replicates of wild type and CD4-Cre⁺ HuR^{fl/fl} mice stimulated for an hour with CD3/CD28 beads. The final products were pooled together so that six samples were sequenced between two lanes. Each pooled Ago associated mRNA sample produced nearly 200 million sequencing reads. Once we filtered and collapsed each pool so that each sequence was only represented once, we had between 20 and 25 million reads for each sample. As mentioned previously, we think this dramatic decrease is due to over sequencing of the sample and also PCR duplication of CLIP tags. We stripped the linker sequences from each read and segregated each sample from the pooled data, the four nucleotide indices are indicated in the table below each sample name. Each sample contributed between close to 4 to 6 million reads, indicating that the samples were sequenced rather evenly. Each sample had roughly 1.5 to 4 million sequences that mapped to unique locations in the mm9 build of the mouse genome (Table 8.1).

As with the other CLIP samples processed for the human dataset, the adapters contained a four nucleotide degenerative sequence. Thus, when these randomly generated

Table 8.1 Ago CLIP Tag Statistics from HuR cKO and WT Lymphocytes.

| | | | | | | |
|--|----------------------|---------------------|----------------------|---------------------|----------------------|---------------------|
| cKO: 1,736,321 WT: 2,318,089 | Pool 1 | | | Pool 2 | | |
| Total Reads | 195,210,749 | | | 179,668,684 | | |
| After Quality Filtering | 143,705,912 | | | 141,577,140 | | |
| Exact Duplicates Collapsed | 20,777,570 | | | 23,331,600 | | |
| | A: cKO (GCAT) 23x | B: WT (GTCA) 24x | C: cKO (ACTG) 20x | D: WT (ACTG) 22x | E: cKO (AGCT) 21x | F: WT (TCGA) 19x |
| Linker Stripped | 4,578,800 | 4,488,975 | 4,190,422 | 4,323,854 | 3,792,646 | 5,746,463 |
| CLIP Adapter Removed | 3,961,605 | 4,007,333 | 3,923,881 | 3,999,408 | 3,584,650 | 5,561,856 |
| mm9 Mapping (novoalign with trimming) | 1,471,464 | 1,451,509 | 2,159,341 | 2,114,094 | 1,959,729 | 3,751,959 |
| PCR Duplicates Collapsed | 261,240 | 182,516 | 927,922 | 461,589 | 547,159 | 1,673,984 |

oligonucleotides were ligated to the RNA they could be used to distinguish between independent Ago binding events at the same locus and PCR duplications of the same Ago interaction by comparing the four-nucleotide barcodes. Thus, we collapsed sequences that had the same start and ending footprint on the genome that also had the same four-nucleotide codes in the linker sequence. In doing so, we can correct for some of the PCR amplification that reduces the true complexity of the sample. The number of PCR cycles used for each sample are listed under the sample names and ranged between 19 and 24 cycles. After this computation, the samples were reduced to almost 200,000 to 2 million unique CLIP tags for each sample. As with the human samples, the colors highlighting each sample correspond to the colors of the CLIP tags viewed on the genome browser (Table 8.1).

Genomic Distribution of Ago Binding Sites

To determine an overview of the Ago binding distributions in wild type and CD4-Cre⁺ HuR^{fl/fl} cells, we examined the regions of transcripts that were targeted in the mouse T cells. We clustered all of the tags together from both the wild type and HuR deficient lymphocytes, specifying that tags needed to overlap at least 5 nucleotides to be included in a cluster. To demand that the clusters were reproducible, we only included clusters that contained CLIP reads from all three of the biologic samples in either the wild type and or the HuR deficient datasets. We specified the cluster as wild type only if there were tags from all three wild type mouse samples and not more than one replicate represented from the HuR cKO data (Figure 8.5A), and the reciprocal for HuR cKO

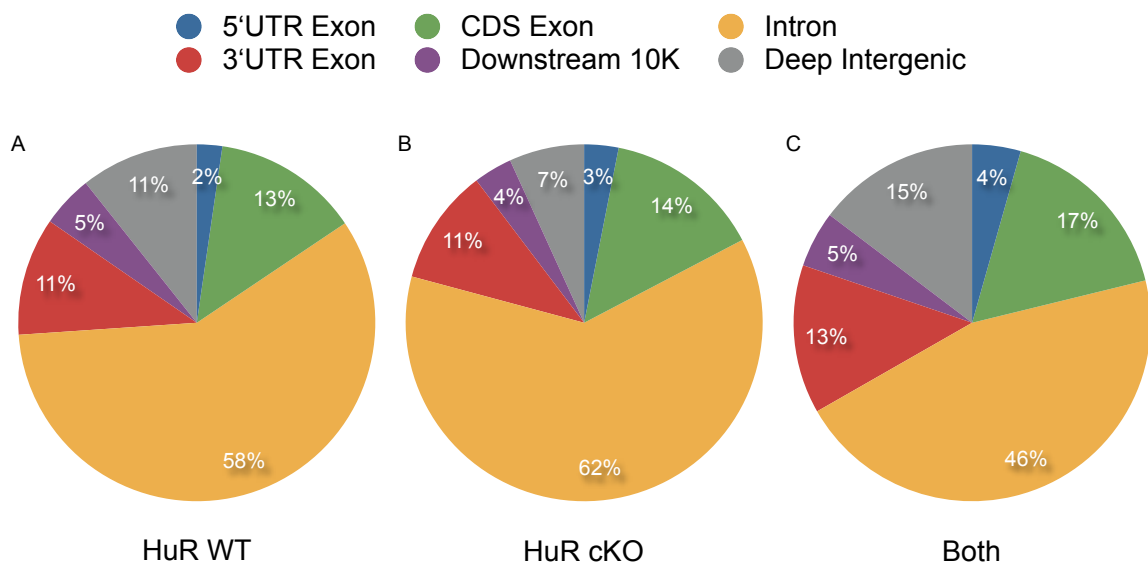


Figure 8.5 Mouse Ago Clusters Genomic Distribution. Distribution of Ago clusters comprised of at 3 biologic replicates exclusively in HuR wild-type mice (CD4-Cre+ HuR^{+/+}, WT), HuR conditional knock out mice (CD4-Cre+ HuR^{fl/fl}, cKO), or in both genotypes.

clusters (Figure 8.5B). All six replicates needed to contribute tags to a cluster for it to be considered present in both biologic samples (Figure 8.5C).

As we saw previously for the Ago and the HuR datasets, the largest pools of robust clusters mapped to intronic regions of target transcripts for all three groups. The next most represented regions were the 3' untranslated regions (UTRs) including the regions ten kilobases downstream of the annotated transcript, and then coding sequences. Interestingly, the proportion of intronic clusters decreased in the group of clusters present in both genotypes, while the percentages of clusters in 3'UTRs and coding sequence exons increased. This may reflect the increased biologic complexity for these samples and possibly an even more robust distribution of binding. Still, the proportion of deep intergenic clusters also increased in this set, while we might expect it to decrease with more stringent cutoffs, signaling that the differences in binding distribution may reflect differences in biology rather than in background signal for the samples.

Ago Binds Egr3 and Ifng in Mouse T cells with or without HuR

To begin our analysis of Ago binding in wild type and HuR cKO T cells, we examined the binding distribution of Ago on the Egr3 and Ifng transcripts. These two transcripts were among the top targets with increased Ago and HuR binding following T cell activation in human lymphocytes. Figure 8.6 shows the distribution of Ago binding to Egr3 in the mouse cells. We included the region downstream of the annotated 3'UTR in the mouse that is homologous to the 3'UTR of the human transcript. This unannotated mouse 3'UTR region includes the largest binding sites for Egr3 in the mouse. It is clear from this binding map that HuR is not necessary for Ago to bind to this transcript with

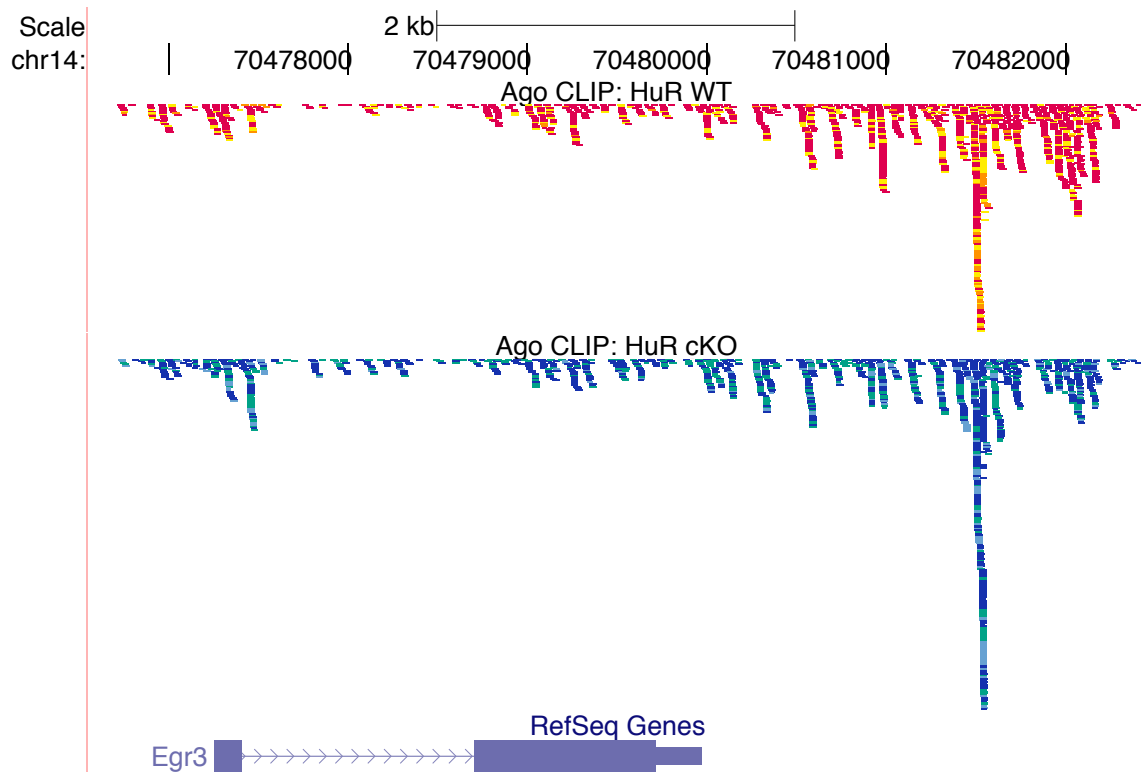


Figure 8.6 Ago Binding on Mouse Egr3. The position of individual Ago unique CLIP tags are plotted relative to their mapped position on the mouse Egr3 transcript. From top to bottom: chromosomal location, Ago CLIP tags from activated HuR wild-type CD8 T cells (colors represent each donor sample as shown in Table 8.1), Ago CLIP tags from activated HuR cKO CD8 T cells, Gene diagram from RefSeq.

lymphocyte activation. Interestingly, while the EGR3 binding map from human lymphocytes mostly excluded binding in intronic regions of the transcript, there are some clusters found in the intron in the mouse. This may reflect slight differences in the regulatory function between species or may be an artifact of a slightly different time course of T cell activation biology in the mouse, even though one hour of stimulation was studied in both systems.

Similarly, HuR was not necessary for Ago to bind to Ifng (Figure 8.7). We found robust Ago binding sites in both wild type and HuR cKO activated T cells. While we found robust intronic binding sites in the Egr3 transcript in mouse but not human, we saw no biologic complexity of three sites in intronic regions for Ifng in the mouse while we did in the human. On the mouse transcript, we saw robust and reproducible binding in the coding sequence and UTRs, but not as much in introns. Furthermore, it appears that the 5'UTR binding in the mouse was limited to the HuR cKO T cells and increased in the coding region and 3'UTR in cells without HuR as well. Therefore, we hypothesize that HuR may help recruit Ago to bind certain sites in Ifng, although this does not explain the differences in intronic binding between the biologic systems.

Revisiting Dynamic Binding Changes from the Human Dataset: IRF9 and SATB1

During the analysis of the human Ago and HuR CLIP data, we identified the IRF9 and SATB1 transcripts as being regulated in overlapping regions by the two RNA binding proteins. We examined the binding patterns on these transcripts in particular, because the binding intensities changed dramatically in the opposite direction for Ago and HuR with T cell activation. For the IRF9 transcript, although Ago binding increased with T cell

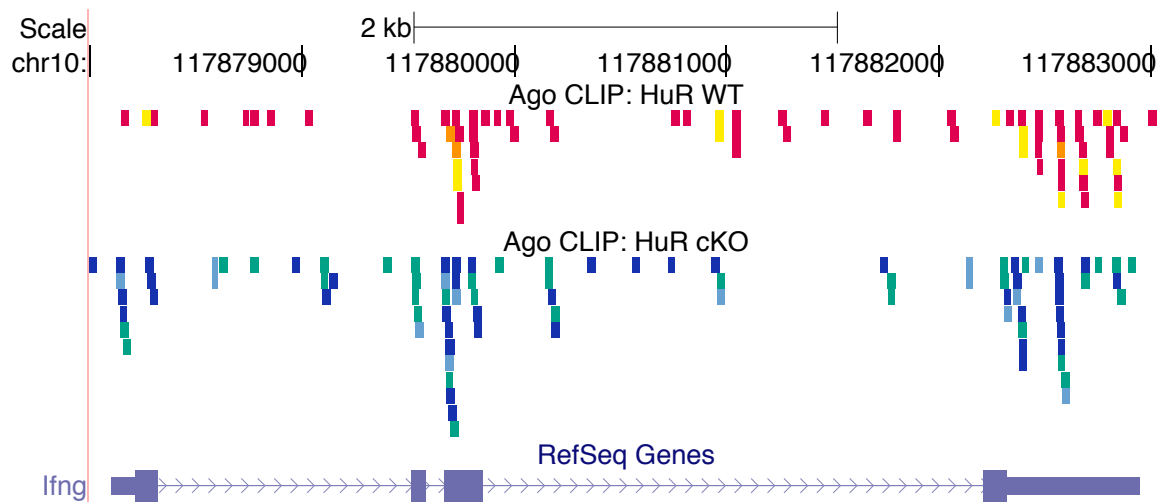


Figure 8.7 Ago Binding on Mouse *Ifng*. The position of individual Ago unique CLIP tags are plotted relative to their mapped position on the mouse *Ifng* transcript. From top to bottom: chromosomal location, Ago CLIP tags from activated HuR wild-type CD8 T cells (colors represent each donor sample as shown in Table 8.1), Ago CLIP tags from activated HuR cKO CD8 T cells, Gene diagram from RefSeq.

stimulation, HuR binding decreased (Figure 8.8A). While there was robust binding in both activation states for both Ago and HuR, this binding pattern shift suggested that the proteins might be interacting antagonistically to exclude each other from this site. Interestingly, in examining the homologous region in the mouse, we found a robust binding site in the wild type activated T cells, matching the human activated state, but only scattered tags in the HuR cKO samples (Figure 8.8B). This suggests that this binding site is conserved across species and that HuR may be necessary for robust Ago binding. There is similarly scattered binding for both genotypes throughout the rest of the transcript, suggesting that there are comparable levels of this transcript available for potential regulation in both groups of mice (data not shown). While Ago and HuR may compete for binding to this site, the mouse data suggests that HuR is necessary for Ago regulation.

The human SATB1 binding map showed the opposite pattern for Ago and HuR in the human T cells. With lymphocyte activation, Ago binding at this 3'UTR site was almost completely depleted, although HuR binding quantitatively increased (Figure 8.9A). Because of the low binding levels of Ago at this site in activated human T cells, it was interesting to find that the corresponding region in the mouse *Satb1* 3'UTR contains the largest region of Ago binding in both wild type and HuR cKO mice. In fact, it appeared that the levels of Ago binding at this site were higher in the wild type mice (Figure 8.9B). Still, this is consistent with the IRF9 transcript, where we found that a possibly antagonistic site in the human transcript required HuR for binding in the mouse. Although the mouse *Satb1* site clearly does not require HuR for Ago binding, as it is

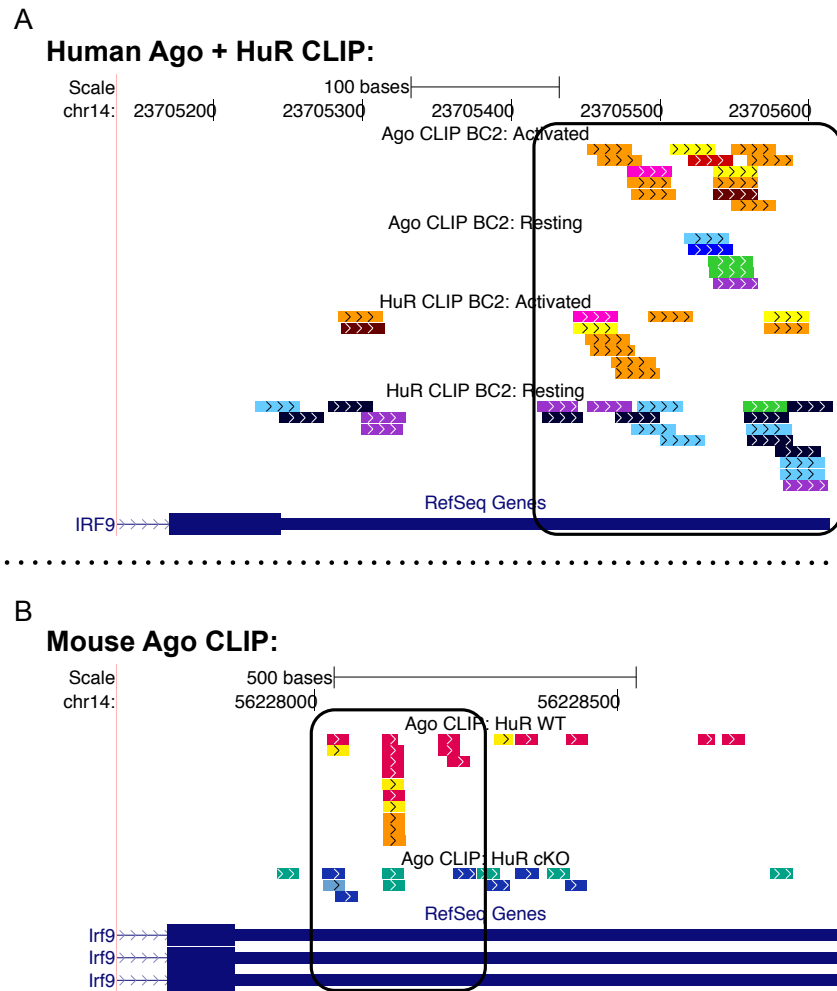


Figure 8.8 Ago and HuR Binding in Human and Mouse: IRF9 3'UTR. (A) The position of individual Ago and HuR unique CLIP tags in biologic complexity two clusters plotted relative to their mapped position on the human IRF9 3'UTR. The CLIP cluster showing dynamic reciprocal Ago and HuR binding changes is outlined in the 3'UTR. From top to bottom: chromosomal location, Ago CLIP tags from activated CD8 T cells (colors represent each donor sample as shown in Table 6.1), Ago CLIP tags from resting CD8 T cells, HuR CLIP tags from activated CD8 T cells, HuR CLIP tags from resting CD8 T cells, Gene diagram from RefSeq. (B) The position of individual Ago unique CLIP tags are plotted relative to their mapped position on the mouse Irf9 3'UTR. The homologous 3'UTR region showing dynamic reciprocal Ago and HuR binding changes on the human transcript is outlined. From top to bottom: chromosomal location, Ago CLIP tags from activated HuR wild-type CD8 T cells (colors represent each donor sample as shown in Table 8.1), Ago CLIP tags from activated HuR cKO CD8 T cells, Gene diagram from RefSeq.

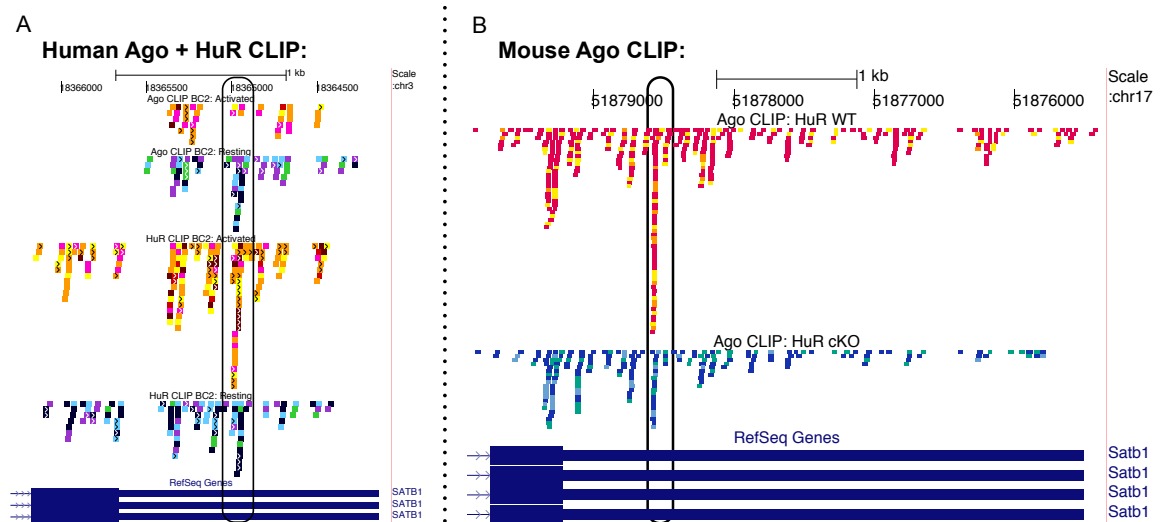


Figure 8.9 Ago and HuR Binding in Human and Mouse: SATB1 3'UTR. (A) The position of individual Ago and HuR unique CLIP tags in biologic complexity two clusters plotted relative to their mapped position on the human SATB1 3'UTR. The CLIP cluster showing dynamic reciprocal Ago and HuR binding changes is outlined in the 3'UTR. From top to bottom: chromosomal location, Ago CLIP tags from activated CD8 T cells (colors represent each donor sample as shown in Table 6.1), Ago CLIP tags from resting CD8 T cells, HuR CLIP tags from activated CD8 T cells, HuR CLIP tags from resting CD8 T cells, Gene diagram from RefSeq. (B) The position of individual Ago unique CLIP tags are plotted relative to their mapped position on the mouse Satb1 3'UTR. The homologous 3'UTR region showing dynamic reciprocal Ago and HuR binding changes on the human transcript is outlined. From top to bottom: chromosomal location, Ago CLIP tags from activated HuR wild-type CD8 T cells (colors represent each donor sample as shown in Table 8.1), Ago CLIP tags from activated HuR cKO CD8 T cells, Gene diagram from RefSeq.

robustly present in the HuR cKO cells, HuR does appear to enhance binding in the wild type cells despite the suggested competition in the human data.

Exploring Ago Binding Changes between HuR Wild type and KO T cells

Although it appeared that generally much of Ago binding was maintained in the HuR cKO cells, we identified sites of Ago regulation that were present only in wild type or HuR cKO cells. We sorted the clusters by biologic complexity and then by tag numbers in each state. The top coding region and 3'UTR binding sites changing between genotypes are listed in Figure 8.10. Figure 8.10A represents binding sites where all three wild type replicate samples are represented in the cluster, but there is no robust binding site in the cells lacking HuR. We suggest that these sites represent potential agonism in the binding of HuR and Ago because HuR would be necessary for Ago to be present at that regulatory site.

Interestingly, the top target in this category was the *Fyb* transcript. This 3'UTR cluster is in the homologous region as the binding changes discussed in the 3'UTR of the human *FYB* transcript in Chapter 6. In the human 3'UTR, we saw overlapping binding of Ago and HuR. While the binding for Ago was biologically complex in both states, actually increasing in biologic complexity with T cell activation, the number of tags represented in the Ago cluster decreased with T cell stimulation. This contrasted with HuR, which had maximal biologic complexity in both states, but increased binding quantitatively with activation (Figure 8.11A). In the mouse system, we see a robust binding site at this 3'UTR location in the wild type animals, but no binding in the HuR cKO mice (Figure 8.11B). This suggests that Ago requires HuR at that site to bind. There is binding of

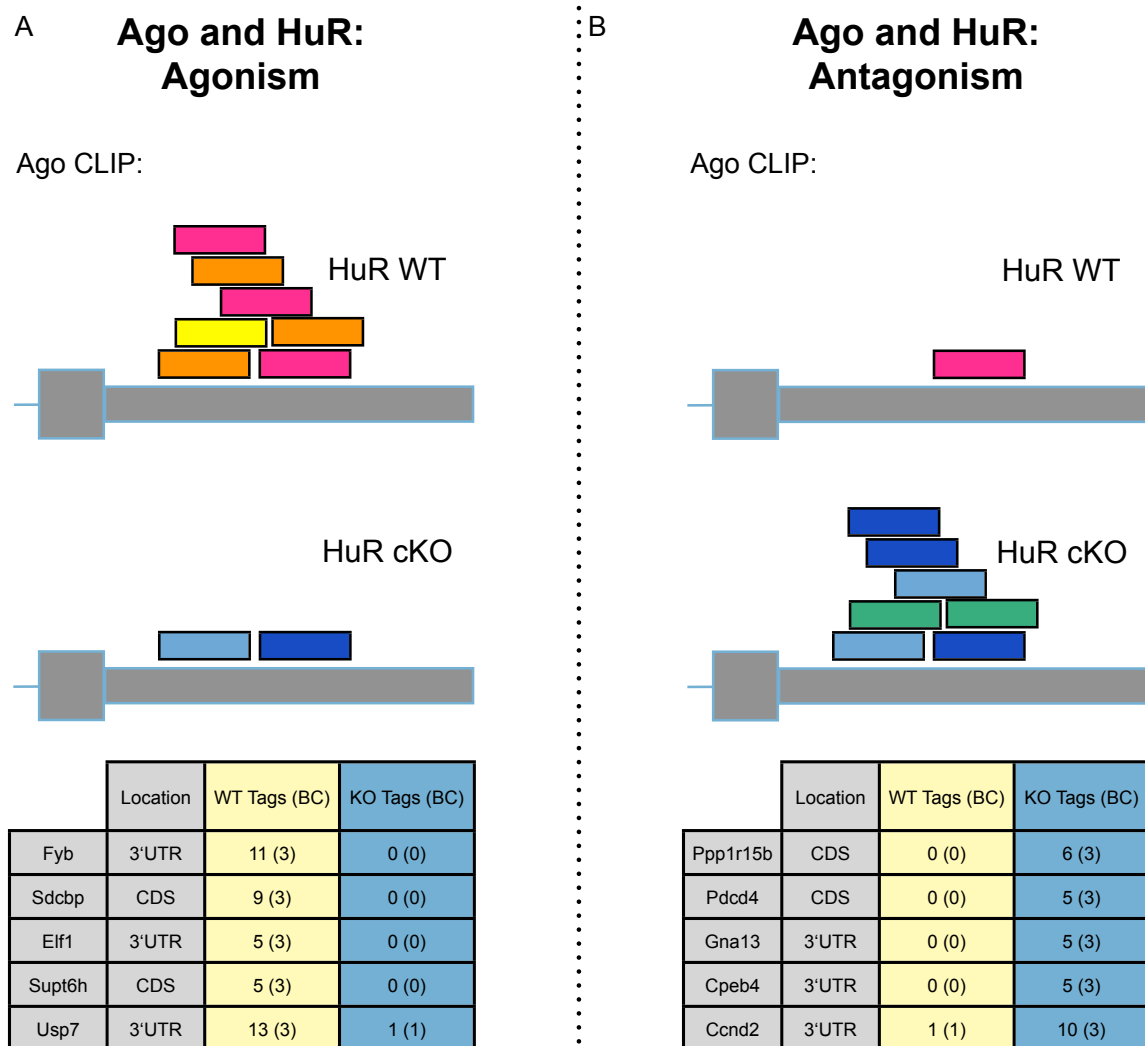


Figure 8.10 Ago and HuR Combinatorial Control. All unique CLIP tags from both wild-type and HuR cKO mice were clustered together based on overlapping genomic positions of at least 5 nucleotides. We sorted the clusters by biologic complexity and then by tag numbers in each state. The top coding region and 3'UTR binding sites changing between genotypes are listed. Each table lists the name of the transcript, the location of the cluster within the transcript, and the number of tags and biologic complexity (BC) of the cluster for each genotype. **(A)** Binding sites where all three wild-type replicate samples are represented in the cluster, but there is no robust binding site in HuR cKO mouse T cells. **(B)** Binding sites where all three HuR cKO replicate samples are represented in the cluster, but there is no robust binding site in wild-type mouse T cells.

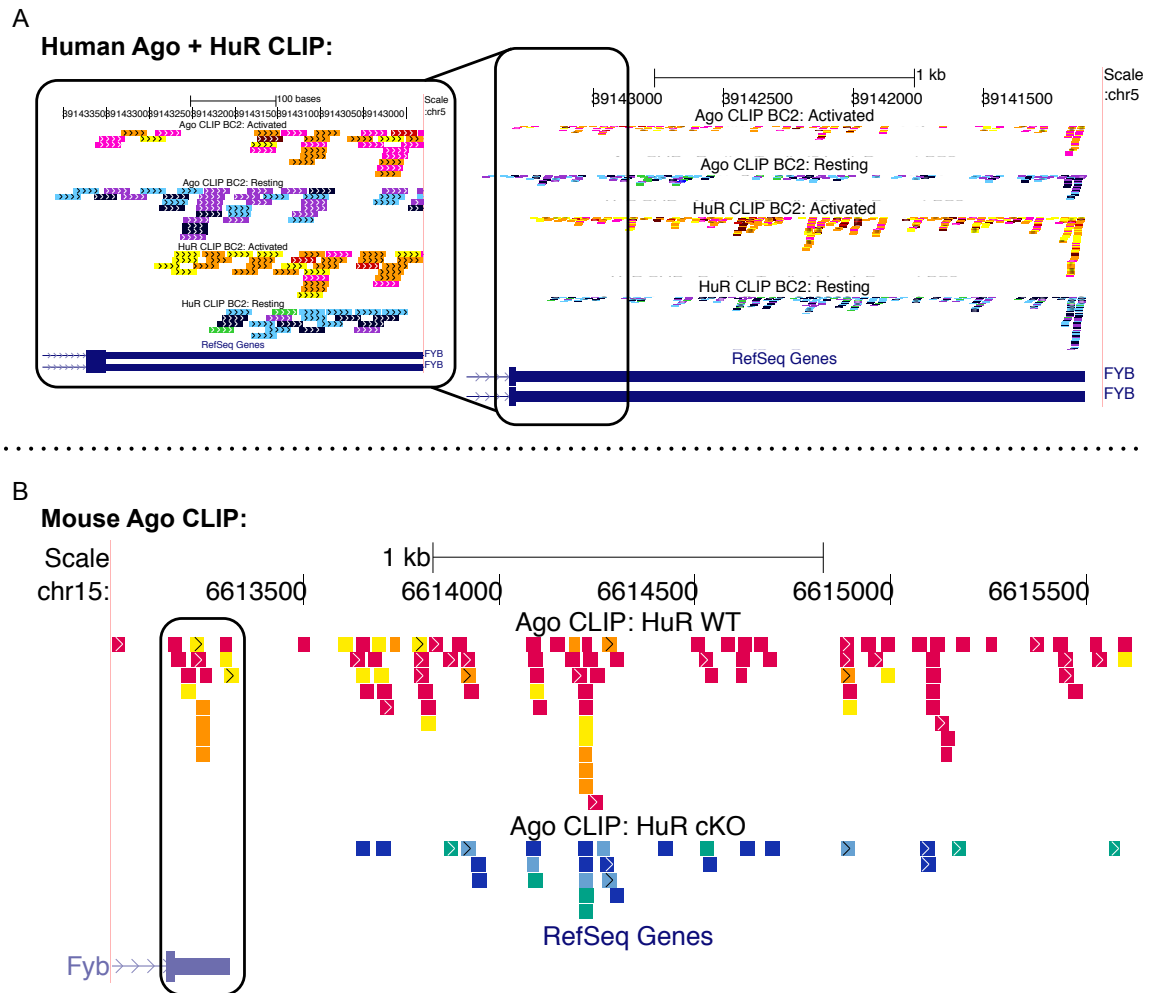


Figure 8.11 Ago and HuR Binding in Human and Mouse: FYB 3'UTR. (A) The position of individual Ago and HuR unique CLIP tags in biologic complexity two clusters plotted relative to their mapped position on the human FYB 3'UTR. The CLIP cluster showing dynamic reciprocal Ago and HuR binding changes is outlined in the 3'UTR. From top to bottom: chromosomal location, Ago CLIP tags from activated CD8 T cells (colors represent each donor sample as shown in Table 6.1), Ago CLIP tags from resting CD8 T cells, HuR CLIP tags from activated CD8 T cells, HuR CLIP tags from resting CD8 T cells, Gene diagram from RefSeq. (B) The position of individual Ago unique CLIP tags are plotted relative to their mapped position on the mouse Fyb 3'UTR. The homologous 3'UTR region showing dynamic reciprocal Ago and HuR binding changes on the human transcript is outlined. From top to bottom: chromosomal location, Ago CLIP tags from activated HuR wild-type CD8 T cells (colors represent each donor sample as shown in Table 8.1), Ago CLIP tags from activated HuR cKO CD8 T cells, Gene diagram from RefSeq.

Ago in other sites along the Fyb transcript in the HuR cKO mouse cells indicating that it is not a lack of the Fyb transcript in these animals that can explain the absence of binding at that site in the HuR cKO mice. The mapped patterns in the human T cells are consistent with a model in which Ago and HuR compete quantitatively to bind in that site. Still, Ago and HuR both display robust binding patterns in both states. Based on the mouse data, HuR binding appears to be necessary for Ago targeting to this 3'UTR region.

We also examined sites of Ago regulation that were present in the HuR cKO mouse cells but not in the wild type lymphocytes. We think these may represent sites of antagonism between HuR and Ago because Ago is only able to bind these RNA regions when HuR is not present in the cells. The top ranked site in this category was in the Ppp1r15b transcript (Figure 8.10B). The cluster was located in the first coding exon and although there were robust Ago binding sites in both genotypes upstream of this binding site, there were no tags seen in the wild type mice in that location (Figure 8.12B). The human data supported this pattern, with a robust HuR binding site matching the same locus without a corresponding Ago site. Upstream of the highlighted region in the exon there were a few small Ago clusters that matched the robust site in the HuR wild type mice. Therefore, it appears that HuR may block Ago from binding to the highlighted site in the coding region of the Ppp1r15b transcript in both mice and human T cells.

Another example of potential Ago and HuR antagonism was in a coding exon in the middle of the Pdcd4 transcript. In this region, there was binding observed in the HuR cKO lymphocytes but not in the wild type cells (Figure 8.13B). In concordance with this observation, there was HuR binding observed at this position in the human T cells

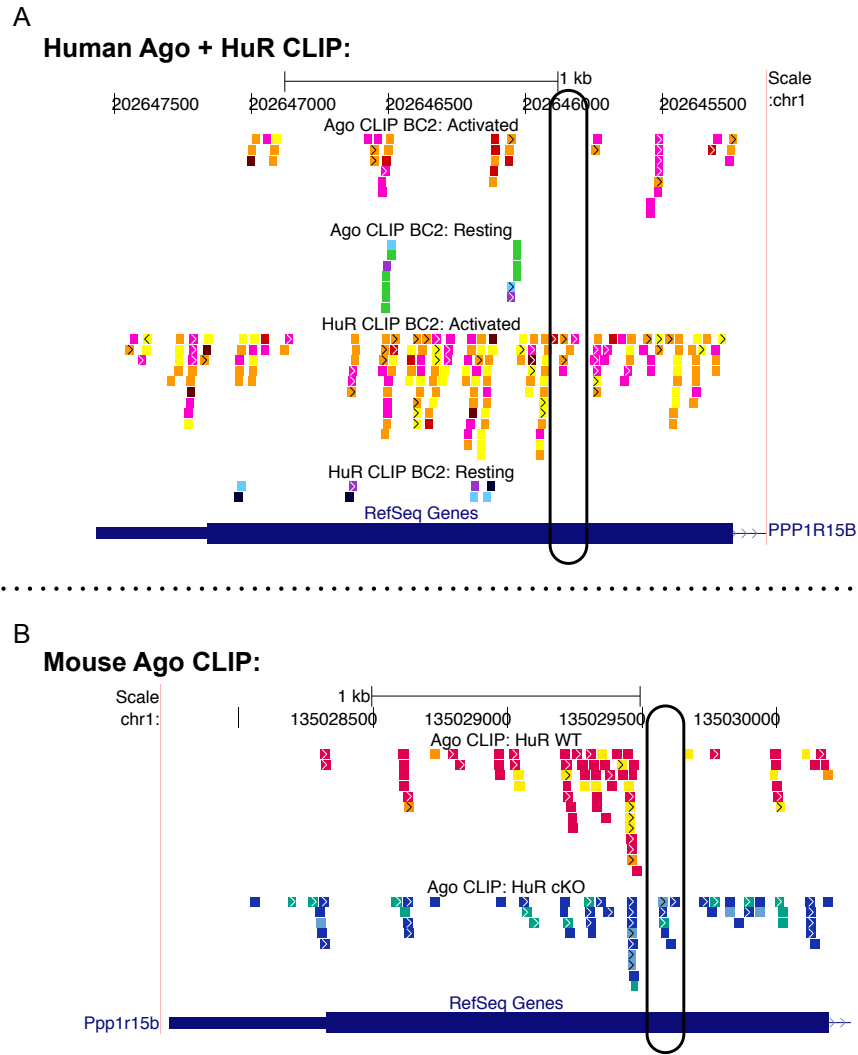


Figure 8.12 Ago and HuR Binding in Human and Mouse: Ppp1r15b Exon. (A) The position of individual Ago and HuR unique CLIP tags in biologic complexity two clusters plotted relative to their mapped position on the human PPP1R15B 3'UTR. The CLIP cluster showing dynamic reciprocal Ago and HuR binding changes is outlined in the 3'UTR. From top to bottom: chromosomal location, Ago CLIP tags from activated CD8 T cells (colors represent each donor sample as shown in Table 6.1), Ago CLIP tags from resting CD8 T cells, HuR CLIP tags from activated CD8 T cells, HuR CLIP tags from resting CD8 T cells, Gene diagram from RefSeq. (B) The position of individual Ago unique CLIP tags are plotted relative to their mapped position on the mouse Ppp1r15b 3'UTR. The homologous 3'UTR region showing dynamic reciprocal Ago and HuR binding changes on the human transcript is outlined. From top to bottom: chromosomal location, Ago CLIP tags from activated HuR wild-type CD8 T cells (colors

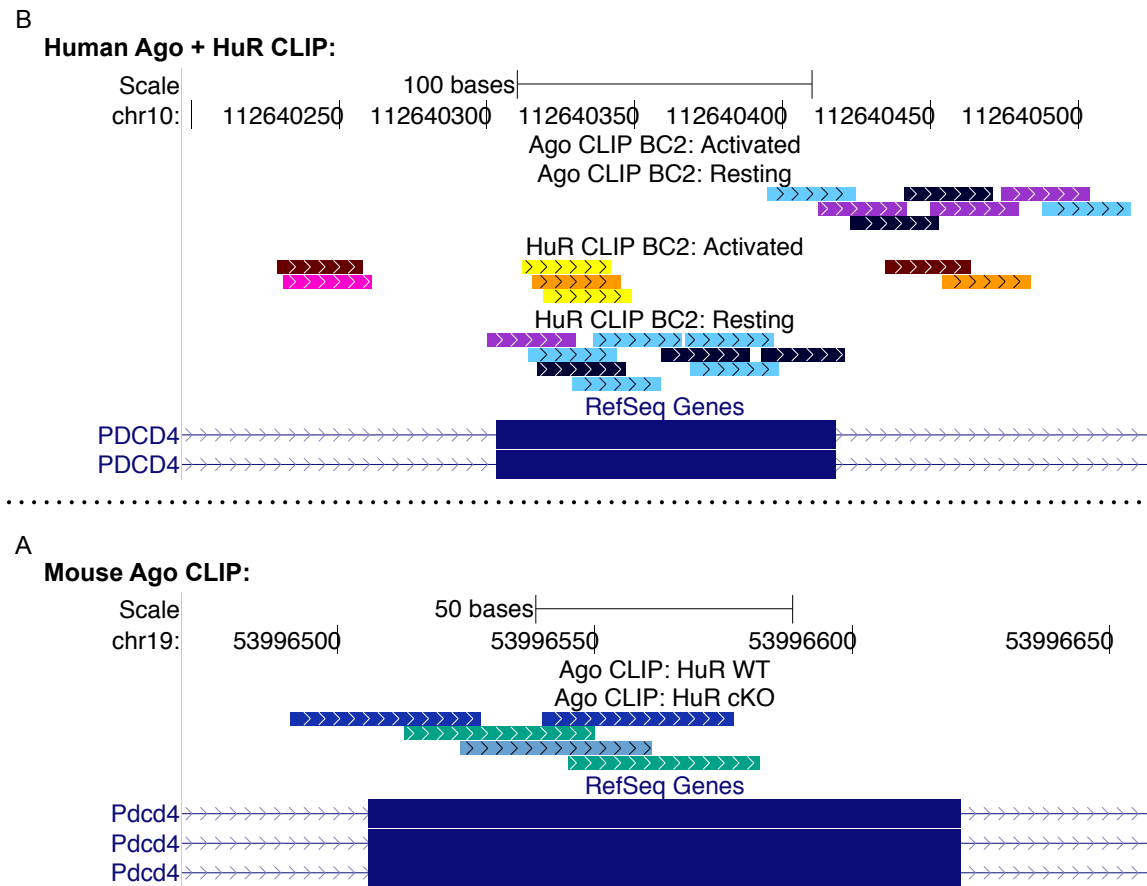


Figure 8.13 Ago and HuR Binding in Human and Mouse: Pdc4 Exon. (A) The position of individual Ago and HuR unique CLIP tags in biologic complexity two clusters plotted relative to their mapped position on the human PDCD4 3'UTR. The CLIP cluster showing dynamic reciprocal Ago and HuR binding changes is outlined in the 3'UTR. From top to bottom: chromosomal location, Ago CLIP tags from activated CD8 T cells (colors represent each donor sample as shown in Table 6.1), Ago CLIP tags from resting CD8 T cells, HuR CLIP tags from activated CD8 T cells, HuR CLIP tags from resting CD8 T cells, Gene diagram from RefSeq. (B) The position of individual Ago unique CLIP tags are plotted relative to their mapped position on the mouse Pdcd4 3'UTR. The homologous 3'UTR region showing dynamic reciprocal Ago and HuR binding changes on the human transcript is outlined. From top to bottom: chromosomal location, Ago CLIP tags from activated HuR wild-type CD8 T cells (colors represent each donor sample as shown in Table 8.1), Ago CLIP tags from activated HuR cKO CD8 T cells, Gene diagram from RefSeq.

without binding of Ago, although there was an intronic cluster just downstream of this position in the resting state (Figure 8.13A). Thus, these binding patterns suggest that HuR binding at this position in the *Pdcd4* transcript precludes binding of Ago.

Discussion

In this chapter we examined the role of Ago in T cells lacking the normally ubiquitous HuR protein. We first began by studying $\text{HuR}^{\text{fl/fl}}$ mice where the *Lck* promoter drove expression of Cre. These mice had been previously described as having aberrant T cell maturation, migration, proliferative responses, and gene expression patterns (Papadaki et al. 2009). We found that although the genotypes of *Lck-Cre+* $\text{HuR}^{\text{fl/fl}}$ mice appeared to be identical, the down regulation of HuR in their lymphocytes was not. Instead we observed that certain mice of this genotype maintained wild type levels of HuR while others showed highly reduced levels of HuR protein. We were able to determine the levels of HuR in lymphocytes by screening the T cells by intracellular staining of HuR and flow cytometry and observed phenotypes in the mouse colony of HuR protein expression of around 5% to 100% of wild type HuR levels by western blot.

In order to have a more phenotypically uniform population of mice with HuR deficient T cells, we bred the $\text{HuR}^{\text{fl/fl}}$ mice to those expressing Cre under control of the CD4 promoter. In contrast to the *Lck-Cre* mice, *CD4-Cre+* $\text{HuR}^{\text{fl/fl}}$ mice showed reliable down regulation of HuR protein in their CD4 and CD8 T cells, which was not seen in CD3 negative cells. We therefore prepared CD8 T cells from pooled groups of *CD4-Cre+* $\text{HuR}^{\text{fl/fl}}$ mice and littermate control wild type mice for Ago CLIP. After isolating CD8 lymphocytes, we activated the cells for one hour with CD3/CD28 beads and crosslinked

them. We monitored the purity of the cells by flow cytometry, the activation state of the cells by qPCR for *Ifng* and did western blotting to confirm that the cells had the correct expression levels of HuR. It is important to note that the isolated CD4-Cre HuR cKO mouse CD8 lymphocytes still maintained a low level of detectable HuR protein. This may be due to contaminating cell populations or small numbers of T cells that escaped deletion of the second exon of HuR. Still, the dramatic reduction in HuR protein expression in these samples provides a useful system for studying the reliance on HuR for Ago regulation in CD8 T cells.

We performed Ago CLIP in the three biologic pools of wild type and HuR cKO CD8 lymphocytes and were able to clone between 180,000 to almost 2 million unique Ago binding sites for each sample. Similar to our human dataset, we found that clusters were most represented in intronic regions of target transcripts, followed by 3'UTRs and then coding sequences. However, in the mouse data, 3'UTR regions were a larger percentage of the total than in the human dataset and there were almost twice the percentage of coding sequences represented here. While these still do not resemble the previously published binding distributions for Ago in the brain or in regulatory CD4 T cells, they are more similar (Chi et al. 2009; Loeb et al. 2012). Thus, in addition to the possibility of the patterns being specific to this cell subset, the differences may also reflect those between Ago regulation in humans and mice.

For the majority of Ago binding sites, the patterns were not greatly altered without the presence of HuR in the T cells. For example, the binding patterns looked very similar in wild type and HuR cKO lymphocytes for the *Egr3* and *Ifng* transcripts. For these two

targets we found that, contrasting in the human cells, Ago binding was apparent in the intronic region of *Egr3* and not reproducibly in the introns of *Ifng*. These may reflect differences in the biology of human and mouse lymphocytes in terms of the targets of Ago regulation or may be due to differences in the time course of the CD3/CD28 induced stimulatory cascades between the two species.

Although we first identified the *IRF9* and *FYB* transcripts in the human dataset as showing potential competitive regulation between Ago and HuR, the results from the mouse data suggest that these suggested quantitative changes in binding might not be as critical as the qualitative ones. It therefore may be more important to examine the binding in the 3'UTR of this transcript as being robustly present for both Ago and HuR rather than trying to dissect quantitative changes in the binding patterns for the two proteins. The cloning of bound RNA may not be reliably enumerative to that degree. Further examination of changes between wild type and HuR cKO Ago maps will provide a guide to interpret HuR dependent changes in Ago binding and will help define its regulatory role as it pertains to transcriptional and translational changes.

This finding also emphasizes the previously discussed results in the human datasets, that the majority of Ago and HuR binding changes seen with activation are congruous. While the two proteins may not always be dependent on each other, such as in the cases of the *Egr3* and *Ifng* transcripts, the small percentage of overlapping clusters that represented possible antagonism between the proteins may only represent a small subset of the interactions between Ago and HuR. Still, it appears that there are cases of Ago and HuR antagonism that are identifiable by studying Ago binding in the HuR cKO CD8

lymphocytes. By overlaying RNAseq and Ribosomal Profiling data in these cells, we will learn more about the cooperative and antagonistic regulatory roles of Ago and HuR in the dynamics of T cell activation.

CHAPTER 9. Exploring Tumor Immunity and Neurologic Autoimmunity in Paraneoplastic Neurologic Degeneration

Introduction

Paraneoplastic disorders are defined as symptoms resulting from damage caused by a malignant neoplasm at a site in the body remote from the tumor and can affect most organs and tissues. This set of disorders can be caused by hormone and cytokine secretion by tumor cells or by an immune response against the tumor. In some patients, tumor cells express proteins that are normally restricted to the brain, termed onconeural antigens. The ectopic expression of onconeural antigens in tumors can elicit a strong immune response against the tumor. It is thought that because the antigens are not normally presented in the body's periphery, the immune system recognizes the antigens as foreign. This can create a strong anti-tumor immune response yielding occult tumors in these patients and good outcomes with cancer treatment. Unfortunately, this immune reaction can also lead to severe autoimmune disease in the brain leading to paraneoplastic neurologic degeneration (PND) (Figure 9.1). This set of disorders represent some of the best-known cases of tumor immunity and are fairly unique in that the antigenic targets of the immune system have been characterized (R. B. Darnell, 1996; R. B. Darnell & Posner, 2003a; 2003b; 2006).

One such paraneoplastic disorder involves the onconeural antigen cerebellar degeneration-related protein 2 (cdr2). While cdr2 is thought to normally be restricted to Purkinje neurons in the brain, this tumor rejection antigen is expressed in many breast and ovarian tumors, 25% and 60%, respectively. In rare cases, an anti-tumor immune

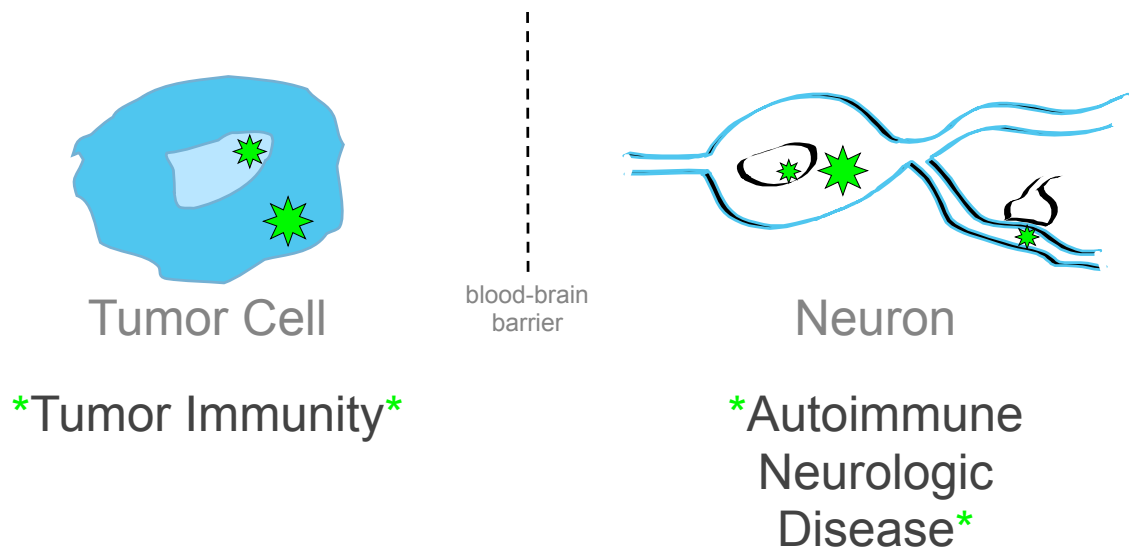


Figure 9.1 Model of Paraneoplastic Neurologic Degeneration. The presence of tumor cells in the periphery that expresses onconeural antigen (represented by green stars) results in an immune response to the onconeural protein that is able to respond to the tumor, resulting in tumor immunity. Trafficking of this immune response to the nervous system targets onconeural antigen-expressing neurons, resulting in neuronal degeneration

response to this onconeural antigen breaks immune tolerance in the brain leading to severe neurodegeneration called paraneoplastic cerebellar degeneration (PCD). Frequently, PCD patients have limited oncologic disease when they are diagnosed with the disorder due to an impressive immunologic rejection of their gynecologic tumor (Albert & Darnell, 2004; Corradi, Yang, Darnell, Dalmau, & Darnell, 1997; J. C. Darnell, Albert, & Darnell, 2000; R. B. Darnell & Posner, 2003a; Peterson, Rosenblum, Kotanides, & Posner, 1992).

A second paraneoplastic neurologic disorder, the Hu Syndrome arises from ectopic expression of the neuronal protein HuD in Small Cell Lung Cancer (SCLC) tumors. It is thought that because HuD is typically restricted to the nervous system, an anti-inflammatory and somewhat immune-privileged site, ectopic expression of HuD in a SCLC tumor stimulates tumor immunity as well as an autoimmune response in the nervous system. Roughly one fifth of SCLC patients have a tumor immune response that breaks tolerance to this onconeural antigen, which is indicated by antibodies to Hu in patient sera. In rare cases, the immune response results in severe autoimmunity in the form of PND called subacute sensory neuropathy and encephalomyelopathy (Figure 9.2). Patients with any HuD immunity display better outcomes with cancer treatment, suggesting that the HuD tumor immune response can be constructive and uncoupled from neuronal autoimmunity (Albert & Darnell, 2004; Dalmau, Furneaux, Gralla, Kris, & Posner, 1990; R. B. Darnell & Posner, 2003b; Rauer & Andreou, 2002).

Although the presence of onconeural antibodies is useful in diagnosing patients with paraneoplastic neurologic degeneration, it is unclear what role they might play in disease

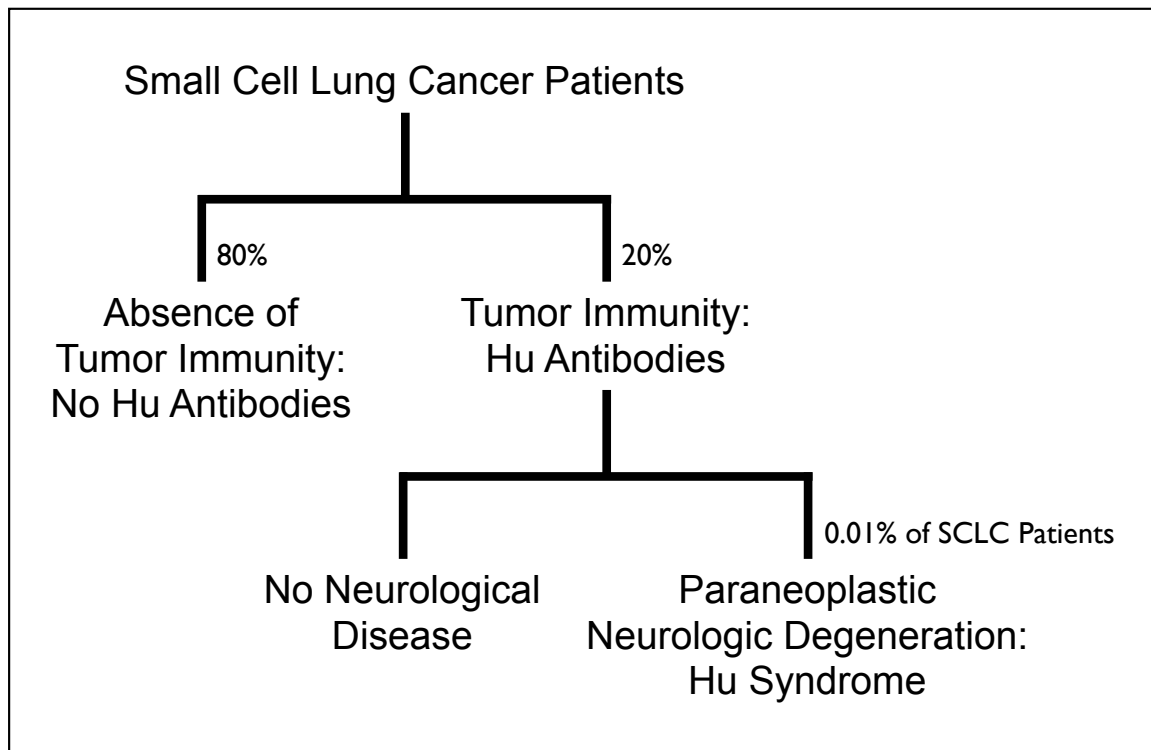


Figure 9.2 Hu Patient Schematic.

progression. Typically, circulating antibodies mediate immune responses to extracellular antigens, while HuD and cdr2 are expressed intracellularly (Okano & Darnell, 1997). Furthermore, disease models utilizing autoantibodies recognizing onconeural antigens have failed to initiate disease (Sakai, Gofuku, Kitagawa, Ogasawara, & Hirose, 1995). Generally, intracellular proteins are presented as peptides extracellularly to the immune system in major histocompatibility complex (MHC) Class I molecule complexes. Each T cell expresses a unique T cell receptor (TCR) that can bind a particular peptide-MHC complex. In this way, T cells can initiate an immune response in an epitope and MHC restricted manner.

Non-self proteins that indicate that a cell has been compromised, such as viral proteins, will be detected on the cell surface by cluster of differentiation eight (CD8) T cells and targeted for killing. Because tumor cells often express unusual protein repertoires, CD8 T cells are prime mediators of tumor immunity (Trombetta & Mellman, 2005). In fact, activated T cells are often found in the cerebral spinal fluid of PND patients and members of the lab have identified cdr2 and HuD-specific CD8 T cells in PND patients (Albert, Austin, & Darnell, 2000; Albert et al., 1998; Roberts et al., 2009). While CD8 T cells can mediate tumor immunity, their priming may rely on help from CD4 lymphocytes. CD4 T cells interact with antigen presenting cells and license the activation of CD8 T cells (Lanzavecchia, 1998; Ridge, Di Rosa, & Matzinger, 1998). Additionally, CD4 lymphocytes interact with B cells to induce the production of antibodies. Thus it is important to consider the role of both CD4 and CD8 T cells to model PND syndromes.

To explore the possibility of using cdr2 as a potential target for immunotherapy of breast and ovarian cancer, the lab identified a peptide derived from human cdr2 (cdr2-290) that stably binds to MHC I molecule HLA-A2.1. Additionally, cdr2-290 specific T cells were identified in HLA-A2.1+ PCD patients' peripheral blood, but not normal HLA-A2.1+ donors, indicating that this epitope is part of the repertoire of the naturally occurring anti-tumor response. Using HLA-A2.1 expressing transgenic mice, high avidity cdr2-290 cytotoxic T lymphocyte clones were isolated which are able to recognize and kill a number of human cancer cell lines that endogenously present cdr2. One murine T cell clone shown to have a strong anti-tumor response against human tumor cell lines was chosen for subsequent analysis. The alpha- and beta-T cell receptor (TCR) genes from the murine T cells were shown to recognize human cdr2-290 presented on HLA-A2.1 and were subsequently cloned. Transfection of RNA derived from this alpha and beta-TCR into normal human donor CD8 T cells afforded the human T cells with the capability to lyse human tumor cell lines endogenously expressing cdr2 (Santomasso et al., 2007).

In order to better understand the varying T cell responses in Hu patients, a murine system was used to study the immune response to HuD. To study the CD8 T cell response to HuD in C57BL/6 mice, the dominant HuD epitope was defined as being peptide 321. The nature of the immune response to HuD in mice was explored by interrogating the difference between immune responses to the neuronal HuD, and the foreign antigen Beta-galactosidase (β -gal). To assay the CD8 T cell responses to these intracellular antigens, groups of mice were immunized with adenovirus expressing either HuD (AdV-HuD) or β -gal (AdV- β -gal). After immunization with the virus and pertussis toxin, an agent which functions as an adjuvant and may help to disrupt the blood brain barrier, and again

with pertussis toxin two days later, CD8 T cells were harvested from the mouse spleens after thirteen days and were stimulated in culture with target cells presenting cognate antigen (Figure 9.3A) (DeLuca, Blachère, Santomasso, & Darnell, 2009).

After wild type C57Bl/6 mice were immunized with AdV-HuD, there was no CD8 T cell IFNG response seen directly *ex vivo* to HuD, but there was an antigen-specific response after *in vitro* T cell stimulation. This suggests that there is peripheral tolerance to the neuronal HuD protein because the HuD-specific T cells are present in the immune repertoire, but they are not active directly *ex vivo* after antigen challenge. In contrast, mice lacking HuD (HuD KO) and immunized with AdV-HuD did not display HuD tolerance. HuD-specific T cells from HuD KO mice were active directly *ex vivo* and after *in vitro* stimulation, because HuD is a foreign antigen in the HuD KO. Similarly, after immunizing wild type mice with AdV- β -gal, there was no immune tolerance observed to the foreign β -gal antigen; there was a detectable response directly *ex vivo* and after *in vitro* stimulation. (Figure 9.3B) (DeLuca et al., 2009). This suggests that the expression of the neuronal HuD protein in a wild type host tolerizes the immune response to HuD epitopes. However, the mechanism is unknown and the critical method by which this tolerance is broken in SCLC patients leading to tumor immunity and the Hu syndrome is not understood. In the future, by mimicking the T cell phenotypes found in PND patients, we intend to model the neurologic degeneration central to these diseases in mice.

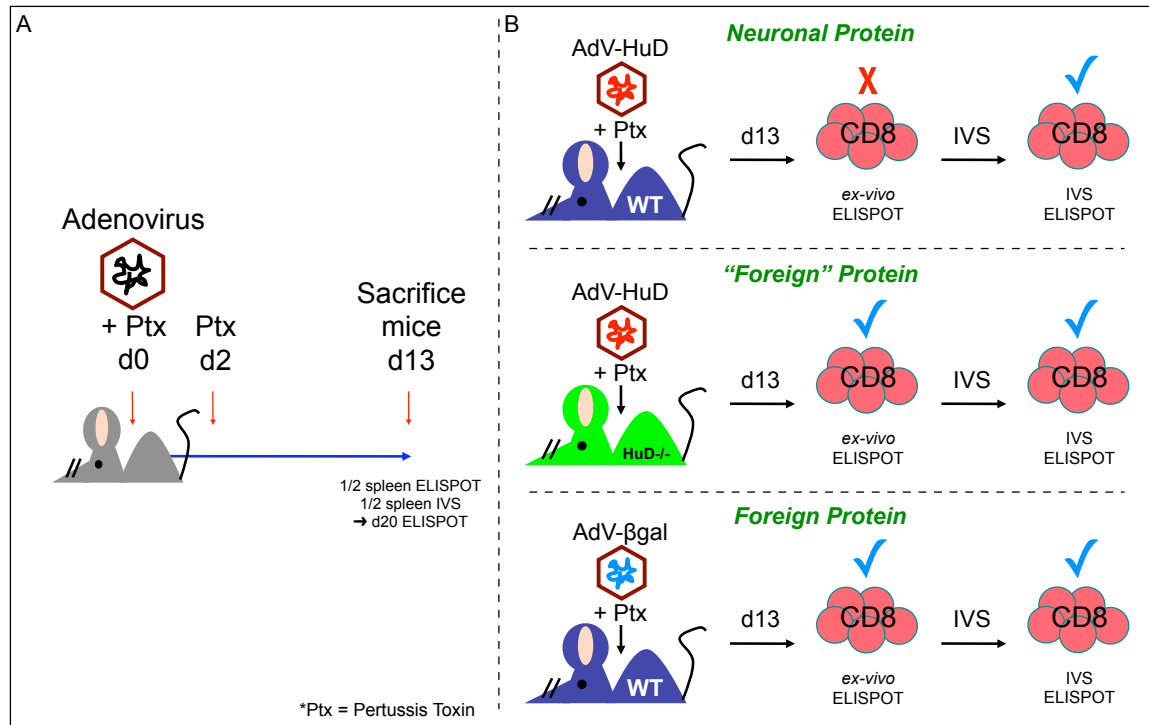


Figure 9.3 Mouse Adenovirus-HuD Immunizations. (A) Cartoon of adenovirus immunization protocol. Mice were immunized on day 0 (d0) with both adenovirus and pertussis toxin. Two days later, they were given another dose of pertussis toxin. The mice were sacrificed on day thirteen and half of the splenocytes were used directly in an *ex vivo* IFNG ELISPOT and the other half were incubated in flasks with peptide for *in vitro* stimulation (IVS). On day 20, the *in vitro* stimulated splenocytes were harvested and used in an IFNG ELISPOT assay. (B) Cartoon representing mouse immunization and ELISPOT results. (Top) Wild-type (WT) mice were immunized with adenovirus-HuD (AdV-HuD). There was no IFNG response directly *ex vivo*, but there was a visible response after IVS. (Middle) HuD knock out (HuD^{-/-}) mice were immunized with AdV-HuD. There was a detectable IFNG response directly *ex vivo* and after IVS. (Bottom) WT mice were immunized with adenovirus-βgal (AdV-βgal). There was a detectable IFNG response directly *ex vivo* and after IVS.

Results

Cdr2 T cell Receptor Optimization

We sought to further characterize the cytotoxic capacity of mouse-derived, human cdr2-reactive CD8 T cell clones in a human system. For this purpose, we engineered the TCR genes from the high avidity cdr2-290 cytotoxic T lymphocyte clone described above (termed Clone 11/12) and from a second clone shown to have good tumor cell line reactivity (Clone 1) to improve the stability of the TCR RNA and increase the abundance of the receptor pair on the cell surface (Santomasso et al., 2007). The TCR genes were originated and cloned from mouse cells but need to be expressed in human cells. To maximize the translational efficiency of the TCRs, human codon-optimized versions of each of the alpha and beta chain genes were generated by *de novo* gene synthesis. Furthermore, it has been demonstrated that an additional cysteine residue in the constant region of each receptor chain helps proper TCR pairing by allowing for an added disulfide bond to form between the correctly paired alpha and beta-receptor chains (Cohen et al., 2007). To enhance the ability of the electroporated cdr2-290 TCRs to pair correctly while competing with the endogenous TCRs in the human CD8 cells, a cysteine codon was incorporated into the constant region of each receptor chain during gene synthesis. We cloned the synthetic TCR constructs into an expression vector for efficient RNA transcription of a polyadenylated mRNA, which was used for T cell electroporations (Figure 9.4) (vector kindly provided by Dr. Eli Gilboa).

We electroporated human CD8 T cells with alpha and beta-chain TCR RNA from Clone 1, Clone 11/12, or with no RNA in a mock electroporation. After allowing the cells to

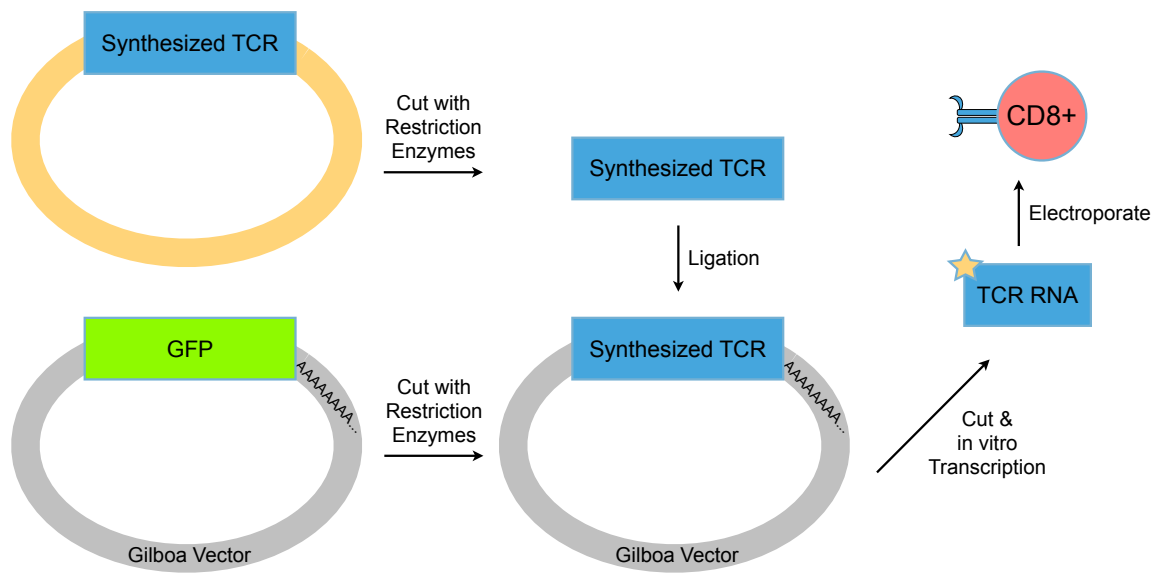


Figure 9.4 cdr2 TCR Optimization Schematic.

rest in culture, we screened the lymphocytes for TCR expression by tetramer staining with a cdr2-290 tetramer or a Flu-M1 tetramer as a negative control. When we stained the electroporated cells with the Flu-M1 tetramer, we saw less than half a percentage of tetramer-positive CD8 cells. This negative result was also seen for the cdr2-290 tetramer staining of mock electroporated cells and cdr2 TCR Clone 1 electroporated cells. This negative result for Clone 1 was expected. The inability of Clone 1 to bind tetramer was one of the main factors for it not being pursued previously, although we are uncertain why it fails to do so. We did see a population of tetramer positive cells comprising ~7% of CD8 lymphocytes electroporated with cdr2 TCR Clone 11/12 (Figure 9.5).

Characterization of Ovarian Cancer Patient Ascites Samples

To study the potency of the electroporated T cells' response to primary cancer tissue, we processed ovarian tumor cells from neurologically healthy oncologic patients' ascites fluid for use *in vitro*. The cancer cells would need to be both cdr2 positive and HLA-A2 positive for the TCR clones to recognize cdr2-290 peptide presented on the cells. To screen the haplotype of the cancer patients, we stained PBMC and analyzed the cells by flow cytometry. We found that three patients were HLA-A2 negative and that five of the eight patients were HLA-A2 positive (Figure 9.6).

In order to determine which tumor samples expressed cdr2, we immunoprecipitated cdr2 from four ovarian ascites samples using sera from PCD patients. Of the four patients tested, three expressed detectable cdr2 protein (data not shown). Importantly, we identified the ascites from patients 4 and 6 as being cdr2 positive and HLA-A2 positive. Therefore, we would expect the cdr2 specific T cells to respond to these tumor cells. The

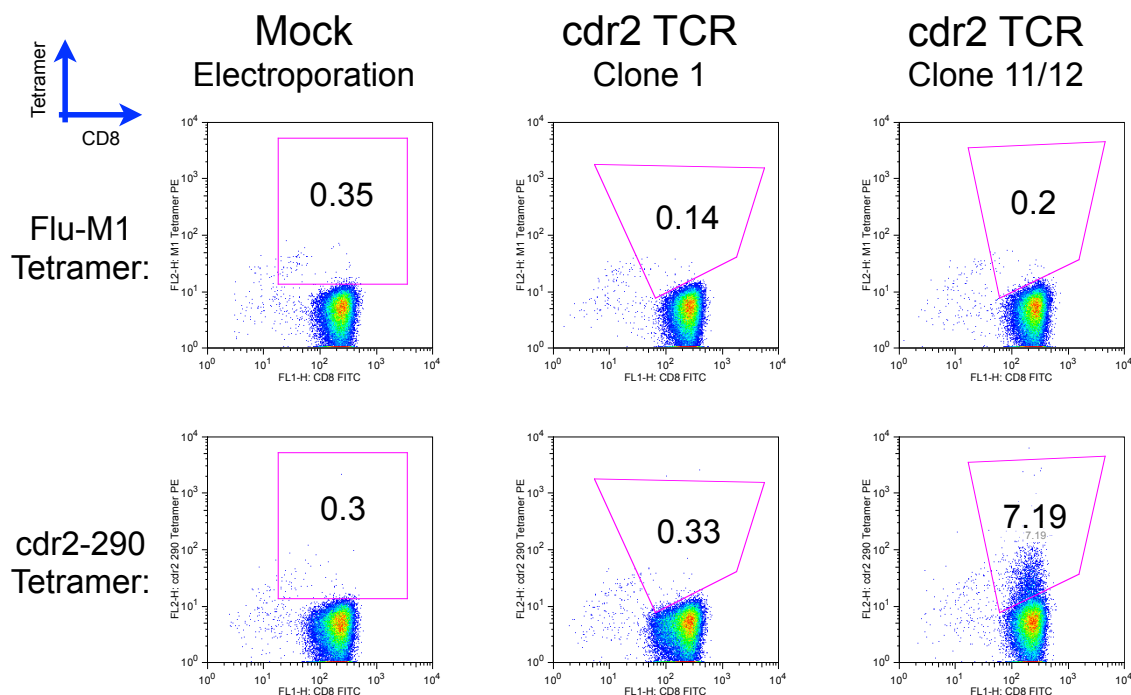


Figure 9.5 cdr2 TCR Tetramer Stain of Electroporated Lymphocytes. Flu-M1 (58-66 peptide) or cdr2 (290-298 peptide) specific HLA-A2.1 tetramer staining of CD8 T cells electroporated with no RNA (Mock) or with the indicated cdr2 TCR Clone RNA (Clone1 or Clone 11/12). The percentages of tetramer-positive cells are noted in the gated populations.

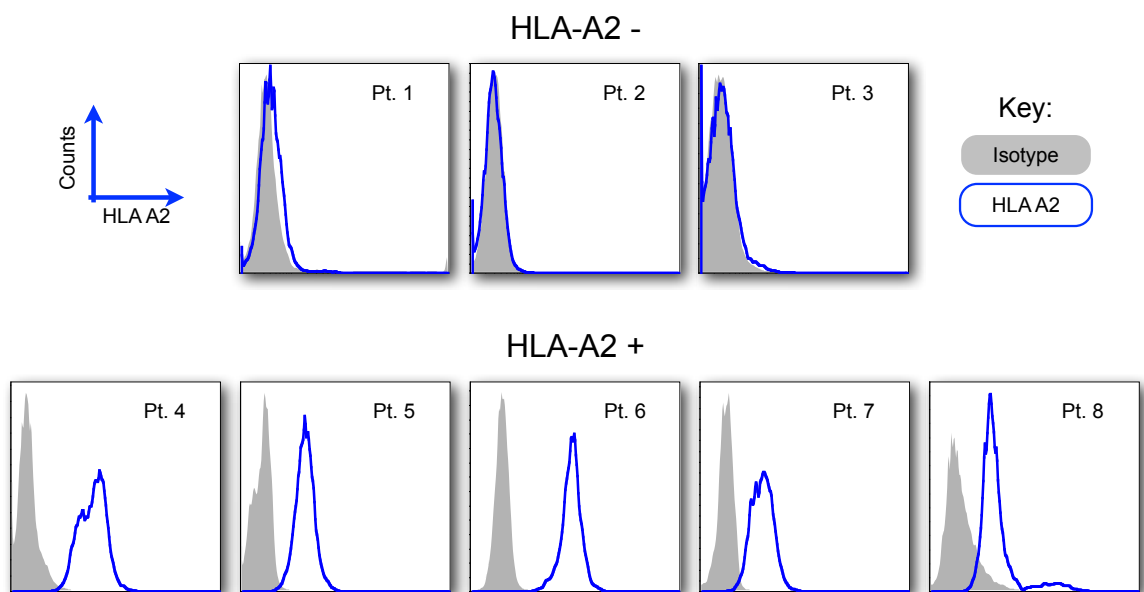
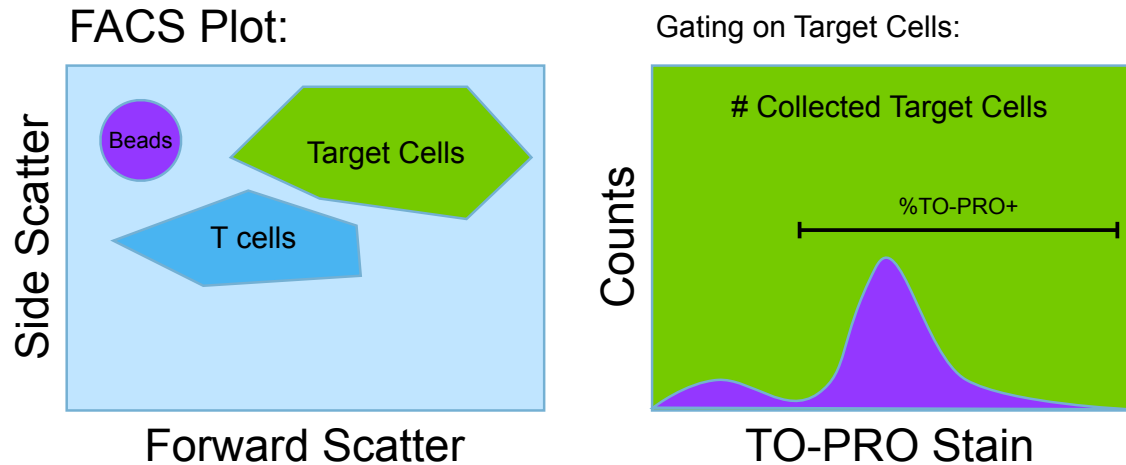


Figure 9.6 HLA-A2 Stain of Ovarian Cancer Patient PBMC. Peripheral blood mononuclear cells (PBMC) from eight ovarian cancer patients were stained with FITC-conjugated HLA-A2 antibody or Isotype Control (BD Biosciences). Cells were washed and analyzed immediately by flow cytometry.

tumor from patient 3 was also cdr2 positive, but because this patient is HLA-A2 negative, the T cell clone should not be able to react to it. Although patient 8 is HLA-A2 positive, the cdr2-290 specific T cells should not be able to engage these cells, as they are cdr2 negative. Thus, we identified tumor samples that should be targeted by the cdr2 specific T cells and also samples that will serve as important negative controls for future work.

Flow Cytometry Based Killing Assay Development

To determine the reactivity of the cdr2 specific lymphocytes against the primary tumor cells, we developed a flow cytometry based killing assay, schematized in Figure 9.7. T cells electroporated with cdr2-290 TCRs or electroporated without RNA (mock) were co-cultured overnight with target cells comprising cancer cell lines and primary ascites samples. After the incubation, all of the cells were harvested from the well, stained with viability dye TO-PRO to designate dead cells and analyzed by flow cytometry. A defined number of non-fluorescent beads were added to each sample as a means to normalize counts, and events were collected by flow cytometry until a set number of beads were captured. In this manner, the number of target cells that had been killed and missing from the well could be distinguished between paired groups of cognate and irrelevant stimulators. The total number of cells killed in the well by cognate T cells could then be calculated by taking the sum of TO-PRO positive dead cells and an estimate of the number of cells missing from the well. Furthermore the percentage of killed target cells could be determined by comparing the killed cells to the number of collected target cells from paired co-cultures of T cells with irrelevant targets.



Killed Cells = Missing Cells + Dead Cells

Missing Cells = (#Collected Target Cells with Mock T cells) - (#Collected Target Cells)

Dead Cells = (#Collected Target Cells) x (%TO-PRO+ Cells) / 100

% Killed = 100 x (Killed Cells) / (#Paired Collected Target Cells with Mock T cells)

Figure 9.7 Tumor Killing Assay Schematic. T cells electroporated with TCR RNA were co-cultured with target cells. After an overnight incubation, the cells were harvested and stained with TO-PRO. An equivalent aliquot of beads were added to each tube and events were collected on the flow cytometer until a set number of beads was collected. The forward and side scatter distribution of the cells was used to gate on target cells as shown in the cartoon. The number of TO-PRO positive cells indicates the dead target cells within the sample. The number of killed target cells was estimated by adding the number of cells missing from the well as determined by the number of paired target cells collected from an incubation with irrelevant T cells and the number of TO-PRO positive cells. From this number, the percentage of killed cells was calculated by comparing the number of killed cells to the total number of paired target cells co-cultured with irrelevant T cells.

Figure 9.8 shows representative data from one replicate of a killing assay set up with cdr2-290 Clone 11/12 TCR and mock electroporated T cells with different tumor cell lines and ascites samples. T cells were co-cultured with T2 cells pulsed with irrelevant Flu-M1 peptide or cognate cdr2-290 peptide. T2 cells are a human lymphoblast cell line deficient in TAP function containing abundant HLA-A2 molecules on the cell surface that can be loaded with exogenous peptide (Salter, Howell, & Cresswell, 1985). The FACS plots in Figure 9.8A show the TO-PRO staining of these target cells. We observed that mock electroporated T cells stimulated with T2 cells pulsed with either peptide gave a background of about 14% TO-PRO positive dead cells and nearly 20,000 total T2 cells were collected. We saw the same results from Clone 11/12 TCR electroporated cells incubated with T2 cells pulsed with Flu-M1 peptide. When cdr2-specific T cells were cultured with cognate T2 cells pulsed with cdr2-290 peptide, we were only able to collect about 5,000 target events and of those events 60% of the cells were dead. Therefore we calculated that approximately 15,000 cells had been eliminated from the well and roughly 3,000 additional cells were dead, but present in the well, leading us to determine that the cdr2-290 Clone 11/12 T cells had killed nearly 90% of the cognate T2 cells.

We calculated the percentage of killed targets for each cell type and have displayed the results in Figure 9.8B. Compared to mock electroporated T cells, cdr2-290 lymphocytes were able to kill ovarian cancer cell line COV413 cells that are both cdr2 and HLA-A2 positive. This killing was not enhanced by adding an irrelevant Flu-M1 peptide, but was greatly increased when the cells were pulsed with cdr2-290. Treating the COV413 cells with IFNG to increase MHC Class I expression and processing of peptides did not increase the killing of these cells.

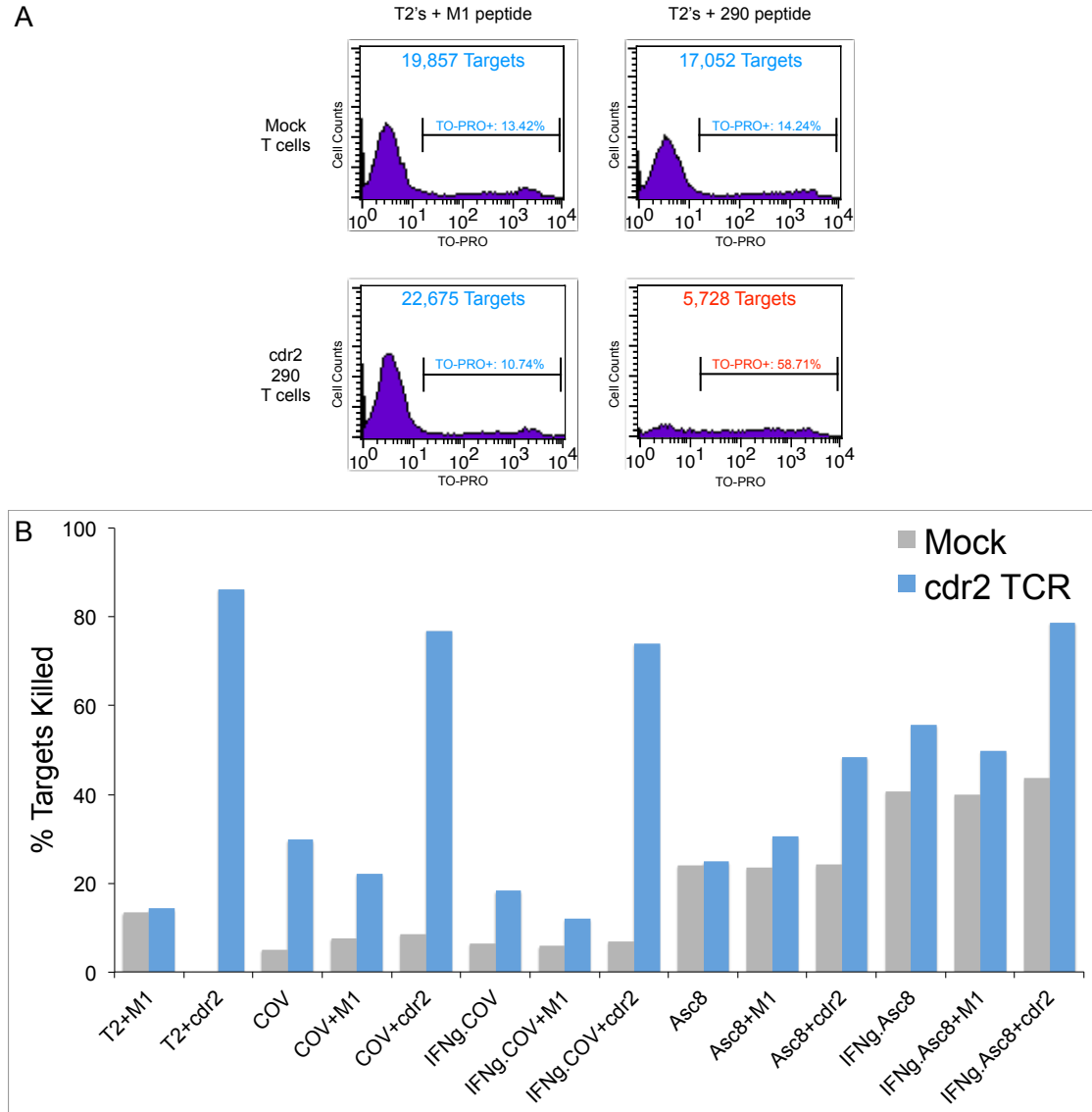


Figure 9.8 cdr2-Specific CD8 T Cell Tumor Killing Assay. (A) Representative histograms of TO-PRO staining of target cells collected for the groups indicated. The total number of targets and percentage of TO-PRO positive cells are indicated for each plot. Targets included T2 cells pulsed with either Flu-M1 peptide or cdr2-290 peptide and the T cells included T cells electroporated without RNA (mock) or T cells electroporated with cdr2-290 specific T cell receptor RNA. (B) Quantification of results from flow cytometry data as in (A). Plotted is the percentage of killed Target cells for each sample (calculations described in Figure 9.7). Targets included T2 cells: HLA-A2 positive and cdr2 negative (T2), COV413: HLA-A2 positive and cdr2 positive (COV), and Ascites Sample 8: HLA-A2 positive and cdr2 negative (Asc8). Some of the target

When we co-cultured lymphocytes with ascites cancer cells from patient 8, we did not see specific killing of tumor cells by the cdr2-290 TCR electroporated cells as compared to the background death of cells co-cultured with T cells that were mock electroporated. This was not surprising given that this tumor sample did not express detectable levels of cdr2 by IP-western blot. Still, this patient was HLA-A2, and the cdr2-TCR electroporated cells were able to target ascites cells pulsed with cdr2-290 peptide. This showed that primary cancer cells could present pre-processed peptide to CD8 lymphocytes for killing. IFNG treatment of the ascites cells increased the background level of dead target cells in the culture. Nevertheless, increased MHC I expression on the cell surface enhanced the killing potential of the cdr2-290 specific T cells in response to the ascites. With IFNG treatment and pulsed with cdr2 peptide, the ascites served as comparable targets to the HLA-A2 cell lines (Figure 9.8B). This suggests that endogenously, the primary tumor cells may display decreased presentation of peptides to help shield them from the surveying immune system. This could serve as a potential problem for T cell therapy although it could potentially be overcome with cytokine treatment. Nevertheless, we were able to see specific targeting of a peptide-pulsed primary ascites tumor sample by cdr2-TCR electroporated lymphocytes. This assay provides the potential to quantify the ability of cytotoxic T cells to kill target cells *in vitro*.

Cdr2-specific CD8 T cell Responses to Primary Human Cancer Cells

In addition to the flow cytometry based killing assay, we examined the responsiveness of the electroporated T cells to target cells in an IFNG ELISPOT assay. Human CD8 T cells were electroporated with either cdr2-290 Clone 1 TCRs, Clone 11/12 TCRs, or GFP

RNA as a negative control. The T cells were co-cultured with target cells in ELISPOT plate wells coated with anti-IFNG antibody to capture the released cytokines from activated T cells. After twenty hours, the cells were washed from the wells and bound IFNG was used to develop spots on the membranes in each well. In this way the number of spot-forming lymphocytes could be counted per million plated T cells.

We found that Clone 1 and Clone 11/12 cdr2-290 TCR electroporated cells were able to respond to both high and low concentrations of cdr2-290 peptide pulsed T2 cells but not to T2 cells pulsed with the irrelevant Flu-M1 peptide. Both were also able to kill humanized mouse kidney epithelial cells infected with adenovirus expressing human cdr2 (AdV-hcdr2). Neither of the T cell clones responded to adenovirus driven expression of mouse cdr2 (AdV-mcdr2) in these cells, showing specificity to the human cdr2-290 peptide (Figure 9.9A). Clone 11/12 had a higher number of spot forming cells than Clone 1 at both concentrations of peptide pulsed T2 cells and with the adenovirus infected cells signaling that it may be a higher avidity T cell clone. The reactivity to the AdV-hcdr2 infected cells is important because it shows that the T cell clones were able to respond to endogenously processed and presented cdr2 peptides, not just cells pulsed with peptide on their cell surfaces.

We also used tumor cell lines and patient ascites cells as targets in the ELISPOT. We found that both cdr2-290 clones were able to respond to COV413 ovarian cancer cells that are HLA-A2 positive and express cdr2. The clones could not respond to the cdr2 expressing HeLa cells that are not HLA-A2 positive, demonstrating that the immune response is HLA restricted. Unfortunately, we did not see any significant response to

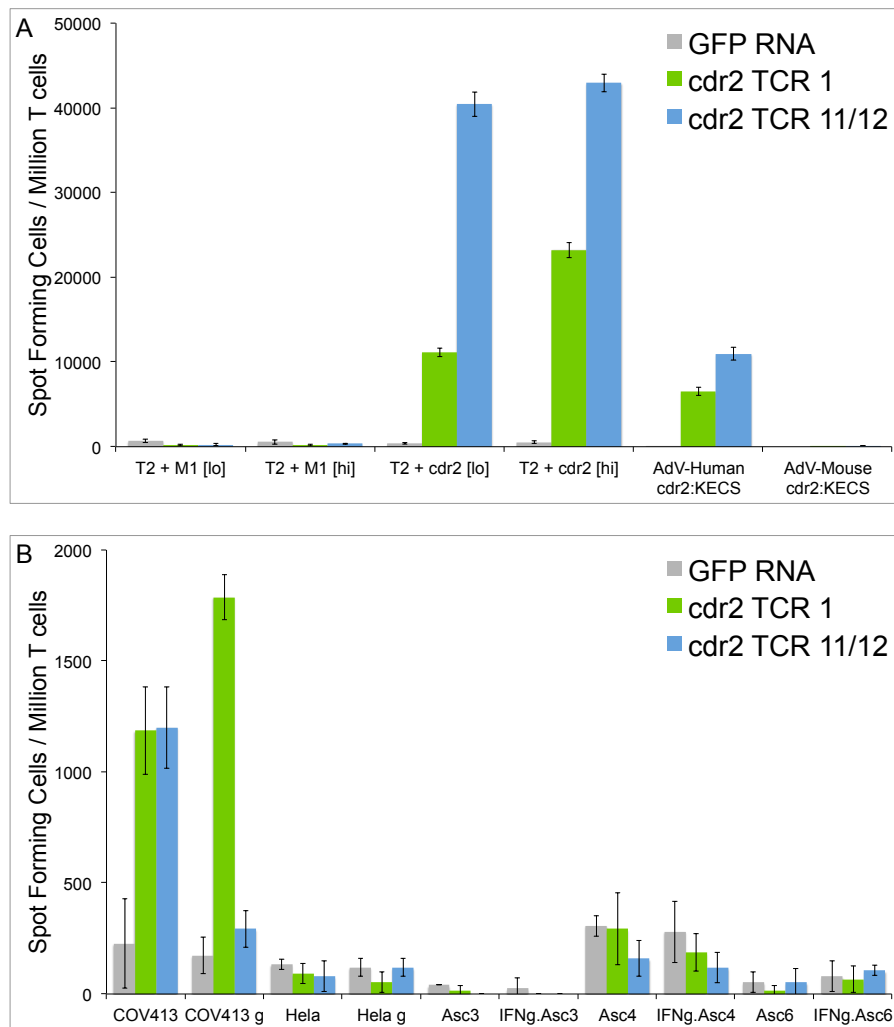


Figure 9.9 cdr2-Specific CD8 T Cell IFNG ELISPOT. To test for recognition of endogenous cdr2 tumors by the electroporated cdr2 specific T cells, cdr2 T cell receptor RNA electroporated T cells (Clone 1 or Clone 11/12) or control GFP RNA electroporated T cells were co-cultured with target cells in a twenty-hour IFNG ELISPOT assay. Values representing spot forming cells per million CD8 T cells, are the average of triplicate wells; error bars indicate standard deviation. **(A)** T cells co-cultured with: T2 cells (HLA-A2 positive and cdr2 negative) pulsed with Flu-M1 peptide (+M1) or cdr2-290 peptide (cdr2) at low [lo] or high [hi] concentrations, humanized kidney epithelial cells (KECS) (HLA-A2 positive and endogenously cdr2 negative) infected with adenoviruses driving expression of either human cdr2 or mouse cdr2. **(B)** T cells co-cultured with: COV413 tumor cells (HLA-A2 positive and cdr2 positive), HeLa tumor cells (HLA-A2 negative and cdr2 positive), ascites sample 3: HLA-A2 negative and cdr2 positive (Asc3), ascites sample 4: HLA-A2 positive and cdr2 positive (Asc4), ascites sample 6: HLA-A2

cdr2 expressing primary ascites samples whether they were HLA-A2 negative (Ascites 3) or HLA-A2 positive (Ascites 4 and 6) with or without IFNG treatment (Figure 9.9B). It is possible that the cdr2 expression in these cells is below the detection of the T cell clones or that the presentation of cdr2-290 on the surfaces of the cells is not efficient.

In order to screen for the effector potential of T cells that were in contact with cognate targets, we stained cdr2-290 TCR electroporated cells for CD107a and TNF following co-culture with target cells as in the ELISPOT assay. Following TCR engagement, the secretion of lytic granules from activated CD8 T cells should lead to the presence of CD107a on the cell surface of the lymphocytes. CD107a that is normally present on the lytic granule membrane will fuse with the cell membrane to release its contents and interrogate the target cell (Betts et al., 2003). After co-culture with T2 cells pulsed with cognate peptide, we saw a dramatic increase in the CD107a expression on the surface of CD8 T cells electroporated with Clone 1 or Clone 11/12 TCRs, but not mock electroporated cells. The expression of TNF also increased in these cells as seen by a shift upward in the scatter plot (Figure 9.10). Interestingly, the percentage of activated cells in this assay greatly exceeds the percentage of tetramer positive cells indicating that tetramer staining may be an underestimate of functional cdr2 specific TCR expressing T cells (Figure 9.5).

In parallel with the results from the IFNG ELISPOT assay, we saw a strong shift in both TNF and CD107a in cdr2-specific T cells in response to humanized KECs infected with AdV-hcdr2 but not AdV-mcdr2 and no response from the mock electroporated T cells. While we did not observe a significant response to the HLA-A2 positive cdr2 positive

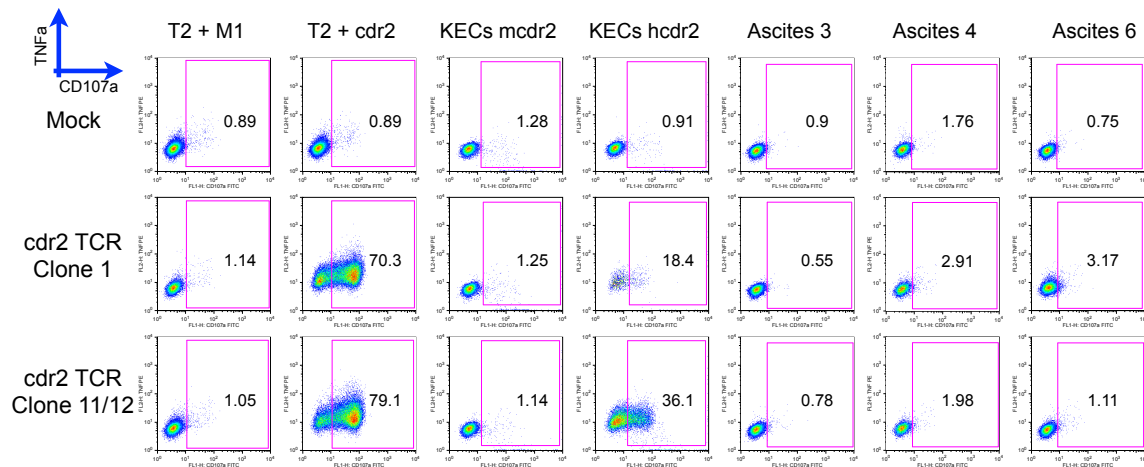


Figure 9.10 cdr2-specific CD8 T Cell CD107a and TNF Assay. FACS analysis for the degranulation marker protein CD107a and TNF was performed after co-culture T cells electroporated without RNA (mock) or T cells electroporated with cdr2-290 specific T cell receptor RNA (Clone 1 or Clone 11/12) with target cells: T2 cells (HLA-A2 positive and cdr2 negative) pulsed with Flu-M1 peptide (+M1) or cdr2-290 peptide (cdr2), humanized kidney epithelial cells (KECs) (HLA-A2 positive and endogenously cdr2 negative) infected with adenoviruses driving expression of either human cdr2 or mouse cdr2, ascites sample 3: HLA-A2 negative and cdr2 positive (Asc3), ascites sample 4: HLA-A2 positive and cdr2 positive (Asc4), ascites sample 6: HLA-A2 positive and cdr2 positive (Asc6). Gating was performed on live lymphocytes based on forward and side scatter characteristics. The percentages of cells staining for CD107a were as indicated.

ascites tumor cells in the ELISPOT assay (Ascites 4 and 6), we did see a slight but detectable increase in CD107a expression on the surface of cdr2-specific T cells in response to the tumors that was not present in response to the HLA-A2 negative cdr2 positive cells (Ascites 3) (Figure 9.10). Although small, this was the first example of a cdr2-specific TCR electroporated lymphocyte response directed against primary human cancer cells.

HuD Specific CD8 T cell Clone Characterization

To isolate a CD8 T cell clone specific for HuD peptide 321, a wild type mouse was immunized with AdV-HuD and pertussis toxin as described previously. Isolated T cells were *in vitro* stimulated with peptide 321 and a bulk line of HuD peptide 321 CD8 T cells was established. The line was plated in limiting dilutions and the clonal T cells were then continually re-stimulated with peptide 321 while being characterized. We chose a peptide 321 HuD clone that proliferated well in culture, was able to specifically recognize targets pulsed with minimal peptide 321 (Figure 9.11A,B), could respond to cells endogenously presenting HuD (Figure 9.11C), was able to specifically kill targets pulsed with peptide 321 (Figure 9.11D), and stained completely with MHC HuD-p321 tetramer as analyzed by flow cytometry (Figure 9.11E).

We isolated RNA from the HuD peptide 321 CD8 T cell clone of interest and amplified cDNA for the alpha- and beta-TCRs using the 5' RACE PCR technique and known TCR constant region sequences. Using gene specific primers, we cloned the entire TCR genes. Isolated HuD peptide 321 TCR genes could now be sub-cloned into a cassette vector and

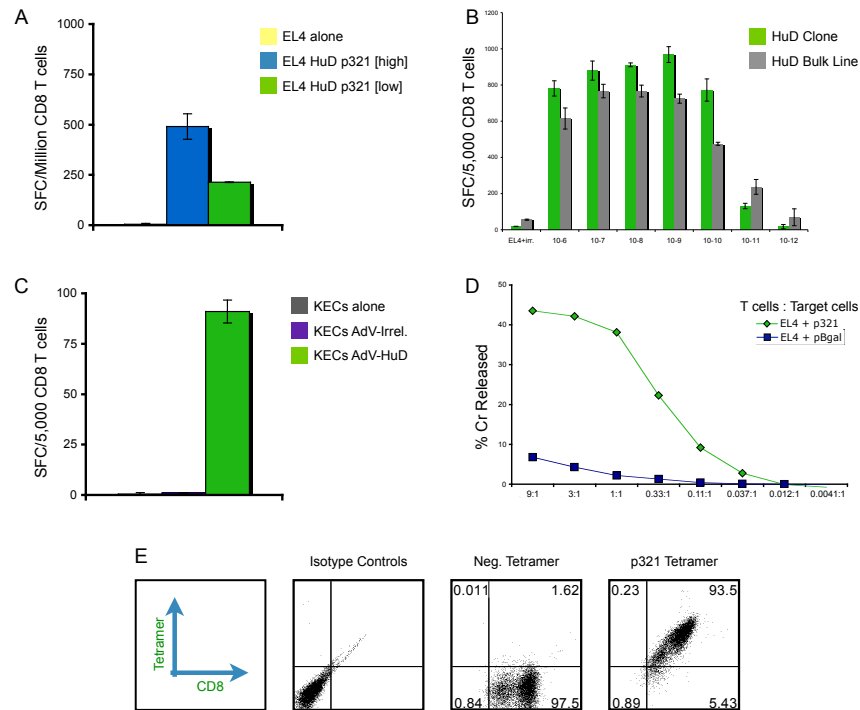


Figure 9.11 HuD peptide 321 CD8 T Cell Clone Characterization. (A) Cloned HuD peptide 321 (p321) T cells specifically recognize peptide 321 pulsed targets. T cells were co-cultured with EL4 cells (HuD negative) alone or with HuD p321 in a low concentration [low] or high concentration [high] in a twenty-hour IFNG ELISPOT assay. Values, representing spot forming cells per million CD8 T cells, are the average of triplicate wells; error bars indicate standard deviation. (B) Cloned HuD p321 T cells respond to targets pulsed with less peptide 321 than the bulk line of T cells. Cloned T cells or bulk HuD T cell line were co-cultured with EL4 cells (HuD negative) with irrelevant peptide (EL4+irr) or with HuD p321 at the μ M concentrations indicated in a twenty-hour IFNG ELISPOT assay. Values, representing spot forming cells per 5,000 CD8 T cells, are the average of triplicate wells; error bars indicate standard deviation. (C) Cloned HuD p321 specific T cells respond to cells presenting endogenously processed HuD. T cells were co-cultured with kidney epithelial cells (KECs) alone or infected with irrelevant (AdV-Irr.) or HuD expressing adenovirus (AdV-HuD) in a twenty-hour IFNG ELISPOT assay. Values, representing spot forming cells per 5,000 CD8 T cells, are the average of triplicate wells; error bars indicate standard deviation. (D) Cloned HuD p321 specific T cells specifically kill targets pulsed with p321. T cells were plated with chromium labeled peptide-pulsed EL4 cells at the indicated T cell to EL4 cell ratios. Values represent the percentage of chromium released from the target cells. (E) Cloned HuD p321 specific T cells were all MHC HuD-p321 tetramer positive. T cells were stained with CD8 antibody and MHC-tetramer specific for cognate HuD peptide or irrelevant peptide. The percentages of tetramer-positive cells are noted in the gated populations.

injected into embryonic cells to create a transgenic mouse where the majority of T cells will have the same HuD-specific TCR (Kouskoff, Signorelli, Benoist, & Mathis, 1995).

Attempts at HuD Specific CD4 T cell Epitope Discovery

To determine the dominant epitope for the CD4 T cell response to HuD, we used an algorithm to predict potential MHC Class II epitopes. To ascertain whether there were HuD T cells specific for any of the predicted peptides in the C57Bl/6 repertoire, we immunized mice with each potential peptide emulsified in the Titermax adjuvant. After seven days, the draining lymph nodes were harvested and CD4 T cells were isolated. The T cells were then plated in a forty-hour IFNG ELISPOT assay with targets pulsed with the cognate peptide or an irrelevant Class II peptide as a negative control. Three out of the six predicted peptides were present in the mouse T cell repertoire (Figure 9.12). Although possible epitopes have now been identified, it is important to characterize the T cell responses to all of these HuD peptides to determine if any of them are naturally processed and presented, and which is optimal. This has proven difficult due to the strong response of CD4 T cells to sera used to grow AdV-HuD for injection into the mice and the dependence on sera to grow the resulting mouse cells in culture.

Exploring Tolerance to HuD Using Wild Type and HuD KO Mouse Bone Marrow

Chimeras

To determine whether the expression of HuD in bone marrow derived cells plays a role in the tolerance to HuD, we transferred bone marrow from wild type and HuD KO mice into sub-lethally irradiated wild type and HuD KO hosts. After bone marrow transplantation,

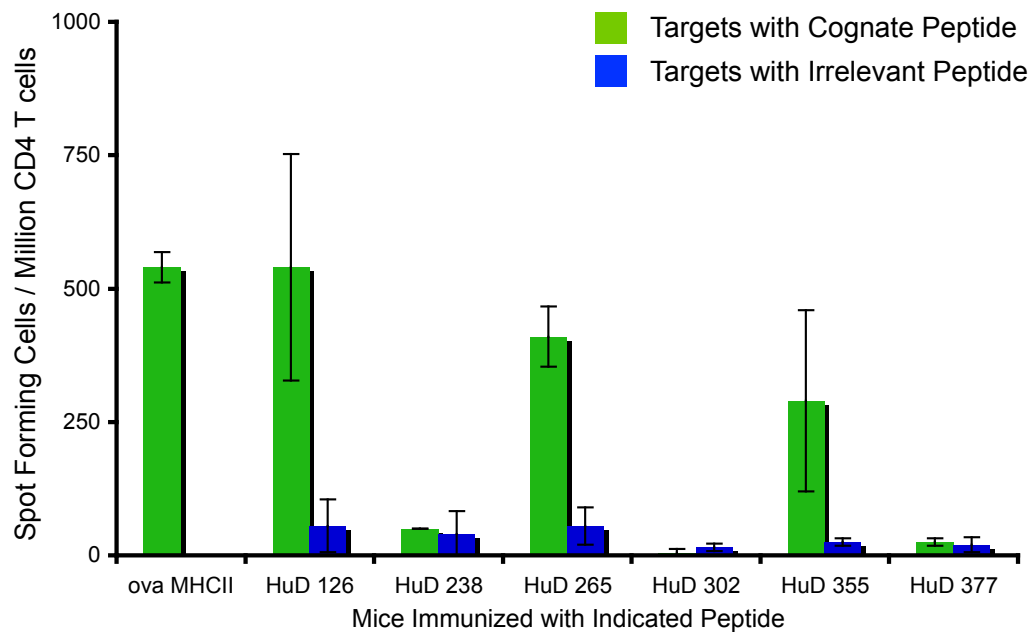


Figure 9.12 IFNG CD4 T Cell HuD Peptide Titermax Experiment. C57BL/6 mice were immunized with individual peptides as indicated in Titermax adjuvant. 7 days later, draining lymph node CD8 T cells were co-cultured in a forty-hour IFNG ELISPOT assay with targets pulsed with cognate or irrelevant peptide. Values, representing spot forming cells per million CD8 T cells, are the average of triplicate wells; error bars indicate standard deviation.

the mice were rested for two months to allow for the new bone marrow to fully reconstitute the host immune system. The mice were then immunized with AdV-HuD and pertussis toxin as previously described (Figure 9.13). We expected that the T cell responses in each mouse would behave like their host. For example, we hypothesized that even with wild type bone marrow the T cells would not be peripherally tolerized in the HuD KO host due to a lack of neuronal HuD expression. Therefore, we expected that the isolated T cells from HuD KO hosts would respond to antigen-specific targets directly *ex vivo* and expanded by *in vitro* stimulation with or without HuD being present in the bone marrow. The T cells from wild type bone marrow or HuD KO bone marrow transferred into wild type hosts were expected to only respond to antigen-specific targets after *in vitro* stimulation because we hypothesized that HuD expression in the host neuronal system would be sufficient to tolerize HuD specific T cell responses regardless of the genotype of the bone marrow derived cells.

The collated results from IFNG ELISPOT assays from two different immunization experiments are summarized in Figure 9.13. In HuD KO hosts reconstituted with transferred HuD KO bone marrow, we were able to recapitulate the HuD KO phenotype in seeing a response to HuD peptide 321 directly *ex vivo* and after *in vitro* stimulation. In contrast, peripheral tolerance to HuD was maintained in wild type hosts reconstituted with either the wild type or HuD KO bone marrow, as these mice maintain expression of HuD in the neuronal system. The peripheral tolerance to HuD was maintained as in a fully wild type mouse and antigen specific responses to HuD peptide 321 were not seen directly *ex vivo*. The T cells from both groups continued to mimic wild type mouse responses and showed antigen-specific activation to HuD peptide 321 after *in vitro*

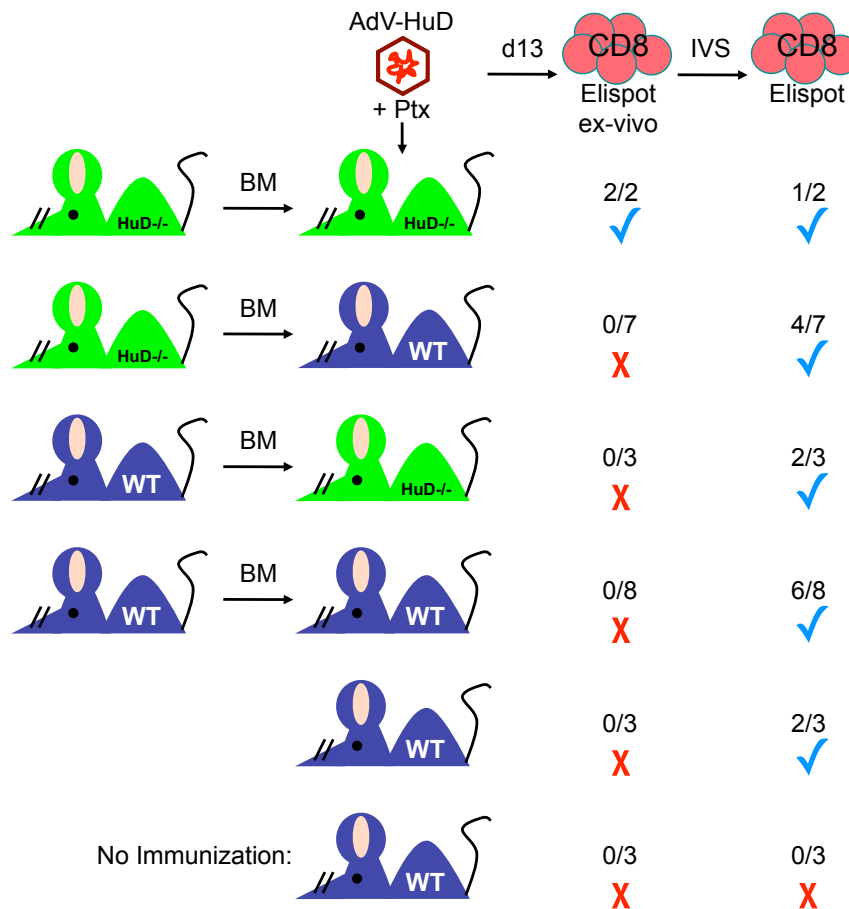


Figure 9.13 HuD Tolerance Bone Marrow Chimera Experiment Summary. Cartoon representing bone marrow chimera genotypes, mouse immunizations, and ELISPOT results. Bone marrow from HuD knock out (green colored animals: HuD^{-/-}) or wild-type mice (purple colored animals: WT) were transferred into sub-lethally irradiated hosts that were either HuD^{-/-} or WT. Control WT mice that were not chimeric are indicated in the bottom two rows. After allowing for bone marrow reconstitution, mice were immunized with adenovirus-HuD (AdV-HuD) and pertussis toxin on day 0 (d0) and again with pertussis toxin on d2, except for control mice represented in the bottom row of the figure as indicated. The mice were sacrificed on d13 and half of the splenocytes were evaluated directly in an *ex vivo* IFNG ELISPOT and the other half were incubated in flasks with peptide for *in vitro* stimulation (IVS). On day 20, the *in vitro* stimulated splenocytes were harvested and analyzed in an IFNG ELISPOT assay. The results of individual mice from two different experiments are enumerated as a ratio of the number of responsive mice to HuD peptide 321 out of the total number of mice assayed between the two experiments. A blue check mark indicates a positive response of the group and a red “X” indicates no HuD p321 response.

stimulation indicating that even the HuD KO derived T cells were able to be tolerized in the wild type host and were not centrally deleted in either case. More specifically, in bone marrow chimeras in wild type hosts, we did not see a response to HuD-specific targets directly *ex vivo*, but did observe T cell expansion and an HuD-specific response after an *in vitro* stimulation with the HuD 321 peptide. Importantly, we did not see HuD-specific responses after *in vitro* stimulation with HuD peptide of T cells from wild type mice that were not immunized with AdV-HuD indicating that the *in vitro* stimulated response was specific to viral immunization (Figure 9.13).

In addition, to explore the role of neuronal antigen absence or expression on the induction of tolerance in bone marrow derived cells from wild type mice, we transferred bone marrow from wild type mice into sub-lethally irradiated HuD KO hosts. Remarkably, the mice also displayed a wild type phenotype. The CD8 T cells did not respond to HuD peptide 321 directly *ex vivo*, but did display an antigen-specific response after *in vitro* stimulation (Figure 9.13). This suggests that even in an HuD KO mouse that does not express the neuronal HuD, the presence of bone marrow derived cells containing a functional HuD gene is enough to tolerize emerging HuD-specific T cells. This implies that the presence of HuD in neurons is not necessary to induce tolerance in T cells to HuD, and that bone marrow derived cells may be sufficient to tolerize CD8 T cells to a neuronal antigen.

Development of Tools to Study Tolerance to HuD

Experiments transferring T cells or bone marrow from wild type or HuD KO mice into different hosts have begun to address whether HuD reactive T cells are being tolerized

and/or deleted in the periphery. One difficulty with these experiments was that we needed to challenge mice with AdV- β -gal in parallel to the mice challenged with AdV-HuD as a positive control for an antigen specific response upon virus challenge. While this helped to control for adenovirus immunization, it was not a control within the same animal and also doubled the number of mice needed for each experiment. A new strategy was tested and adopted to intradermally immunize with both AdV-HuD and AdV- β -gal on opposite sides of the same mouse. In these experiments, we observed a response to β -gal directly *ex vivo* while we were still unable to detect an HuD-specific response at this time. We were able to recover a response to HuD after *in vitro* stimulation (Figure 9.14). The magnitudes of the response to both antigens after the double adenovirus immunization were comparable to the responses to that antigen in a singly immunized mouse. With this new approach, we can recapitulate the phenotypes we observe with single immunizations in a mouse immunized with both viruses. This strategy internally controls for natural variability or abnormalities in the immune response in a mouse specific manner.

In parallel, an approach for double immunization with Titermax emulsified peptides was also explored. We observed that a mouse immunized with different Titermax emulsified peptides in each of the back footpads mounts a detectable antigen-specific response in the corresponding draining popliteal and inguinal lymph nodes. Interestingly, we only see the response in the draining lymph nodes from each footpad and not on the opposite side of the same doubly immunized mouse. Furthermore, the response to each peptide in the double immunized mouse is of the same magnitude of a singly immunized mouse (Figure

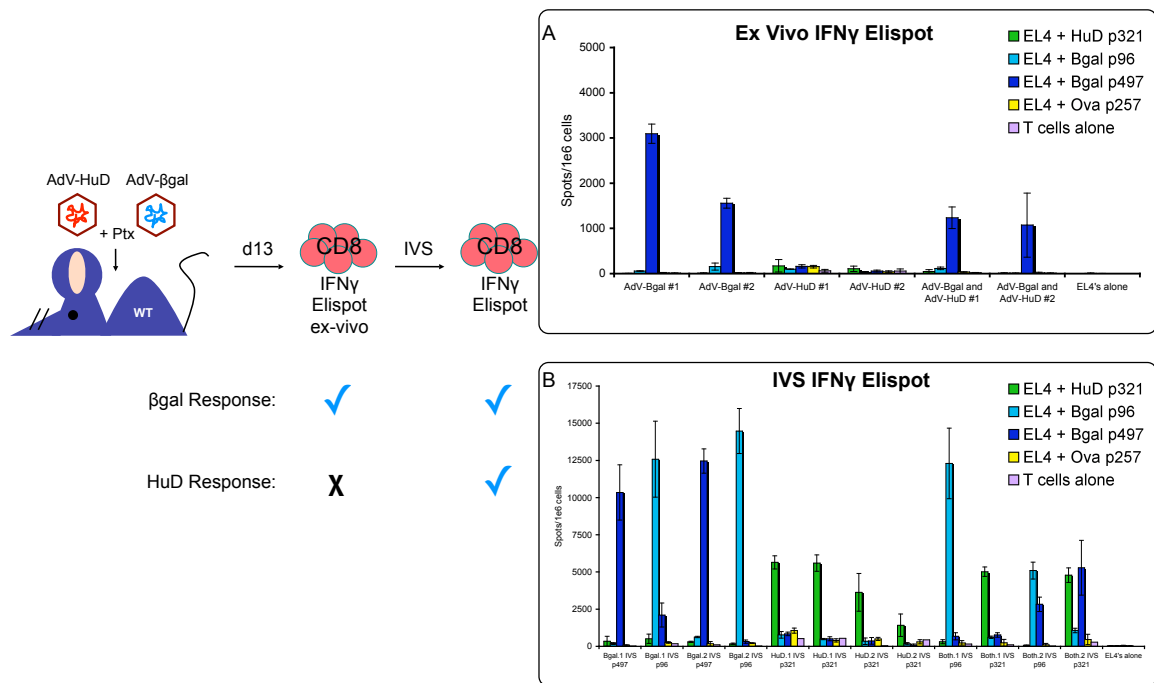


Figure 9.14 Tools to Study Tolerance to HuD: Double Adenovirus Immunization.

Two mice were immunized with adenovirus-β-Gal (AdV-β-Gal), adenovirus-HuD (AdV-HuD) or both adenoviruses with pertussis toxin on day 0 (d0) and again with pertussis toxin on d2. The mice were sacrificed on d13 and half of the splenocytes were evaluated directly in an *ex vivo* ELISPOT and the other half were split into two flasks and incubated with HuD peptide 321 (p321), β-Gal peptide 96 (p96), or β-Gal peptide 297 (p297) for *in vitro* stimulation (IVS). On day 20, the *in vitro* stimulated splenocytes were harvested analyzed in an ELISPOT assay. In the twenty-hour IFNG ELISPOT assays, T cells were co-cultured with EL4 cells (HuD and β-Gal negative) with HuD p321, β-Gal p96, β-Gal p497, irrelevant Ova peptide 257, or alone. Values, representing spot forming cells per million CD8 T cells, are the average of triplicate wells; error bars indicate standard deviation. (A) *Ex vivo* IFNG ELISPOT Results from each immunized mouse are shown. (B) IVS IFNG ELISPOT results from each immunized mouse stimulated in two flasks each with either β-Gal peptide (AdV-β-Gal immunized mice), replicate stimulations of HuD p321 (AdV-HuD immunized mice), or β-Gal p96 and HuD p321 (AdV-β-Gal and AdV-HuD immunized mice) as indicated.

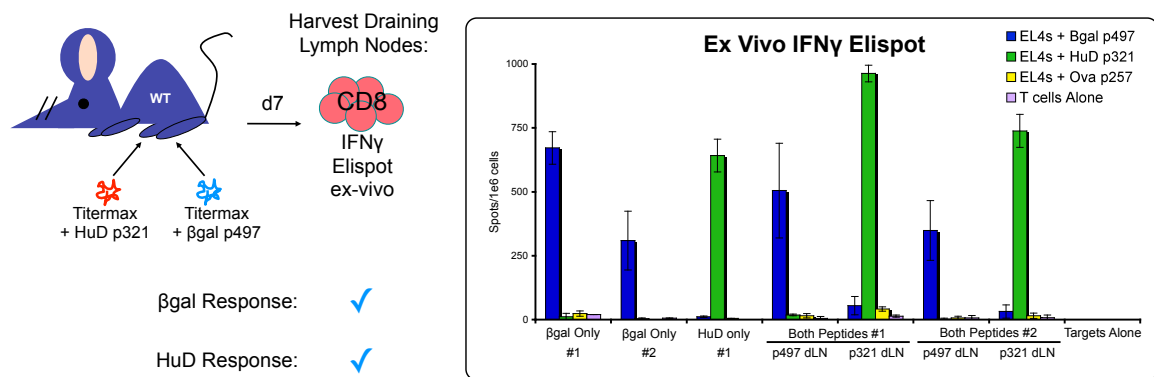


Figure 9.15 Tools to Study Tolerance to HuD: Double Peptide-Titermax Immunization. C57BL/6 mice were immunized with individual peptides into one footpad with β-Gal peptide 497 (p497) or HuD peptide 321 (p321), or with individual peptides (p497 and p321) in either back footpads in Titermax adjuvant as indicated. 7 days later, draining lymph node CD8 T cells were co-cultured in a twenty-hour IFNγ ELISPOT assay with EL4 cells (HuD and β-Gal negative) with β-Gal p497, HuD p321, irrelevant Ova peptide 257, or alone. Values, representing spot forming cells per million CD8 T cells, are the average of triplicate wells; error bars indicate standard deviation.

9.15). With this internal control, we have a better way to monitor the effectiveness of our bone marrow or T cell transfers and for abnormal responses in an animal specific control.

Discussion

In this chapter we examined the immune responses to onconeural antigens. We were able to deliver cdr2-specific T cell receptors to human CD8 T cells by electroporation of TCR alpha- and beta-chain RNA. Using optimized TCR genes for two different mouse-derived human cdr2-specific clones, we were able to confer cdr2-290 peptide immunity to normal human donor cells. Although the majority of cells showed cdr2 reactivity in functional assays, it is unclear why such small percentages of cells were stained by cdr2-290 tetramer. If we increased the TCR expression further, it is possible that the T cells could confer an even more promising functional outcome.

We demonstrated specific targeting of HLA-A2 cdr2-expressing tumor cell lines by both TCR clones. Furthermore, working with primary tumor cells collected from ovarian cancer patient ascites samples, we were able to show reactivity to primary samples that were HLA-A2 positive and expressed cdr2. Still, the magnitude of this immune reaction would need to be improved to consider the possibility of cancer treatment. We also need to repeat the flow cytometry based killing assays with both cdr2-specific TCR Clone 1 and Clone 11/12 with HLA-A2 and cdr2 positive primary ascites samples. By exploring the ability of the electroporated lymphocytes to recognize and attack primary tumor cells endogenously expressing cdr2, these future experiments would explore the potential of using adoptively transferred cdr2-290 TCR T cells in clinical therapy for breast and ovarian cancer.

We have previously described the dominant CD8 T cell epitope of HuD in C57BL/6 mice, peptide 321 (p321) (DeLuca et al., 2009). Here we described establishing clonal HuD-specific CD8 T cells and characterizing their responses to targets expressing HuD. Although potential CD4 T cell epitopes have been established, future work is needed to identify the CD4 T cell dominant HuD epitope. We have cloned the TCR genes from optimal CD8 T cell clones and this could be repeated for the CD4 T cell epitope. The identified TCR genes could be used to make transgenic mice expressing HuD-specific CD4 or CD8 TCRs.

There is currently no animal model for the Hu syndrome. The laboratory's discovery of two different kinds of CD8 T cells in Hu patients suggests that generating HuD-specific transgenic T cells may allow us to learn how to skew HuD-specific CD8 T cells to different phenotypes and monitor the functional consequences (Roberts et al., 2009). Also, nothing is known about CD4 T cell responses in the Hu syndrome. We believe that a critical component in determining whether patients are tolerant of their tumor or react to it may be related to the presence or absence of effective CD4 T cell responses. Therefore, both proposed HuD TCR transgenic mice would be critical tools for understanding the immune response to HuD.

In future work, we propose to characterize the persistence of TCR transgenic CD4 and CD8 T cells in WT and HuD KO hosts. It is possible that the transgenic lymphocytes would be deleted due to their recognition of native antigen, but as in a WT mouse, we expect the HuD-specific T cells would persist, even if in small quantities. Therefore, it will be important to study the transgenic T cells' migration patterns in the thymus and

throughout the mice and to study their proliferation patterns. We would also study the presence of the lymphocytes in the nervous system and whether they cause damage to neurons expressing HuD. We would expect the transgenic cells to be tolerized to HuD and therefore not cause damage to neurons in a resting state. We hypothesize that by challenging mice with a peripheral tumor expressing HuD and providing disruptions to the blood brain barrier, using agents such as pertussis toxin, we may be able to uncover a link to promote an escape from tolerance and possibly lead to neuronal degeneration.

By making bone marrow chimeras of wild type and HuD KO mice, we were able to further study the peripheral tolerance to HuD. As expected, we recapitulated the HuD KO mouse phenotype when transferring HuD KO bone marrow into a KO host. In these animals, we were able to detect an active immune response to HuD peptide 321 directly *ex vivo* following immunization with AdV-HuD and pertussis toxin. This immunity was also seen after *in vitro* stimulation of splenocytes with the HuD peptide. Also as anticipated, having either HuD KO or wild type bone marrow in a wild type host produced tolerance to HuD in the peripheral T cells. For these mice, no immune response to HuD was seen directly *ex vivo* after immunization, but was recovered after *in vitro* stimulation. We consider this response to be a case of tolerance because although the HuD specific T cells were present in the mice, we were not able to detect their activity until they were propagated in culture. Interestingly, we saw this same wild type phenotype in HuD KO mice with transferred wild type bone marrow. We did not expect to see the presence of a functional HuD gene in bone marrow derived cells be able to confer tolerance in an otherwise HuD deficient animal, when HuD is thought to be

restricted to the nervous system. Further work is needed to explore the source of HuD expression in bone marrow derived cells and its role in tolerance in a normal mouse.

With transgenic T cells, we could challenge the mice to mimic possible Hu syndrome initiating events and follow the migration of the HuD-specific cells in the mouse, including the CNS. By conducting transfer experiments using the transgenic TCR mice in combination with wild type and HuD KO littermates, we aim to elucidate the mechanism mediating the anergy of HuD-specific T cells and understand how this tolerance is broken in Hu syndrome patients. Understanding the tumor immune response and the autoimmune neurologic disease for both PCD and the Hu Syndrome are of major clinical importance and could lead to new interventions for disease.

CHAPTER 10. General Discussion

Summary

The careful control of the adaptive immune response allows for the host to respond to rapid changes in its homeostasis and protect against the invasion of pathogens and other systemic injury. While the processes mediating these important retaliations have been studied in extensive detail, the acute molecular processes of regulatory control in T cell activation have still not been completely elucidated. Lymphocytes have the ability to react quickly to confront the presence of cognate antigen within their host. They initiate and terminate cytotoxic and inflammatory pathways abruptly to contain the damage of the invading offense and simultaneously protect the surrounding environment from their own dangerous defense mechanisms. The induction of new transcription is important to shaping these responses. Nonetheless, the rapid control of translation post-transcriptionally is also critical to the immediate function of these cells.

RNA-binding proteins, such as Ago and HuR, have previously been shown to mediate both the proper development of lymphocytes and the regulation of their translational responses. Though there is a vast literature analyzing the targets of Ago and HuR control, the majority of work has been done in non-physiologic *in vitro* systems and little is known about the dynamics of their regulation *in vivo*. The results presented here represent the determination of Argonaute (Ago) and HuR RNA-binding maps in *ex vivo* normal healthy donor cluster of differentiation eight (CD8) lymphocytes before and after T cell stimulation. By overlaying the transcriptional and translational status of these

dynamically changing lymphocytes, we provide a system to functionally decipher the roles of these regulatory proteins and their impacts on the inflammatory response.

Overlapping RNA-Binding of Ago and HuR

We observed that 40% of Ago clusters and 14% of HuR clusters overlap each other, within 64-nucleotides up or downstream of their peak binding positions. Interestingly, not only do many Ago and HuR clusters overlap within a small distance, but also their peak positions are highly superimposable. This implies that in a large proportion of their binding sites, the two proteins are found in the same position. While CLIP data represents the binding specificities of a population of cells and not necessarily a map of a single RNA molecule, this propensity of two such distinct proteins to preferentially bind the same loci is remarkable. These binding similarities were not limited to one T cell stimulation state and quantitative differences in binding for both proteins were often similarly reflective of the transcriptional levels of the targets. This suggests that Ago and HuR may bind these sites cooperatively or in a step-wise fashion to instigate regulatory control. In this way the two proteins could work together or antagonistically to regulate function.

Because the majority of Ago binding was preserved in the HuR cKO mice, it is unlikely that Ago is dependent on HuR as a rule. Still we were able to observe clusters that were present in either one of the mouse genotypes and not in the other, so HuR may be necessary for the binding of Ago to some regulatory sites and may preclude Ago binding in others. We propose that while the binding of these proteins to the same message may in some cases be independent, that their regulatory capacities are still intertwined.

Rapid Changes in RNA-Binding with CD8 T cell Activation

Ago and HuR display rapid changes in binding patterns with CD3/CD28 stimulation of CD8 lymphocytes. While viewing the distributions of binding at one hour represents an early point in the T cell activation regulatory cascade, it is clear that we could learn much from the regulatory states of these cells at both even earlier and later time points. For example, assessing Ago and HuR de novo binding to a transcript at early time points after stimulation may allow a determination of whether there is an ordered hierarchy of binding between these two proteins. Repeating a time course in HuR cKO T cells would complement such studies.

One model to address the binding of Ago and HuR to the same RNA sequence domains is that Ago and HuR do not bind simultaneously to their joint targets. In this model, if binding of one protein proceeds the other in binding pre-processed RNA, then the ratios of binding events in the intronic regions of transcripts to the exonic regions, that will remain in the final mature mRNA, may be indicative of a time line of regulation. For example, in the activated lymphocyte Ago CLIP map of IFNG (Figure 6.2), the larger binding sites in the 3'UTR as compared to intronic regions may indicate that Ago is binding later in the life cycle of the mRNA than HuR. HuR is bound more evenly in its introns and exons, even though it too shows some preference for 3'UTR binding. It is possible that HuR is important in the immediate processing of the IFNG transcript in the nucleus and that the large induction of transcription needs to be tempered by Ago after processing to mediate translational control as time progresses in the stimulatory cascade.

Assaying the timing and efficiency of mRNA processing in the wild type and HuR cKO T cells could help define this regulation.

Studying the transcriptional and translational statuses of T cells at later time points may also help resolve the functional outcome of Ago and HuR binding events. Because both proteins often displayed correlative changes in binding with transcript levels, it is possible that the large changes in transcript abundance with T cell activation may be occluding our ability to identify the regulatory consequences of these binding events. While we have largely focused in our examples on messages that had increased binding and message levels with activation, it is important to note that we also see the reverse as well. Understanding the rapid changes in RNA-protein interactions may give us clues to the eventual stability and translational control of the message, and the interactions between both Ago and HuR may dictate these fates.

For example, within one hour of activation, the levels of IFNG transcript can increase by a factor of 10^2 - 10^3 . Since Ago and HuR robustly bind this message, it is not surprising that their interactions with IFNG would increase in this time period. Still, the eventual effect of Ago binding, for example, is most likely to help degrade this message in a pattern common to the decreases seen in many early activation genes quickly increased after transcription. While HuR may be functioning synergistically with Ago, it is more likely from previous work that it is helping to stabilize or steer copies of the message to translational machinery to balance this repressive Ago response. This kind of balanced regulation could be critical for IFNG so that too much cytokine is not produced after T cell stimulation, which could be detrimental to healthy cells in the immediate

environment of the lymphocyte. While Ago may be necessary to dampen IFNG expression for host safety, rapid translational increases in IFNG protein mediated by HuR stabilization may be just as critical to the inflammatory response. With considerable increased message being made at one hour, even if Ago were mediating degradation of IFNG, we would still observe this as an overall rise in transcript levels. Therefore, it may be informative to look at later times for transcription level responses of targets, when the immediate escalation of the activation has quelled, to determine the functional outcomes of these early binding events. Looking at IFNG levels over time in the HuR KO mice could also help assess this.

Analysis of CLIP Data in the Context of Translational Status

With both proteins changing binding patterns congruently with the dynamic variations in transcript expression, it appears that the large changes in message levels may be obscuring Ago and HuR mediated dynamic changes in transcript stability, or that these proteins often work together to modify transcript abundance. This differs from the results of the ribosomal profiling work. While it is hard to define a single general rule for shifts in ribosomal occupancy of Ago and HuR targets with T cell activation, it is clear that these messages do not automatically enter the translational machinery in proportion to their levels.

In the analysis of Ago and HuR 3'UTR targets, we see that the binding patterns of the proteins correlate well with the patterns in gene expression changes of the messages. For example, in Figure 7.12A, as the ratio of message levels between the resting and activated state shifts from left to right on the axis, signifying transcripts with more RNA

in the resting state on the left or more RNA in the activated state on the right, HuR binding patterns also shift from having more binding in the resting state to more in the activated state shown by points changing in color from blue to yellow. If this pattern were reflected in the translational state of each message, the plotted points would resemble the $y=x$ line. Instead, we see a scattering of points mainly around the origin of the graph. This pattern suggests that for many HuR targets, the translational changes (vertical shifts, up or down) are greater than transcriptional changes (horizontal shifts, left or right). These rapid changes suggest that HuR is part of a critical and complex network of translational regulation shortly after lymphocyte stimulation. Differences in the translational responses of individual transcripts with activation may reflect the interactions of HuR, or analogously Ago, with other factors such as other RNA-binding proteins or subcellular localization changes to mediate translational control.

We have reported multiple examples of dynamic reciprocal changes in Ago and HuR binding patterns in overlapping sites throughout this work. For messages such as FYB and SATB1, we described shifts where the binding levels for HuR increased with activation and Ago decreased with activation, although both represented biologically reproducible binding in both states. This corresponded to CLIP binding maps in the mouse data, where dynamically changing but robust binding of Ago and HuR in the human reflected a preference for binding in wild type cells as compared to HuR cKO. We propose that these may be examples where robust binding in both states in the human is more salient than quantitative differences observed in CLIP tag numbers with activation for predicting the necessity of coincident binding for Ago and HuR in the mouse. As shown in Table 10.1, while we saw subtle shifts in the transcript levels of

Table 10.1 Dynamic Changes in Ago and HuR binding and Translational Efficiency.

| | Human Ago | Human HuR | Resting RPF (RPKM) | Resting mRNA (RPKM) | Resting TE RPF/mRNA | Activated RPF (RPKM) | Activated mRNA (RPKM) | Activated TE RPF/mRNA |
|-------|-----------|-----------|----------------------|---------------------|---------------------|-----------------------|-----------------------|-----------------------|
| EGR3 | Act | Act | --- | --- | --- | 1533 | 1418 | 1.08 |
| IFNG | Act | Act | --- | --- | --- | 22,375 | 6871 | 3.26 |
| IRF9 | Act | Rest | 51 *8 cloned tags | 72 | 0.70 | 67 *18 cloned tags | 60 | 1.11 |
| SATB1 | Rest | Act | 187 | 273 | 0.69 | 134 | 199 | 0.67 |
| FYB | Rest | Act | 500 | 496 | 1.01 | 364 | 384 | 0.95 |

these genes in human T cells, which both decreased with activation, we did not see dynamic shifts in the translational efficiency. The binding patterns of Ago and HuR are similar in these sites and may suggest that the decrease with Ago binding of these transcripts with activation is linked to the reduction in message, while HuR maintains the correlative translational status of these targets.

In the case of the IRF9 transcript, we saw the opposite binding pattern changes for Ago and HuR in the human T cells with activation. Ago binding increased with T cell activation, while HuR binding decreased. Again, both binding sites were still reproducible in both states even though their levels shifted in opposite directions. Analyzing the homologous site in the mouse suggests that HuR is supportive of Ago binding because there was more binding seen in the wild type mice than in the HuR cKO. Interestingly, we did see a shift in translational efficiency for the IRF9 mRNA in human T cells with activation. In the resting state, there was less ribosomal occupancy than message, but the opposite was true after T cell activation (Table 10.1). Although these changes represent differences in relatively small numbers of cloned tags and therefore need to be independently validated, including with additional human samples and in the mouse, these results suggest that HuR may help recruit Ago binding to IRF9 and that with T cell activation this translates into increased ribosomal occupancy.

Generally, we have observed large dynamic shifts in translational status acutely with T cell activation that are often not mediated by similar transcriptional changes. Still, there does not appear to be a single universal rule governing all of the effects of Ago and HuR binding on target transcripts. This is likely due to the complexity of the regulatory

systems in which these proteins interact, and suggest that individual transcripts have evolved to be differentially regulated by the same Ago and HuR proteins. There are many possibilities for how this might happen, such as via the action of additional factors, by the timing of their binding events, or due to the effects of Ago and HuR binding different regions within the transcript such as the coding sequence versus the 3'UTR or even more subtle differences in the precise binding positions of Ago compared to HuR. With more replicates and analysis of translational profiles in the HuR cKO mouse system, it will be interesting to try to define patterns in these changes and to determine pathways of regulation by these proteins that can be separated out from the massive changes in cellular states.

Genomic Distribution of Ago and HuR Regulation in CD8 Lymphocytes

Previous work on Ago and HuR regulatory control of target mRNA has largely focused on their binding interactions with 3' untranslated regions (3'UTRs). However, the analysis described here indicates the first role for Ago and HuR interaction in intronic regions of transcripts. While the rapid increase in transcription with T cell stimulation might indicate a large pool of newly synthesized RNA available for RNA-binding, these patterns are maintained in both the resting and the activated states. Additionally, the predominance of intronic mapping of Ago CLIP tag clusters in the HuR cKO T cells indicates that Ago binding in these regions is not dependent on the presence of HuR. The data suggest that these proteins are deposited on transcripts either co-transcriptionally or soon after transcription.

In the mouse brain, Hu proteins most frequently bind to 3'UTRs, but also bind to intronic sequences and can mediate alternative splicing of neuronal transcripts (Ince-Dunn et al. 2012). HuR has also been shown to bind intronic sequences in human cell lines and its potential role in splicing and the possible link between pre-mRNA processing and transcript stability inferred. The stability of RNA targets was more greatly impacted in HuR knockdown experiments if the RNA contained HuR binding sites in both the 3'UTR and the intron than either of the two alone (Lebedeva et al. 2011; Mukherjee et al. 2011). Still, the interaction of HuR and Ago in these intronic regions has not been previously explored. We propose that the formerly described effects of HuR on pre-mRNA processing and mRNA stability involve interactions with Ago. HuR and Ago may interact with target transcripts in the nucleus to direct splicing events, although it is currently unclear whether they function cooperatively or antagonistically in this process to control the mature message. It is possible that the binding of HuR or Ago could not only direct the sites of splicing, but could also regulate the timing of splicing events by interfering with splicing machinery and other RNA-binding proteins. Their binding could help mediate processing or sequester the RNA, similar to their roles in the cytoplasm. Analysis of Ago target transcripts in the HuR cKO mice might help elucidate a clearer model of control.

Furthermore, the role of immediate binding of HuR and Ago to nascent RNA may serve an even more important role in the regulation of immune function than in previously studied systems. As previously described, the abundant initiation of transcription with the induction of an immune reaction needs to be carefully titrated to secure that cytotoxic and inflammatory signals are directed properly. Binding of RNA by both HuR and Ago

in the nucleus may ensure that when being shuttled into the cytoplasm, that the messages are already being directed for the appropriate fate. They could be directed by HuR directly to active polysomes, or filtered by Ago into cytoplasmic foci such as P-bodies and stress granules for quick interactions with other RNA-binding proteins, or simply degraded.

It would be interesting to consider the binding positions of HuR and Ago on transcripts at further time points after T cell activation. We propose that if HuR and Ago are deposited co-transcriptionally on pre-processed RNA, that after the message has been spliced and shuttled to the cytoplasm, that we may observe the resolution of these intronic sites in an increase in binding in the 3'UTRs more similar to what is seen in the steady state of the brain. Still, the binding events in the intronic regions appear to be sequence specific and present in the resting state as well. Thus, the regulation of the timing and sites of splicing by HuR and Ago may represent another level of post-transcriptional control, whereby target mRNAs could have different availabilities for maturation and processing in the nucleus due to their interrogation by Ago and HuR. The quick shuttling of HuR out of the nucleus with T cell activation could therefore represent the transportation of targets to the cytoplasm or also the release of nuclear targets for the availability of processing.

Ago and HuR and microRNA Regulation

The regulation of RNA processing by Ago and HuR is not only restricted to mRNA. We observed robust binding sites for both proteins in primary microRNA transcript loci. In the example of the microRNA-17-92 locus, we see binding of Ago to microRNA stem loop regions that are greater in length than mature microRNA sequences. This binding is

robust in both the resting and the activated states, indicating that microRNA processing is active in both groups of cells. Ago has been shown to aid Dicer in microRNA processing, or in the case of miR-451, microRNA can be processed by Ago without Dicer involvement (Cheloufi et al. 2010; Cifuentes et al. 2010; Diederichs and Haber 2007). Our data reveals that *in vivo*, Ago associates with microRNA before they are mature species. Interestingly, there is an increase in binding of Ago to regions between stem loops with stimulation induced transcript level induction, indicating that Ago may bind to microRNA transcripts in the nucleus with T cell activation. This may indicate a new role for Ago in the processing of microRNA and may have been previously missed due to the predominant analyses of steady state biology.

We also see an impressive increase in binding in the miR-17-92 region by HuR, mirroring the increase in transcript levels with lymphocyte activation. Thus, HuR may play a role in regulating the dynamics of processing immediately following transcription of microRNA message. Furthermore, the HuR binding pattern is distinct from Ago. Most notably, unlike Ago, the predominant binding sites appear to match sequences between the microRNA stem loops and not as frequently in sites that will eventually make up the mature microRNA 22-mers. We therefore propose that HuR is involved in the processing of microRNAs in the nucleus and would expect to see differences in the levels of mature microRNA bound to Ago in the HuR cKO T cells.

Interestingly, the levels of Ago binding in the mouse miR-17-92 cluster vary in some regions between the wild type and HuR cKO T cells. Although some of these CLIP tags are 22-nucleotides in length and represent mature microRNA, we did not specifically

clone the microRNA population and so our analysis is limited mostly to mRNA binding sites. While there are robust Ago binding events in both animals, even though there are less total unique reads in the HuR cKO dataset, there are quantitatively more binding sites specifically on what will be the mature miR-92a and miR-20a transcripts. The rest of the microRNAs have similar binding patterns in both mice (Figure 10.1).

There is little Ago or HuR binding to or around miR-92a in the human dataset, so it is hard to infer a conclusion about this change in the mouse system. However, miR-20a had a unique pattern of HuR binding in human T cells among this cluster of microRNA. HuR displayed binding sites covering the stem loop region instead of being restricted to only up or downstream of the mature microRNA site. Thus, it is very interesting that Ago binding would be increased preferentially for this microRNA in the HuR cKO cells. This suggests that HuR binding to miR-20a impedes efficient binding of Ago and may explain why their binding patterns are almost exclusive of each other in other parts of this region in the human dataset. We hypothesize that because HuR binding mostly excludes mature microRNA message, HuR plays a role in loading microRNAs into Ago and that binding of HuR to eventual mature sequences would inhibit Ago association in those sites.

Intriguingly, most of the top 7-mers represented in Ago clusters that overlap HuR were microRNAs that were cloned in low frequencies in Ago CLIP. And conversely, the seed matches from the most highly represented microRNA from Ago CLIP, miR-142-3p, was preferentially not found in these sites, but rather in sites where Ago binding did not overlap HuR. This suggests that HuR binding together with Ago may enrich for target sites utilizing more rare microRNAs in T cells. Furthermore, it supports our model that

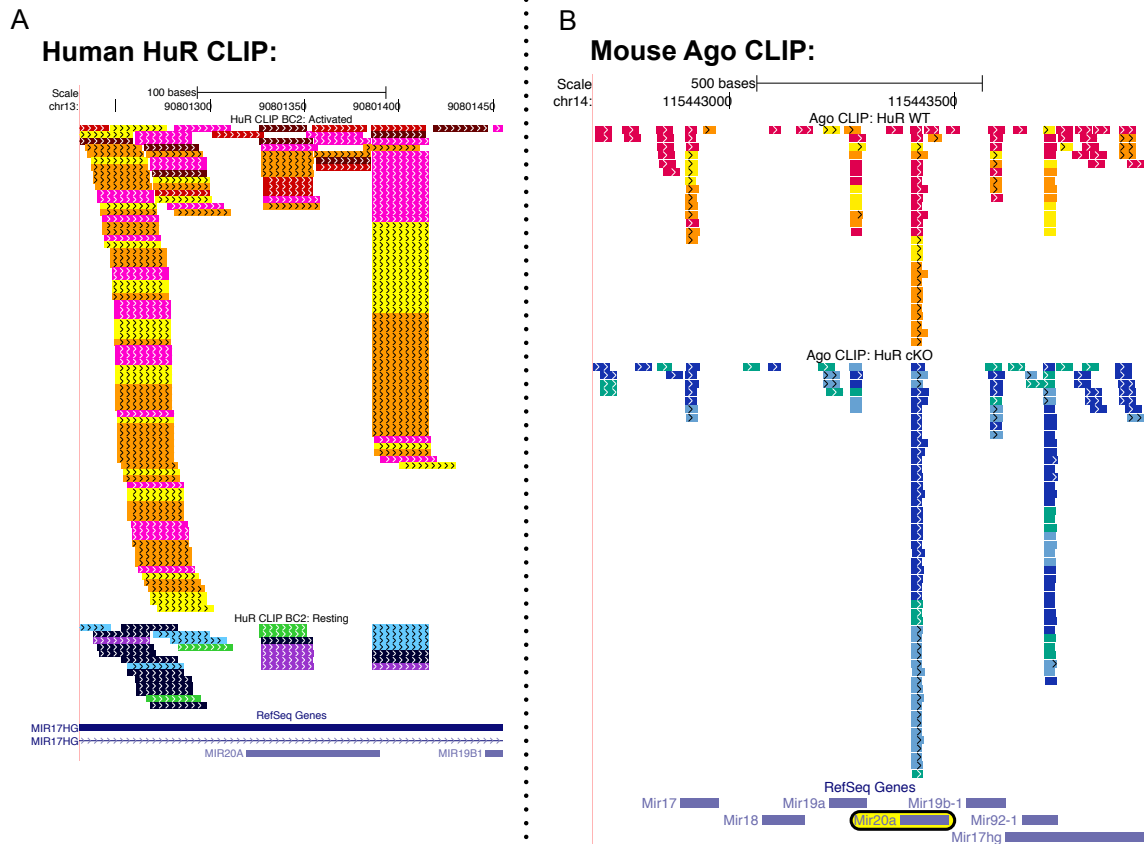


Figure 10.1 Ago and HuR Binding in Human and Mouse: microRNA-17-92 Locus.

(A) The position of individual Ago and HuR unique CLIP tags in biologic complexity two clusters plotted relative to their mapped position on the human microRNA-17-92 locus. From top to bottom: chromosomal location, Ago CLIP tags from activated CD8 T cells (colors represent each donor sample as shown in Table 6.1), Ago CLIP tags from resting CD8 T cells, HuR CLIP tags from activated CD8 T cells, HuR CLIP tags from resting CD8 T cells, Gene diagram from RefSeq. (B) The position of individual Ago unique CLIP tags are plotted relative to their mapped position on the mouse microRNA-17-92 locus, with microRNA-20a highlighted. From top to bottom: chromosomal location, Ago CLIP tags from activated HuR wild-type CD8 T cells (colors represent each donor sample as shown in Table 8.1), Ago CLIP tags from activated HuR cKO CD8 T cells, Gene diagram from RefSeq.

HuR could be a chaperone for loading Ago with microRNAs or for Ago message targeting and it is possible that without this interaction, Ago would not show a binding preference for these rare microRNA seed sites. This might not be necessary for highly abundant microRNAs such as miR-142-3p. Additional analysis of Ago-microRNA association in the HuR cKO animals is needed to further explore this model.

Conclusion

The results presented in this thesis represent the identification and careful characterization of Ago and HuR RNA-binding in the activation of CD8 lymphocytes. Studying normal healthy donor CD8 T cells, we have characterized a system to investigate lymphocyte stimulation *ex vivo* to probe the regulation of this important immune function. These studies also serve as a useful surrogate system for understanding larger issues of dynamic control of RNA regulation in other cellular stress conditions. We demonstrated the reproducibility of our methods to robustly identify Ago and HuR RNA-binding events in human biologic samples representing two cellular states. Furthermore, we identified the transcriptional and translational status of each lymphocyte activation state using ribosomal profiling and RNA sequencing, providing a means to functionally interpret the Ago and HuR binding maps. Moreover, by studying the binding maps for Ago in mouse CD8 T cells with or without HuR, we establish a system for investigating the dependence of Ago on HuR for its target specificities in the mouse, and for focusing on regions in which Ago and HuR binding is likely to be interdependent following the stimulation of human T cells.

REFERENCES

- Abdelmohsen, Kotb, Rudolf Pullmann, Ashish Lal, Hyeon Ho Kim, Stefanie Galban, Xiaoling Yang, Justin D Blethrow, Mark Walker, Jonathan Shubert, David A Gillespie, Henry Furneaux, and Myriam Gorospe. 2007. "Phosphorylation of HuR by Chk2 Regulates SIRT1 Expression.." *Molecular Cell* 25(4): 543–57.
- Abdelmohsen, Kotb, Subramanya Srikantan, Yuki Kuwano, and Myriam Gorospe. 2008. "miR-519 Reduces Cell Proliferation by Lowering RNA-Binding Protein HuR Levels.." *Proceedings of the National Academy of Sciences of the United States of America* 105(51): 20297–302.
- Akamatsu, Wado, Hiroaki Fujihara, Takayuki Mitsuhashi, Masato Yano, Shinsuke Shibata, Yoshika Hayakawa, Hirotaka James Okano, Shin-Ichi Sakakibara, Hiroshi Takano, Toshiya Takano, Takao Takahashi, Tetsuo Noda, and Hideyuki Okano. 2005. "The RNA-Binding Protein HuD Regulates Neuronal Cell Identity and Maturation.." *Proceedings of the National Academy of Sciences of the United States of America* 102(12): 4625–30.
- Akool, El-Sayed, Hartmut Kleinert, Farid M A Hamada, Mohamed H Abdelwahab, Ulrich Förstermann, Josef Pfeilschifter, and Wolfgang Eberhardt. 2003. "Nitric Oxide Increases the Decay of Matrix Metalloproteinase 9 mRNA by Inhibiting the Expression of mRNA-Stabilizing Factor HuR.." *Molecular and cellular biology* 23(14): 4901–16.
- Albert, M L, J C Darnell, A Bender, L M Francisco, N Bhardwaj, and R B Darnell. 1998. "Tumor-Specific Killer Cells in Paraneoplastic Cerebellar Degeneration.." *Nature medicine* 4(11): 1321–24.
- Albert, M L, L M Austin, and R B Darnell. 2000. "Detection and Treatment of Activated T Cells in the Cerebrospinal Fluid of Patients with Paraneoplastic Cerebellar Degeneration.." *Annals of neurology* 47(1): 9–17.
- Albert, Matthew L, and Robert B Darnell. 2004. "Paraneoplastic Neurological Degenerations: Keys to Tumour Immunity.." *Nature reviews Cancer* 4(1): 36–44.
- Ambros, Victor. 2004. "The Functions of Animal microRNAs.." *Nature* 431(7006): 350–55.
- Anderson, Paul. 2008. "Post-Transcriptional Control of Cytokine Production.." *Nature Immunology* 9(4): 353–59.
- Anderson, Paul. 2010. "Post-Transcriptional Regulons Coordinate the Initiation and Resolution of Inflammation.." *Nature reviews Immunology* 10(1): 24–35.

- Atasoy, U, J Watson, D Patel, and J D Keene. 1998. "ELAV Protein HuA (HuR) Can Redistribute Between Nucleus and Cytoplasm and Is Upregulated During Serum Stimulation and T Cell Activation." *Journal of cell science* 111 (Pt 21): 3145–56.
- Baek, Daehyun, Judit Villén, Chanseok Shin, Fernando D Camargo, Steven P Gygi, and David P Bartel. 2008. "The Impact of microRNAs on Protein Output.." *Nature* 455(7209): 64–71.
- Banchereau, J, and R M Steinman. 1998. "Dendritic Cells and the Control of Immunity." *Nature*.
- Bartel, David P. 2004. "MicroRNAs: Genomics, Biogenesis, Mechanism, and Function.." *Cell* 116(2): 281–97.
- Bartel, David P. 2009. "MicroRNAs: Target Recognition and Regulatory Functions." *Cell* 136(2): 215–33.
- Barton, Gregory M. 2008. "A Calculated Response: Control of Inflammation by the Innate Immune System.." *The Journal of clinical investigation* 118(2): 413–20.
- Bazzini, A A, M T Lee, and A J Giraldez. 2012. "Ribosome Profiling Shows That miR-430 Reduces Translation Before Causing mRNA Decay in Zebrafish." *Science (New York, NY)* 336(6078): 233–37.
- Betts, Michael R, Jason M Brenchley, David A Price, Stephen C De Rosa, Daniel C Douek, Mario Roederer, and Richard A Koup. 2003. "Sensitive and Viable Identification of Antigen-Specific CD8+ T Cells by a Flow Cytometric Assay for Degranulation.." *Journal of immunological methods* 281(1-2): 65–78.
- Bhattacharyya, S N, R Habermacher, U Martine, E I Closs, and W Filipowicz. 2006a. "Stress-Induced Reversal of microRNA Repression and mRNA P-Body Localization in Human Cells." *Cold Spring Harbor symposia on quantitative biology* 71: 513–21.
- Bhattacharyya, Suvendra N, Regula Habermacher, Ursula Martine, Ellen I Closs, and Witold Filipowicz. 2006b. "Relief of microRNA-Mediated Translational Repression in Human Cells Subjected to Stress." *Cell* 125(6): 1111–24.
- Blackshear, P J. 2002. "Tristetraprolin and Other CCCH Tandem Zinc-Finger Proteins in the Regulation of mRNA Turnover.." *Biochemical Society Transactions* 30(Pt 6): 945–52.
- Boczkowski, D, S K Nair, D Snyder, and E Gilboa. 1996. "Dendritic Cells Pulsed with RNA Are Potent Antigen-Presenting Cells in Vitro and in Vivo.." *The Journal of experimental medicine* 184(2): 465–72.
- Boehm, U, T Klamp, M Groot, and J C Howard. 1997. "CELLULAR RESPONSES to INTERFERON- γ ." *Annual review of immunology* 15(1): 749–95.

- Boldin, M P, K D Taganov, D S Rao, L Yang, J L Zhao, M Kalwani, Y Garcia-Flores, M Luong, A Devrekanli, J Xu, G Sun, J Tay, P S Linsley, and D Baltimore. 2011. "miR-146a Is a Significant Brake on Autoimmunity, Myeloproliferation, and Cancer in Mice." *Journal of Experimental Medicine*.
- Bradley, J R. 2008. "TNF-Mediated Inflammatory Disease.." *The Journal of pathology* 214(2): 149–60.
- Bregues, Muriel, Daniela Teixeira, and Roy Parker. 2005. "Movement of Eukaryotic mRNAs Between Polysomes and Cytoplasmic Processing Bodies." *Science (New York, NY)* 310(5747): 486–89.
- Brennan, C M, and J A Steitz. 2001. "HuR and mRNA Stability.." *Cellular and molecular life sciences : CMLS* 58(2): 266–77.
- Brown, V, P Jin, S Ceman, J C Darnell, W T O'Donnell, S A Tenenbaum, X Jin, Y Feng, K D Wilkinson, J D Keene, R B Darnell, and S T Warren. 2001. "Microarray Identification of FMRP-Associated Brain mRNAs and Altered mRNA Translational Profiles in Fragile X Syndrome.." *Cell* 107(4): 477–87.
- Burute, Mithila, Kamal Gottimukkala, and Sanjeev Galande. 2012. "Chromatin Organizer SATB1 Is an Important Determinant of T-Cell Differentiation.." *Immunology and cell biology* 90(9): 852–59.
- Cantrell, D A. 2002. "T-Cell Antigen Receptor Signal Transduction - Cantrell - 2002 - Immunology - Wiley Online Library." *Immunology*.
- Casolaro, Vincenzo, Xi Fang, Brian Tancowny, Jinshui Fan, Fan Wu, Subramanya Srikantan, S Yukiko Asaki, Umberto De Fanis, Shau-Ku Huang, Myriam Gorospe, Ulus X Atasoy, and Cristiana Stellato. 2008. "Posttranscriptional Regulation of IL-13 in T Cells: Role of the RNA-Binding Protein HuR.." *The Journal of allergy and clinical immunology* 121(4): 853–54.
- Chang, Sung-Hee, Yi-Chien Lu, Xi Li, Wan-Ying Hsieh, Yuquan Xiong, Mallika Ghosh, Todd Evans, Olivier Elemento, and Timothy Hla. 2012. "Antagonistic Function of the RNA-Binding Protein HuR and miR-200b in Post-Transcriptional Regulation of VEGF-a Expression and Angiogenesis.." *The Journal of biological chemistry*.
- Chaulk, Steven G, Gina L Thede, Oliver A Kent, Zhizhong Xu, Emily M Gesner, Richard A Veldhoen, Suneil K Khanna, Ing Swie Goping, Andrew M MacMillan, Joshua T Mendell, Howard S Young, Richard P Fahlman, and J N Mark Glover. 2011. "Role of Pri-miRNA Tertiary Structure in miR-17~92 miRNA Biogenesis.." *RNA biology* 8(6): 1105–14.
- Cheloufi, Sihem, Camila O Dos Santos, Mark M W Chong, and Gregory J Hannon. 2010. "A Dicer-Independent miRNA Biogenesis Pathway That Requires Ago Catalysis." *Nature* 465(7298): 584–89.

- Chen, Chang-Zheng, Ling Li, Harvey F Lodish, and David P Bartel. 2004. "MicroRNAs Modulate Hematopoietic Lineage Differentiation.." *Science (New York, NY)* 303(5654): 83–86.
- Chi, Sung Wook, Gregory J Hannon, and Robert B Darnell. 2012. "An Alternative Mode of microRNA Target Recognition.." *Nature structural & molecular biology* 19(3): 321–27.
- Chi, Sung Wook, Julie B Zang, Aldo Mele, and Robert B Darnell. 2009. "Argonaute HITS-CLIP Decodes microRNA-mRNA Interaction Maps." *Nature* 460(7254): 479–86.
- Cifuentes, D, H Xue, D W Taylor, H Patnode, Y Mishima, S Cheloufi, E Ma, S Mane, G J Hannon, N D Lawson, S A Wolfe, and A J Giraldez. 2010. "A Novel miRNA Processing Pathway Independent of Dicer Requires Argonaute2 Catalytic Activity." *Science (New York, NY)* 328(5986): 1694–98.
- Cobb, B S. 2005. "T Cell Lineage Choice and Differentiation in the Absence of the RNase III Enzyme Dicer." *Journal of Experimental Medicine* 201(9): 1367–73.
- Cohen, Cyrille J, Yong F Li, Mona El-Gamil, Paul F Robbins, Steven A Rosenberg, and Richard A Morgan. 2007. "Enhanced Antitumor Activity of T Cells Engineered to Express T-Cell Receptors with a Second Disulfide Bond.." *Cancer research* 67(8): 3898–3903.
- Corradi, J P, C Yang, J C Darnell, J Dalmau, and R B Darnell. 1997. "A Post-Transcriptional Regulatory Mechanism Restricts Expression of the Paraneoplastic Cerebellar Degeneration Antigen Cdr2 to Immune Privileged Tissues." *The Journal of neuroscience : the official journal of the Society for Neuroscience* 17(4): 1406–15.
- Dalmau, J, H M Furneaux, R J Gralla, M G Kris, and J B Posner. 1990. "Detection of the Anti-Hu Antibody in the Serum of Patients with Small Cell Lung Cancer--a Quantitative Western Blot Analysis." *Annals of neurology* 27(5): 544–52.
- Darnell, J C, M L Albert, and R B Darnell. 2000. "Cdr2, a Target Antigen of Naturally Occurring Human Tumor Immunity, Is Widely Expressed in Gynecological Tumors." *Cancer research* 60(8): 2136–39.
- Darnell, R B. 1996. "Onconeural Antigens and the Paraneoplastic Neurologic Disorders: at the Intersection of Cancer, Immunity, and the Brain.." *Proceedings of the National Academy of Sciences of the United States of America* 93(10): 4529–36.
- Darnell, Robert B, and Jerome B Posner. 2003a. "Observing the Invisible: Successful Tumor Immunity in Humans." *Nature Immunology* 4(3): 201.
- Darnell, Robert B, and Jerome B Posner. 2003b. "Paraneoplastic Syndromes Involving the Nervous System." *The New England journal of medicine* 349(16): 1543–54.

- Darnell, Robert B, and Jerome B Posner. 2006. "Paraneoplastic Syndromes Affecting the Nervous System." *Seminars in oncology* 33(3): 270–98.
- de Silanes, Isabel López, Ming Zhan, Ashish Lal, Xiaoling Yang, and Myriam Gorospe. 2004. "Identification of a Target RNA Motif for RNA-Binding Protein HuR." *Proceedings of the National Academy of Sciences of the United States of America* 101(9): 2987–92.
- DeLuca, Ilana, Nathalie E Blachère, Bianca Santomasso, and Robert B Darnell. 2009. "Tolerance to the Neuron-Specific Paraneoplastic HuD Antigen.." *PloS one* 4(6): e5739.
- Diederichs, Sven, and Daniel A Haber. 2007. "Dual Role for Argonautes in microRNA Processing and Posttranscriptional Regulation of microRNA Expression.." *Cell* 131(6): 1097–1108.
- Diehn, Maximilian, Ash A Alizadeh, Oliver J Rando, Chih Long Liu, Kryn Stankunas, David Botstein, Gerald R Crabtree, and Patrick O Brown. 2002. "One Path to Costimulation Is Through NFAT." *Science's STKE* 2002(149): 335tw–335.
- Doller, Anke, Josef Pfeilschifter, and Wolfgang Eberhardt. 2008. "Signalling Pathways Regulating Nucleo-Cytoplasmic Shuttling of the mRNA-Binding Protein HuR.." *Cellular signalling* 20(12): 2165–73.
- Fan, X C, and J A Steitz. 1998a. "HNS, a Nuclear-Cytoplasmic Shuttling Sequence in HuR." *Proceedings of the National Academy of Sciences of the United States of America* 95(26): 15293–98.
- Fan, X C, and J A Steitz. 1998b. "Overexpression of HuR, a Nuclear-Cytoplasmic Shuttling Protein, Increases the in Vivo Stability of ARE-Containing mRNAs." *The EMBO journal* 17(12): 3448–60.
- Galfrè, G, and C Milstein. 1981. "Preparation of Monoclonal Antibodies: Strategies and Procedures.." *Methods in enzymology* 73(Pt B): 3–46.
- Gallouzi, I E, C M Brennan, and J A Steitz. 2001. "Protein Ligands Mediate the CRM1-Dependent Export of HuR in Response to Heat Shock.." *RNA* 7(9): 1348–61.
- Gallouzi, I E, C M Brennan, M G Stenberg, M S Swanson, A Eversole, N Maizels, and J A Steitz. 2000. "HuR Binding to Cytoplasmic mRNA Is Perturbed by Heat Shock.." *Proceedings of the National Academy of Sciences of the United States of America* 97(7): 3073–78.
- Ghosh, Mallika, Hector Leonardo Aguila, Jason Michaud, Youxi Ai, Ming-Tao Wu, Annabrita Hemmes, Ari Ristimäki, Caiying Guo, Henry Furneaux, and Timothy Hla. 2009. "Essential Role of the RNA-Binding Protein HuR in Progenitor Cell Survival in Mice.." *The Journal of clinical investigation* 119(12): 3530–43.

- Glorian, V, G Maillot, S Polès, J S Iacovoni, G Favre, and S Vagner. 2011. “HuR-Dependent Loading of miRNA RISC to the mRNA Encoding the Ras-Related Small GTPase RhoB Controls Its Translation During UV-Induced Apoptosis.” *Cell Death and Differentiation* 18(11): 1692–1701.
- Griffiths, E K, C Krawczyk, Y Y Kong, M Raab, S J Hyduk, D Bouchard, V S Chan, I Kozieradzki, A J Oliveira-Dos-Santos, A Wakeham, P S Ohashi, M I Cybulsky, C E Rudd, and J M Penninger. 2001. “Positive Regulation of T Cell Activation and Integrin Adhesion by the Adapter Fyb/Slap..” *Science (New York, NY)* 293(5538): 2260–63.
- Gruber, Andreas R, Jörg Fallmann, Franz Kratochvill, Pavel Kovarik, and Ivo L Hofacker. 2011. “AREsite: a Database for the Comprehensive Investigation of AU-Rich Elements..” *Nucleic Acids Research* 39(Database issue): D66–D69.
- Guo, Huili, Nicholas T Ingolia, Jonathan S Weissman, and David P Bartel. 2010. “Mammalian microRNAs Predominantly Act to Decrease Target mRNA Levels.” *Nature* 466(7308): 835–40.
- Guo, Xu, Yuehan Wu, and Rebecca S Hartley. 2009. “MicroRNA-125a Represses Cell Growth by Targeting HuR in Breast Cancer..” *RNA biology* 6(5): 575–83.
- Hao, Shengli, and David Baltimore. 2009. “The Stability of mRNA Influences the Temporal Order of the Induction of Genes Encoding Inflammatory Molecules..” *Nature Immunology* 10(3): 281–88.
- Harding, Heather P, Marcella Calfon, Fumihiko Urano, Isabel Novoa, and David Ron. 2002. “Transcriptional and Translational Control in the Mammalian Unfolded Protein Response..” *Annual review of cell and developmental biology* 18: 575–99.
- Harding, Heather P, Yuhong Zhang, Huiquing Zeng, Isabel Novoa, Phoebe D Lu, Marcella Calfon, Navid Sadri, Chi Yun, Brian Popko, Richard Paules, David F Stojdl, John C Bell, Thore Hettmann, Jeffrey M Leiden, and David Ron. 2003. “An Integrated Stress Response Regulates Amino Acid Metabolism and Resistance to Oxidative Stress..” *Molecular Cell* 11(3): 619–33.
- Hargreaves, Diana C, Tiffany Horng, and Ruslan Medzhitov. 2009. “Control of Inducible Gene Expression by Signal-Dependent Transcriptional Elongation..” *Cell* 138(1): 129–45.
- Harlow, Ed, and David P Lane. 1988. *Antibodies: a Laboratory Manual*. CSHL Press.
- Hendrickson, David G, Daniel J Hogan, Heather L McCullough, Jason W Myers, Daniel Herschlag, James E Ferrell, and Patrick O Brown. 2009. “Concordant Regulation of Translation and mRNA Abundance for Hundreds of Targets of a Human microRNA..” *PLoS biology* 7(11): e1000238.

- Henke, Jura Inga, Dagmar Goergen, Junfeng Zheng, Yutong Song, Christian G Schüttler, Carmen Fehr, Christiane Jünemann, and Michael Niepmann. 2008. "microRNA-122 Stimulates Translation of Hepatitis C Virus RNA.." *The EMBO journal* 27(24): 3300–3310.
- Hillman-Jackson, Jennifer, Dave Clements, Daniel Blankenberg, James Taylor, Anton Nekrutenko, Galaxy Team. 2012. "Using Galaxy to Perform Large-Scale Interactive Data Analyses.." *Current protocols in bioinformatics / editorial board, Andreas D. Baxevanis ... [et al.]* Chapter 10: Unit10.5.
- Hoffmann, A. 2002. "The Ikappa B-NF-Kappa B Signaling Module: Temporal Control and Selective Gene Activation." *Science (New York, NY)* 298(5596): 1241–45.
- Horvath, C M. 2000. "STAT Proteins and Transcriptional Responses to Extracellular Signals.." *Trends in biochemical sciences* 25(10): 496–502.
- Ince-Dunn, Gulayse, Hirotaka J Okano, Kirk B Jensen, Woong-Yang Park, Ru Zhong, Jernej Ule, Aldo Mele, John J Fak, Chingwen Yang, Chaolin Zhang, Jong Yoo, Margaret Herre, Hideyuki Okano, Jeffrey L Noebels, and Robert B Darnell. 2012. "Neuronal Elav-Like (Hu) Proteins Regulate RNA Splicing and Abundance to Control Glutamate Levels and Neuronal Excitability." *Neuron* 75(6): 1067–80.
- Ingolia, Nicholas T, Gloria A Brar, Silvia Rouskin, Anna M McGeachy, and Jonathan S Weissman. 2012. "The Ribosome Profiling Strategy for Monitoring Translation in Vivo by Deep Sequencing of Ribosome-Protected mRNA Fragments.." *Nature protocols* 7(8): 1534–50.
- Ingolia, Nicholas T, Sina Ghaemmamghami, John R S Newman, and Jonathan S Weissman. 2009. "Genome-Wide Analysis in Vivo of Translation with Nucleotide Resolution Using Ribosome Profiling.." *Science (New York, NY)* 324(5924): 218–23.
- Izquierdo, José M. 2008. "Hu Antigen R (HuR) Functions as an Alternative Pre-mRNA Splicing Regulator of Fas Apoptosis-Promoting Receptor on Exon Definition.." *The Journal of biological chemistry* 283(27): 19077–84.
- Jacobsen, Anders, Jiayu Wen, Debora S Marks, and Anders Krogh. 2010. "Signatures of RNA Binding Proteins Globally Coupled to Effective microRNA Target Sites." *Genome research* 20(8): 1010–19.
- Janeway, Charles A Jr, and Ruslan Medzhitov. 2002. "Innate Immune Recognition." *Science Signaling* 20(1): 197.
- Jenkins, M K, P S Taylor, S D Norton, and K B Urdahl. 1991. "CD28 Delivers a Costimulatory Signal Involved in Antigen-Specific IL-2 Production by Human T Cells.." *The Journal of*

- Jeyaraj, Selvi C, Mamata Singh, Dina A Ayupova, Suman Govindaraju, and Beth S Lee. 2010. "Transcriptional Control of Human Antigen R by Bone Morphogenetic Protein.." *The Journal of biological chemistry* 285(7): 4432–40.
- Jiang, Shan, Chaoran Li, Virginie Olive, Erik Lykken, Feng Feng, Jose Sevilla, Ying Wan, Lin He, and Qi-Jing Li. 2011. "Molecular Dissection of the miR-17-92 Cluster's Critical Dual Roles in Promoting Th1 Responses and Preventing Inducible Treg Differentiation.." *Blood* 118(20): 5487–97.
- Jopling, Catherine L, Minkyung Yi, Alissa M Lancaster, Stanley M Lemon, and Peter Sarnow. 2005. "Modulation of Hepatitis C Virus RNA Abundance by a Liver-Specific MicroRNA.." *Science (New York, NY)* 309(5740): 1577–81.
- Jordan, Martha S, Andrew L Singer, and Gary A Koretzky. 2003. "Adaptors as Central Mediators of Signal Transduction in Immune Cells.." *Nature Immunology* 4(2): 110–16.
- Jousse, Céline, Seiichi Oyadomari, Isabel Novoa, Phoebe Lu, Yuhong Zhang, Heather P Harding, and David Ron. 2003. "Inhibition of a Constitutive Translation Initiation Factor 2alpha Phosphatase, CReP, Promotes Survival of Stressed Cells.." *The Journal of cell biology* 163(4): 767–75.
- Katsanou, V, M Dimitriou, and D L Kontoyiannis. 2006. "Post-Transcriptional Regulators in Inflammation: Exploring New Avenues in Biological Therapeutics." *Ernst Schering Foundation symposium proceedings* (4): 37–57.
- Katsanou, Vicky, Olympia Papadaki, Stavros Milatos, Perry J Blackshear, Paul Anderson, George Kollias, and Dimitris L Kontoyiannis. 2005. "HuR as a Negative Posttranscriptional Modulator in Inflammation." *Molecular Cell* 19(6): 777–89.
- Katsanou, Vicky, Stavros Milatos, Anthie Yiakouvaki, Nikos Sgantzis, Anastasia Kotsoni, Maria Alexiou, Vaggelis Harokopos, Vassilis Aidinis, Myriam Hemberger, and Dimitris L Kontoyiannis. 2009. "The RNA-Binding Protein Elavl1/HuR Is Essential for Placental Branching Morphogenesis and Embryonic Development." *Molecular and cellular biology* 29(10): 2762–76.
- Kawai, Tomoko, Ashish Lal, Xiaoling Yang, Stefanie Galban, Krystyna Mazan-Mamczarz, and Myriam Gorospe. 2006. "Translational Control of Cytochrome C by RNA-Binding Proteins TIA-1 and HuR.." *Molecular and cellular biology* 26(8): 3295–3307.
- Kaye, Jonathan. 2000. "Regulation of T Cell Development in the Thymus." *Immunologic Research* 21(2-3): 71–82.
- Kedersha, N L, M Gupta, W Li, I Miller, and P Anderson. 1999. "RNA-Binding Proteins TIA-1 and TIAR Link the Phosphorylation of eIF-2 Alpha to the Assembly of Mammalian Stress Granules.." *The Journal of cell biology* 147(7): 1431–42.

- Kedersha, N, and P Anderson. 2002. "Stress Granules: Sites of mRNA Triage That Regulate mRNA Stability and Translatability." *Biochemical Society Transactions* 30(Pt 6): 963–69.
- Kim, Hyeon Ho, Yuki Kuwano, Subramanya Srikantan, Eun Kyung Lee, Jennifer L Martindale, and Myriam Gorospe. 2009. "HuR Recruits Let-7/RISC to Repress C-Myc Expression." *Genes & Development* 23(15): 1743–48.
- Kishore, Shivendra, Lukasz Jaskiewicz, Lukas Burger, Jean Hausser, Mohsen Khorshid, and Mihaela Zavolan. 2011. "A Quantitative Analysis of CLIP Methods for Identifying Binding Sites of RNA-Binding Proteins." *Nature Methods* 8(7): 559–64.
- Kouskoff, V, K Signorelli, C Benoist, and D Mathis. 1995. "Cassette Vectors Directing Expression of T Cell Receptor Genes in Transgenic Mice." *Journal of immunological methods* 180(2): 273–80.
- Krol, Jacek, Volker Busskamp, Ilona Markiewicz, Michael B Stadler, Sebastian Ribi, Jens Richter, Jens Duebel, Silvia Bicker, Hans Jörg Fehling, Dirk Schübeler, Thomas G Oertner, Gerhard Schratt, Miriam Bibel, Botond Roska, and Witold Filipowicz. 2010. "Characterizing Light-Regulated Retinal microRNAs Reveals Rapid Turnover as a Common Property of Neuronal microRNAs.." *Cell* 141(4): 618–31.
- Kundu, Pradipta, Marc R Fabian, Nahum Sonenberg, Suvendra N Bhattacharyya, and Witold Filipowicz. 2012. "HuR Protein Attenuates miRNA-Mediated Repression by Promoting miRISC Dissociation From the Target RNA.." *Nucleic Acids Research* 40(11): 5088–5100.
- Lai, W S, E Carballo, J R Strum, E A Kennington, R S Phillips, and P J Blackshear. 1999. "Evidence That Tristetraprolin Binds to AU-Rich Elements and Promotes the Deadenylation and Destabilization of Tumor Necrosis Factor Alpha mRNA.." *Molecular and cellular biology* 19(6): 4311–23.
- Lal, Ashish, Krystyna Mazan-Mamczarz, Tomoko Kawai, Xiaoling Yang, Jennifer L Martindale, and Myriam Gorospe. 2004. "Concurrent Versus Individual Binding of HuR and AUF1 to Common Labile Target mRNAs.." *The EMBO journal* 23(15): 3092–3102.

- Landgraf, Pablo, Mirabela Rusu, Robert Sheridan, Alain Sewer, Nicola Iovino, Alexei Aravin, Sébastien Pfeffer, Amanda Rice, Alice O Kamphorst, Markus Landthaler, Carolina Lin, Nicholas D Socci, Leandro Hermida, Valerio Fulci, Sabina Chiaretti, Robin Foà, Julia Schliwka, Uta Fuchs, Astrid Novosel, Roman-Ulrich Müller, Bernhard Schermer, Ute Bissels, Jason Inman, Quang Phan, Minchen Chien, David B Weir, Ruchi Choksi, Gabriella De Vita, Daniela Frezzetti, Hans-Ingo Trompeter, Veit Hornung, Grace Teng, Gunther Hartmann, Miklos Palkovits, Roberto Di Lauro, Peter Wernet, Giuseppe Macino, Charles E Rogler, James W Nagle, Jingyue Ju, F Nina Papavasiliou, Thomas Benzing, Peter Lichter, Wayne Tam, Michael J Brownstein, Andreas Bosio, Arndt Borkhardt, James J Russo, Chris Sander, Mihaela Zavolan, and Thomas Tuschl. 2007. "A Mammalian microRNA Expression Atlas Based on Small RNA Library Sequencing." *Cell* 129(7): 1401–14.
- Lanzavecchia, A. 1998. "Immunology. Licence to Kill." *Nature* 393(6684): 413–14.
- Lebedeva, Svetlana, Marvin Jens, Kathrin Theil, Björn Schwanhäusser, Matthias Selbach, Markus Landthaler, and Nikolaus Rajewsky. 2011. "Transcriptome-Wide Analysis of Regulatory Interactions of the RNA-Binding Protein HuR." *Molecular Cell* 43(3): 340–52.
- Leung, Anthony K L, Amanda G Young, Arjun Bhutkar, Grace X Zheng, Andrew D Bosson, Cydney B Nielsen, and Phillip A Sharp. 2011. "Genome-Wide Identification of Ago2 Binding Sites From Mouse Embryonic Stem Cells with and Without Mature microRNAs.." *Nature structural & molecular biology* 18(2): 237–44.
- Leung, Anthony K L, and Phillip A Sharp. 2007. "microRNAs: a Safeguard Against Turmoil?." *Cell* 130(4): 581–85.
- Leung, Anthony K L, and Phillip A Sharp. 2010. "MicroRNA Functions in Stress Responses.." *Molecular Cell* 40(2): 205–15.
- Leung, Anthony K L, J Mauro Calabrese, and Phillip A Sharp. 2006. "Quantitative Analysis of Argonaute Protein Reveals microRNA-Dependent Localization to Stress Granules.." *Proceedings of the National Academy of Sciences of the United States of America* 103(48): 18125–30.
- Levy, David E, and J E Darnell. 2002. "Stats: Transcriptional Control and Biological Impact.." *Nature reviews. Molecular cell biology* 3(9): 651–62.
- Li, Qi-Jing, Jacqueline Chau, Peter J R Ebert, Giselle Sylvester, Hyeyoung Min, Gwen Liu, Ravi Braich, Muthiah Manoharan, Juergen Soutschek, Petra Skare, Lawrence O Klein, Mark M Davis, and Chang-Zheng Chen. 2007. "miR-181a Is an Intrinsic Modulator of T Cell Sensitivity and Selection." *Cell* 129(1): 147–61.

- Licatalosi, Donny D, Aldo Mele, John J Fak, Jernej Ule, Melis Kayikci, Sung Wook Chi, Tyson A Clark, Anthony C Schweitzer, John E Blume, Xuning Wang, Jennifer C Darnell, and Robert B Darnell. 2008. "HITS-CLIP Yields Genome-Wide Insights Into Brain Alternative RNA Processing." *Nature* 456(7221): 464–69.
- Lindstein, T, C H June, J A Ledbetter, G Stella, and C B Thompson. 1989. "Regulation of Lymphokine Messenger RNA Stability by a Surface-Mediated T Cell Activation Pathway.." *Science (New York, NY)* 244(4902): 339.
- Liston, Adrian, Li-Fan Lu, Dónal O'Carroll, Alexander Tarakhovsky, and Alexander Y Rudensky. 2008. "Dicer-Dependent microRNA Pathway Safeguards Regulatory T Cell Function.." *Journal of Experimental Medicine* 205(9): 1993–2004.
- Liu, Gwen, Hyeyoung Min, Sibiao Yue, and Chang-Zheng Chen. 2008. "Pre-miRNA Loop Nucleotides Control the Distinct Activities of Mir-181a-1 and Mir-181c in Early T Cell Development" ed. Edathara Abraham. *PloS one* 3(10): e3592.
- Loeb, Gabriel B, Aly A Khan, David Canner, Joseph B Hiatt, Jay Shendure, Robert B Darnell, Christina S Leslie, and Alexander Y Rudensky. 2012. "Transcriptome-Wide miR-155 Binding Map Reveals Widespread Noncanonical MicroRNA Targeting." *Molecular Cell*: 1–11.
- Lu, Li-Fan, Mark P Boldin, Ashutosh Chaudhry, Ling-Li Lin, Konstantin D Taganov, Toshikatsu Hanada, Akihiko Yoshimura, undefined author, and Alexander Y Rudensky. 2010. "Function of miR-146a in Controlling Treg Cell-Mediated Regulation of Th1 Responses.." *Cell* 142(6): 914–29.
- Lu, Li-Fan, To-Ha Thai, Dinis Pedro Calado, Ashutosh Chaudhry, Masato Kubo, Kentaro Tanaka, Gabriel B Loeb, Hana Lee, Akihiko Yoshimura, Klaus Rajewsky, and Alexander Y Rudensky. 2009. "Foxp3-Dependent microRNA155 Confers Competitive Fitness to Regulatory T Cells by Targeting SOCS1 Protein.." *Immunity* 30(1): 80–91.
- Ma, W J, S Cheng, C Campbell, A Wright, and H Furneaux. 1996. "Cloning and Characterization of HuR, a Ubiquitously Expressed Elav-Like Protein.." *The Journal of biological chemistry* 271(14): 8144–51.
- Malter, J S. 1989. "Identification of an AUUUA-Specific Messenger RNA Binding Protein.." *Science (New York, NY)* 246(4930): 664–66.
- Mathonnet, Géraldine, Marc R Fabian, Yuri V Svitkin, Armen Parsyan, Laurent Huck, Takayuki Murata, Stefano Biffo, William C Merrick, Edward Darzynkiewicz, Ramesh S Pillai, Witold Filipowicz, Thomas F Duchaine, and Nahum Sonenberg. 2007. "MicroRNA Inhibition of Translation Initiation in Vitro by Targeting the Cap-Binding Complex eIF4F.." *Science (New York, NY)* 317(5845): 1764–67.

- Mazan-Mamczarz, Krystyna, Stefanie Galban, Isabel López de Silanes, Jennifer L Martindale, Ulus Atasoy, Jack D Keene, and Myriam Gorospe. 2003. "RNA-Binding Protein HuR Enhances P53 Translation in Response to Ultraviolet Light Irradiation.." *Proceedings of the National Academy of Sciences of the United States of America* 100(14): 8354–59.
- Meisner, Nicole-Claudia, and Witold Filipowicz. 2010. "Properties of the Regulatory RNA-Binding Protein HuR and Its Role in Controlling miRNA Repression.." *Advances in experimental medicine and biology* 700: 106–23.
- Mili, Stavroula, and Joan A Steitz. 2004. "Evidence for Reassociation of RNA-Binding Proteins After Cell Lysis: Implications for the Interpretation of Immunoprecipitation Analyses." *RNA* 10(11): 1692–94.
- Monticelli, Silvia, K Mark Ansel, Changchun Xiao, Nicholas D Socci, Anna M Krichevsky, To-Ha Thai, Nikolaus Rajewsky, Debora S Marks, Chris Sander, Klaus Rajewsky, Anjana Rao, and Kenneth S Kosik. 2005. "MicroRNA Profiling of the Murine Hematopoietic System.." *Genome biology* 6(8): R71.
- Moulton, Vaishali R, Vasileios C Kyttaris, Yuang-Taung Juang, Bhabadeb Chowdhury, and George C Tsokos. 2008. "The RNA-Stabilizing Protein HuR Regulates the Expression of Zeta Chain of the Human T Cell Receptor-Associated CD3 Complex.." *The Journal of biological chemistry* 283(29): 20037–44.
- Mu, Ping, Yoon-Chi Han, Doron Betel, Evelyn Yao, Massimo Squatrito, Paul Ogradowski, Elisa de Stanchina, Aleco D'Andrea, Chris Sander, and Andrea Ventura. 2009. "Genetic Dissection of the miR-17~92 Cluster of microRNAs in Myc-Induced B-Cell Lymphomas.." *Genes & Development* 23(24): 2806–11.
- Mukherjee, Neelanjana, David L Corcoran, Jeffrey D Nusbaum, David W Reid, Stoyan Georgiev, Markus Hafner, Manuel Ascano, Thomas Tuschl, Uwe Ohler, and Jack D Keene. 2011. "Integrative Regulatory Mapping Indicates That the RNA-Binding Protein HuR Couples Pre-mRNA Processing and mRNA Stability.." *Molecular Cell* 43(3): 327–39.
- Mukherjee, Neelanjana, Patrick J Lager, Matthew B Friedersdorf, Marshall A Thompson, and Jack D Keene. 2009. "Coordinated Posttranscriptional mRNA Population Dynamics During T-Cell Activation." *Molecular systems biology* 5(1): 288.
- Muljo, Stefan A, K Mark Ansel, Chryssa Kanellopoulou, David M Livingston, Anjana Rao, and Klaus Rajewsky. 2005. "Aberrant T Cell Differentiation in the Absence of Dicer.." *The Journal of experimental medicine* 202(2): 261–69.
- Murphy, Kenneth M. 2006. "Stress Management for T Helper Differentiation." *Nature Immunology* 7(6): 553–55.
- Myer, V E, X C Fan, and J A Steitz. 1997. "Identification of HuR as a Protein Implicated in AUUUA-Mediated mRNA Decay." *The EMBO journal* 16(8): 2130–39.

- Nathan, Carl. 2002. "Points of Control in Inflammation.." *Nature* 420(6917): 846–52.
- Neilson, Joel R, Grace X Y Zheng, Christopher B Burge, and Phillip A Sharp. 2007. "Dynamic Regulation of miRNA Expression in Ordered Stages of Cellular Development." *Genes & Development* 21(5): 578–89.
- Nelson, Peter T, Mariangels De Planell-Saguer, Stella Lamprinaki, Marianthi Kiriakidou, Paul Zhang, Una O'Doherty, and Zissimos Mourelatos. 2007. "A Novel Monoclonal Antibody Against Human Argonaute Proteins Reveals Unexpected Characteristics of miRNAs in Human Blood Cells.." *RNA* 13(10): 1787–92.
- O'Carroll, D, I Mecklenbrauker, P P Das, A Santana, U Koenig, A J Enright, E A Miska, and A Tarakhovsky. 2007. "A Slicer-Independent Role for Argonaute 2 in Hematopoiesis and the microRNA Pathway." *Genes & Development* 21(16): 1999–2004.
- Okano, H J, and R B Darnell. 1997. "A Hierarchy of Hu RNA Binding Proteins in Developing and Adult Neurons." *The Journal of neuroscience : the official journal of the Society for Neuroscience* 17(9): 3024–37.
- Olsen, P H, and V Ambros. 1999. "The Lin-4 Regulatory RNA Controls Developmental Timing in *Caenorhabditis Elegans* by Blocking LIN-14 Protein Synthesis After the Initiation of Translation.." *Developmental biology* 216(2): 671–80.
- Papadaki, Olympia, Stavros Milatos, Sofia Grammenoudi, Neelanjan Mukherjee, Jack D Keene, and Dimitris L Kontoyiannis. 2009. "Control of Thymic T Cell Maturation, Deletion and Egress by the RNA-Binding Protein HuR." *Journal of immunology (Baltimore, Md : 1950)* 182(11): 6779–88.
- Peng, S S, C Y Chen, N Xu, and A B Shyu. 1998. "RNA Stabilization by the AU-Rich Element Binding Protein, HuR, an ELAV Protein.." *The EMBO journal* 17(12): 3461–70.
- Peterson, E J, M L Woods, S A Dmowski, G Derimanov, M S Jordan, J N Wu, P S Myung, Q H Liu, J T Pribila, B D Freedman, Y Shimizu, and G A Koretzky. 2001. "Coupling of the TCR to Integrin Activation by Slap-130/Fyb.." *Science (New York, NY)* 293(5538): 2263–65.
- Peterson, K, M K Rosenblum, H Kotanides, and J B Posner. 1992. "Paraneoplastic Cerebellar Degeneration. I. a Clinical Analysis of 55 Anti-Yo Antibody-Positive Patients." *Neurology* 42(10): 1931–37.
- Piecyk, M, S Wax, A R Beck, N Kedersha, M Gupta, B Maritim, S Chen, C Gueydan, V Kruys, M Streuli, and P Anderson. 2000. "TIA-1 Is a Translational Silencer That Selectively Regulates the Expression of TNF-Alpha.." *The EMBO journal* 19(15): 4154–63.

- Pillai, Ramesh S, Suvendra N Bhattacharyya, Caroline G Artus, Tabea Zoller, Nicolas Cougot, Eugenia Basyuk, Edouard Bertrand, and Witold Filipowicz. 2005. "Inhibition of Translational Initiation by Let-7 MicroRNA in Human Cells.." *Science (New York, NY)* 309(5740): 1573–76.
- Ramirez-Carrozzi, Vladimir R, Daniel Braas, Dev M Bhatt, Christine S Cheng, Christine Hong, Kevin R Doty, Joshua C Black, Alexander Hoffmann, Michael Carey, and Stephen T Smale. 2009. "A Unifying Model for the Selective Regulation of Inducible Transcription by CpG Islands and Nucleosome Remodeling." *Cell* 138(1): 114–28.
- Rauer, Sebastian, and Ioanna Andreou. 2002. "Tumor Progression and Serum Anti-HuD Antibody Concentration in Patients with Paraneoplastic Neurological Syndromes." *European neurology* 47(4): 189–95.
- Rebane, Ana, Alar Aab, and Joan A Steitz. 2004. "Transportins 1 and 2 Are Redundant Nuclear Import Factors for hnRNP A1 and HuR.." *RNA* 10(4): 590–99.
- Ridge, J P, F Di Rosa, and P Matzinger. 1998. "A Conditioned Dendritic Cell Can Be a Temporal Bridge Between a CD4+ T-Helper and a T-Killer Cell." *Nature* 393(6684): 474–78.
- Roberts, Wendy K, Ilana J Deluca, Ashby Thomas, John Fak, Travis Williams, Noreen Buckley, Athanasios G Dousmanis, Jerome B Posner, and Robert B Darnell. 2009. "Patients with Lung Cancer and Paraneoplastic Hu Syndrome Harbor HuD-Specific Type 2 CD8+ T Cells." *The Journal of clinical investigation* 119(7): 2042–51.
- Rock, K L, and A L Goldberg. 1999. "Degradation of Cell Proteins and the Generation of MHC Class I-Presented Peptides." *Annual review of immunology*.
- Rodriguez, Antony, Elena Vigorito, Simon Clare, Madhuri V Warren, Philippe Couttet, Dalya R Soond, Stijn van Dongen, Russell J Grocock, Partha P Das, Eric A Miska, David Vetrie, Klaus Okkenhaug, Anton J Enright, Gordon Dougan, Martin Turner, and Allan Bradley. 2007. "Requirement of Bic/microRNA-155 for Normal Immune Function.." *Science (New York, NY)* 316(5824): 608–11.
- Roman, Jessica, Tirumalai Rangasamy, Jia Guo, Siva Sugunan, Nida Meednu, Gopinath Packirisamy, Larissa A Shimoda, Amit Golding, Gregg Semenza, and Steve N Georas. 2010. "T-Cell Activation Under Hypoxic Conditions Enhances IFN-Gamma Secretion.." *American journal of respiratory cell and molecular biology* 42(1): 123–28.
- Sakai, K, M Gofuku, Y Kitagawa, T Ogasawara, and G Hirose. 1995. "Induction of Anti-Purkinje Cell Antibodies in Vivo by Immunizing with a Recombinant 52-kDa Paraneoplastic Cerebellar Degeneration-Associated Protein." *Journal of neuroimmunology* 60(1-2): 135–41.

- Sakai, Koichiro, Yoko Kitagawa, Misuzu Saiki, Shinji Saiki, and Genjiro Hirose. 2003. "Binding of the ELAV-Like Protein in Murine Autoimmune T-Cells to the Nonameric AU-Rich Element in the 3' Untranslated Region of CD154 mRNA.." *Molecular immunology* 39(14): 879–83.
- Salaun, Bruno, Takuya Yamamoto, Bassam Badran, Yasuko Tsunetsugu-Yokota, Antoine Roux, Lukas Baitsch, Redouane Rouas, Hussein Fayyad-Kazan, Petra Baumgaertner, Estelle Deveau, Anirudh Ramesh, Marion Braun, Daniel Speiser, Brigitte Autran, Philippe Martiat, Victor Appay, and Pedro Romero. 2011. "Differentiation Associated Regulation of microRNA Expression in Vivo in Human CD8+ T Cell Subsets." *Journal of Translational Medicine* 9(1): 44.
- Salter, R D, D N Howell, and P Cresswell. 1985. "Genes Regulating HLA Class I Antigen Expression in T-B Lymphoblast Hybrids.." *Immunogenetics* 21(3): 235–46.
- Santomasso, Bianca D, Wendy K Roberts, Ashby Thomas, Travis Williams, Nathalie E Blachère, Mark E Dudley, Alan N Houghton, Jerome B Posner, and Robert B Darnell. 2007. "A T-Cell Receptor Associated with Naturally Occurring Human Tumor Immunity.." *Proceedings of the National Academy of Sciences* 104(48): 19073–78.
- Scheu, Stefanie, Daniel B Stetson, R Lee Reinhardt, Jess H Leber, Markus Mohrs, and Richard M Locksley. 2006. "Activation of the Integrated Stress Response During T Helper Cell Differentiation." *Nature Immunology* 7(6): 644–51.
- Schwanhäusser, Björn, Dorothea Busse, Na Li, Gunnar Dittmar, Johannes Schuchhardt, Jana Wolf, Wei Chen, and Matthias Selbach. 2011. "Global Quantification of Mammalian Gene Expression Control.." *Nature* 473(7347): 337–42.
- Selbach, Matthias, Björn Schwanhäusser, Nadine Thierfelder, Zhuo Fang, Raya Khanin, and Nikolaus Rajewsky. 2008. "Widespread Changes in Protein Synthesis Induced by microRNAs.." *Nature* 455(7209): 58–63.
- Shao, H, D H Kono, L Y Chen, E M Rubin, and J Kaye. 1997. "Induction of the Early Growth Response (Egr) Family of Transcription Factors During Thymic Selection.." *The Journal of experimental medicine* 185(4): 731–44.
- Sheth, Ujwal, and Roy Parker. 2006. "Targeting of Aberrant mRNAs to Cytoplasmic Processing Bodies.." *Cell* 125(6): 1095–1109.
- Shuai, Ke, and Bin Liu. 2003. "Regulation of JAK–STAT Signalling in the Immune System." *Nature reviews Immunology* 3(11): 900–911.
- Smale, Devn, M Bhatt, Amy Pandya-Jones, Ann-Jay Tong, Iros Barozzi, Michellen, M Lissner, Gioacchino Natoli, Douglas, L Black, Stephenn, T, Amy Pandya-Jones, Ann-Jay Tong, Iros Barozzi, Michelle M Lissner, Gioacchino Natoli, Douglas L Black, and Stephen T Smale. 2012. "Transcript Dynamics of Proinflammatory Genes Revealed by Sequence Analysis of Subcellular RNA Fractions." *Cell* 150(2): 279–90.

- Stark, G R, I M Kerr, B R Williams, R H Silverman, and R D Schreiber. 1998. "How Cells Respond to Interferons.." *Annual review of biochemistry* 67: 227–64.
- Stark, George R, and James E Darnell. 2012. "The JAK-STAT Pathway at Twenty.." *Immunity* 36(4): 503–14.
- Sureban, Sripathi M, Nabendu Murmu, Pavel Rodriguez, Randal May, Reeti Maheshwari, Brian K Dieckgraefe, Courtney W Houchen, and Shrikant Anant. 2007. "Functional Antagonism Between RNA Binding Proteins HuR and CUGBP2 Determines the Fate of COX-2 mRNA Translation.." *Gastroenterology* 132(3): 1055–65.
- Taylor, G A, E Carballo, D M Lee, W S Lai, M J Thompson, D D Patel, D I Schenkman, G S Gilkeson, H E Broxmeyer, B F Haynes, and P J Blackshear. 1996. "A Pathogenetic Role for TNF Alpha in the Syndrome of Cachexia, Arthritis, and Autoimmunity Resulting From Tristetraprolin (TTP) Deficiency.." *Immunity* 4(5): 445–54.
- Thai, To-Ha, Dinis Pedro Calado, Stefano Casola, K Mark Ansel, Changchun Xiao, Yingzi Xue, Andrew Murphy, David Frendewey, David Valenzuela, Jeffery L Kutok, Marc Schmidt-Supprian, Nikolaus Rajewsky, George Yancopoulos, Anjana Rao, and Klaus Rajewsky. 2007. "Regulation of the Germinal Center Response by microRNA-155.." *Science (New York, NY)* 316(5824): 604–8.
- Thompson, C B, T Lindsten, J A Ledbetter, S L Kunkel, H A Young, S G Emerson, J M Leiden, and C H June. 1989. "CD28 Activation Pathway Regulates the Production of Multiple T-Cell-Derived Lymphokines/Cytokines." *Proceedings of the ...* 86(4): 1333–37.
- Tian, B. 2005. "Identification of Direct Genomic Targets Downstream of the Nuclear Factor- B Transcription Factor Mediating Tumor Necrosis Factor Signaling." *The Journal of biological chemistry* 280(17): 17435–48.
- Trombetta, E Sergio, and Ira Mellman. 2005. "Cell Biology of Antigen Processing in Vitro and in Vivo." *Annual review of immunology* 23: 975–1028.
- Trujillo, Robin Deis, Si-Biao Yue, Yujie Tang, William E O'Gorman, and Chang-Zheng Chen. 2010. "The Potential Functions of Primary microRNAs in Target Recognition and Repression.." *The EMBO journal* 29(19): 3272–85.
- Ule, Jernej, Kirk B Jensen, Matteo Ruggiu, Aldo Mele, Aljaz Ule, and Robert B Darnell. 2003. "CLIP Identifies Nova-Regulated RNA Networks in the Brain." *Science (New York, NY)* 302(5648): 1212–15.
- Ule, Jernej, Kirk Jensen, Aldo Mele, and Robert B Darnell. 2005. "CLIP: a Method for Identifying Protein-RNA Interaction Sites in Living Cells." *Methods (San Diego, Calif)* 37(4): 376–86.

- Vasudevan, Shobha, and Joan A Steitz. 2007. "AU-Rich-Element-Mediated Upregulation of Translation by FXR1 and Argonaute 2." *Cell* 128(6): 1105–18.
- Vasudevan, Shobha, Yingchun Tong, and Joan A Steitz. 2007. "Switching From Repression to Activation: microRNAs Can Up-Regulate Translation." *Science (New York, NY)* 318(5858): 1931–34.
- Vasudevan, Shobha, Yingchun Tong, and Joan A Steitz. 2008. "Cell-Cycle Control of microRNA-Mediated Translation Regulation." *Cell cycle (Georgetown, Tex)* 7(11): 1545–49.
- Ventura, Andrea, Amanda G Young, Monte M Winslow, Laura Lintault, Alex Meissner, Stefan J Erkeland, Jamie Newman, Roderick T Bronson, Denise Crowley, James R Stone, Rudolf Jaenisch, Phillip A Sharp, and Tyler Jacks. 2008. "Targeted Deletion Reveals Essential and Overlapping Functions of the miR-17 Through 92 Family of miRNA Clusters.." *Cell* 132(5): 875–86.
- Villarino, Alejandro V, Shoshana D Katzman, Eugenio Gallo, Omer Miller, Shuwei Jiang, Michael T McManus, and Abul K Abbas. 2011. "Posttranscriptional Silencing of Effector Cytokine mRNA Underlies the Anergic Phenotype of Self-Reactive T Cells.." *Immunity* 34(1): 50–60.
- Vogel, Christine, Raquel de Sousa Abreu, Daijin Ko, Shu-Yun Le, Bruce A Shapiro, Suzanne C Burns, Devraj Sandhu, Daniel R Boutz, Edward M Marcotte, and Luiz O Penalva. 2010. "Sequence Signatures and mRNA Concentration Can Explain Two-Thirds of Protein Abundance Variation in a Human Cell Line.." *Molecular systems biology* 6: 400.
- Wang, Jia-huai, and Ellis L Reinherz. 2002. "Structural Basis of T Cell Recognition of Peptides Bound to MHC Molecules." *Molecular immunology* 38(14): 1039–49.
- Wang, Jin Gene, Mark Collinge, Vinod Ramgolam, Oran Ayalon, Xinhao Cynthia Fan, Ruggero Pardi, and Jeffrey R Bender. 2006. "LFA-1-Dependent HuR Nuclear Export and Cytokine mRNA Stabilization in T Cell Activation." *Journal of immunology (Baltimore, Md : 1950)* 176(4): 2105–13.
- Wang, W, H Furneaux, H Cheng, M C Caldwell, D Hutter, Y Liu, N Holbrook, and M Gorospe. 2000. "HuR Regulates P21 mRNA Stabilization by UV Light.." *Molecular and cellular biology* 20(3): 760–69.
- Weiss, A, and D R Littman. 1994. "Signal Transduction by Lymphocyte Antigen Receptors.." *Cell* 76(2): 263–74.
- Wu, Haoquan, Joel R Neilson, Priti Kumar, Monika Manocha, Premalata Shankar, Phillip A Sharp, and N Manjunath. 2007. "miRNA Profiling of Naïve, Effector and Memory CD8 T Cells." *PloS one* 2(10): e1020.

- Wu, Ligang, Jihua Fan, and Joel G Belasco. 2006. "MicroRNAs Direct Rapid Deadenylation of mRNA.." *Proceedings of the National Academy of Sciences of the United States of America* 103(11): 4034–39.
- Wu, Tuoqi, Andreas Wieland, Koichi Araki, Carl W Davis, Lilin Ye, J Scott Hale, and Rafi Ahmed. 2012. "Temporal Expression of microRNA Cluster miR-17-92 Regulates Effector and Memory CD8+ T-Cell Differentiation.." *Proceedings of the National Academy of Sciences of the United States of America* 109(25): 9965–70.
- Xiao, Changchun, and Klaus Rajewsky. 2009. "MicroRNA Control in the Immune System: Basic Principles.." *Cell* 136(1): 26–36.
- Xiao, Changchun, Lakshmi Srinivasan, Dinis Pedro Calado, Heide Christine Patterson, Baochun Zhang, Jing Wang, Joel M Henderson, Jeffrey L Kutok, and Klaus Rajewsky. 2008. "Lymphoproliferative Disease and Autoimmunity in Mice with Increased miR-17-92 Expression in Lymphocytes.." *Nature Immunology* 9(4): 405–14.
- Yarovinsky, Timur O, Noah S Butler, Martha M Monick, and Gary W Hunninghake. 2006. "Early Exposure to IL-4 Stabilizes IL-4 mRNA in CD4+ T Cells via RNA-Binding Protein HuR." *Journal of immunology (Baltimore, Md : 1950)* 177(7): 4426–35.
- Yue, Si-Biao, Robin Deis Trujillo, Yujie Tang, William E O'Gorman, and Chang-Zheng Chen. 2011. "Loop Nucleotides Control Primary and Mature miRNA Function in Target Recognition and Repression.." *RNA biology* 8(6): 1115–23.
- Zhang, Nu, and Michael J Bevan. 2010. "Dicer Controls CD8+ T-Cell Activation, Migration, and Survival.." *Proceedings of the National Academy of Sciences* 107(50): 21629–34.
- Ørom, Ulf Andersson, Finn Cilius Nielsen, and Anders H Lund. 2008. "MicroRNA-10a Binds the 5'UTR of Ribosomal Protein mRNAs and Enhances Their Translation.." *Molecular Cell* 30(4): 460–71.